

GENETIC AND FUNCTIONAL INVESTIGATION OF INHERITED NEUROPATHIES

Ellen Cottenie

MRC Centre for Neuromuscular Diseases, UCL Institute of Neurology

Supervisors: Professor Mary M.
Reilly, Professor Henry Houlden and Professor Mike Hanna

Thesis submitted for the degree of Doctor of Philosophy

University College London

2015

Declaration

I, Ellen Cottenie, confirm that the work presented in this thesis is my own. Where information has been derived from other sources, I confirm that this has been indicated in the thesis.

Abstract

With the discovery of next generation sequencing techniques the landscape of pathogenic gene discovery has shifted drastically over the last ten years. For the purpose of this thesis, focus was applied on finding genetic causes of inherited neuropathies, mainly Charcot-Marie-Tooth disease, by using both old and new genetic techniques and the accompanying functional investigations to prove the pathogenicity of these variants. Mutations in *ATPase 6*, the first mitochondrially encoded gene responsible for an isolated neuropathy, were found in five families with CMT2 by a traditional Sanger sequencing approach. The same approach was used to expand the phenotype associated with *FIG4* mutations, known as CMT4J. Compound heterozygous mutations were found in a patient with a proximal and asymmetric weakness and rapid deterioration of strength in a single limb, mimicking CIDP.

Several appropriate cohorts were screened for mutations in candidate genes with the traditional Sanger sequencing approach; however, no new pathogenic genes were found. In the case of the *HINT1* gene, the originally stated frequency of 11% could not be replicated and a founder effect was suggested, underlying the importance of considering the ethnic background of a patient when screening for mutations in neuropathy-related genes. After the incorporation of exome sequencing, five CMT families were provided with a genetic diagnosis due to mutations in three novel genes and two previously known pathogenic genes. Many more families are currently under investigation and candidate genes have been found in some.

Lastly, a series of divergent functional techniques was used to investigate the pathogenicity of *IGHMBP2* mutations in 11 families with CMT2. *IGHMBP2* mutations normally lead to SMARD1 and fibroblast and lymphoblast studies indicate that the *IGHMBP2* protein levels are significantly higher in CMT2 than SMARD1, but lower than controls, suggesting that the clinical phenotype differences correlate to the *IGHMBP2* protein levels.

Acknowledgments

First of all, I would like to express my gratefulness and gratitude to my supervisors Professor Mary Reilly, Professor Henry Houlden and Professor Mike Hanna, for giving me the chance to work on this thesis under their guidance. I immensely appreciate the opportunities they have given me to grow as a person, both professionally and personally.

None of this would have been possible without the endless support from my family and friends, old and new. I would especially like to thank my mum for always being there, for her encouragement and belief in me, and her never-ending care. My dad, who made moving countries so much easier and was always there to help, and my grandma for her continuous supply of cakes and stews from home. A special thanks to Julia, for keeping me sane and crazy at the same time; Elodie, the most amazing colleague I am so pleased to call my friend and Alice and Siobhan, who made me want to go sit in the office every day and provided entertaining distractions during long days in the lab and were so kind to welcome me amongst their friends. Marta and Ellie, for all the lovely coffees and dinners we had together and their tremendous support and help. All the other people from the lab that helped me along the way, especially Qiang, Amelie, Kira, Sybille, Alex H, Alex R, James, Mary, Cathy, Ese, Jason and Jacky, Chris and Matilde at the centre, and everyone from the ION Department of Molecular Neuroscience and the MRC centre for their help, advice, and friendship during my PhD.

I also would like to thank all of my friends in London and my lovely housemates, Nicol and Ramona, for making me feel at home and being there in the best and worst times. For sharing their wisdom, cooking recipes and nail polish and putting up with some of my weird habits. My friends in Belgium, for always welcoming me back and not forgetting about me. Especially Karolien and Mireille, two of the most wonderful women I know. Annemie, Mairo, Laura and Willeke, girls I've known since first grade and I know will always be there for me.

Table of Contents

Declaration	2
Abstract	3
Acknowledgments	4
Figure list	11
Table list	15
List of abbreviations	17
List of publications	23
Chapter 1: Introduction	25
1.1 Phenotypic spectrum of peripheral neuropathies	25
1.1.1 The peripheral nervous system	25
1.1.2 Peripheral neuropathies	26
1.1.3 Charcot-Marie-Tooth disease	27
1.2 Genetic diversity and classification of CMT	27
1.2.1 Demyelinating CMT	28
1.2.2 Axonal CMT	32
1.2.3 Intermediate CMT	37
1.2.4 Hereditary Sensory and Autonomic Neuropathy.....	39
1.2.5 Distal Hereditary Motor Neuropathy	42
1.2.6 X-linked CMT	47
1.3 Pathogenic pathways involved in Charcot-Marie-Tooth.....	49
1.3.1 Myelin assembly and Schwann cell dynamics	49
1.3.2 Altered protein synthesis, sorting and/or degradation	50
1.3.3 Axonal transport Altered Transport Processes	53
1.3.4 Alterations of the Cytoskeleton	56
1.3.5 Mitochondrial network dynamics and ATP production	58
1.3.6 tRNA synthetase genes	61
1.3.7 Unknown pathways	62
1.4 Thesis aims	63
Chapter 2: Material and methods	64
2.1 Genetic studies	64
2.1.1 Ethical approval and patient selection	64

2.1.2 DNA extraction.....	64
2.1.3 DNA concentration and purity.....	65
2.1.4 Polymerase Chain Reaction (PCR).....	65
2.1.5 Agarose gel electrophoresis of PCR products	67
2.1.6 DNA purification	67
2.1.7 Sequencing.....	68
2.1.8 Clean-up reaction.....	68
2.1.9 Sequence analysis	69
2.1.10 Restriction endonuclease analysis	69
2.1.11 Fragment analysis to look at the C9orf72 expansion repeat.....	69
2.1.12 Exome Sequencing	70
2.1.13 Linkage analysis	72
2.1.14 Haplotyping	72
2.2 Cell Culture	73
2.2.1 Fibroblast culture	73
2.2.2 HEK293T Cell culture	74
2.2.3 Lymphoblast cell culture	74
2.3 Molecular biology	74
2.3.1 Constructs and generation of mutations by site-directed mutagenesis	74
2.3.2 Heat-shock transformation of competent Top10 E.Coli.....	75
2.3.3 Purification	76
2.3.4 Stable transfection for Co-immunoprecipitation	76
2.3.5 Stable transfection for ATPase assay	77
2.4 Protein Biochemistry for HEK293T cell lines	77
2.4.1 Cell harvesting for Co-immunoprecipitation.....	77
2.4.2 Co-immunoprecipitation.....	77
2.4.3 Cell harvesting for ATPase assay	78
2.4.4 ATPase assay	78
2.5 Protein biochemistry for fibroblast cell lines	79
2.5.1 Cell harvesting for mRNA extraction.....	79
2.5.2 mRNA extraction.....	80
2.5.3 cDNA synthesis	80
2.5.4 Quantitative PCR	80
2.5.5 Cell harvesting for western blot.....	82

2.5.6 Protein estimation	82
2.5.7 Western blot.....	82
2.6 Immunocytochemistry	83
2.6.1 Subcellular localisation of proteins in patient fibroblasts.....	83
2.6.2 Colocalisation	84
2.6.3 Endocytosis investigation	84
2.6.4 Basal mitochondrial membrane potential	85
2.6.5 Response to mitochondrial toxins.....	86
2.7 Statistical analysis	86
Chapter 3: Mitochondrial mutations in CMT2.....	88
3.1 Introduction	88
3.1.1 A role for mitochondria in neurodegenerative diseases	88
3.1.2 The oxidative phosphorylation system	89
3.1.3 Mutations in the OXPHOS genes in patients with peripheral neuropathy	92
3.1.4 Mutations in ATP synthase.....	93
3.1.5 Mitochondrial genetics in humans.....	93
3.1.6 Structural results of mutations in the ATPase 6 gene.....	98
3.2 Results	99
3.2.1 Genetic screening of the ATPase 6 and ATPase 8 genes resulted in a mutation frequency of 1.4%	99
3.2.2 Segregation analysis and the use of heteroplasmy investigation.....	100
3.2.3 Family A	100
3.2.4 Family B	102
3.2.5 Family C.	103
3.2.6 Sporadic case	104
3.2.7. Estimating pathogenicity of unknown variations in the mitochondrial genome.....	105
3.3 Discussion	106
3.3.1 Clinical details	106
3.3.2 Pattern of disease severity	106
3.3.3 Blue native gels.....	108
3.3.4 Explanation for the phenotypic spectrum is unknown	108
3.3.5 Guidelines for mutational analysis in patients with CMT2	109
3.3.6 Cohort study.....	109

Chapter 4: Candidate gene screening in patients with CMT2.....	111
4.1 Introduction	111
4.1.1 Expanding clinical spectrum of known disease genes.....	111
4.1.2 Frequency of genetic subtypes.....	116
4.1.3 Mouse models as an example to screen new genes	122
4.2 Results	123
4.2.1 FIG4.....	123
4.2.2 C9orf72	127
4.2.3 HINT1	128
4.2.4 SCN9A.....	129
4.2.5 ARL1 and ARL6ip1	131
4.3 Discussion	132
4.3.1 FIG4	132
4.3.2 C9orf72	133
4.3.3 HINT1	133
4.3.4 SCN9A.....	133
4.3.5 ARL1 and ARL6ip1	134
4.3.6 Overall discussion.....	134
Chapter 5: Whole exome sequencing	135
5.1 Introduction	135
5.1.1 Previous ways to identify disease genes	135
5.1.1 Discovering new genes with the use of whole exome sequencing	136
5.1.2 The usage of linkage analysis in combination with whole exome sequencing	136
5.1.3 Prioritizing variants to find a favourable candidate gene	137
5.1.4 The ubiquitous variants of unknown significance	137
5.2 Results	139
5.2.1 Success rate of exome sequencing in rare diseases	139
5.2.2 Family D	139
5.2.3 Family E.....	153
5.2.4 Family F	161
5.2.5 Family G	167
5.2.6 Family H	171
5.2.7 Family I.....	173

5.2.8 Family J	177
5.2.9 Family K	180
5.2.10 Family L.....	182
5.3. Discussion	183
Chapter 6: Genetic and functional analysis of <i>IGHMBP2</i>	186
6.1 Introduction	186
6.1.1 Spinal Muscular Atrophy with Respiratory distress 1	186
6.1.2 Immunoglobulin mu binding protein 2 protein	189
6.1.3 nmd mouse.....	192
6.1.4 Treatment and management.....	193
6.1.5 Future directions	193
6.2 Results	195
6.2.1 Clinical details of two siblings with CMT2.....	195
6.2.2 Exome sequencing revealed a mutation in the <i>IGHMBP2</i> gene	196
6.2.3 Genetic screening.....	197
6.2.4 Clinical details	197
6.2.5 Mutation spectrum	203
6.2.6 Localisation of the missense mutations within the structural domains of <i>IGHMBP2</i>	206
6.2.7 Haplotyping	208
6.2.8 mRNA analysis of <i>IGHMBP2</i> nonsense mutations.....	210
6.2.9 Subcellular localisation of <i>IGHMBP2</i> in patient fibroblasts	211
6.2.10 Protein levels of <i>IGHMBP2</i> in patient fibroblasts.....	211
6.2.11 Protein levels of <i>IGHMBP2</i> in lymphoblastoid cell lines	219
6.2.12 <i>IGHMBP2</i> expression studies.....	219
6.2.13 mRNA levels of <i>IGHMBP2</i> in fibroblasts.....	219
6.2.14 mRNA levels of <i>IGHMBP2</i> in lymphoblasts	223
6.2.15 Co-immunoprecipitation of <i>IGHMBP2</i> with proteins implicated in Amyotrophic lateral sclerosis	224
6.2.16 Subcellular localisation of TDP43	226
6.2.17 Colocalisation of <i>IGHMBP2</i> with TDP43.....	227
6.2.18 Co-immunoprecipitation of <i>IGHMBP2</i> with proteins implicated in CMT	228
6.2.19 Visualisation of <i>IGHMBP2</i> in the CMT2 protein network	229

6.2.20 ATPase activity of the IGHMBP2 protein in transfected HEK cells	229
6.3 Discussion	235
Chapter 7: General conclusions.....	238
Appendix I	247
Appendix II	249
Appendix III	251
Appendix IV.....	255
Appendix V	259
References	265

Figure list

Figure 1-1 Proteins of the endocytic pathway implicated in CMT.	51
Figure 1-2 Proteins in axonal transport or cytoskeleton, implicated in CMT.	55
Figure 2-1 Circular map of the pCMV-Tag 4 vector.	75
Figure 2-2 Sample plot of the amplification curves (left) and the dissociation curves (right) for the selected primers of the qPCR experiment in lymphoblasts.	81
Figure 3-1 The oxidative phosphorylation system in the inner mitochondrial membrane.	90
Figure 3-2 The human ATP synthase.	92
Figure 3-3 Genotype-phenotype correlation for the m.8993T>G transversion.	98
Figure 3-4 Sequencing results for the m.9.185T>C variant.	100
Figure 3-5 Pedigree of Family A.	102
Figure 3-6 Pedigree of family B.	103
Figure 3-7 Pedigree of Family C.	104
Figure 3-8 Pedigree of the sporadic case.	105
Figure 3-9 Correlation between heteroplasmic content of mutant DNA and severity of the disease	107
Figure 4-1 Electropherograms of compound heterozygous mutations found in <i>FIG4</i> .	123
Figure 4-2 MRI of the patient.	125
Figure 4-3 Sural nerve biopsy at age 14 years.	127
Figure 4-4 Example of fragment analysis in <i>C9orf72</i> .	128
Figure 4-5 Missense variant in <i>SCN9A</i> .	131
Figure 5-1 Exome sequencing workflow, starting from the return of the data to the choice of a candidate gene.	138
Figure 5-2 Pedigree of CMT2 family D.	140
Figure 5-3 (A) Electropherograms of the m.12441delC variant in the blood and muscle of the index patient and blood of the mother (III.2) in comparison with a control. (B) Localisation of the m.12241delC frameshift variant in tRNA serine 2 (C) Conservation of the basepair amongst different species.	143
Figure 5-4 Electropherograms and conservation of the novel missense variants found in the CMT2 patient cohort.	146

Figure 5-5 cDNA analysis of the nonsense variant in <i>TRAK2</i> .	147
Figure 5-6 Localisation experiments of TRAK2 in transfected COS7 cells.	148
Figure 5-7 Localisation of TRAK2 in patient fibroblasts in comparison with a MFN2 patient and two controls.	149
Figure 5-8 Percentage of mitochondrial membrane potential of patient fibroblasts and MFN2 positive control in comparison with normal control fibroblasts.	150
Figure 5-9 Confocal images of the mitochondrial membrane potential of patient fibroblasts in comparison with a MFN2 positive control and normal control fibroblasts.	151
Figure 5-10 Pedigree of family F	153
Figure 5-11 Conservation of Glycine 367 in γ -adducin.	155
Figure 5-12 Time course of transferrin internalisation in controls (•) and patients (▪) fibroblast cell lines.	157
Figure 5-13 Transferrin intensity in the different fibroblast cell lines.	157
Figure 5-14 Representative confocal images for the uptake of transferrin in human fibroblasts after an incubation period of 30 minutes.	158
Figure 5-15 Physiology of the mitochondrial network in patient and control fibroblasts.	159
Figure 5-16 Mitochondrial membrane potential in the different fibroblast cell lines.	159
Figure 5-17 Pedigree of Family F.	163
Figure 5-18 Linkage areas of family F on chromosomes 1, 5, 7, 15 and 19.	164
Figure 5-19 Pedigree of Family G.	167
Figure 5-20 Linkage areas of Family G on chromosomes 1,13,14 and 17.	168
Figure 5-21 Conservation of Proline 266 in the <i>WDR48</i> gene.	171
Figure 5-22 Pedigree of Family H.	172
Figure 5-23 Pedigree of family I.	174
Figure 5-24 Conservation of the variants in the <i>RGMb</i> (upper frame) and <i>MORC2</i> (lower frame) genes.	175
Figure 5-25 Pedigree of Family J.	177
Figure 5-26 Conservation of the variant in the <i>FAM126A</i> gene.	180
Figure 5-27 Pedigree of Family K.	181
Figure 5-28 Electropherograms of mutations in <i>BICD2</i> .	181
Figure 5-29 Coverage of the <i>MFN2</i> variant in the original exome sequencing	182

Figure 6-1 Location of all missense, nonsense and frameshift mutations in the structure of <i>IGHMBP2</i> .	190
Figure 6-2 Electropherograms of the segregational analysis in families A-D.	199
Figure 6-3 Localisation of the newly found mutations in <i>IGHMBP2</i> in CMT2 patients in comparison with the already known pathogenic mutations in SMARD1 patients.	204
Figure 6-4 Conservation of the novel variants found in <i>IGHMBP2</i> .	205
Figure 6-5 Conservation of Proline 531 of <i>IGHMBP2</i> in primates.	206
Figure 6-6 Mapping of the missense mutations of families O, P, Q, U, V and W on to the <i>IGHMBP2</i> structure.	207
Figure 6-7 Haplotyping results for families M, N and O.	209
Figure 6-8 Sequence electropherograms of the c.138T>A mutation in the mRNA of lymphoblasts and fibroblasts of CMT2 individuals and carriers, the c.1813C>T mutation in fibroblasts of CMT2 individuals, and frameshift mutations in fibroblasts of SMARD1 individuals.	210
Figure 6-9 Localisation of the <i>IGHMBP2</i> protein in fibroblasts.	212
Figure 6-10 Comparison of the different antibodies for <i>IGHMBP2</i> in different cell types.	214
Figure 6-11 Ponceau staining of different fibroblast cell lines during a period of bacterial infections in the tissue culture labs.	215
Figure 6-12 Steady-state protein levels of <i>IGHMBP2</i> in fibroblast cell lines.	217
Figure 6-13 Western blot results for 2 sets of identical samples, harvested and processed on different days.	218
Figure 6-14 Existence of a degradation band around 70–80 kDa in individuals with CMT2 and a combination of the p.Cys46Ter and p.Arg971Glufs*4 mutations.	218
Figure 6-15 Western blot showed the presence of an extra band at ~130 kDa in fibroblasts under stressful conditions.	218
Figure 6-16 Steady-state protein levels in lymphoblastoid cell lines.	220
Figure 6-17 Expression of <i>IGHMBP2</i> (top row) in various human tissues as compared to the housekeeping gene <i>GAPDH</i> (bottom row).	221
Figure 6-18 mRNA expression levels in different tissues at different stages of life.	221
Figure 6-19 mRNA expression levels of <i>IGHMBP2</i> in fibroblast cell lines.	222

Figure 6-20 mRNA expression levels of <i>IGHMBP2</i> in lymphoblastoid cell lines.	223
Figure 6-21 Co-immunoprecipitation experiments carried out in HEK293-T cells transfected with wild type construct of <i>IGHMBP2</i> show no interaction between <i>IGHMBP2</i> and FUS or SOD1.	224
Figure 6-22 Co-immunoprecipitation experiments carried out in HEK293-T cells transfected with wild type or mutated construct of <i>IGHMBP2</i> show that TDP43 interacts with <i>IGHMBP2</i> .	225
Figure 6-23 Immunostaining of TDP43 in the anterior horn cells of the spinal cord of a SMARD1 patient with mutations in <i>IGHMBP2</i> .	226
Figure 6-24 Localisation of TDP43 and colocalisation of <i>IGHMBP2</i> and TDP43 in human fibroblasts.	227
Figure 6-25 Pierson's correlation coefficient for the colocalisation of <i>IGHMBP2</i> and TDP43 in different human fibroblast cell lines.	228
Figure 6-26 Co-immunoprecipitation experiments carried out in HEK293-T cells transfected with wild type construct of <i>IGHMBP2</i> show no interaction between <i>IGHMBP2</i> and selected proteins involved in CMT2.	229
Figure 6-27 Protein network of CMT2 proteins and <i>IGHMBP2</i> .	230
Figure 6-28 Coomassie blue staining of the different conditions for the optimisation of <i>IGHMBP2</i> purification.	232
Figure 6-29 Purification of wild type- <i>IGHMBP2</i> with condition 2 and 3x 15 cm ² dishes.	232
Figure 6-30 Coomassie Blue staining for the different conditions used for further <i>IGHMBP2</i> purification with conditions 5,6 and 7.	233
Figure 6-31 ATPase assay for different construct of <i>IGHMBP2</i> .	234
Figure 6-32 ATPase assay for different construct of <i>IGHMBP2</i> with a positive CIP control.	235

Table list

Table 1-1 Classification of demyelinating CMT according to genotype.	31
Table 1-2 Classification of axonal CMT according to genotype.	35
Table 1-3 Classification of intermediate CMT according to genotype.	38
Table 1-4 Classification of Hereditary sensory and autonomic neuropathy according to genotype.	41
Table 1-5 Classification of Distal Hereditary Motor Neuropathy according to genotype.	46
Table 1-6 Classification of X-linked CMT.	49
Table 2-1 List of transcripts used for sequencing of genes.	65
Table 2-2 Standard 60-50 touchdown PCR reaction.	66
Table 2-3 Primer sequences for the <i>ATPase6</i> and 8 genes.	67
Table 2-4 PCR reaction. Steps 2 to 4 were repeated 30 times.	67
Table 2-5 Primer sequences for the <i>C9orf72</i> expansion repeat (5' to 3').	70
Table 2-6 PCR reaction for the <i>C9orf72</i> expansion repeat.	70
Table 2-7 Microsatellite markers used for haplotyping of the c.Cys46Ter mutation in the <i>IGHMBP2</i> gene.	72
Table 2-8 Primer sequences for mutagenesis of the <i>IGHMBP2</i> construct.	75
Table 2-9 Antibodies used for western blotting to detect interactions with the <i>IGHMBP2</i> protein after Co-immunoprecipitation.	78
Table 2-10 Protocol for quantitative PCR. Steps 3-5 were repeated 40 times.	81
Table 2-11 Primary antibodies used for western blotting.	83
Table 2-12 Primary and secondary antibodies used for Confocal imaging.	84
Table 3-1 Possible mutations amongst variants found in the <i>ATPase 6/8</i> genes in the mitochondrial genome.	105
Table 3-2 Variants of unknown significance found in the <i>ATPase 6</i> gene in our cohort.	109
Table 4-1 Variants found in the <i>FIG4</i> gene.	124
Table 4-2 Nerve conduction studies at ages 13,19 and 26.	126
Table 4-3 Phenotype for the 127 patients analysed for mutations in the <i>HINT1</i> gene.	128
Table 4-4 Variants found in the <i>HINT1</i> gene.	129

Table 4-5 Patient cohort for the screening of <i>SCN9A</i> .	129
Table 4-6 Coding changes found in the <i>SCN9A</i> gene.	130
Table 4-7 Variants found in the <i>ARL1</i> gene.	131
Table 4-8 Variants found in the <i>ARL6ip1</i> gene.	132
Table 5-1 List of eleven candidates genes for Family F within the linkage areas.	165
Table 5-2 List of novel variants outside the linkage areas in family F.	166
Table 5-3 Shared, novel, nonsynonymous variants in family G.	170
Table 5-4 Shared, novel, nonsynonymous variants in family I.	176
Table 5-5 Shared, novel, nonsynonymous variants in Family J.	179
Table 6-1 List of all patients with CMT2 and mutations in <i>IGHMBP2</i> .	198
Table 6-2 Clinical features of all patients with CMT2 and <i>IGHMBP2</i> mutations.	201
Table 6-3 Polymorphic microsatellite markers used for the haplotyping of the nonsense and frameshift mutations in <i>IGHMBP2</i> in families M, N and O.	208
Table 6-4 List of all the available fibroblast and lymphoblast cell lines in the <i>IGHMBP2</i> project.	213
Table 6-5 Different buffers used for the optimisation of <i>IGHMBP2</i> purification.	231
Table 6-6 Order of different buffers used for further optimisation of <i>IGHMBP2</i> purification.	233

List of abbreviations

AA	Amino acid
AAV9	Adeno-associated virus 9
ABI	Applied Biosystems
ACD	Acid citrate dextrose
ADP	Adenosine diphosphate
AD	Autosomal dominant
ALS	Amyotrophic Lateral Sclerosis
ANOVA	Analysis of variance
AONs	Antisense oligonucleotides
AR	Autosomal recessive
ARS	Aminoacyl tRNA synthetases
ATP	Adenosine 5'-triphosphate
BAC	Bacterial artificial chromosome
BMP	Bone morphogenetic protein
BN	Blue native
BN-PAGE	Blue native-polyacrylamide gel electrophoresis
BSA	Bovine serum albumin
CCP	Clathrin-coated pit
CDE	Clathrin-dependent endocytosis
cDNA	Complementary deoxyribonucleic acid
CIDP	Chronic inflammatory demyelinating polyneuropathy
CIP	Congenital insensitivity to pain
CIPA	Congenital insensitivity to pain with anhidrosis
CMAP	Compound muscle action potential
CMT	Charcot-Marie-Tooth disease
CNS	Central nervous system
CO2	Carbon dioxide
COOH-terminus	Carboxy-terminus
COS7	CV-1 (simian) in Origin, and carrying the SV40 genetic material
COX	Cytochrome c oxidase

C _t	Threshold cycle
DAPI	4',6-Diamidino-2-phenylindole
DCSMA	Dominant congenital spinal muscular atrophy
dbSNP	Single nucleotide polymorphism database
dHMN	Distal hereditary motor neuropathy
DMEM	Dulbecco's modified eagle medium
DMSO	Dimethyl sulfoxide
DNA	Deoxyribonucleic acid
dNTP	Deoxyribonucleotide triphosphate
DPBS	Dulbecco's phosphate buffered saline
DRG	Dorsal root ganglia
DTT	Dithiothreitol
ECACC	European Collection of Cell Cultures
ECL	Electrochemiluminescence
EDTA	Ethylenediaminetetraacetic acid
EEG	Electroencephalogram
EMG	Electromyogram
ENT	Ear nose and throat
ER	Endoplasmic reticulum
ES	Exome sequencing
EST	Expressed sequence tag
ETC	Electron transport chain
EVS	Exome variant server
FAD	Flavin adenine dinucleotide
FADH ₂	Flavin adenine dinucleotide (reduced)
FAM	Fluorescein
FBS	Foetal bovine serum
FCCP	Carbonyl cyanide-4-(trifluoromethoxy) phenylhydrazone
FCD	Fleck corneal dystrophy
FDIO	First dorsal interosseous
FMN	Flavin mononucleotide
FS	Frameshift
FSGS	Focal segmental glomerulosclerosis
FTLD	Frontotemporal lobar degeneration

GABAA	Type-A γ -aminobutyric acid receptor
GAPDH	Glyceraldehyde-3-phosphate dehydrogenase
GERP	Genomic evolutionary rate profiling
GFP	Green fluorescent protein
GSK	Glycogen synthase kinase
GTP	Guanosine-5'-triphosphate
HBT	Human brain transcriptome
HBSS	Hank's balanced salt solution
HCC	Hypomyelination and congenital cataract
HD	Huntington's disease
HEK293	Human embryonic kidney 293
HEPES	4-(2-Hydroxyethyl)-1-piperazineethanesulfonic acid
HGK	Hepatocyte progenitor kinase-like
HIV	Human immunodeficiency virus
HMSN	Hereditary motor and sensory neuropathy
HRP	Horseradish peroxidase
HSAN	Hereditary sensory and autonomic neuropathy
HSP	Hereditary spastic paraplegia
IEM	Inherited erythromelalgia
IGF1	Insulin-like growth factor 1
ION	Institute of Neurology
IP	Immunoprecipitation
IPS (cell)	Induced pluripotent stem (cell)
KDa	Kilodalton
LB	Luria broth
LDS	Lithium dodecyl sulfate
LOD	Logarithm (base 10) of odds
LS	Leigh syndrome
MAF	Minor allele frequency
MAPS	Motor action potentials
MELAS	Mitochondrial encephalomyopathy, lactic acidosis, and stroke-like episodes
MERFF	Myoclonic epilepsy with ragged-red fibers
MES	2-(N-morpholino) ethanesulfonic acid

MILS	Maternally inherited Leigh syndrome
MLPA	Multiplex ligation-dependent probe amplification
MNCV	Motor nerve conduction velocity
MND	Motor neurone disease
MRC	Mitochondrial respiratory chain
MRC (Centre)	Medical Research Council (Centre)
MRI	Magnetic resonance imaging
mRNA	Messenger ribonucleic acid
MT	Mitochondrial transcript
mTOR	Mammalian target of rapamycin
NA	Not applicable
NAD ⁺	Nicotinamide adenine dinucleotide (oxidised)
NADH	Nicotinamide adenine dinucleotide (reduced)
NARP	Neurogenic muscle weakness, ataxia, and retinitis pigmentosa
NCBI	National centre for biotechnology information
NCS	Nerve conduction study
NCV	Nerve conduction velocity
NF	Neurofilament
NGS	Next-generation sequencing
NH2-terminus	NH2-terminus
NHNN	National hospital for neurology and neurosurgery
NMD	Nonsense-mediated decay
NP40 ⁺	Nonyl phenoxypolyethoxylethanol
NSC	Neuronal stem cell
OMIM	Online mendelian inheritance in man
OXPHOS	Oxidative phosphorylation
PBMC	Peripheral blood mononuclear cell
PBS	Phosphate buffered saline
PCR	Polymerase chain reaction
PD	Parkinson disease
PDC	Pyruvate dehydrogenase complex
PEI	Polyethulenimine
PEPD	Paroxysmal extreme pain disorder
PET	Positron emission tomography

PFA	Paraformaldehyde
PI	Phosphatidylinositol
PNS	Peripheral nervous system
POLG	Polymerase (DNA directed), gamma
PTC	Premature termination codons
qPCR	Quantitative polymerase chain reaction
RAN	Repeat-associated non-ATG
RC-DC	Reducing agent and detergent compatible
RNA	Ribonucleic acid
ROS	Reactive oxygen species
RPMI	Roswell park memorial institute
RT	Reverse transcription
RT-qPCR	Real-time reverse transcription polymerase chain reaction
RTT	Rett syndrome
SCA	Spinocerebellar ataxias
SDS	Sodium dodecyl sulphate
shRNA	Short hairpin ribonucleic acid
SIFT	Sorting intolerated from tolerated
siRNA	Small interfering RNA
SMA	Spinal muscular atrophy
SMA-LED	Spinal muscular atrophy with lower extremity predominance
SMARD1	Spinal muscular atrophy with respiratory distress type 1
SNP	Single nucleotide polymorphism
TBE	Tris/borate/EDTA
TCA	Tricarboxylic acid
TLC	Thin layer chromatography
TMRM	Tetramethylrhodamine methyl ester
TNF	Tumour necrosis factor
tRNA	Transfer RNAs
TTX	Tetrodotoxin
UCL	University College London
UCSC	University of California, Santa Cruz
UMN	Upper motor neurone
UTR	Untranslated region

UPR	Unfolded protein response
UV	Ultraviolet
WES	Whole exome sequencing
WGS	Whole genome sequencing
WT	Wild type
$\Delta\Psi_m$	Mitochondrial membrane potential

List of publications

Absence of HINT1 mutations in a UK and Spanish cohort of patients with inherited neuropathies. 2015 Horga A, *Cottenie E*, Tomaselli PJ, Rojas-García R, Salvado M, Villarreal-Pérez L, Gamez J, Márquez-Infante C, Houlden H, Reilly MM. *J Neurol*. 262(8):1984-6

Truncating and Missense Mutations in IGHMBP2 Cause Charcot-Marie Tooth Disease Type 2 2014 *Cottenie E*, Kochanski A, Jordanova A, Bansagi B, Zimon M, Horga A, Jaunmuktane Z, Saveri P, Rasic VM, Baets J, Bartsakouli M, Ploski R, Teterycz P, Nikolic M, Quinlivan R, Laura M, Sweeney MG, Taroni F, Lunn MP, Moroni I, Gonzalez M, Hanna MG, Bettencourt C, Chabrol E, Franke A, von Au K, Schilhabel M, Kabzińska D, Hausmanowa-Petrusewicz I, Brandner S, Lim SC, Song H, Choi B, Horvath R, Chung K, Zuchner S, Pareyson D, Harms M, Reilly MM, Houlden H. *Am. J Hum Genet*. 95(5):590-601

Mutations in γ adducin are associated with inherited cerebral palsy. 2013 Kruer MC, Jepperson T, Dutta S, Steiner RD, *Cottenie E*, Sanford L, Merkens M, Russman BS, Blasco PA, Fan G, Pollock J, Green S, Woltjer RL, Mooney C, Kretzschmar D, Paisán-Ruiz C, Houlden H. *Ann Neurol*. 74(6):805-14.

Mutations in BICD2 cause dominant congenital spinal muscular atrophy and hereditary spastic paraparesia. 2013 Oates EC, Rossor AM, Hafezparast M, Gonzalez M, Speziani F, MacArthur DG, Lek M, *Cottenie E*, Scoto M, Foley AR, Hurles M, Houlden H, Greensmith L, Auer-Grumbach M, Pieber TR, Strom TM, Schule R, Herrmann DN, Sowden JE, Acsadi G, Menezes MP, Clarke NF, Züchner S; UK10K, Muntoni F, North KN, Reilly MM. *Am J Hum Genet*. 92(6):965-73

Rapidly progressive asymmetrical weakness in Charcot-Marie-Tooth disease type 4J resembles chronic inflammatory demyelinating polyneuropathy. 2013 *Cottenie E*, Menezes MP, Rossor AM, Morrow JM, Yousry TA, Dick DJ, Anderson JR, Jaunmuktane Z, Brandner S, Blake JC, Houlden H, Reilly MM. *Neuromuscul Disord*. 23(5):399-403

Genetic dysfunction of MT-ATP6 causes axonal Charcot-Marie-Tooth disease.
2013 Pitceathly RD, Murphy SM, *Cottenie E*, Chalasani A, Sweeney MG, Woodward C, Mudanohwo EE, Hargreaves I, Heales S, Land J, Holton JL, Houlden H, Blake J, Champion M, Flinter F, Robb SA, Page R, Rose M, Palace J, Crowe C, Longman C, Lunn MP, Rahman S, Reilly MM, Hanna MG. *Neurology*. 79(11):1145-54.

All publications can be found on the additional disk included at the end of this thesis.

Chapter 1:

Introduction

1.1 Phenotypic spectrum of peripheral neuropathies

1.1.1 The peripheral nervous system

The main function of the peripheral nervous system (PNS) is to transfer information from the limbs to and from the central nervous system (CNS), which consists of brain and the spinal cord. The nerves responsible for this include the cranial nerves that link to the brainstem and 31 pairs of spinal nerves with their roots and rami that branch out between each of the vertebrae of the spine, connecting to the spinal cord. Considering this is a two-way system, a division is made between the afferent nerves that convey information from the sensory organs and limbs to the brainstem and the spinal cord – the sensory nerves – and the efferent nerves that transfer information from the brainstem and the spinal cord to the neuromuscular junctions at the muscles – the motor nerves. Working in conjunction with this, there is the autonomic nervous system that extends out of the CNS and regulates the visceral organs, which is also regarded as part of the PNS (Hubbard et al., 1974).

Characteristic of the peripheral nerves are the long axons, extending to the extremities of the body. The axons can be both unmyelinated and myelinated and are

organised in multiple bundles or fascicles, together with their supporting elements, in the peripheral nerves. Unmyelinated axons are solely enveloped by a single layer of Schwann cell cytoplasm whilst myelinated axons are surrounded by concentric layers of the Schwann cell plasma membrane which form the myelin sheath. This myelin sheath serves as an insulating layer resulting in a higher conduction velocity depending on the diameter of the sheath. In the context of peripheral neuropathies, abnormalities can be found in both the axon and the myelin sheath, causing different phenotypes (Hubbard, 1974).

1.1.2 Peripheral neuropathies

Whether abnormalities are found in the axon or the myelin sheath or in the cell body, the covering term for diseases affecting the PNS is peripheral neuropathies. Causes for peripheral neuropathies can be multiple, such as hereditary, infectious, inflammatory, exposure to toxins, metabolic or traumatic. These mainly result in an overall phenotype of muscle weakness and/or sensory loss and sometimes pain. Depending on the cause of disease, peripheral neuropathies can have an acute or chronic progression. When only one single nerve is affected, the term mononeuropathy is used and localised trauma or infection is suspected to be the most likely cause of disease. The myelin sheath or part of the axon can be damaged due to long-term pressure on a nerve due to swelling or injury. Multiple mononeuropathy or mononeuritis multiplex is characterised by two or more nerves being affected simultaneously or sequentially where the pattern is asymmetric. These can be caused by multiple medical conditions, such as diabetes mellitus, lupus erythematosus or HIV, and are sometimes difficult to distinguish from the polyneuropathies when their progress becomes more symmetrical (Dyck, 1927).

Polyneuropathies such as Charcot-Marie-Tooth (CMT) disease and Chronic Inflammatory Demyelinating Polyneuropathy (CIDP) are characterised by the involvement of multiple nerves and the effects can encompass the whole body. Peripheral neuropathies can be manifested as part of a more widespread neurological or multisystem disorder or they can be the sole part of disease (Dyck, 1927). For the purpose of this thesis, the main focus will be on the latter and in particular on the different forms of Charcot-Marie-Tooth disease (CMT).

1.1.3 Charcot-Marie-Tooth disease

CMT, also known as hereditary motor and sensory neuropathy (HMSN), functions as a term covering a group of clinically and genetically heterogeneous inherited neuropathies (Skre, 1974). Their prevalence in the general population can vary but has an overall estimation of 1 in 2500. Depending on the genetic defect, the severity and age of onset, the disease can be extensively divergent. Clinical symptoms are determined by the type of peripheral nerve that is affected (Harding et al., 1980). This results in a broad primary classification in the following three groups:

- CMT, both motor and sensory nerves are affected
- Hereditary Sensory and Autonomic Neuropathy (HSAN), predominantly sensory and autonomic features are affected
- Distal Hereditary Motor Neuropathy (dHMN), only motor neurons are affected.

A clear distinction cannot always be made between these different groups and especially patients presenting with dHMN on first examination can develop sensory symptoms later on in life and be classified as having CMT.

Due to the phenotypic variability, classification of CMT is not only based on clinical presentation, but also on neurophysiology and/or genetic testing. An important concept in this classification is motor nerve conduction velocity (MNCV). Uniformly slow MNCV less than 38 m/s in the arms is characteristic for demyelinating CMT1 while MNCV above this cut-off is typical of axonal CMT2. The intermediate form of CMT has intermediate electrophysiological features, i.e. MNCV from 25 to 45 m/s (Harding et al., 1980).

1.2 Genetic diversity and classification of CMT

Next to the phenotypic variability seen in patients with CMT, there is also a very heterogeneous genotypic presence that characterises this disease. Mutations in more than 80 genes have been found so far and more are being unravelled. The genetic background plays an important role in the classification of the disease and will be crucial to find common pathways to explain the characteristic features seen in most patients. In this section, the different subgroups of CMT will be discussed and the

most important causative genes that have been involved in each of these subgroups will be highlighted (Braathen, 2012).

1.2.1 Demyelinating CMT

For the demyelinating form of CMT, genes are often associated with Schwann cells and the myelin sheath surrounding the axon (Table 1.1), although their function can be very disparate, which causes a phenotypic heterogeneity (Nave et al., 2007; Berger et al., 2006). Inheritance can be dominant, recessive or X-linked and the autosomal dominant form of demyelinating CMT is often referred to as CMT1, accounting for at least two thirds of all patients with CMT.

PMP22 as the most common mutated gene in CMT1

The most prevalent mutation, which occurs in more than 70% of the European cases with autosomal dominant inheritance, is the duplication of a region containing the Peripheral myelin protein 22 (*PMP22*) gene on chromosome 17, and is classified as CMT1A (Raeymaekers et al., 1991). This duplication results in the presence of three copies of the *PMP22* gene instead of two and it is believed that the higher levels of *PMP22* result in CMT1A (Lupsik et al., 1992). These altered levels of the protein have been shown to influence the production of cholesterol, causing reduced myelin thickness and shortened internodes during the development of peripheral nerves. This may partially explain the slowed conduction velocity observed in CMT1A (Li et al., 2013).

Patients with autosomal dominant CMT1A present in the first two decades with a classical CMT phenotype, starting with foot deformities and difficulty walking. There is mainly distal involvement with wasting and weakness of the muscles and sensory loss. This occurs more prominent in the lower limbs than the upper limbs. In the absence of the duplication, CMT1 can also be caused by missense mutations in the *PMP22* gene, which results in a more severe phenotype in the patients and a classification of CMT1E (Reilly, 2007). In contrast to the duplication, mutations in *PMP22* result in protein aggregates in Schwann cells and are believed to exert a toxic gain of function (Li et al., 2013).

Mutations in MPZ cause CMT1B

Another important protein involved in autosomal dominant CMT is Myelin Protein Zero (*MPZ*), which causes CMT1B. In comparison to CMT1A, patients present with a more severe and earlier onset of the disease or a milder late-onset form. *MPZ* is the major component of myelin, comprising up to 50% of the myelin sheath (Siskind et al., 2013). Mutations in this gene have been shown to disrupt the myelination process and the compaction of myelin, subsequently failing to be incorporated in the plasma membrane or disrupting its structure due to a dominant negative effect (Berger et al., 2006).

Rare causes of AD CMT1

The remaining cases of autosomal dominant CMT1 can be explained by mutations in the Lipopolysaccharide-Induced TNF Factor (*LITAF*), Early Growth Response 2 (*EGR2*) or Neurofilament Light Chain (*NEFL*) genes, each on its own being a very rare cause of CMT1 with only few families reported (Houlden et al., 2006). The role of *EGR2* protein in myelination is crucial and mice harbouring mutations in this gene present with nerves devoid of myelin. *EGR2* serves as a transcription factor directly working on *MPZ*, which explains its involvement in demyelinating CMT.

Mutations in *LITAF* are known to affect ubiquitination, sorting and/or degrading of the myelin, but the exact pathway that causes the CMT1C phenotype is not known yet (Berger et al., 2006). This is in contrast with the NF-L protein, which was originally described in the context of axonal CMT2. It has an important role within the cytoskeleton of axons and it has been speculated that it exerts an effect on the myelin sheath via the axon-myelin interactions (Houlden et al., 2006).

Autosomal Recessive CMT4

The occurrence of autosomal recessive CMT1, also known as CMT4, is relatively rare in the general population, although this varies depending on the community (Schenone et al., 2011). The autosomal recessive neuropathies tend to have an earlier onset and a more severe progression than the autosomal dominant varieties. Except in the case of consanguinity, they appear only in sibs or as simplex cases (Espinosa et al., 2012). So far, fifteen genes have been described that cause an autosomal recessive inheritance pattern and several different molecular genetic subtypes of demyelinating AR CMT have been identified. These molecular genetic subtypes all

show a demyelinating phenotype but often have distinct clinical and nerve biopsy features (Reilly et al., 2011). Some of the genes implicated in the autosomal dominant form of CMT, such as *PMP22*, *EGR2* or *MPZ*, are predominantly found in patients with CMT1, but are known to also cause the recessive variant in rare cases. Others are only found to cause the recessive form but have a distinctive link to demyelinating features. One example of the latter is Periaxin (*PRX*), part of the complex responsible for linking Schwann cells to the basal lamina.

Whilst all the above-mentioned genes appear to be involved in myelin pathways, a considerable number of genes play a role in the mitochondrial compartment. One of these has been shown to cause autosomal recessive CMT1. Ganglioside-induced Differentiation Associated Protein 1 (*GDAP1*) is a tail-anchored protein in the outer mitochondrial membrane, implicated in mitochondrial fission. Mutations in this protein cause a range of early onset demyelinating, intermediate, and/or axonal forms of CMT (CMT4A, CMTRIA, CMT2K). Since mutations in the Mitofusin 2 (*MFN2*) gene - involved in mitochondrial fusion - are the main cause for axonal CMT, it is surprising that mutations in this mitochondrial fission protein mainly lead to a demyelinating neuropathy. It has been established that mitochondrial dynamics are a very important feature in the maintenance of the nerves and have a significant role in the pathogenicity of axonal neuropathies. It remains a mystery so far how these mutations in *GDAP1* correlate with a primary myelin defect in the peripheral nerves (Berger et al., 2006; Tazir et al., 2013).

Apart from these two examples, there are many more genes responsible for autosomal recessive CMT (Table 1.1), for which I will not go into further detail. However, as mentioned before, the majority of these have specific clinical features that can be of guidance in finding a molecular diagnosis. For example, mutations in the SH3 domain and tetratricopeptides repeats 2 gene (*SH3TC2*) are often found in patients with severe scoliosis and recent reports have suggested mutations in this gene to be the commonest form of autosomal recessive CMT (Houlden et al., 2009).

CMT1	Gene/Locus	Function
Autosomal dominant		
CMT1		
CMT 1A	Dup 17p (<i>PMP22</i>)	Myelin structure and formation
CMT 1B	<i>MPZ</i>	Myelin structure
CMT 1C	<i>LITAF</i>	Vesicular transport
CMT 1D	<i>EGR2</i>	Transcription factor, including myelin proteins
CMT 1E	<i>PMP22</i> (Point mutations)	Myelin structure and formation
CMT 1F	<i>NEFL</i>	Cytoskeleton component
Autosomal recessive		
CMT1		
CMT4A	<i>GDAP1</i>	Mitochondrial dynamics
CMT4B1	<i>MTMR2</i>	Vesicular transport, Active phosphatase of PI(3,5)P2 and PI(3)P
CMT4B2	<i>MTMR13</i>	Vesicular transport, Inactive phosphatase of PI(3,5)P2 and PI(3)P
CMT4B3	<i>MTMR5</i>	Vesicular transport
CMT4C	<i>SH3TC2</i>	Endocytic recycling
CMT4D	<i>NDRG1</i>	Signalling protein
CMT4E	<i>EGR2</i>	Transcription factor, including myelin proteins
CMT4F	<i>PRX</i>	Myelin structure
CMT4G (HMSN Russe)	<i>HK1</i>	Glucose metabolism
CMT4H	<i>FGD4</i>	Cytoskeletal remodelling
CMT4J	<i>FIG4</i>	PI (3,5)P2 5-phosphatase / endocytotic recycling
AR CMT1	<i>PMP22</i> (point mutations)	Myelin structure and formation
Other	<i>SURF1</i>	Assembly factor of OXPHOS complex
CCFDN	<i>CTDP1</i>	Phosphatase in transcription

Table 1-1 Classification of demyelinating CMT according to genotype. AR, autosomal recessive; Dup, duplication; *PMP-22*, peripheral myelin protein 22; *MPZ*, myelin protein zero; *LITAF*, lipopolysaccharide-induced tumour necrosis factor; *EGR2*, early growth response 2; *NEFL*, neurofilament, light polypeptide 68 kDa; *GDAP1*, ganglioside-induced differentiation-associated protein 1; *MTMR2*, myotubularin-related protein 2; *MTMR13*, myotubularin-related protein 13; *MTMR13*, myotubularin-related protein 5; *SH3TC2*, SH3 domain and tetratricopeptides repeats 2; *NDRG1*, N-myc downstream-regulated gene 1; *PRX*, periaxin; *HK*, Hexokinase 1; *FGD4*, FYVE, RhoGEF and PH domain containing 4; *FIG4*, Phosphoinositide phosphatase 4; *SURF1*: Surfeit locus

protein 1; *CCFDN*, Congenital Cataracts, Facial Dysmorphism & Neuropathy Syndrome; *CTDPI*, carboxy-terminal domain RNA polymerase II polypeptide A phosphatase subunit 1.

1.2.2 Axonal CMT

Autosomal dominant CMT2

Several genes are known to cause AD CMT2, but only a quarter of the patients receive a molecular diagnosis. There is no main gene responsible for the majority of cases in the way that *PMP22* is the main gene explaining the AD CMT1 phenotype. From a genetic point of view, point mutations in the *MFN2* gene account for 20% of patients and are the most common cause of CMT2 (Zuchner et al., 2004). Eleven additional genes have been identified to date causing the dominant variant of this disease, most of them ubiquitously expressed (Table 1.2). The majority of these genes were not specifically associated with the function of the axon before mutations were discovered. By discovering these mutations, important pathways were revealed that are necessary for maintaining the axonal integrity; for example the mitochondrial fusion and fission process, in which not only *MFN2* but also *GDAPI* participates (Patzkó et al., 2011), alterations of the cytoskeleton, mitochondrial dynamics and endocytosis, have all been found to be affected by mutations that cause CMT2 (Niemann et al, 2006).

Classic CMT2 phenotype

A distinction between three different subtypes can be made according to the clinical presentation of the patients. Most patients present with the classical CMT phenotype, and differentiation between AD CMT2 and CMT1 is difficult before neurophysiology is performed. The presence of reduced motor action potentials (MAPS) with normal or near normal NCVs will confirm the diagnosis of CMT2 (Reilly, 2007). The majority of these patients will be diagnosed with mutations in the *MFN2* gene, which frequently results in an early-onset, more severe phenotype. Interestingly, up to 20% of mutations in *MFN2* are de novo, making it more difficult to decide on the pathogenicity of a new variant. *MFN2* is a GTPase located in the outer mitochondrial membrane and serves as a regulator for mitochondrial fusion and tethering to the endoplasmic reticulum. Together with *MFN1*, homo-oligomeric and hetero-oligomeric complexes are formed between opposing mitochondria to facilitate fusion of the outer membrane (Milone et al., 2012). Disruptions in this process lead to increased mitochondrial fragmentation, where part of the fragmented

mitochondria lose their membrane potential and show impaired mitochondrial transport (Chen et al., 2003). In the context of disease, it has been suggested that this altered physiology and/or lack of healthy mitochondria at the distal parts of the axons could lead to the degeneration of the axons (Niemann et al., 2009).

Apart from *MFN2* mutations, the classical phenotype can also be caused by mutations in three genes known to cause CMT1: *NEFL*, *MPZ* or *GDAP1* - although this accounts for only a very small percentage of patients (Reilly et al., 2011).

After the myelin and mitochondrial groups of genes, recent discoveries found mutations in a range of tRNA synthetase genes, causing CMT. One of these, the Alanyl tRNA synthetase (*AARS*) gene, can also be responsible for the typical CMT2 phenotype. However, an accurate estimate of the prevalence of these mutations has not been established yet (Latour et al., 2010; McLaughlin et al., 2012). Other tRNA synthetase genes have been found in different CMT phenotypes and will be discussed in section 1.3.6. Even though it was first only found to be involved in the recessive form of axonal neuropathies, mutations in the leucine rich repeat and sterile alpha motif containing 1 (*LRSAM1*) gene were reported in several families with a dominant inheritance, suggesting the phenotypes of these mutations might expand further than causing recessive CMT2 (Weterman et al., 2012; Nicolaou et al., 2013). Lastly, a mutation in the dehydrogenase E1 and transketolase domain-containing 1 (*DHTKD1*) gene was found in a large Chinese family with five affected generations. This gene has been implied to have a role in the degradation pathways of several amino acids, but no further investigations regarding to disease pathways have been made (Xu et al., 2012).

CMT2 with prominent sensory features

Patients with CMT2 can also present with more prominent sensory features. Two main genes have been described causing this phenotype: Ras-related protein 7 (*RAB7A*) and Serine palmitoyltransferase, long chain base subunit 1 (*SPTLC1*). Characteristically, patients suffer from lack of sensation and complications of sensory loss leading to ulcerations, osteomyelitis, and even amputations. This is very similar to patients with HSAN and it can be difficult to distinguish between the two forms, especially since patients with mutations in *SPTLC1* are frequently classified

as having HSAN. These patients often suffer from neuropathic pain, which is the main determining feature that differentiates them from patients with mutations in *RAB7A* (Houlden et al., 2006).

CMT2 with major motor involvement

The last phenotype associated with AD CMT2 has a large overlap with dHMN, since patients present with major motor involvement due to mutations in six different genes: Glycyl tRNA synthetase (*GARS*), heat shock protein beta-1 (*HSPB1*), heat shock protein beta-8 (*HSPB8*), Transient receptor potential cation channel subfamily V member 4 (*TRPV4*), dynein, cytoplasmic 1, heavy chain 1 (*DYNC1H1*) or *ATPase 6*. Whilst mutations in the heat shock protein genes are a very rare cause of AD CMT2 and are more frequently known to cause a purely motor phenotype, mutations in *TRPV4* not only cause CMT2C, but can lead to a spectrum of inherited neuropathies with varying clinical features. However, caution has to be applied before diagnosing these patients since asymptomatic carriers and polymorphisms in the gene have been reported (Zimon et al., 2010; Fawcett et al., 2012).

It was not surprising when mutations in dynein were reported to cause CMT, considering it is the primary motor protein responsible for retrograde axonal transport in neurons. Mouse model studies have shown that mutations affect the processivity of the protein and the ability to move along the microtubule (Ori-McKenney et al., 2010; Weedon et al., 2011).

As mentioned before, a small subset of genes mutated in CMT encode mitochondrial proteins, the most common of which is *MFN2*. All of these are encoded by the nuclear DNA, but our research recently showed that mutations in the mitochondrially encoded *ATPase6* gene could lead to axonal neuropathy with predominantly motor involvement. More detail can be found in Chapter 3.

Mutations in *GARS* cause CMT2D, which can be distinguished by involvement of the small hand muscles (Reilly et al., 2011). *GARS* was the first aminoacyl tRNA synthetase identified in 2003 by Antonellis et al. to be causative for a human genetic disease and after its discovery, five more aminoacyl tRNA synthetase genes have been implicated in CMT disease, one of which is the *AARS* gene, mentioned before.

CMT2	Gene/locus	Function
Autosomal dominant		
CMT2		
CMT 2A	<i>KIF1Bβ</i>	Axonal transport
CMT 2A	<i>MFN 2</i>	Mitochondrial dynamics
CMT 2B	<i>RAB7</i>	GTPase in vesicular transport
CMT 2C	<i>TRPV4</i>	Calcium homeostasis
CMT 2D	<i>GARS</i>	Aminoacyl synthetase
CMT 2E	<i>NEFL</i>	Cytoskeleton component
CMT 2F	<i>HSPB1</i>	Heat shock protein/cytoskeleton remodelling
CMT 2G	12q12-q13.3	
CMT 2 I/J	<i>MPZ</i>	Myelin protein
CMT 2K	<i>GDAP1</i>	Mitochondrial dynamics
CMT 2L	<i>HSPB8</i>	Heat shock protein/cytoskeleton remodelling
CMT 2M	<i>DNM2</i>	Instability of microtubule and endocytosis
CMT 2N	<i>AARS</i>	Aminoacyl synthetase
CMT 2O	<i>DYNC1H1</i>	Axonal transport
CMT 2P	<i>LRSAM1</i>	E3-Ubiquitin Protein Ligase
CMT 2Q	<i>DHTKD1</i>	Degradation of AA
	<i>MT-ATPase6</i>	ATP production
Autosomal recessive CMT 2		
CMT 2B1	<i>LMNA</i>	Intermediate filaments protein
CMT 2B2	<i>MED25</i>	Transcription regulation
CMT 2H	<i>GDAP1</i>	Mitochondrial dynamics
CMT 2P	<i>LRSAM1</i>	E3-Ubiquitin Protein Ligase
CMT 2R	<i>TRIM2</i>	E3-Ubiquitin Protein Ligase
ARAN-NM	<i>HINT1</i>	Purine phosphoramidase

Table 1-2 Classification of axonal CMT according to genotype. *KIF1Bβ*: kinesin family member 1B; *MFN 2*: Mitofusin 2; *RAB7*: Ras-related protein 7; *TRPV4*: Transient receptor potential cation channel subfamily V member 4; *GARS*: Glycyl tRNA synthetase; *NEFL*: neurofilament, light polypeptide 68 kDa; *HSPB1*: Heat Shock Protein 27 kDa; *MPZ*: myelin protein zero; *GDAP1*: ganglioside-induced differentiation-associated protein 1; *HSPB8*: Heat shock protein, 22 kDa; *DNM2*: Dynamin-2; *AARS*: Alanyl tRNA synthetase; *DYNC1H1*: dynein, cytoplasmic 1, heavy chain 1;

LRSAM1: leucine rich repeat and sterile alpha motif containing 1; *DHTKD1*: dehydrogenase E1 and transketolase domain-containing 1; *LMNA*: Lamin A/C; *MED25*: mediator complex subunit 25; *TRIM2*: tripartite motif containing 2; *HINT1*: histidine triad nucleotide–binding protein 1

It has been suggested that mutations in this gene lead to an impaired GARS enzyme activity and a GARS localisation defect that is predominantly present in the longest axons due to a higher need in localised protein synthesis (Antonellis et al., 2006).

Autosomal recessive CMT2

Axonal autosomal recessive neuropathies are very rare and most cases found to date have been restricted to specific geographical areas or families. In a recent study, mutations in the histidine triad nucleotide–binding protein 1 (*HINT1*) gene have been found in 11% of AR CMT patients with neuromyotonia, comprising a new disease identity. In patients with AR CMT2 and neuromyotonia, this percentage went up to 76%. Most of these families were eastern European and presented with the same homozygous mutation, suggesting a founder effect (Zimon et al., 2012).

In North Africa, multiple families were found with mutations in Lamin A/C (*LMNA*), causing CMT2B1. *LMNA* mutations can cause a variety of phenotypes, ranging from peripheral neuropathies and cardiac disorders to lipodystrophy and premature aging disorders. More than ten different phenotypes have been shown to be caused by mutations in this gene and many of them show overlapping clinical features (Tazir et al., 2013).

Only one large consanguineous Costa Rican family was found with a mutation in the mediator complex subunit 25 (*MED25*) gene (Leal et al., 2009), classifying this as a very rare cause of AR CMT2. In very few cases, *GDAP1*, normally causing AR CMT1, can also be found to cause AR CMT2. One paper by Guernsey et al. investigating a large Canadian family suggested a missense mutation of a splice site acceptor in the leucine rich repeat and sterile alpha motif containing 1 (*LRSAM1*) gene as cause of the disease. This encodes for an E3-Ubiquitin protein ligase important for vesicle fusion. More recently, this gene has also been found to cause the autosomal dominant form, as mentioned above.

In 2013, a patient was reported with a mutation in the tripartite motif containing 2 (*TRIM2*) gene, which also encodes for an E3-Ubiquitin ligase (Ylikalio et al., 2013). Loss of either of these proteins in mouse models leads to neurodegeneration, indicating an important role for these proteins. In rare cases, genes known to cause the dominant form of the disease are found to be the responsible gene in families with a recessive inheritance, such as *NEFL* (Abe et al., 2009), *HSPB1* (Houlden et al., 2008) and *MFN2* (Polke et al., 2011).

1.2.3 Intermediate CMT

So far, five genes and one locus are known to specifically cause dominant intermediate CMT, whereas the recessive form can be caused by three different genes (Table 1.3). Intermediate CMT is characterised by patients having NCS values in the intermediate range (25-45 m/s). In rare cases, genes that normally cause a demyelinating or axonal form of disease can mimic intermediate conditions and be classified as intermediate CMT. Patients with mutations in *MPZ* normally have NCV< 38m/s, however more recently several missense mutations have been shown to result in NCV of the motor median nerve varying from <38 m/s to normal (De jonghe et al., 1999; Banchs et al., 2010).

Similar results have been shown for mutations in *GDAP1*, where NCVs were between 25 and 35 m/s and peripheral nerve pathology showed axonal as well as demyelinating changes (Senderek et al., 2003). Apart from mutations in genes implicated in the myelin pathway and mitochondrial dynamics, dysfunction of cytoskeleton can also lead to intermediate forms of CMT. Dynamin-2 (*DNM2*) has a dual role in the regulation of the dynamic instability of microtubules and in endocytosis. Different mutations can have their effect on either of these pathways and result in intermediate CMT (Tanabe et al., 2012). So do mutations in inverted formin-2 (*INF2*), a member of the diaphanous-related formin family involved in remodelling the microtubule cytoskeleton and actin (Rodriguez et al., 2013). Whilst a connection with CMT is apparent in these patients, the pathologic mechanisms that cause intermediate CMT in patients with mutations in the other genes such as *GNB4* and *PLEKHG5* are not known yet (Azzedine et al., 2013; Soong et al., 2013).

Intermediate CMT	Gene/locus	Function
Dominant intermediate CMT (CMTDI)		
CMTDIA		
	<i>10q24.1-q25.1.</i>	
	<i>DNM2</i>	Instability of microtubule and endocytosis
CMTDIB		
	<i>YARS</i>	Aminoacyl synthetase
CMTDIC		
	<i>MPZ</i>	Myelin structure
CMTDID		
	<i>INF2</i>	Cytoskeletal remodelling
CMTDIE		
	<i>GNB4</i>	Signal transduction
Recessive intermediate CMT (CMTRI)		
CMTRIA	<i>GDAP1</i>	Mitochondrial dynamics
CMTRIB	<i>KARS</i>	Aminoacyl synthetase
CMTRIC	<i>PLEKHG5</i>	Signal transduction

Table 1-3 Classification of intermediate CMT according to genotype. *DNM2*: Dynamin-2; *YARS*: tyrosyl tRNA synthetase; *MPZ*, myelin protein zero; *INF2*: inverted formin, FH2 and WH2 domain containing; *GNB4*: guanine nucleotide binding protein (G protein), beta polypeptide 4; *GDAP1*, ganglioside-induced differentiation-associated protein 1; *KARS*: lysyl-tRNA synthetase; *PLEKHG5*: pleckstrin homology domain containing, family G.

Three years after the discovery of the *GARS* gene, mutations in the tyrosyl tRNA synthetase (*YARS*) gene were found, making it the second aminoacyl synthetase responsible for causing CMT. A dominant-negative effect on the normal function and distribution of YARS in the neuronal endings was observed when the protein was mutated. Even though the exact pathway leading to CMT is still a mystery, the specific subcellular localisation of YARS to the nerve endings – which was not observed in other tRNA synthetases studied – indicates an important function at the neuronal endings (Jordanova et al., 2006). Four years later, another tRNA synthetase gene was discovered to be involved in intermediate CMT - lysyl-tRNA synthetase (*KARS*). In these cases, compound heterozygous mutations resulted in a loss-of-function effect on the protein (McLaughlin et al., 2010). The presence of a null allele in combination with a hypomorphic allele significantly reduces the charging activity

to a level where barely any functionality remains, effects that have also been seen in several *GARS* mutations (Antonellis et al., 2008).

1.2.4 Hereditary Sensory and Autonomic Neuropathy

Patients presenting with mainly sensory involvement and autonomic features are classified as having HSAN. Sensory loss, insensitivity to pain, a variable degree of muscle weakness and wasting, as well as autonomic features have been observed. This can occur in both dominant and recessive form and can be subdivided into six different groups according to the age of onset, inheritance and characteristic clinical features (Rotthier et al., 2010; Table 1.4).

Autosomal Dominant HSAN

All dominant forms are classified under the HSAN1 subtype and can be caused by mutations in five known genes and one locus for which the gene has not been found yet. As mentioned above, there is a significant overlap with some of the AD axonal phenotypes with predominantly sensory features and mutations in *SPTLC1* and *RAB7A* are known to cause phenotypes with varying degree of motor involvement. These two phenotypes are very similar, apart from an overall sensory loss in the somatosensory system in patients with *RAB7A*. Next to mutations in subunit 1 of the serine palmitoyltransferase, mutations in subunit 2 can cause the same phenotype, which are indistinguishable. The presence of lancinating pain can differentiate these patients from others (Rotthier et al., 2010).

Two other genes are known to cause autosomal dominant HSAN: Atlastin-1 (*ATL1*), which has a role in ER formation, and DNA methyltransferase 1 (*DNMT1*), important in DNA methylation and gene regulation. Most of these genes act in the cell body, but a common pathway for these genes resulting in HSAN has not been established (Rotthier et al., 2012). Some families present with sensory loss, cough and gastroesophageal reflux, also classified as HSAN-1B, but no gene responsible for this phenotype has been found so far and linkage has narrowed it down to chromosomal location 3p22–p24 (Kok et al., 2003).

Autosomal Recessive HSAN

While all phenotypes of autosomal dominant HSAN are classified under the HSAN1 subtype, there are several different sub classifications for autosomal recessive

HSAN. HSAN II is characterised by distal numbness and progressive loss of pain, temperature and touch sensation and can be caused by mutations in three different genes: WNK lysine deficient protein kinase 1 (*WNK1*), involved in sodium, chloride and potassium homeostasis; Family with sequence similarity 134, Member B (*FAM134B*), a component of the cis-golgi matrix, and kinesin family member 1A (*KIF1A*), which has a role in anterograde axonal transport. So far, a link between these different genes has not been documented, although an interaction has been found between *KIF1A* and the domain of *WNK1* that is primarily mutated (Riviere et al., 2011).

HSAN III is also known as Riley-Day syndrome or Familial Dysautonomia and is caused by mutations in the inhibitor of kappa light polypeptide gene enhancer in B-cells, kinase complex-associated protein (*IKBKAP*). This gene encodes for the I κ B kinase complex-associated protein (ELP1), an important subunit of the RNA polymerase II complex, necessary for transcriptional elongation. Disruptions in this gene result in prominent, widespread autonomic disturbances, as well as small-fibre sensory dysfunction and are almost solely seen in patients with eastern European Jewish ethnicity. Only three mutations have been found so far, of which one accounts for more than 99% of the patients, suggesting a founder effect.

Patients with a more severe form of this disease, also involving prominent autonomic features, are classified as having HSAN VI, linking to mutations in Dystonin (*DST*). The neuronal isoform of *DST* has been shown to link actin filaments to the microtubule to maintain the neuronal cytoskeleton organisation. Interestingly, *DST* is upregulated in fibroblasts of patients with mutations in *IKBKAP*, suggesting a compensatory mechanism. The RNA polymerase II complex has been shown to interact with the microtubuli and microtubule disorganisation was observed in fibroblasts, explaining the possibility of a compensatory mechanism by *DST* (Edvardson et al., 2012).

In some cases, HSAN is accompanied by insensitivity to temperature and pain and generalised anhidrosis, known as congenital insensitivity to pain with anhidrosis (CIPA) or HSAN IV. Several families of different ethnicities and more than 40 different mutations have been found with mutations in the neurotrophic tyrosine

kinase, receptor, type 1 (*NTKRI*) gene. This encodes for the high-affinity nerve growth factor receptor Trk-A protein, a kinase involved in neurotrophin signalling supporting neurite outgrowth and survival of neurons.

HSAN	Gene/Locus	Function
Autosomal Dominant HSAN		
HSAN-I	<i>SPTLC1</i>	Sphingolipid biosynthesis pathway
HSAN-I	<i>SPTLC2</i>	Sphingolipid biosynthesis pathway
HSAN-I	<i>ATL1</i>	GTPase in the Endoplasmatic Reticulum
CMT2B/HSAN-I	<i>RAB7A</i>	GTPase in vesicular transport
HSAN-I with dementia and hearing loss	<i>DNMT1</i>	DNA methylation, gene regulation
HSAN-IB	3p24–p22	
Autosomal recessive HSAN		
HSAN-II	<i>WNK1</i>	Regulator of ion channels
HSAN-II	<i>FAM134B</i>	Structural protein of the <i>cis</i> golgi-body
HSAN-II	<i>KIF1A</i>	Axonal transport
HSAN-III	<i>IKBKAP</i>	Scaffold protein for transcriptional elongation
HSAN-IV	<i>NTRK1</i>	Neurotrophin signalling
HSAN-V	<i>NGFB</i>	Neurotrophin signalling
HSAN-VI	<i>DST</i>	Adhesion junction protein
HSAN with spastic paraplegia	<i>CCT5</i>	Molecular chaperone

Table 1-4 Classification of Hereditary sensory and autonomic neuropathy according to genotype.
SPTLC1: Serine palmitoyltransferase, long chain base subunit 1; *SPTLC2*: Serine palmitoyltransferase, long chain base subunit 2; *ATL1*: Atlastin-1; *RAB7A*: Ras-related protein 7; *DNMT1*: DNA methyltransferase 1; *WNK1*: WNK lysine deficient protein kinase 1; *FAM134B*: Family with sequence similarity 134, Member B; *KIF1A*: kinesin family member 1A; *IKBKAP*: inhibitor of kappa light polypeptide gene enhancer in B-cells, kinase complex-associated protein; *NTRK1*: neurotrophic tyrosine kinase, receptor, type 1; *NGFB*: nerve growth factor, beta-subunit; *DST*: Dystonin; *CCT5*: chaperonin containing TCP1-complex subunit 5.

A very similar phenotype is seen in patients with HSAN V, although patients suffer from hypohidrosis instead of anhidrosis. This phenotype is also caused by mutations in a gene important in neurotrophin signalling, called nerve growth factor (*NGF*),

encoding for the β -NGF protein. β -NGF serves downstream as a ligand for Trk-A, which will autophosphorylate to activate downstream signalling pathways (Einarsdottiret al., 2004; Carvalho et al., 2011).

The last phenotype associated with recessive HSAN is accompanied with spastic paraplegia and can be explained by mutations in the chaperonin containing TCP1-complex subunit 5 (*CCT5*) gene. This protein is important for the protein folding and assembly of a range of proteins, and it has been suggested that disruptions in this process lead to protein misfolding and ER-stress, causing the phenotype (Bouhouche et al., 2006). Previous reports have also shown that this particular subunit is important for the binding of the CCT5 protein to actin and tubulin (Llorca et al., 2000). Patients with this phenotype can also be classified as having Hereditary Spastic Paraplegia (HSP), when the lower extremity spastic weakness is the primary clinical symptom (Fink, 2013).

1.2.5 Distal Hereditary Motor Neuropathy

In contrast to patients with HSAN, a significant group of patients present with predominantly motor involvement. Distal hereditary motor neuropathy (dHMN) is characterised by the selective loss of motor neurons and/or their long axons in the peripheral nervous system. Apart from the absence of sensory abnormalities, distal HMN closely resembles axonal CMT2 and clinical overlap is ever-present, often dependent on the stage of disease and the age of the patient. Recurrently, mutations in the same gene may cause either dHMN or CMT2. In some cases, minor sensory involvement is present, comparable to the symptoms seen in other motor neuron diseases such as Amyotrophic Lateral Sclerosis (ALS), Spinal Muscular Atrophy (SMA) or Kennedy's disease. dHMN is often referred to as distal Spinal Muscular Atrophy (dSMA) or Spinal CMT, since various hypotheses have suggested that the primary pathological process is located in the cell body of the anterior horn.

Similarly to the previous subgroups, dHMN is also classified according to inheritance, age of onset and phenotype, even though multiple genes can cause the same subtype of dHMN (Table 1.5). Seven subtypes of dHMN have been described, which will be discussed below depending on their mode of inheritance (Rossor et al., 2012).

Autosomal dominant dHMN

Of the seven subtypes of dHMN, four have an autosomal dominant mode of inheritance: Types I, II, V and VII. Patients presenting with typical dHMN phenotype are classified as type I or II, depending on whether they have a childhood or adult onset respectively. Clinical features are very similar to CMT2, apart from the absence of sensory abnormalities.

dHMN I and II

The childhood onset (dHMN I) can be caused by mutations in either *HSPB1*, *HSPB8*, *GARS* or dynein, cytoplasmic 1, heavy chain 1 (*DYNC1H1*). As seen before, all these genes have already been implemented in respectively CMT 2F, CMT 2L, CMT 2D or CMT 2O. Depending on the development of sensory signs, these will be classified amongst dHMN or CMT2 and a significant amount of overlap can occur.

Interestingly, mutations in the *HSPB1* and *HSPB8* genes can also cause the adult onset subtype of dHMN II. Both of these genes encode for small heat-shock proteins and are part of a group of stress-induced chaperone proteins that are ubiquitously expressed. When mutated, protein aggregates are formed and it has been suggested that mutations also influence the chaperone function (Carra et al., 2010). By using a candidate gene approach screening, mutations in the heat-shock protein 27-like protein (*HSPB3*) were also found to be responsible for the adult onset subtype (Kolb et al., 2010).

Apart from faulty chaperones, dHMN II can also be caused by mutations in the Berardinelli–Seip Congenital Lipodystrophy type 2 gene (*BSCL2*), known to cause Congenital Generalised Lipodystrophy type 2 in a recessive manner. *BSCL2* encodes for Seipin, a glyco-protein present in the Endoplasmatic reticulum (ER). Previous reports have suggested that malfunction of Seipin leads to incorrect folding and activation of the Unfolded Protein response (UPR) in the ER, a pathway implied in many neurodegenerative diseases (Ito et al., 2008; Liu et al., 2003).

Lastly, a recent paper by Sumner et al. in 2013 reported mutations in F-box protein 38 (*FBXO38*) to cause an adult onset of dHMN.

dHMN V

In the event of more predominant upper limb symptoms, classification will lean towards dHMN V. This can be caused by both the *GARS* and *BSCL2* genes. The latter protein has been implied in a variety of diseases, such as classical Silver Syndrome, severe spastic paraplegia with amyotrophy predominantly affecting the lower limbs, dHMN II as mentioned before and dHMN V (Irobi et al., 2006). Inter- and intrafamilial variability has been shown in 14 unrelated Austrian families, which raises the question of modifying factors (Auer-Grumbach et al., 2005). In both cases, families with a recessive inheritance have been found which will still be classified as dHMN V. More recently, a new splice site mutation was found in receptor accessory protein 1 (*REEP1*) in a family with dHMN and dHMN V. Missense mutations in this gene normally lead to HSP, due to a loss-of-function mechanism. Whilst the majority of mutations found in HSP result in nonsense-mediated decay, the suspected skipping of exon 5 would not result in a frameshift, which could account for the difference in phenotype (Beetz et al., 2012).

dHMN VII

The last autosomal dominant dHMN subtype is characterised by an adult onset of upper limb before lower limb involvement and the main distinguishing feature is the presence of vocal cord paralysis. Four loci have been found to be linked to the dHMN VII phenotype, three of which have been narrowed down to a specific gene. The first gene encodes for the P150Glued subunit of Dynactin (*DCTN1*), a microtubule motor protein important in the retrograde axonal transport. As seen before, compromised axonal transport is an important molecular pathway leading to disease and previous reports have shown that mutations in *DCTN1* interfere with the binding of dynactin to the microtubule (Puls et al., 2003).

The second locus overlapped with one of the genes already known for CMT2; *TRPV4*. Whilst mutations in dynactin lead to issues with axonal transport, *TRPV4* encodes for a non-selective cation channel. In normal conditions it exhibits a moderate permeability to calcium, which will be affected when mutations are present. There have been contradicting studies about the effects of mutations on the calcium import, but recent studies in neuronal derived cell lines have shown a toxic

gain of function, with a higher level of calcium import in comparison to basal levels (Fecto et al., 2011).

The most recent gene responsible for the dHMN VII phenotype is the solute carrier family 5, member 7 (*SLC5A7*). This is a choline transporter in the cholinergic neurons, dependent on sodium and chloride. A dominant-negative mutation was found, resulting in reduced protein levels (Barwick et al., 2012).

SMA-LED

A separate entity of patients shows autosomal dominant inheritance with muscle weakness predominantly affecting the proximal lower extremities and is classified as SMA-LED. This can be caused by two different genes: *DYNC1H1* and bicaudal D homolog 2 (*BICD2*). Dynein has already been implicated in CMT disease and is known to have an important role in axonal transport. The *BICD2* protein was discovered by three groups simultaneously (Oates et al., 2013; Peeters et al., 2013; Neveling et al., 2013) and is known to bind to the dynactin-dynein complex to transport cargo such as mRNA, Golgi, and secretory vesicles. Mutations in *BICD2* affect the binding to this complex and the small GTPase RAB6 and will be more extensively discussed in Chapter 5.

Autosomal recessive dHMN

The remaining three subtypes of dHMN have a recessive pattern of inheritance and are classified as subtypes III, IV and VI. For both dHMN III and IV, the causative gene has not been found yet. Classification of these two subtypes depends on the severity of disease and the presence of diaphragmatic palsy (Harding et al., 1980; Pearn et al., 1979). Both have been linked to the same locus on chromosome 11q13, which encompasses the immunoglobulin μ binding protein 2 (*IGHMBP2*), responsible for dHMN VI. However, genetic studies rule out this gene as the causative factor for disease and further studies in multiple families managed to narrow down the linkage area to a region of 1Mb, telomeric to the *IGHMBP2* gene. Ten known genes are located in this area, but none of these were shown to segregate with disease (Viollet et al., 2004).

dHMN	Gene/Loci	Function
Autosomal Dominant		
dHMN		
dHMN I	<i>HSPB1</i>	Heat shock protein
	<i>HSPB8</i>	Heat shock protein
	<i>GARS</i>	Aminoacyl synthetase
	<i>DYNC1H1</i>	Axonal transport
dHMN II	<i>HSPB1</i>	Heat shock protein
	<i>HSPB8</i>	Heat shock protein
	<i>HSPB3</i>	Heat shock protein
	<i>BSCL2</i>	Glyco protein in the Endoplasmatic Reticulum
	<i>FBXO38</i>	Neuronal axon outgrowth and repair
dHMN V	<i>GARS</i>	Aminoacyl synthetase
	<i>BSCL2</i>	Glyco protein in the Endoplasmatic Reticulum
	<i>REEP1</i>	Olfactory receptor binding
dHMN VII	<i>DCTN1</i>	Axonal transport
	<i>TRPV4</i>	Calcium homeostasis
	<i>SLC5A7</i>	Choline transporter
	<i>2q14</i>	
SMA-LED	<i>DYNC1H1</i>	Axonal transport
	<i>BICD2</i>	Motor adaptor protein
Autosomal recessive		
dHMN		
dHMN III	<i>11q13</i>	
dHMN IV	<i>11q13</i>	
dHMN VI	<i>IGHMBP2</i>	ATP-dependent helicase in RNA translation

Table 1-5 Classification of Distal Hereditary Motor Neuropathy according to genotype. *HSPB1*: Heat Shock 27kDa Protein 1; *HSPB8*: Heat Shock 22kDa Protein 8; *GARS*: Glycyl tRNA synthetase; *DYNC1H1*: dynein, cytoplasmic 1, heavy chain 1; *HSPB3*: Heat Shock 27kDa Protein 3; *BSCL2*: Berardinelli–Seip Congenital Lipodystrophy type 2; *FBXO38*: F-box protein 38; *REEP1*: receptor accessory protein 1; *DCTN1*: P150Glued subunit of Dynactin; *TRPV4*: Transient receptor potential cation channel subfamily V member 4; *SLC5A7*: solute carrier family 5, member 7; *BICD2*: bicaudal D homolog 2; *IGHMBP2*: immunoglobulin μ binding protein 2.

As mentioned in the previous paragraph, dHMN VI is caused by mutations in the *IGHMBP2* gene and results in a phenotype of Spinal Muscular Atrophy with Respiratory Distress 1 (SMARD1). Patients typically present in early childhood with a very severe neuropathy and diaphragmatic paralysis and rarely survive the first decade. *IGHMBP2* functions as an ATP-dependent 5'-3' helicase and unwinds RNA and DNA duplexes. Further detail can be found in Chapter 6 of this thesis.

1.2.6 X-linked CMT

Demyelinating CMTX1

The second commonest form of CMT is characterised by an X-linked inheritance and mutations in the Gap Junction Protein Beta 1 (*GJPB1*) gene, encoding for the connexin 32 protein (Cx32). Consistent with an X-linked disease, males typically present with a more severe phenotype than females. Central nervous system manifestations can also occur in these cases.

Connexin 32 is expressed by Schwann cells and oligodendrocytes that fail to assemble functional gap junctions or assemble defective gap junctions when mutated. Being important for myelin homeostasis, disruptions in the function of these gap junctions will lead to a demyelinating neuropathy (Scherer et al., 2012).

CMTX2 and CMTX3

One family with CMTX2 has been studied by Ionasescu et al., showing a disease phenotype similar to CMT1 but showing both demyelinating and axonal involvement in electrophysiological studies. This family showed an infantile onset, with two out of five affected individuals having mental retardation and carrier females being unaffected. Linkage analysis showed peak scores on Xp22.2 (Table 1.6).

So far, three families have been reported with CMTX3 (Ionasescu et al., 1991; Huttner et al., 2006; Brewer et al., 2008). All families presented with juvenile onset of distal muscle atrophy and weakness and electromyography data showed variable NCVs, both above and below 38 m/s. Again, carrier females were unaffected. In two of the families, the majority of patients reported pain and paraesthesia as the initial sensory symptom before the onset of sensory loss. Linkage analysis carefully refined

the locus to a 2.5-Mb region on Xq26.3-27.1, consisting of 10 genes that showed no variants.

Axonal CMTX

Three other types of CMTX are predominantly axonal: CMTX4, CMTX5 and CMTX6. CMTX4 - also known as Cowchock syndrome - is characterised by early onset polyneuropathy, sensorineural hearing loss and mental retardation, caused by mutations in the apoptosis- inducing factor (*AIF*) gene (Rinaldi et al., 2012).

Rosenburg-Chutorian syndrome, CMTX5, is caused by mutations in the phosphoribosyl pyrophosphate synthetase 1 (*PRPS1*) gene. Patients present with a very severe neuropathy, deafness and optic atrophy and can also be referred to as having Rosenberg-Chutorian syndrome (Kim et al., 2007).

The last X-linked axonal form has only been found in one family so far and has been linked to mutations in the Pyruvate dehydrogenase kinase, isoenzyme 3 (*PDK3*) gene (Kennerson et al., 2013).

X-linked dHMN

So far, only one gene has been found to be responsible in families with X-linked dHMN. ATPase, Cu⁺⁺ transporting, alpha polypeptide (*ATP7A*) encodes for a copper-transporting ATPase 1 that is located to the transmembrane from the golgi in response to copper. When mutated, there is a significant accumulation of this protein at the plasma membrane, interfering with the copper metabolism (Kennerson et al., 2010). Originally, mutations in this gene were found to cause Menke's disease, characterised by an infantile onset of cerebral and cerebellar neurodegeneration, failure to thrive, kinky hair and connective-tissue abnormalities. The mutation spectrum of Menke's disease does not include either of the mutations found in the dHMN families, which suggest the mutation spectrum might have an influence on the phenotype.

X-linked	Gene/locus	Function
X-linked CMT		
CMTX1	<i>GJB1</i>	Myelin assembly/Myelin transport
CMTX2	<i>Xp22.2</i>	
CMTX3	<i>Xq26</i>	
CMTX4	<i>AIF</i>	Apoptotic pathway
CMTX5	<i>PRPS1</i>	Purine metabolism and nucleotide biosynthesis
CMTX6	<i>PDK3</i>	Regulation of glucose metabolism
X-linked HMN	<i>ATP7A</i>	Copper-transporting ATPase

Table 1-6 Classification of X-linked CMT. *GJB1*: Gap Junction Protein Beta 1; *AIF*: apoptosis- inducing factor. *PRPS1*: phosphoribosyl pyrophosphate synthetase 1; *PDK3*: Pyruvate dehydrogenase kinase, isoenzyme 3; *ATP7A*: ATPase, Cu⁺⁺ transporting, alpha polypeptide.

1.3 Pathogenic pathways involved in Charcot-Marie-Tooth

1.3.1 Myelin assembly and Schwann cell dynamics

Not surprisingly, the first genes involved in CMT were found to be part of the myelin pathway. In a normal situation, myelin will reduce the capacitance of the internodal axonal membrane and cluster ion channels at nodes to facilitate saltatory conduction. Demyelination increases internodal capacitance and disrupts the organisation of ion channels in the nodal region, resulting in conduction slowing and even conduction block.

The majority of demyelinating neuropathies result from defects in the development and functioning of Schwann cells and the myelin sheath they produce by mutations in genes such as *PMP22*, *MPZ*, *GJB1* and *PRX*. Axonal loss will occur as a secondary outcome, displaying a higher correlation with the severity of disease than the initial demyelination (Fledrich et al., 2012). Demyelination can be the result of disrupted structure of the myelin sheath (*MPZ*), formation of aggresomes and actin/PI4-5P2 positive vacuoles (*PMP22*), retention of the proteins in the ER (*PMP22*), alterations of the gap junctions between compact and uncompact myelin (*Cx32*) or interruption of the Schwann cell-ECM connection (*PRX*, *PMP22*). Different mutations in the same gene can lead to distinct effects, as is the case for

MPZ: depending on the location of the mutation, there is disruption of the myelin structure or direct axonal loss, thought to arise from aberrant Schwann cell-axon interactions (Berger et al., 2006). The effects do not limit themselves to the structure of myelin. For example, mutations in *PMP22* will also result in misregulation of apoptosis. How and whether this will be a determining factor for the observed phenotype has not been established yet.

As evidenced by the pathogenic results of the altered dosage of the *PMP22*, protein levels have to be tightly regulated to control myelination. An important transcription factor in this pathway is *EGR2*, which is likely to control the expression of myelin proteins such as *MPZ* (LeBlanc et al., 2006). Mice lacking this gene are devoid of peripheral nerve myelin, and the phenotype in humans with mutations generally results in severe demyelination or dysmyelination.

1.3.2 Altered protein synthesis, sorting and/or degradation

The internalisation and subsequent endosomal trafficking or recycling of proteins and membrane along the endocytic pathway is a fundamental cellular process. Cells can internalise components in diverse ways, such as phagocytosis, caveolea or clathrin-dependent endocytosis (CDE). Along the latter pathway, several genes have been found to result in a CMT phenotype when mutated (Fig. 1.1). At the early stages, *DNM2* is involved as a large GTPase to constrict and deform membranes; including pinching off newly formed clathrin-coated vesicles. Mutations are mainly located in the pleckstrin-homology domain and can either cause axonal or intermediate versions of CMT. This results in a reduced binding of *DNM2* to vesicles, leading to a reduction of CDE (Zuchner et al., 2005; Durieux et al., 2010). Few mutations will maintain the membrane localisation but instead affect the microtubule-dependent membrane transport (Tanabe et al., 2012).

Further in the endocytic pathway at the late endosome-/lysosome state, a small GTPase, *RAB7*, regulates endosomal sorting, biogenesis of lysosomes and phagocytosis (Zhang et al., 2009). Mutant forms of the protein exhibited lower GTPase activity, with a predisposition for GTP binding leading to a more activated state of *RAB7* (Spinosa et al., 2008).

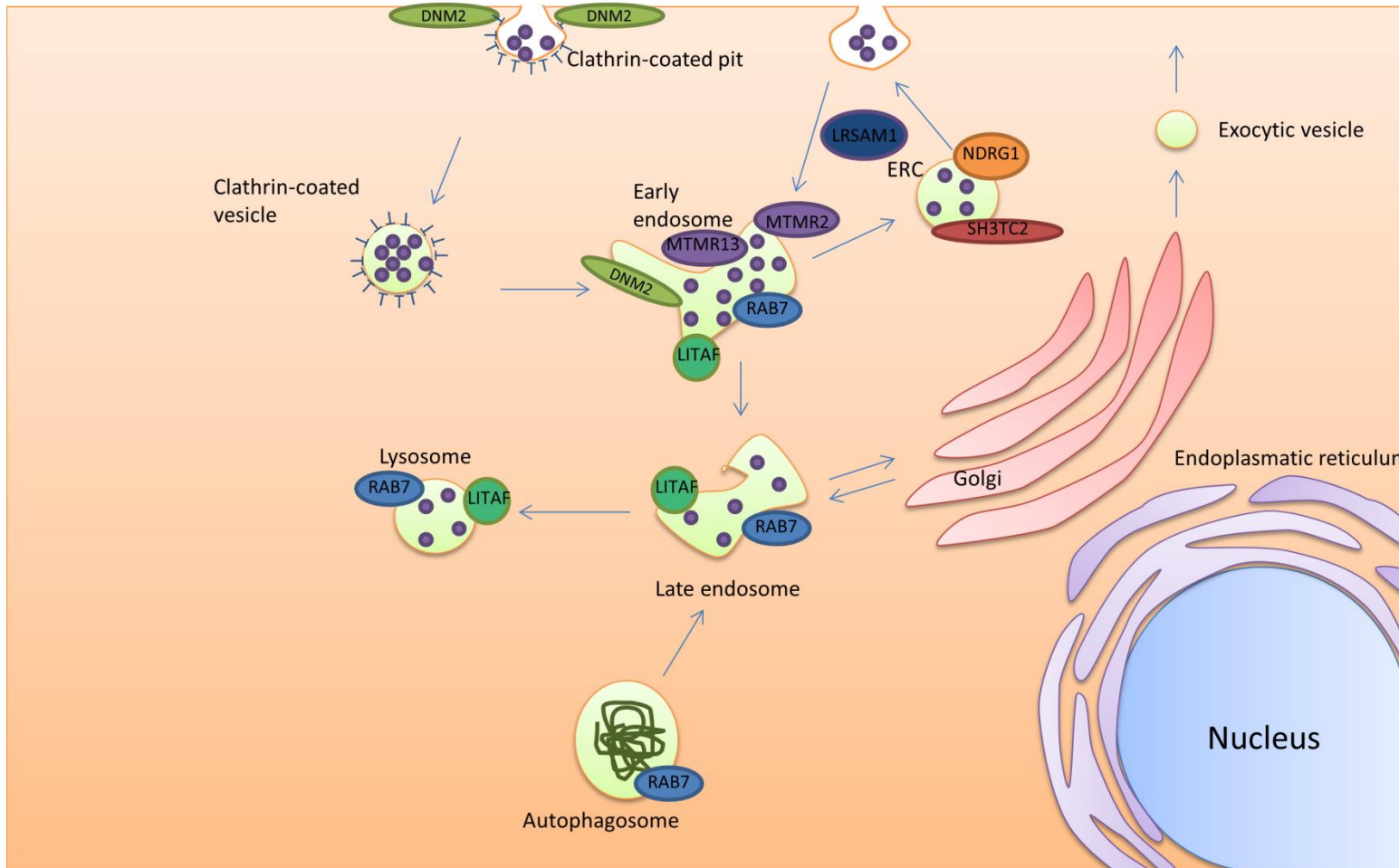


Figure 1-1 Proteins of the endocytic pathway implicated in CMT. ERC = Endocytic recycling compartment.

As mentioned in section 1.2.2, the axonal phenotype with prominent sensory features that originates from mutations in *RAB7A* has an extensive similarity with the *SPTLC1*-phenotype, involved in sphingolipid synthesis, suggesting the pathogenic mechanism originates from the transport or endocytosis of sphingolipids. Another small GTPase, RAB11, interacts with SH3TC2 to target the intracellular recycling endosome, responsible for the recycling of internalised membrane and receptors back to the plasma membrane. Mutant forms of SH3TC2 are unable to associate with Rab11, resulting in a loss of recycling endosome localisation. Phenotypically, this will result in progressive demyelination of the peripheral nerves (Roberts et al., 2010).

Recently, one more autosomal recessive demyelinating form of CMT, linked to mutations in the *NDRG1* gene, has also been implicated in vesicular transport. Even though the exact function is not known yet, evidence shows localisation to the recycling/sorting endosomes for E-cadherin transport and recycling (Kachhap et al., 2007).

As a whole, the endocytic pathway is subject to regulation by phosphoinositides (PIs), phosphorylated versions of phosphatidylinositol, a minor component on the cytosolic side of cell membranes. Whilst phosphatidylinositol-4,5-bisphosphate [PI(4,5)P₂] is the main PI present, accountable for initiation of clathrin-coated pit (CCP) formation, generation of phosphatidylinositol-3,4-bisphosphate [PI(3,4)P₂] and dephosphorylation of [PI(4,5)P₂] later in the pathway are necessary for the regulation of CCP maturation and vesicle uncoating. [PI(3)P] is localised on early endosomes and, together with [PI(3,3)P₂], can be dephosphorylated by active myotubularins such as MTMR2 and MTMR13. Mutant forms of these enzymes in demyelinating CMT show reduced phosphatase activity and indicate a necessity for a tight control of PI levels along the endocytic pathway (Berger et al., 2002). [PI(3,5)P₂] is one of the other PIs localised on the endosomal membranes, although in a concentration almost 100-fold lower than [PI(4,5)P₂]. Concentration of [PI(3,5)P₂] is tightly regulated by the PAS complex, containing both a phosphoinositide kinase and phosphatase. Part of the phosphatase contains the FIG4 protein, mutated in recessive demyelinating CMT (McCartney et al., 2014) and will be more extensively discussed in Chapter 4.

Regulating the same pathway, SIMPLE/LITAF was first linked to the late endosome, identifying as an E3 Ubiquitin ligase due to a C-rich domain resembling the RING finger motif. However, recent studies suggest it is an early endosomal membrane protein, regulating cell signalling by promoting endosome-to-lysosome trafficking and degradation of signalling receptors (Lee et al., 2012; Chin et al., 2013). Mutations will result in mislocalisation to the mitochondria, inhibiting endosomal trafficking and lysosomal degradation of proteins (Lacerda et al., 2014). Again, this will lead to a demyelinating phenotype.

Lastly, LRSAM1 has been identified as an E3 Ubiquitin ligase exhibiting an opposite effect on the pathway. Ubiquitination by LRSAM1 will cause the disassembly of sorting complexes, leading to a prolonged signalling of the activated receptors (Engeholm et al., 2014). Mutant forms will lead to an axonal phenotype in patients, with both dominant and recessive cases being reported (Guernsey et al., 2010; Engeholm et al., 2014). The regulation of cell surface receptors throughout the endocytic pathway will modulate the intensity and duration of signal transduction in cells.

None of these proteins are exclusively expressed in neuronal cell types and the occurrence of demyelinating CMT indicates Schwann cells might be particularly susceptible to defects in endosomal trafficking. Whilst in some cases, direct links could be found with ERK1/2 activation, leading to demyelination (Lee et al., 2012), the link between endocytic dysregulation and axonal neuropathies is less clear.

1.3.3 Axonal transport Altered Transport Processes

Axonal transport regulates the movement of different cell organelles such as mitochondria, vesicles or lipids and proteins throughout the axon in a bidirectional way. Anterograde transport directs the cargo from the cell body to the periphery, with retrograde transport being responsible for transferring cargo along the microtubule from periphery to the cell body.

Anterograde transport uses a class of motor proteins called kinesins to drive the cargo over the microtubule towards the plus end, located at the periphery (Fig. 1.2).

Each step is catalysed by the hydrolysis of ATP into ADP, releasing energy (Hirokawa et al., 2005). Multiple members exist in the human kinesin superfamily, exhibiting individual functions. In relation to CMT, only one family has been found with a mutation in the *KIF1B* gene, causing axonal neuropathy (Zhao et al., 2001). Two different isoforms are encoded by the *KIF1B* gene and show affinity for different cargos. KIF1B- α mediates transport of mitochondria, while KIF1B- β associates with synaptic vesicles precursors. The mutation is located in the ATP binding domain, which is part of both isoforms but heterozygous mice only showed a defect in synaptic vesicle transport together with progressive muscle weakness. This led to the suggestion that haploinsufficiency of the protein and impaired transport of synaptic vesicle precursors could lead to the axonal neuropathy. Many years later, truncating, recessive mutations in *KIF1A* were linked to patients with HSAN. All mutations were found downstream of the motor domain, in an alternatively spliced exon of *KIF1A* mainly expressed in the nervous system. *KIF1A* is responsible for fast anterograde transport of synaptic vesicles and Y2H studies indicated *KIF1A* interacted with the HSN2 exon of *WNK1*, another gene implied in HSAN (Riviere et al., 2011).

In the same way for retrograde transport, dynein-dynactin complexes function as motor proteins, transporting the cargo from the periphery to the cell body. The first mutation was reported in *DCTN1* in 2003, in patients with dHMN (Puls et al., 2003). Dynactin links the specific cargo with the microtubule and cytoplasmic dynein. Mutant forms have shown a lower affection for microtubule, impairing the dynactin function and leading to aggregates that associate with mitochondria and induce cell death (Levy et al., 2006). Axonal transport will both be inhibited by the lower interaction and the toxic gain-of-function effect from the aggregates, leading to axonal neuropathy. More recently, mutations in *DYNH1C1*, the heavy chain of dynein, were found in CMT2 patients (Weedon et al., 2011). One year later, different mutations in the same gene were appointed as the cause for SMA-LED (Tsurusaki et al., 2012). All of these mutations are located in the homodimerisation domain, resulting in a decreased affinity of dynein for the microtubule during the ATP step, impairing motor domain co-ordination and subsequently reducing dynein-driven retrograde transport (Harms et al., 2012).

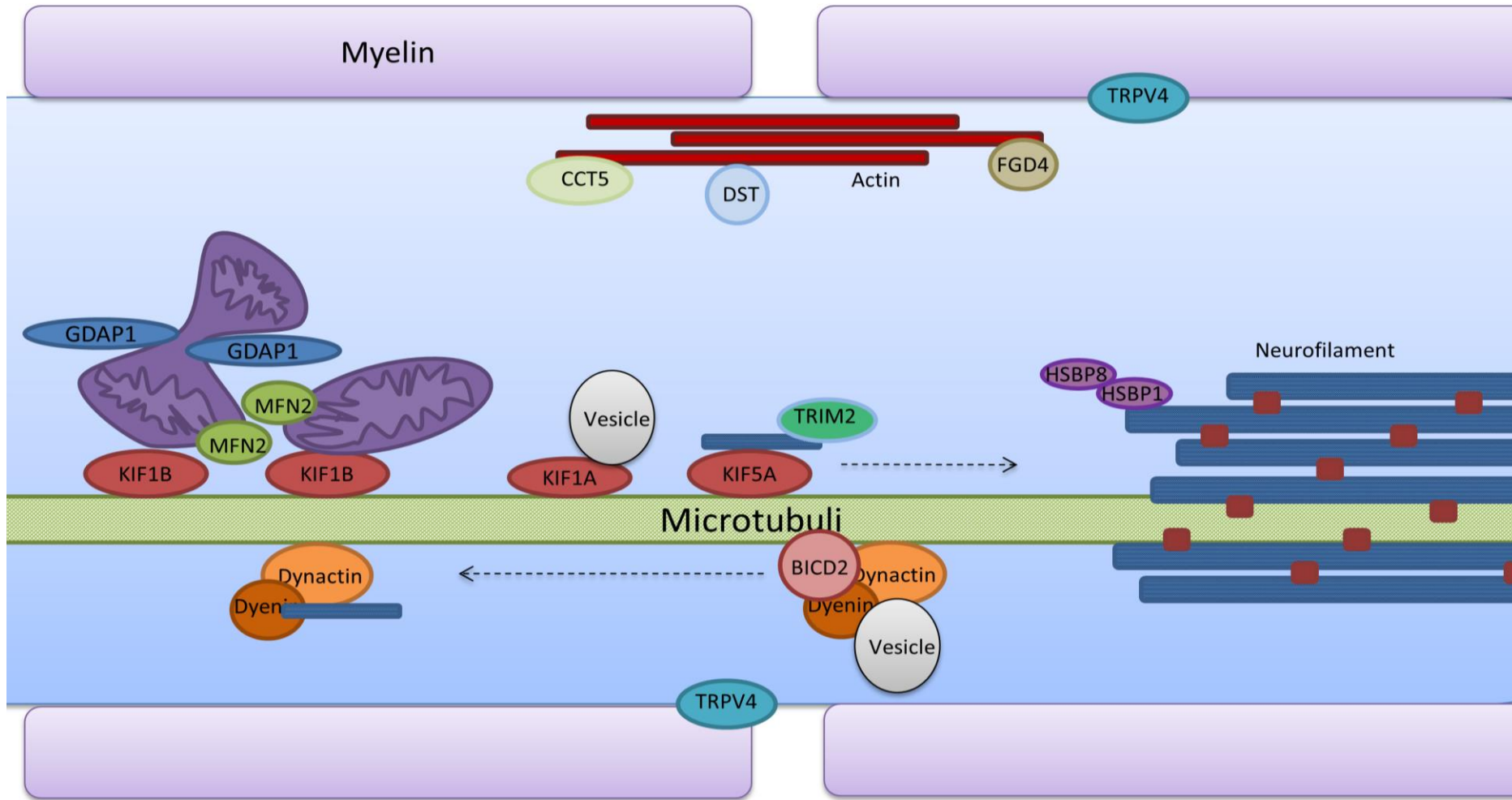


Figure 1-2 Proteins in axonal transport or cytoskeleton, implicated in CMT.

Further research showed profoundly modified mitochondrial morphology and respiration due to these mutations, indicating that dynein is required for the maintenance of mitochondrial morphology (Eschbach et al., 2013). Whilst dynein is ubiquitously expressed, motor neurons seem to be most vulnerable to defects in dynein function.

Important factors in the regulation of dynein-based vesicle motility, function and localisation are a group of proteins called Bicaudal D. These were first identified in *Drosophila* flies and have two homologs in mammals: BICD1 and BICD2 (Kardon et al., 2009). Mutations in the latter have been found in patients with a very similar phenotype to *DYNC1HI*-associated SMA-LED, indicating the pathogenicity of these mutations (Oates et al., 2013; Peeters et al., 2013; Neveling et al., 2013). This will be further discussed in Chapter 5.

Another way to regulate mitochondrial transport is through the levels of Ca^{2+} along the neuron. High Ca^{2+} levels will recruit more mitochondria to take up the excess Ca^{2+} through the uniporter into intracellular stores. Mutations in *TRPV4*, a cation channel mediating calcium influx, result in a dominant axonal neuropathy and different hypothesis have been suggested in regards to the pathomechanism of these mutations. Whilst initial studies showed a loss of function due to cytoplasmic retention of the channels and decreased calcium channel activity of the mutant form (Auer-Grumbach et al., 2010), other studies proposed a gain of function mechanism, showing physiological localisation and an increased calcium channel activity, leading to an increased intracellular calcium influx (Fecto et al., 2011). Apart from causing dominant axonal neuropathies, mutations in this gene can lead to a range of skeletal and neuromuscular disorders, with a high variability even within families (Auer-Grumbach et al., 2010).

1.3.4 Alterations of the Cytoskeleton

Not only can mutations occur directly in the molecular motors for axonal transport or their modulators, mutations in proteins of the cytoskeleton can indirectly influence the working of axonal transport. Alterations in the cytoskeleton will result in an impaired axonal transport, reduced axon diameter and a reduced capacity for nerve regeneration. One of the major components of the neuronal cytoskeleton is

neurofilament, which functions to provide structural support and regulate the axon diameter (Lariviere et al., 2004). Neurofilament is built from three building blocks, with names based on the molecular weight of each subunit: Neurofilament light chain (NF-L: 62 kDa), medium chain (NF-M: 168 kDa) and heavy chain (NF-H: 200 kDa). After synthesis in the cell body, neurofilament will be transported along the microtubule to the nerve terminals, where NF-L functions as a scaffold for the assembly of NF-M and NF-H (Ching et al., 1993; Xia et al., 2003). More than a decade ago, the first mutations in the neurofilament light chain gene (*NEFL*) were found to cause axonal CMT2, with further reports expanding the phenotype to demyelinating CMT1 (Mersiyanova et al., 2000; Jordanova et al., 2003). Different *NEFL* mutations exert various effects on NF biology, such as interference with the transport of mitochondria, axonal transport of mutant neurofilament and neurofilament assembly (Brownlees et al., 2002; Perez-Olle et al., 2004), but no genotype/phenotype correlations have been established so far (Miltenberger-Miltenyi et al., 2007). *NEFL* knockout mice did not exert a CMT2 phenotype, whilst the introduction of missense mutations led to a severe peripheral neuropathy, indicating the dominant missense mutations do not cause loss-of-function (Zhu et al., 1997; Lee et al., 1994). In one of our families with axonal neuropathy, mutations were found in the neurofilament heavy chain, which will be discussed in Chapter 5. Interestingly, studies have shown that dynein is partially responsible for the movement of neurofilament along the axons, via an interaction with NF-M. Inhibition of the dynein/dynactin complex leads to accumulation of neurofilaments in the axon (Wagner et al., 2004; Motil et al., 2007).

The organisation of the neurofilament network requires the assistance of small heat shock proteins such as HSP27, encoded by *HSPB1*, that regulate interactions that occur between filaments in their cellular networks (Perng et al., 1999). Mutations in *HSPB1* disrupt the neurofilament network (Evgrafov et al., 2004) by hyperphosphorylation of the neurofilaments, reducing anterograde transport and subsequently leading to dominant axonal neuropathy or dHMN (Holmgren et al., 2013). The role of HSP22, another protein implicated in CMT, has not been characterised as extensively. Even though it does not directly interact with neurofilament, it might play a role in the architecture of the cytoskeleton via interaction with HSP27 (Sun et al., 2004). NF-L metabolism is also regulated by

TRIM2, an E3 Ubiquitin ligase. Studies have shown TRIM2 is responsible for the ubiquitination of NF-L and mutant forms lead to a reduction of NF-L ubiquitination with subsequent NF-L accumulation in aggregates (Balastik et al., 2008). Only one patient with axonal neuropathy has been found so far with compound heterozygous mutations in this gene (Ylikallio et al., 2013).

Most of the mutated genes implied in the neuronal cytoskeleton metabolism will result in axonal CMT with the exception of NF-L, which has been shown to also lead to demyelinating CMT. However, no consistent differences could be found in between the mutations causing either axonal or demyelinating CMT, with several mutations causing both (Miltenberger-Miltenyi et al., 2007).

A characteristic component of the cytoskeleton for all cell lines is microfilament, consisting of linear polymers of actin which, in neurons, are located at nodes of Ranvier and post synaptic densities and in dendritic spines. They are situated right under the plasma membrane of the axon and provide mechanical strength to the cell or link transmembrane proteins to cytoplasmic proteins. Multiple genes have been found to be mutated in demyelinating CMT or HSAN that influence the actin cytoskeleton as mentioned before, such as *CCT5* –involved in the folding of actin–, *DST* –linking actin filaments to microtubule–, and *FGD4* –mediating actin cytoskeleton changes (Bouhouche et al., 2006; Edvardson et al., 2012; Delague et al., 2007). All of these present with a recessive mode of inheritance but so far, none have been extensively studied to hypothesise the pathogenic pathway involved.

1.3.5 Mitochondrial network dynamics and ATP production

Another concept important in the maintenance of axons is the dynamics of the mitochondrial network. Due to high energy requirements and low intrinsic energy reserves, neurons require a constant delivery of mitochondria, producing ATP. Not only low ATP levels, but also high Ca^{2+} levels attract a flux of mitochondria, which will take up the excess Ca^{2+} through the mitochondrial Ca^{2+} uniporter, as mentioned before. Mutations in different genes affecting the function, transport, fusion, fission or interactions with mitochondria have been found in patients with CMT. Mitochondria are known as the ‘Powerhouses of the cell’ and defects in their function can lead to a broad spectrum of diseases, most commonly called

mitochondrial diseases. Mitochondrial diseases tend to present as multisystemic disorders and are generally progressive. Despite the phenotypic variability, more cases of neurodegenerative disorders due to mitochondrial defects are being discovered, such as Alzheimer's disease, Amyotrophic lateral sclerosis, Huntington disease and hereditary spastic paraplegia (Lin et al., 2006; Schon et al., 2011).

Whilst initially these disorders were mainly characterised by defects in mitochondrial respiration, genes are being discovered that lead to faults in mitochondrial trafficking, interorganellar communication and quality control defects when mutated. Section 1.3.3 already showed examples of cases where the transport of mitochondria was affected due to mutations in motor proteins, but many more are implied in the context of CMT. As mentioned before, *MFN2* is a GTPase located in the outer membrane of the mitochondria and regulates mitochondrial fusion and tethering. The fusion/fission process plays a critical role in maintaining healthy mitochondria, for example after metabolic or environmental stress. Fusion will help to diffuse stress by mixing contents of healthy mitochondria with partially damaged mitochondria, whilst fission is needed to create new mitochondria. Mutant forms of *MFN2* will not only cause defects in the fusion of mitochondria (Detmer et al., 2007), but also compromise the axonal transport of mitochondria leading to mitochondrial clustering in the perikaryon (Baloh et al., 2007). Axonal degeneration correlated with the alteration of proper mitochondrial distribution along the axon, due to disruption of local axonal energy sensing and positioning mechanisms. Initial hypothesis explained the vulnerability of long axons to the delay or prevention of newly synthesised mitochondria from reaching the most distal ends, but more recent data suggests this might be due to a deficit in the regulation of local transport and distribution of mitochondria (Misko et al., 2012). Additionally, mutations in *MFN2* resulted in a reduced mitochondrial membrane potential together with an energetic coupling defect (Loiseau et al., 2007).

Even though mutations in *MFN2* lead to axonal CMT, mutations in the mitochondrial fission protein *GDAP1* most frequently lead to demyelinating CMT and in some cases to intermediate or axonal forms. Phenotypically, recessive mutations result in a more severe disease than dominant mutations. Recessive mutant forms have lost mitochondrial fragmentation activity (Niemann et al., 2005), whilst

dominant forms interfere with mitochondrial fusion and result in an increased production of reactive oxygen species (Niemann et al., 2009). Silencing of *GDAP1* also influences Ca^{2+} homeostasis by reducing Ca^{2+} inflow through store-operated Ca^{2+} entry (Pla-Martin et al., 2013). However, the exact pathological changes that lead to axonal or demyelinating changes have not been elucidated yet. Knockout mouse models have been developed, showing progressive decreased nerve conduction velocities, accompanied by mild hypomyelination. Investigations show larger mitochondria in knockout mice axons and cultured sensory neurons showed impaired mitochondrial transport (Niemann et al., 2014).

GDAP1 fission is dependent on *Drp1* (also known as *DNM1L*), a highly conserved mitochondrial fission factor that regulates the interaction between mitochondria and ER, and silencing *Drp1* expression resulted in mitochondrial elongation and reduced fragmented mitochondria (Niemann et al., 2009). Whilst mutations in this gene are lethal, one of the upstream regulators, inverted formin 2 (*INF2*), has been shown to be mutated in intermediate CMT. One postulation is that ER-localised *INF2* assembles actin at the mitochondria-ER constriction sites, providing initial mitochondrial constriction and enhancing further constriction by *Drp1* before rapidly depolymerizing actin (Korobova et al., 2013). Originally, mutations in *INF2* were found to cause focal segmental glomerulosclerosis (FSGS) after which the phenotype was expanded to dominant intermediate CMT with FSGS (Boyer et al., 2011).

Secondly, mutations can also interfere with the production of ATP in the mitochondrion itself. When pyruvate is transported along the mitochondrial membrane it enters the Krebs cycle after conversion to acetyl CoA, and results in ATP and reduced FADH_2 and NADH that will be transported to the electron transport chain. CMT2-causing genes have been found at different stages of this process, all leading to a neuropathy. The first step of oxidative decarboxylation of pyruvate is catalysed by the pyruvate dehydrogenase complex (PDC). PDC deficiency normally leads to developmental delay, hypotonia, seizures and abnormal cerebral neuroimaging with selected cases associated with peripheral neuropathy (Patel et al., 2012). This complex is regulated by four pyruvate dehydrogenase kinase isoenzymes (PDKs), each exhibiting tissue-specific expression. PDK3, the isoenzyme expressed in brain and spinal cord, has been found mutated in one family

with X-linked CMT, resulting in overactivity of the isoenzyme leaving PDC in a predominantly phosphorylated inactive state, which may lead to impaired ATP production (Kennerson et al., 2013).

Although extremely rare, cases have been reported with mutations in the enzymes of the Krebs cycle, leading to metabolic diseases (Rustin et al., 1997). The first and only mutation leading to axonal neuropathy was found in the dehydrogenase e1 and transketolase domains-containing protein 1 (*DHTKD1*) which has been postulated to function as a 2-oxoglutarate-dehydrogenase E1 component in the Krebs cycle. Silencing of this protein resulted in severely reduced levels of ATP and NADH and haploinsufficiency due to rapid mRNA degradation via nonsense mediated decay of the nonsense mutation is suggested to lead to insufficient energy production and dysfunction of peripheral nerves (Xu et al., 2012).

In Chapter 3, the mitochondrial oxidative phosphorylation system and discovery of mutations in complex V will be discussed extensively. There we found mutations in CMT2 patients in the mitochondrially encoded *ATP6* gene, normally known to cause mitochondrial disorders such as Leigh syndrome or NARP. Not long after that discovery, mutations in a different gene in the same pathway that normally causes Leigh syndrome were found in patients with recessive, demyelinating CMT (*SURF1*). All three patients presented with an isolated peripheral neuropathy and very little multisystem involvement (Echaniz-Laguna et al., 2013). *SURF1* is one of the at least 6 assembly factors of Cytochrome c oxidase (COX), also known as complex IV in the electron transport chain, and mutant forms result in a markedly reduced assembly and activity of COX. The exact pathways that lead from a COX defect to an isolated peripheral neuropathy have not been elucidated yet.

1.3.6 tRNA synthetase genes

Aminoacyl tRNA synthetases are enzymes responsible for charging the appropriate amino acid to their cognate tRNA before transferring the amino acid onto a growing peptide. The first amino-acyl tRNA synthetase discovered to cause axonal neuropathy was glycyl tRNA synthetase (Antonellis et al., 2003). This led to the subsequent discovery of an additional five amino-acyl tRNA synthetases implicated in peripheral neuropathy: tyrosyl-tRNA synthetase (Jordanova et al., 2006); alanyl-

tRNA synthetase (Latour et al., 2010); lysyl-tRNA synthetase (McLaughlin et al., 2010); histidyl-tRNA synthetase (Vester et al., 2013) and methionyl-tRNA synthetase (Gonzalez et al., 2013). Different hypothesis have been suggested to explain the pathogenicity of mutations in tRNA synthetase genes and have been predominantly studied in *GARS*, due to the earlier discovery and the majority of mutations being located in this gene. Considering the mutation in *AARS* was present in the editing domain, misincorporation of amino acids has been observed, leading to misfolded proteins and the activation of the unfolded protein response which could lead to the observed neurodegeneration (Lee et al., 2006). However, *GARS* does not have an editing domain since the active site is conformationally constrained to only accept glycine and only few mutations would adjust the dimer interface leading to misincorporation, suggesting this would not be the pathological mechanism (Stum et al., 2011). Most functional approaches to prove pathogenicity of these ARS enzymes involve aminoacylation and yeast growth assays. When performed on nine different *GARS* mutations, all mutations affected the aminoacylation activity of the protein in comparison with wild type and the majority of mutations also dramatically reduced yeast cell viability (Griffin et al., 2014). Whilst this indicates pathogenicity of novel mutations and insight in the functional consequences, it provides no further elucidation about the pathomechanism in axons. Research has suggested a role in local translation in axons (Giuditta et al., 2002) and studies have shown a punctate structure of wild type endogenous *GARS* in peripheral axons, which is impaired in certain mutated forms (Griffin et al., 2014). However, additional research needs to be performed to establish a link between impaired function and the observed axonal or intermediate neuropathy in these six ARS found so far.

1.3.7 Unknown pathways

Apart from the previous recurring themes in the pathogenicity of peripheral neuropathies, there are multiple genes involved that do not fit in any of these pathways or have not had their pathogenic role clarified yet. Some of them affect the same pathway, indicating the importance in neuropathy; others stand alone with a function not related to other proteins mutated. Examples are proteins involved in RNA metabolism (*HINT1*, *IGHMBP2*, *CTDP1*), sphingolipid biosynthesis (*SPTLC1*, *SPTLC2*) or development (*WNK1*, *IKBKAP*, *FBXO38*) or isolated proteins such as *LMNA*, *HK1* or *SLC5A7*. The majority of genes implicated in CMT are not restricted

to one specific function and in many cases, it is not clear which exact function is impaired in the mutant forms of the protein.

1.4 Thesis aims

The aim of this thesis was to contribute to the knowledge of the genetic heterogeneity and mechanism of disease of inherited neuropathies, in particular, CMT. My work combined the use of genetic studies and functional analysis with the overall aims of:

1. Investigating the presence of mutations in the mitochondrial genome leading to CMT (Chapter 3).
2. Estimating the frequency of newly discovered genes in selected cohorts (Chapter 4).
3. Screening new candidate genes in appropriate cohorts by the use of Sanger sequencing (Chapter 4).
4. Using exome sequencing to establish the genetic cause of disease in undiagnosed families with inherited neuropathy (Chapter 5).
5. Investigating the molecular mechanism of mutations in *IGHMBP2* leading to both SMARD1 and CMT2 (Chapter 6).

Chapter 2:

Material and methods

Materials: The country of origin is only indicated for companies that do not have registered UK subsidiaries.

2.1 Genetic studies

2.1.1 Ethical approval and patient selection

This study has been granted ethical approval by the National Research Ethics Service Committee of the National Hospital for Neurology and Neurosurgery (NHNN) in Queen Square, London, UK. Written informed consent was obtained from all patients, parental guardians and/or included family members. Patients were identified by Professors Mary Reilly and Henry Houlden primarily and collaborations were made with several additional clinicians around the world.

2.1.2 DNA extraction

DNA extraction was performed in the neurogenetics lab by the clinical diagnostic service of the National Hospital for Neurology and Neurosurgery. This was performed using either automated purification of DNA from 1–5 ml or 5–10 ml samples of fresh or frozen whole blood using Autopure reagents on the Autopure LS or by manual extraction with the Qiagen Flexigene kit (Qiagen).

2.1.3 DNA concentration and purity

DNA concentration and purity were assessed using the NanoDrop ND-1000 spectrophotometer as per the manufacturer's instructions (NanoDrop Technologies). Concentration was assessed at 260 nm. Purity was estimated by the 260/280 and 260/230 absorbance ratios, to assess contamination with respectively proteins or other contaminants such as phenol, ethanol or other compounds. Absorbance ratios between the spectrum of 1.8-2 and 1.8-2.2 respectively were required for DNA of decent quality.

2.1.4 Polymerase Chain Reaction (PCR)

Human genome sequences were obtained from Ensembl Genome Browser (<http://www.ensembl.org/index.html>), genome assembly build 37 (GRCh37; GCA_000001405.14). Transcripts were chosen according to the project, depending on previous papers or the full length of the transcript. Genes for which the whole gene was sequenced are listed below (Table 2.1). Transcripts for exome sequencing variants were chosen according to the exome data.

Gene	Transcript
<i>MT-ATP6</i>	ENST00000361899
<i>MT-ATP8</i>	ENST00000361851
<i>FIG4</i>	ENST00000230124
<i>C9orf72</i>	ENST00000380003
<i>HINT1</i>	ENST00000304043
<i>ARL1</i>	ENST00000261636
<i>ARL6ip1</i>	ENST00000304414
<i>SCN9A</i>	ENST00000409672
<i>BICD2</i>	ENST00000356884
<i>TRAK2</i>	ENST00000332624
<i>ADD3</i>	ENST00000356080
<i>IGHMBP2</i>	ENST00000255078

Table 2-1 List of transcripts used for sequencing of genes.

Designing of primers

Primers were designed using the Primer3 software (<http://primer3.ut.ee/>, Rozen and Skaletsky, 2000) unless stated otherwise, to amplify the exons and exon-intron boundaries. Primers were chosen to be a length of 18-23 basepairs long, resulting in

a product size between 500-700 basepairs. Melting temperatures were between 57°C and 62°C and the percentage of G or C bases in the primer was ~50%. Primers with a high self-complementarity were excluded. All primers are available on request.

Nuclear DNA

PCR reaction mix was made up to a volume of 25 µL with sterile deionised H₂O and included 10 µmol of each primer, 20 to 50 ng DNA and 12.5 µL of FastStart PCR master (Roche). When necessary, 10% DMSO was included in the PCR reaction. PCR was performed on an Eppendorf Mastercycler thermal cycler at a previously determined optimal annealing temperature. Cycling conditions used for PCR amplification reactions are described in Table 2.2. PCR reactions were maintained at 4°C after cycling and stored at -20°C.

Step	Reactionstep	Time	Temperature
1	Initial denaturation	10 min	95°C
2	Denaturation	30 sec	94°C
3	Annealing primers	30 sec	60°C (-0.4°C/cycle)
4	Elongation	45 sec	72°C
5	Denaturation	30 sec	94°C
6	Annealing primers	30 sec	50°C
7	Elongation	45 sec	72°C
8	Final elongation	10 min	72°C

Table 2-2 Standard 60-50 touchdown PCR reaction. Steps 2 to 4 were repeated 25 times; steps 5-7 were repeated 12 times. Annealing temperature in step 3 was 60°C (-0.4°C/cycle) for the majority of exons sequenced.

Mitochondrial DNA

The whole length of 841 nucleotides of the *ATPase 6* and *ATPase 8* genes, with a surrounding hundreds of nucleotides, was divided into three overlapping fragments (Table 2.3). Primer sequences were originally designed as a set to screen the complete mitochondrial genome in overlapping segments and the remaining primers are available on request. All forward primers had a -21 M13 primer tail (TGTAAAACGACGGCCAGT) and all reverse primers a M13 reverse tail (CAGGAAACAGCTATGACC). PCRs were made up to a volume of 25 µL with sterile deionised H₂O and included 10 pmol of each primer, 50 ng DNA and 12.5 µL of AmpliTaq Gold 360 Mastermix (ABI) with conditions listed in Table 2.4

Fragment	Primer Forward	Length (nt)	Nucleotide location
	Primer Reverse		
1	5'- acagttcatgccatcgct-3' 3'- gttcgcccttagtgttg -5'	530	8196-8726
2	5'- ccgactaatcaccaccaac -3' 3'- ggttttactatatgataggc -5'	598	8646-9244
3	5'- atccaaggctacgtttcac -3' 3'- ctgaggcttgtaggagggt -5'	593	9151-9744

Table 2-3 Primer sequences for the *ATPase6* and 8 genes.

Step	Reaction step	Time	Temperature
1	Initial denaturation	10 min	95°C
2	Denaturation	30 sec	95°C
3	Annealing primers	30 sec	58°C
4	Elongation	30 sec	72°C
5	Final Elongation	7 min	72°C

Table 2-4 PCR reaction. Steps 2 to 4 were repeated 30 times.

2.1.5 Agarose gel electrophoresis of PCR products

1.3% w/v agarose gel was prepared by adding 1g of agarose powder (Roche) to 75 mL of 1xTBE buffer (10x TBE: 121.1 g Tris (Sigma-Aldrich), 61.8 g anhydrous boric acid (Merck-Millipore), 7.4 g EDTA (VWR), made up with dH₂O; pH to 8.3) and heating up the mixture in the microwave to dissolve. After cooling, 2 µL of 10 mg/mL ethidium bromide (Promega) was added to visualise DNA by intercalation between the strands. After PCR amplification, length of PCR products was verified by loading 5 µL of the PCR product mixed with 2 µL Orange G loading dye (60% glycerol, 40% dH₂O, teaspoon of orange G powder (Sigma-Aldrich)). Electrophoresis was run on 80V for 30 minutes to allow a good separation of the bands and visualised under a UV transilluminator. Digital photographs were obtained using the Syngene GeneGenius image acquisition system and GeneSnap software (Synoptics).

2.1.6 DNA purification

To ensure PCR products were free of unincorporated single strand DNA oligonucleotides and dNTPs, two different methods were used. Millipore

multiscreen^{hts} PCR filter plates were used up until 5/2/13, after this date ExoSap was used.

Millipore

Vacuum at 25 inches Hg was applied for 5-10 minutes after which the samples were reconstituted in 50 µL of nanopure water. Samples were mixed on a plate mixer for 30 minutes, where after the purified PCR product was retrieved from each well.

ExoSap

PCR products were purified using 2µL of Exo-Fast (50µL Exo I, 200µL Fast-AP, 750µL Water) per 5 µL of amplified DNA by incubating at 37°C for 30 minutes and 80°C for 15 minutes. The resulting product was stored at 4°C before sequencing reaction was performed.

2.1.7 Sequencing

Bi-directional sequencing was performed using a DNA sequencing kit (Big Dye Terminator 3.1; Applied Biosystems). Each reaction was made up to 10 µL of sterile deionised H₂O and included 3.2 µmol of primer, 3.5 µL of PCR product, 2 µL of 5X BigDye Terminator v3.1 sequencing buffer (Life Technologies) and 0.5 µL of BigDye Terminator v3.1 reaction mix (Life Technologies). The cycling conditions were the following: (96°C, 10 sec.; 50°C, 5 sec.; 60°C, 4 min) x25.

2.1.8 Clean-up reaction

To remove unincorporated dye terminators from the sequencing reaction, two different methods were used. Before February 2013, the dye terminator removal kit (Thermo Fisher Scientific) was used according to the manufacturer's protocol. Before loading onto the separation plate, samples were adjusted to 20 µL with water. After centrifugation for 3 min at 950xg the samples were collected in a sterile 96 well plate.

After February 2013, Corning® FiltrEX™ 96 well filter plates, 0.66 mm glass fibre filter, polystyrene (Sigma-Aldrich) were used and columns were manually created with 350µL of Sephadex G-50 Bioreagent (Sigma-Aldrich) by dissolving 1.9g of Sephadex in 40mL of sterile deionised water per plate. Plates were spun for 3 minutes at 750xg before adding the samples. After adding the entire volume of the

sequencing reaction (10 μ L) onto the Sephadex columns, plates were spun for 5 minutes at 910xg and samples were collected in a sterile 96 well plate.

2.1.9 Sequence analysis

Samples were run on the ABI PRISM 3730xl Genetic Analyzer and were manually analysed using the SeqScape v2.5 program (ABI).

2.1.10 Restriction endonuclease analysis

A fragment of the *ATPase 6* gene, which includes the mutation site, was amplified using the sense mismatch primer (9,161–9,184) ACGTTTCACACTTCTAGTGGGCC, and antisense Primer (9,273–9,253) AGAGGGCCCTGTTAGGGGTC, hereby introducing a BSP12OI restriction site (GGGCC) in the mutant but not in the wild type mtDNA. To calculate the percentage of heteroplasmy, a FAM fluorophore (6-carboxyfluorescein) was attached to the 5' end of the antisense primer. The same conditions as stated above in Table 2.4 were used, with an annealing temperature of 57°C and a repetition of steps 2–4 for 18 times.

Following amplification, restriction enzyme digestion by 10 units of BSP12OI was performed to cleave the 113 nucleotides PCR product of mutant DNA into 89 and 24 nucleotide fragments. The reaction mix was then incubated for two hours at 37°C. To denature the PCR products, 12 μ L of formamide was added to 1 μ L of product. 0.3 μ L of Liz 600 (ABI) was used as a size standard. The resulting mixture was heated at 95°C for 3 minutes, after which it was put on ice immediately. It was then loaded on the 3730xl DNA analyser and the ratio of cut to uncut DNA was calculated with the GeneMapper (ABI) program. This was all performed in triplicate, after which the mean value was calculated.

2.1.11 Fragment analysis to look at the C9orf72 expansion repeat

The repeat expansion was assayed with a repeat-primed PCR which included a gene-specific fluorescently labelled forward primer in the C9orf72 exon 1a and two reverse primers. The use of triplet-primed PCR (TP-PCR) for the detection of repeat expansions was first suggested by Warner et al. in 1996, with the principle of the technique relying on the use of locus-specific PCR primers in combination with a primer designed across the repeated sequence. After PCR reaction, products of different sizes will be produced, according to the number of repetitions. If an

expansion occurs, a continuous ladder of PCR amplification fragments exceeding the normal range will be visualised. For this project, one reverse primer consisted of four GGGGCC repeat units and an anchor sequence, while the second reverse primer contained the anchor sequence. Before PCR reaction, a primer mix was constituted according to volumes stated in Table 2.5. 1 μ L of this primer mix was used in combination with 10 μ L of Extensor mix, 10 μ L of Betaine and 1 μ L of DNA. PCR conditions are stated in Table 2.6. A cohort of 185 patients with dHMN was screened.

Primer mix	V (µL)
F1: 6fam-agtgcgttagaggcgaaagc	20
R1: tacgcattccagttgagacggggccggggccggggccggggccgggg	10
R2: tacgcattccagttgagacg	10
H ₂ O	50

Table 2-5 Primer sequences for the *C9orf72* expansion repeat (5' to 3').

Step	Reaction step	Time	Temperature
1	Initial denaturation	10 min	98°C
2	Denaturation	35 sec	97°C
3	Annealing primers	2 min	53°C
4	Elongation	2 min	68°C
5	Denaturation	35 sec	97°C
6	Annealing primers	2 min	53°C
7	Elongation	2 min	68°C
8	Final elongation	10 min	68°C

Table 2-6 PCR reaction for the *C9orf72* expansion repeat. Steps 2-4 were repeated 10 times, steps 5-8 were repeated 25 times.

To denature PCR products, 9.2 μ L of formamide was added to 1.5 μ L of product. 0.3 μ L of Liz 500 (ABI) was used as a size standard. The resulting mixture was heated at 95°C for 3 minutes, after which it was put on ice immediately. It was then loaded on the 3730xl DNA analyser and allele identification and scoring was accomplished using GeneMapper v3.7 software (ABI).

2.1.12 Exome Sequencing

Enrichment of coding exons and flanking intronic regions was performed externally with the use of the Illumina's TruSeq Exome Enrichment Kit, Nimblegen EZ

Capture og Agilent SureSelect in combination with HiSeq2000 sequencing. Poor quality samples were repeated with the same technology or done in-house with the HiSeq 2500 in High output mode. Primary data analysis including image analysis, base calling, alignment and variant calling, copy number variations and structural variations was performed by AROS or in-house. The exome sequencing performed in-house by Dr Deborah Hughes and Dr Alan Pittman at the UCL ION was mapped to the human reference genome build UCSC hg19 by Novoalign Software (Novocraft, Malaysia). After removal of PCR duplicates using Picard (<http://picard.sourceforge.net>) as well as reads without a unique mapping location, variants were extracted using the Maq model in SAMtools and filtered by the following criteria: consensus quality >30, SNP quality >30 and root mean square mapping quality >30. These variants were further filtered against the dbSNP 135 and 1000 Genomes databases by use of Annovar (<http://www.openbioinformatics.org/annovar/>). The data filtering of the results were performed by me. Depending on the location in the genome, some genes, exons or genomic areas may not be covered fully by the hybridisation probe design, leading to a variable number of independent reads at a particular base pair, the read depth. Therefore, gene coverage and read depths of known disease-associated genes and candidates genes were determined by exploring BAM files using the GenomeBrowse software (Golden Helix, USA). A base was considered poorly covered if it had less than 15-20 times coverage. These were still included in the analysis but were regarded as potentially false positives.

After confirming known mutations causing CMT disease or variants in candidate genes were not present, SNPs present in public databases with a frequency higher than 0.5% or a segmental duplication region higher than 0.96 were omitted, as variants within these regions are frequently false positive calls. Synonymous SNPs were excluded and the appropriate disease model was applied to the remaining list of variants. Shared variants files were made in the event where multiple patients were available. Further prioritising of variants was done by combining linkage analysis results or based on individual gene function and expression. In-silico predictions of pathogenicity and conservation between species were assessed and details of gene expression in various tissues and location of the mutated amino acid within the protein were examined to prioritise candidate gene lists.

2.1.13 Linkage analysis

Genotyping was performed on the Illumina CytoSNP 12 array with a complete panel of 200,000 genome-wide tag SNPs and markers targeting all regions of known cytogenetic importance. Raw data was processed using GenomeStudio software (Illumina, San Diego, CA). Uninformative markers with low call rates (<90%) and monomorphic SNPs (MAF <0.5%) were removed and a subset of 5000-6000 randomly select markers was extracted for use in linkage analysis with PLINK (Purcell et al., 2007; <http://pngu.mgh.harvard.edu/purcell/plink/>). Parametric linkage analysis was run on MERLIN (Abecasis et al., 2002) for an autosomal dominant model, specified with an estimated allele frequency of 0.0001 and 90% penetrance.

2.1.14 Haplotyping

Haplotype sharing analysis between families with the c.Cys46Ter mutation in *IGHMBP2* was performed using five microsatellite markers (D11S1889, D11S4178, D11S4113, D11S4095, D11S4139) surrounding the *IGHMBP2* region. These were amplified with fluorescently labelled primers (Table 2.7) and denatured by adding 9.2 µL of formamide to 1.5 µL of PCR product. 0.3 µL of Liz 500 (ABI) was used as a size standard. The resulting mixture was heated at 95°C for 3 minutes, after which it was put on ice immediately. It was then loaded on the 3730xl DNA analyser and the results were analysed with the GeneMapper (ABI) program.

Microsatellite	Chromosome	Allele size	Primers	Sequence
Marker	location			
D11S1889	11:67313143-	183-207	Forward	5'- agctggacttcacagaatg - 3'
	67313325		Reverse	5'- caagaggctggtagaagggtg - 3'
D11S4178	11:68189108-	237 - 260	Forward	5'- caggcccagtctctg - 3'
	68189359		Reverse	5'- cgtgtccagatgaaagtg - 3'
D11S4113	11:68765634-	218 - 262	Forward	5'- acctcacggtaatccc - 3'
	68765859		Reverse	5'- cttgaagcccatcttgc - 3'
D11S4095	11:69268159-	173 - 205	Forward	5'- tccctggctatctgaatc - 3'
	69268361		Reverse	5'- ctgactgggtccacg - 3'
D11S4139	11:70504269-	151 - 195	Forward	5'- tatagacttcagccctgctgc - 3'
	70504461		Reverse	5'- cctctgttaggatcgagtgg - 3'

Table 2-7 Microsatellite markers used for haplotyping of the c.Cys46Ter mutation in the *IGHMBP2* gene.

2.2 Cell Culture

2.2.1 Fibroblast culture

With ethical approval and informed consent, punch biopsies were taken from the upper arm of controls, carriers and affected individuals using a standard technique. This tissue was dissected and the fibroblasts grown under standard tissue culture conditions at 37 °C in 5% CO₂ in DMEM with 1% L-Glutamine (Invitrogen) supplemented with 10% fetal bovine serum (Heat-inactivated, Life Technologies) and 1% PenStrep (Penicillin + Streptomycin; Invitrogen). Controls were obtained from the MRC Centre for Neuromuscular Disorders Biobank Dubowitz Centre, UCL Institute of Child Health (ICH) by Dr Diana Johnson, or were sent to us by our collaborators. Patients and controls for the ADD3 project were provided by Dr. Kruer's lab. Patients II.1 and II.2 of family O were sent to us by Dr. Vedrana Milic Rasic and patient S1 was a contribution of Prof. Rita Horvath. S2 was obtained from GOSH and S3 + S4 were sent to us by Dr. Katja Von Au from Germany.

Cells were grown in standard 75 cm² flasks and media was changed every 2-3 days. Cultures were passaged after reaching 70-80% confluence. Media was removed from the flasks and 5mL of sterile NaCl/P_i (Life technologies) was used to wash. 2 mL of 0.05% 1x Trypsin-EDTA (Life technologies) was added and flasks were placed in the incubator at 37°C for 5 minutes. In case of unsufficient detachment, flasks were tapped against the surface before adding 7 mL of pre-warmed media to stop the reaction. To split cells, 3 mL was added to three new 75 cm² flasks and medium was topped up to 15 mL. To freeze cells, contents of the flask were collected and centrifuged at 1,200 rpm for 5 minutes after which media was discarded. Cell pellet was resuspended in 3 mL of FBS with 10% DMSO (Sigma-Aldrich) and added to cryovials (1 mL per cryovial). Cryovials were placed in a Mr. Frosty freezing container (Thermo scientific) to achieve a rate of cooling very close to -1°C/minute, the optimal rate for cell preservation, and frozen at -80°C. For long-term storage, cells were transferred to liquid nitrogen. For usage, cells were defrosted in a 37°C water bath and resuspended in 5 mL of media before centrifugation at 1,200 rpm for 5 minutes. Supernatant was removed, 5 mL of media was added to the pellet and cells were seeded in a new flask.

2.2.2 HEK293T Cell culture

HEK293T cells were obtained from ATCC (line identifier CRL-1573) and grown under standard tissue culture conditions at 37 °C in 5% CO₂ in DMEM (Invitrogen) supplemented with 10% fetal bovine serum (Life Technologies). HEK293 cells are a specific cell line originally derived from human embryonic kidney cells grown in tissue culture and were chosen due to their easiness to work with and to transfect. Cell culture techniques were the same as fibroblast techniques, although grown in 175 cm² flasks. For passaging, 3 mL of .05% 1x Trypsin-EDTA (Life technologies) was added and flasks were placed in the incubator at 37°C for 5 minutes. 9 mL of pre-warmed media was added to stop the reaction and 4 mL of the solution was added to three new 175 cm² flasks to split cells. These were topped up to 25 mL.

2.2.3 Lymphoblast cell culture

Peripheral blood mononuclear cells were isolated from ACD blood by the Ficoll-Hypaque method (BD vacutainer CPT) and were send off to the European Collection of Cell Cultures (ECACC) for transformation with the Epstein Barr Virus. Two immortalised SMARD1 lymphoblastoid cell lines were send to us by Dr. Katja Von Au. Immortalised cells were grown in suspension in 75 or 175 cm² flasks in an upright position, in approximately 15 or 30 mL of RPMI-1640 (Invitrogen) medium that contained 2 mM L-glutamine and 20% (v/v) fetal bovine serum (FBS) and maintained in a humidified 5% CO₂ incubator at 37 °C. Media was routinely changed every 2 days by removing the medium above the settled cells and replacing it with an equal volume of fresh medium. Cells were counted by adding 10 µL of suspension to 10 µL of 0.4% trypan blue (Sigma-Aldrich). The result was pipetted onto a disposable slide and counted with an automated cell counter (Life technologies). For freezing, 1 mL of freezing media, consisting of RPMI-1640 with 10% DMSO, was added per 6 million cells and placed in a microvial.

2.3 Molecular biology

2.3.1 Constructs and generation of mutations by site-directed mutagenesis

FLAG epitope tagged wild type *IGHMBP2* construct was a kind contribution of Prof. Fischer in Germany. The backbone for this construct was a pCMV-Tag 4b (Fig. 2.1). To generate mutant forms of *IGHMBP2*, site directed mutagenesis was carried out using the QuikChange II mutagenesis kit (Agilent, Santa Clara, CA,

USA) according to the manufacturer's instructions. PCR product was then incubated with the restriction endonuclease Dpn1 for 1 hr at 37 °C to digest the parental supercoiled dsDNA and subsequently transformed into competent Top10 cells (Section 2.3.2). Constructs were sequenced prior to use and primer sequences used for the mutagenesis are listed in Table 2.8.

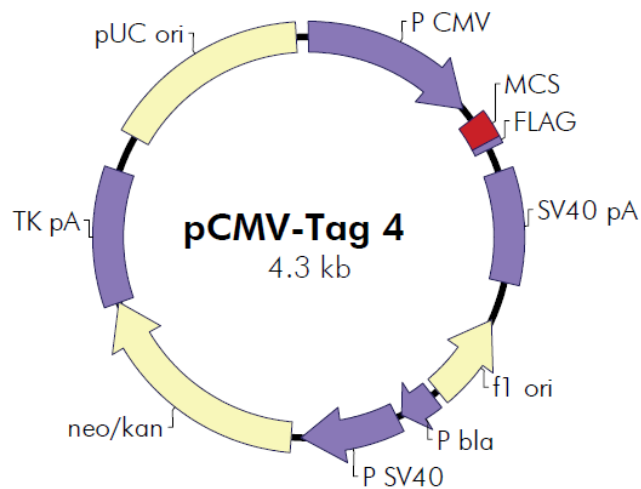


Figure 2-1 Circular map of the pCMV-Tag 4 vector.

Source: Instruction manual catalog #211174, Agilent technologies.

Mutation	Primer	Sequence
c.238A>G	Forward	5' – cgcggcagcttcccgtaacagcttacttc – 3'
	Reverse	5' – gaagtaaagctgttaccggaaagagctgccg – 3'
c.1591C>A	Forward	5' – ggtggacgctggttacagccgtg – 3'
	Reverse	5' – cacgggctgtaacaccagcgtccacc – 3'
c.1738G>A	Forward	5' – ccgtgatactgtccttcatcagatccaacaggaaa – 3'
	Reverse	5' – ttcctgttggatctgtgaaggacagtatcacgg – 3'

Table 2-8 Primer sequences for mutagenesis of the *IGHMBP2* construct.

2.3.2 Heat-shock transformation of competent Top10 E.Coli

Constructs were transformed into One Shot TOP10 Chemically Competent E.Coli cells (Invitrogen) using the manufacturer's protocol. 50 ng of DNA was added to 25 µL of competent cells and kept on ice for 30 minutes. The mixture was then placed in a 42°C water bath for 30-40 seconds to perform the heat-shock and returned on ice for a further 2 minutes. 200 µL of LB medium without antibiotics (20 g of LB broth

powder (Sigma-Aldrich) dissolved in 1 L dH₂O, followed by autoclaving) was then added under sterile conditions and was incubated in a shaker for 1 hour at 37°C. After this, transformed bacteria were grown on kanamycin-selective LB-agar plates (35 g of LB agar powder (Sigma-Aldrich) dissolved in 1 L dH₂O, followed by autoclaving) by spreading 100 µL of the mixture on the plate and incubating it at 37°C overnight.

2.3.3 Purification

Single bacterial colonies from agar plates were selected from LB-plates and added to 5 mL of LB broth containing 50 µg/mL of kanamycin. The cells were incubated overnight at 37°C under constant agitation. 2 mL of the resulting mixture was pelleted by centrifugation at 9000g for 3 minutes and DNA was extracted using the Qiagen GenElute™ Plasmid Miniprep Kit (Qiagen) according to the manufacturer's protocol. Glycerol stocks were made by adding 500 µL of 50% glycerol to 500 µL of bacterial mixture.

For large scale purification, 5mL of LB broth from the bacterial colony was incubated for 8 hours before inoculating a larger flask consisting of 150 mL of LB broth and containing 50 µg/mL of kanamycin with 300 µL of starter culture. This was incubated with vigorous shaking overnight and harvested the next morning by centrifugation at the maximum speed for 20 minutes. DNA was extracted using the Qiagen QiaFilter Plasmid Maxi kit (Qiagen) according to the manufacturer's protocol. Pelleted DNA was resuspended in 50 µL of sterile deionised water and concentration/ purity was measured according to section 2.1.2.

2.3.4 Stable transfection for Co-immunoprecipitation

2 µg of plasmid DNA and 4 µL polyethylenimine (PEI, Polysciences, Warrington, PA, USA) were each dissolved in 250 µL DMEM in a separate sterile eppendorf tube before mixing the two solutions together and leaving them to incubate for a minimum of 20 minutes at room temperature. During this incubation period, one or more 80% confluent 175 cm² flasks of HEK293T cells were trypsinised and collected in a 15 mL sterile tube. One 175cm² flask is sufficient for four 10 cm² dishes. After 20 minutes, the resulting mixture was plated on the appropriate number of 10 cm² dishes by covering the surface with drops. 3mL of suspended HEK293T cells were added to one 10cm² dish and media was topped up to 10mL. Transfected

cells were incubated for 48 hr post-transfection to obtain maximal levels of gene expression. PEI solution treated HEK293T cells were used throughout the study as control samples.

2.3.5 Stable transfection for ATPase assay

10 µg of plasmid DNA and 20 µL polyethylenimine (PEI, Polysciences, Warrington, PA, USA) were each dissolved in 500 µL DMEM in a separate sterile eppendorf tube before mixing the two solutions together and leaving them to incubate for a minimum of 20 minutes at room temperature. During this incubation period, three 80% confluent 175 cm² flasks of HEK293T cells were trypsinised and collected in a 50 mL sterile tube. One 175cm² flask is sufficient for two 15cm² dishes. After 20 minutes, the resulting mixture was plated on the appropriate number of 15cm² dishes by covering the surface with drops. 5mL of suspended HEK293T cells were added to a 15 cm² dish and media was topped up to 20mL. Transfected cells were incubated for 48 hr post-transfection to obtain maximal levels of gene expression. PEI solution treated HEK293T cells were used throughout the study as control samples.

2.4 Protein Biochemistry for HEK293T cell lines

2.4.1 Cell harvesting for Co-immunoprecipitation

Forty-eight hours after transfection, 10 cm² dishes of transfected HEK293T cells were washed with 2mL of ice-cold phosphate buffered saline (NaCl/Pi) prior to lysis. Cells were gently scraped off in NaCl/Pi, placed in a sterile Eppendorf tube and spun down for 1 minute at 4000 rpm. Pellet was resuspended in 350 µL of NP40⁺ buffer (50 mMTris pH 8, 150 mM NaCl, 0.5% NP40⁺) containing 1 × complete protease inhibitor cocktail (Roche, Indianapolis, IN, USA). Subsequently cell lysates were incubated for 10 minutes at 4 °C and freeze-thawed twice before spinning them at 14 000xg for 10 minutes to remove cell debris by centrifugation at maximum speed for 10 minutes. Supernatant was used straight away or stored at -80°C.

2.4.2 Co-immunoprecipitation

Lysates were thawed on ice or used straight after harvesting. 0.2% (v/v) RNase A was added and incubated at 37°C to detect RNA-independent interactions. Meanwhile, 30µL of ANTI-FLAG® M2 Affinity Gel (Sigma-Aldrich) was washed with 1mL of NP40⁺ buffer for 10 minutes at RT. Beads were spun down by centrifugation at 8000 rpm for 1 minute. 250 µL of the wild type and *IGHMBP2*

transfected cell lines was added to the beads and incubated overnight at 4 °C. The remaining 100 µL was kept for western blotting purposes. Depending on the species of the primary antibody (Table 2.9), goat anti-mouse IgG-HRP or goat anti-rabbit IgG-HRP was used in a 1:5000 dilution for the secondary antibody (Santa Cruz).

Primary antibody	Species	Concentration
Hint1, (Sigma-Aldrich)	Rabbit Polyclonal	1:1000
TDP43, clone AC-40 (Proteintech)	Rabbit Polyclonal	1:3000
FUS, AV40278 (Sigma-Aldrich)	Rabbit Polyclonal	1:10 000
SOD1, ADI-SOD-100 (Enzo Life sciences)	Rabbit Polyclonal	1:1000
HSP27, #2402 (Cell Signalling)	Mouse monoclonal	1:500
LAS11, SAB1409160 (Sigma-Aldrich)	Mouse polyclonal	1:5000

Table 2-9 Antibodies used for western blotting to detect interactions with the *IGHMBP2* protein after Co-immunoprecipitation.

2.4.3 Cell harvesting for ATPase assay

Forty-eight hours after transfection, 15 cm² dishes of transfected HEK293T cells were washed with ice-cold phosphate buffered saline (NaCl/P_i) prior to lysis. This was achieved by gently scraping off cells in 3 mL of NaCl/P_i, placing the solution in 2 sterile Eppendorf tubes and spinning down for 1 minute at 4000 rpm. Pellet was resuspended in 1 mL of NP40⁺ buffer (50 mMTris pH 8, 150 mM NaCl, 0.5% NP40⁺) containing 1 × complete protease inhibitor cocktail (Roche, Indianapolis, IN, USA). Subsequently cell lysates were incubated for 30 minutes at 4 °C and freeze-thawed twice before spinning them at 14 000xg for 10 minutes to remove cell debris by centrifugation at maximum speed for 30 minutes. Supernatant was used straight away or stored at -80°C.

2.4.4 ATPase assay

Frozen down lysates were thawed on ice or used straight after harvesting. 900 µL of the wild type and mutant *IGHMBP2* supernatants were incubated with 40 µL ANTI-FLAG® M2 Affinity Gel (Sigma-Aldrich) overnight at 4 °C, after preparing the beads by washing 2x with cold PBS. The next day beads were washed 2 × in each of three wash buffers (20 mM Tris, 1000-200 mM NaCl, 1% Triton) before being eluted in elution buffer (50 mMTris pH 8, 150 mM NaCl, 0.5% NP40⁺, 1x protease inhibitor cocktail) with 150 ng·µL⁻¹ FLAG peptide (Sigma-Aldrich) for 40 minutes at

4 °C. Eluted protein was then incubated with assay buffer (20 mM Hepes, pH 7.2, 2 mM MgCl₂, 1 mM dithiothreitol and 0.05% BSA) and [α^{32} P]ATP (5 μ Ci; Perkin Elmer, Waltham, MA, USA) was added to each reaction. Samples were incubated at 37 °C with vigorous shaking and 2 μ L aliquots were removed at time points from 0 to 120 minutes and spotted onto TLC plates (Sigma-Aldrich). Samples were then subjected to rising TLC under 1 M formic acid and 1.2 M LiCl. After drying the plates they were exposed to Kodak biomax films (Kodak, Rochester, NY, USA) overnight and developed the following day using a Kodak developer. The remaining samples were denatured in 4 \times SDS loading buffer (NuPage SDS sample buffer, Life Technologies) with 1% DTT at 75 °C for 10 minutes and loaded onto 4–12% Bis Tris gels (Life Technologies). Proteins were then transferred to Hybond ECL Nitrocellulose membrane (GE life sciences), blocked with 5% milk in NaCl/P_i-Tween (NaCl/P_i + 1% Tween-20) and probed with primary antibodies at 4 °C overnight (1: 1000 Mouse anti-IGHMBP2, clone mAb11-24, millipore). The next day membranes were washed three times in NaCl/P_i-Tween and incubated for 1 h with secondary antibodies in 1% milk in NaCl/P_i-Tween at room temperature followed by another three washes and incubation with Pierce ECL substrate. Finally membranes were exposed to Kodak biomax films (Kodak, Rochester, NY, USA) and developed on a Kodak developer according to the manufacturer's instructions.

2.5 Protein biochemistry for fibroblast cell lines

2.5.1 Cell harvesting for mRNA extraction

2 mL of 0.05% 1x Trypsin-EDTA (Life technologies) was added to a confluent 75cm² flask of fibroblasts and placed in the incubator at 37°C for 5 minutes. In case of unsufficient detachment, flasks were tapped against the surface before adding 7 mL of pre-warmed media to stop the reaction. Cell were pelleted by centrifugation at 1200 rpm for 5 minutes and resuspended in 6mL of media. 1mL was added in duplicate to 1 well of a 6 well plate and remaining solution was used to passage the cell line. After 24-48h, cells were harvested by adding 1mL of cold NaCl/P_i on ice, gently scraping off the cells to transfer to a new sterile Eppendorf tube and spinning down the pellet by centrifugation at 4000 rpm for 1 minute. Pellet was resuspended in 350 μ L of QIAzol® reagent (Invitrogen, United States) and used straight away or kept at -80°C.

2.5.2 mRNA extraction

RNA was extracted from fibroblasts using the miRNeasy Mini kit (Qiagen). An amount of 1 million cells was used, correlating to the amount of cells in a confluent well of a 6-well plate. A volume of 350 µL of 70% ethanol was added to the QIAzol® cell suspension and mixed well by pipetting up and down. Sample was transferred to a RNeasy mini spin column placed in a 2mL collection tube and centrifuged at 8000g for 15 minutes. RNA was extracted following the manufacturer's protocol, and eluate was suspended in 50 µL of RNase-free water. Concentration and purity was estimated as stated in section 2.1.2 with altered absorbance ratios for RNA. Samples were expected to have a value of >2.0 for the 260/280 ratio and in the range of 2.2-2.2 for 260/230.

2.5.3 cDNA synthesis

cDNA was synthesised using 500 ng total RNA, random primers and SuperScript II reverse transcriptase (Invitrogen, United states) following the manufacturer's protocol. The resulting cDNA was used to perform a standard PCR reaction with cDNA primers spanning the exon/intron boundaries. Subsequent agarose gel electrophoresis was used to confirm the expression of cDNA in the fibroblasts. Sequencing analysis was performed to investigate the presence of genomic DNA mutations in the RNA of patients and to assess nonsense mediated decay.

2.5.4 Quantitative PCR

The *IGHMBP2* cDNA transcript levels were determined in triplicate using Glyceraldehyde-3-phosphate dehydrogenase (*GAPDH*) and hypoxanthine phosphoribosyltransferase 1 (*HPRT1*) as reference genes. 1µL of cDNA at 500 ng/µL was added to 12.5 µL of SybrGreen, 1 µM of each primer and topped up to 25 µL with RNase-free water. Primers used for *IGHMBP2* cDNA levels were used from the paper by Guenther et al., in 2009. Reference genes primers were validated beforehand by other groups in the department. Accumulation of PCR products was monitored through SYBR green incorporation on an Stratagene/Agilent MX3000P with the protocol stated in Table 2.10.

Step	Reaction step	Temperature	Time
1	Carryover prevention	50°C	2 min
2	PCR initial activation step	95°C	10 min
3	Denaturation	95°C	15 sec
4	Annealing primers	60°C	30 sec
5	Elongation	72°C	30 sec
6	Final elongation	72°C	10 min

Table 2-10 Protocol for quantitative PCR. Steps 3-5 were repeated 40 times.

Relative quantities were calculated with the $\Delta\Delta Ct$ method (Schmittgen et al., 2008) in relation to the two housekeeping genes. Gene expression levels were calculated by the ratio between the amount of target gene and two endogenous reference genes, which is present in all samples. The Ct threshold value is chosen as the cycle in which there is a significant increase in reporter signal. This value is related to the initial amount of DNA in inverse proportion to the expression level of the gene (Fig. 2.2). Firstly, the ΔCt between the target gene and the reference genes was calculated for each sample ($\Delta Ct = Ct_{\text{target}} - Ct_{\text{reference gene}}$). Then the difference between the ΔCt of the patient and the ΔCt of the controls was calculated, giving the $\Delta\Delta Ct$ value: $\Delta\Delta Ct = (Ct_{\text{target}} - Ct_{\text{reference}})_{\text{control}} - (Ct_{\text{target}} - Ct_{\text{reference}})_{\text{patient}}$. The normalised target amount in the sample is then equal to $2^{-\Delta\Delta Ct}$ and can be used to compare expression levels in samples. The data were depicted as a mean with standard deviation.

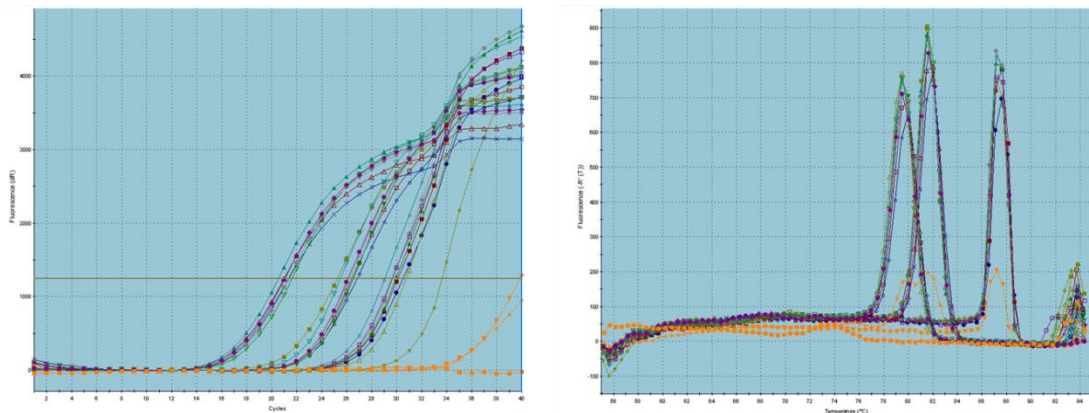


Figure 2-2 Sample plot of the amplification curves (left) and the dissociation curves (right) for the selected primers of the qPCR experiment in lymphoblasts. The orange-coloured curves not reaching the threshold of detection represent the “no template” controls.

2.5.5 Cell harvesting for western blot

2 mL of 0.05% 1x Trypsin-EDTA (Life technologies) was added to a confluent 75cm² flask of fibroblasts and placed in the incubator at 37°C for 5 minutes. In case of unsufficient detachment, flasks were tapped against the surface before adding 7 mL of pre-warmed media to stop the reaction. Cell were pelleted by centrifugation at 1200 rpm for 5 minutes and washed in 1 mL of cold NaCl/Pi. Cells were pelleted again by centrifugation at 4000 rpm for 1 minute and resuspended in 50 µL of NP40⁺ buffer (50 mMTris pH 8, 150 mM NaCl, 0.5% NP40⁺) containing 1 × complete protease inhibitor cocktail (Roche, Indianapolis, IN, USA). Subsequently cell lysates were incubated for 10 minutes at 4 °C and freeze-thawed twice before spinning them at 14 000xg for 10 minutes to remove cell debris by centrifugation at maximum speed for 10 minutes. Pellet was stored in -80 °C and supernatant was used straight away or stored at -80°C.

2.5.6 Protein estimation

1 µL of each sample was pipetted in triplicate on a 96-well plate together with a BSA standard ranging from 0-7 µg/µL. 1 µL of NP40⁺ buffer was added to each well of the standard to account for background signal. RC DC™ Protein Assay (BioRad) was used according to the manufacturer's protocol and cell sample protein concentrations were calculated from the standard curve prepared by plotting the average blank-corrected 562nm measurement for each BSA standard vs. its average concentration in µg/µL.

2.5.7 Western blot

60 µg of protein was mixed with 1x NuPage LDS sample buffer (Invitrogen), 1% DL-Dithiothreitol (Invitrogen) and made up to the same volume with the NP40⁺ buffer before denaturation at 75°C for 10 minutes. Samples, accompanied by a marker, were run on a 4-12% Bis-Tris gel for 90 minutes under 150 V in 1xMES running buffer (100 mL 20x NuPAGE MES SDS running buffer (Life Technologies) in 1,900 mL dH₂O.). All gels were electro-blotted to Hybond ECL membrane (GE lifesciences) in transfer buffer (20% methanol, 10% Tris-glycine electroblotting buffer 10X (National Diagnostics, USA) and 70% dH₂O) and the membrane was immersed in Ponceau red (Sigma-Aldrich) to verify protein transfer. Blocking was performed in 5% (w/v) milk powder in 1x NaCl/Pi (1 PBS tablets (Life Technologies) dissolved in 500 mL of dH₂O) for 1 hr at room temperature.

Membranes were incubated overnight with the primary antibody at 4°C, diluted to their respective concentrations in 1% milk in NaCl/Pi-Tween (Table 2.11). The following day, after 3x washing in 1x NaCl/Pi-Tween for 10 minutes, the membrane was incubated for 60 min at room temperature with horseradish peroxidase-conjugated secondary antibody (Santa Cruz). Depending on the species of the primary antibody, goat anti-mouse IgG-HRP or goat anti-rabbit IgG-HRP was used in a 1:5000 dilution. An ECL kit with each ECL reagent at a 1:1 ratio (Thermo Fisher Scientific) was used as a substrate and antibody binding was detected in a dark room on Super Rx X-ray film (Fujifilm, Japan) in an Amersham autoradiography cassette (GE Healthcare). β-Actin was used as a loading control for normalisation and analysis was performed with the ImageJ program (Rasband, W.S., ImageJ, U. S. National Institutes of Health, Bethesda, Maryland, USA, <http://imagej.nih.gov/ij/>, 1997-2014).

Primary antibody	Species	Concentration
IGHMBP2, clone mAb11-24 (Millipore)	Mouse monoclonal	1:1000
B-Actin, A3853 (Sigma-Aldrich)	Mouse monoclonal	1:20 000
TDP43, clone AC-40 (Proteintech)	Rabbit polyclonal	1:3000

Table 2-11 Primary antibodies used for western blotting.

2.6 Immunocytochemistry

2.6.1 Subcellular localisation of proteins in patient fibroblasts

Fibroblasts were cultured onto 13 mm autoclaved glass coverslips in 24-well plates in standard DMEM + Glutamax media supplemented with 10% FBS and 1% PenStrep after placing the plate under UV light for at least 20 min. After 24h, cells were washed with cold NaCl/Pi and fixed in 4% paraformaldehyde (PFA) for 15 minutes. Cells were washed again with NaCl/Pi and permeabilised in 0.05% Triton X-100 for 10 minutes. After three more washes with NaCl/Pi, cells were then blocked in 10% FBS in NaCl/Pi for one hour. Cover slips were incubated with 40 µL of primary antibody for 60 minutes (Table 2.12), washed three times with NaCl/Pi and incubated with the appropriate Alexa Fluor secondary antibody for 60 minutes (Invitrogen, United States). Following, the cover slips were washed with NaCl/Pi and mounted on microscope slides with Prolong Gold Antifade with 4',6-diamidino-2-phenylindole (DAPI) (Life Technologies) and imaged using a Zeiss 710 confocal

microscope (Carl Zeiss AG, Germany) with the 63x oil immersion objective. A negative control (incubated overnight in blocking solution only, with no primary antibody) was included to assess the specificity of the secondary antibody.

Antibody	Species	Concentration
TRAK2 Antibody 13770-1-AP (Protein Tech)	Rabbit polyclonal	1:1000
TDP43, clone AC-40 (Proteintech)	Rabbit monoclonal	1:3000
IGHMBP2, clone mAb11-24 (Millipore)	Mouse monoclonal	1:1000
Alexa Fluor 488-A11008 secondary antibody	Goat anti- rabbit	1:2000
Alexa Fluor 488-A11001 secondary antibody	Goat anti-mouse	1:2000
Alexa Fluor 555-A21428 secondary antibody	Goat anti-rabbit	1:2000

Table 2-12 Primary and secondary antibodies used for Confocal imaging.

2.6.2 Colocalisation

Fibroblasts were prepared as described in section 2.6.1. After cells were blocked in 10% FBS in NaCl/Pi for one hour, cover slips were incubated with 40 µL of the combined primary antibodies for 60 minutes (Table 2.12), washed three times with NaCl/Pi and incubated with a combination of Alexa Fluor secondary antibodies for 60 minutes (Invitrogen, United States). Following, the cover slips were washed with NaCl/Pi and mounted on microscope slides with Prolong Gold Antifade with 4',6-diamidino-2-phenylindole (DAPI) (Life Technologies) and imaged using a Zeiss 710 confocal microscope (Carl Zeiss AG, Germany) with the 63x oil immersion objective. A negative control (incubated overnight in blocking solution only, with no primary antibody) was included to assess the specificity of the secondary antibody. Image processing and evaluation were performed using the Volocity software (Perkin Elmer). Thresholds were set manually by drawing a region of interest and the global Pearson's correlation coefficients were extracted. The experiment was performed in triplicate and the average global Pearson's correlation coefficient of selected cells of the field of view was calculated from 3 images per cover slip.

2.6.3 Endocytosis investigation

Fibroblasts were grown overnight on 13 mm cover slips in standard DMEM + Glutamax media supplemented with 10% FBS and 1% PenStrep. Cover slips were then incubated at 37°C in labelling medium (F12 containing 10 mM HEPES, pH 7.3 and 0.2% w/v BSA) for 1h, where after they were labelled for 1h on ice with 50

$\mu\text{g/mL}$ Alexa-Fluor 488-transferrin (Invitrogen) in labelling medium. Excess label was washed off by rinsing twice with warm labelling medium and cells were incubated for either 20 or 30 minutes at 37°C to allow transferrin uptake. Following, the cells were fixed with 2% paraformaldehyde in NaCl/P_i for 30 minutes at room temperature, washed twice with 1x NaCl/P_i and mounted on microscope slides with Prolong Gold Antifade with DAPI and imaged using a Zeiss 710 confocal microscope (Carl Zeiss AG, Germany) with the 63x oil immersion objective.

Image processing and evaluation were performed using the Volocity software (Perkin Elmer). The experiment was performed in duplicate and triplicate for the respective incubation times of 20 and 30 minutes and the average fluoresce/volume of selected cells of the field of view was calculated from 9 images after an incubation time of 30 minutes.

2.6.4 Basal mitochondrial membrane potential

The basal mitochondrial membrane potential ($\Delta\Psi_m$) was measured using the tetramethylrhodamine methyl ester (TMRM) lipophilic cationic dye. This dye accumulates in the mitochondria and is released in the cytosol when the mitochondria become depolarised, which results in a decrease of signal intensity. The fluorescence intensity of the dye is representative of the $\Delta\Psi_m$ as a more polarised (more negative) $\Delta\Psi_m$ will accumulate more dye and give a stronger fluorescence signal, whereas depolarised mitochondria accumulate less dye and exhibit a lower TMRM signal. Patient and control fibroblasts were grown in standard media and plated overnight on 25 mm cover slips in 6 well plates. An extra cell line with fibroblasts from the patient with the p.Ser700Ile variant was used as a control. Fibroblasts were incubated for 40 minutes at room temperature with 25 nM TMRM (Invitrogen) in a HBSS solution composed of 156 mM NaCl , 3 mM KCl , 2 mM MgSO_4 , 1.25 mM KH_2PO_4 , 2 mM CaCl_2 , 10 mM glucose and 10 mM HEPES; pH adjusted to 7.35 with NaOH. The dye was present throughout the experiment. The Zeiss 710 confocal microscope (Carl Zeiss AG, Germany) was used to obtain z-stack images using a 63x oil immersion objective and a 560 nm laser to excite the dye. Data was analysed using the Zeiss image analysis software (Zeiss). To control for mitochondrial mass, the TMRM signal was averaged across all the voxels corresponding to mitochondria whose fluorescence was greater than the set threshold.

2.6.5 Response to mitochondrial toxins

For analysis of response to mitochondrial toxins, 25 mm cover slips were used after measurement of the mitochondrial membrane potential. Images were recorded continuously from a single focal plane and a time-series was used to add the mitochondrial toxins. After measuring baseline TMRM intensity for 2-3 min, oligomycin from *Streptomyces diastatochromogenes* (2 µg/mL; Sigma-Aldrich) was added and fluorescence measured until a plateau was reached, after which rotenone (10 µM; Sigma-Aldrich) was added. Lastly, 1 µM FCCP ($\geq 98\%$; Sigma-Aldrich) was added and recordings were stopped when the mitochondria had fully depolarised. The effects of each drug are the following:

Oligomycin: Complex V inhibitor

If ATPase function is reversed to maintain the $\Delta\Psi_m$, there will be a decline in TMRM fluorescence

Rotenone: Complex I inhibitor

This will cause a small decline in TMRM fluorescence; if cells rely more on complex I than complex II, there will be a greater decline.

FCCP: Uncouples oxidation from phosphorylation so ATP synthesis cannot occur. This will result in an immediate depolarisation of the $\Delta\Psi_m$ and loss of fluorescence.

Time-series data were analysed using the Zeiss Zen software (Carl Zeiss AG). A total of 10-20 areas were selected for analysis and the average dye intensity across these areas was plotted on the y-axis against time on the x-axis. The change in TMRM intensity after addition of each toxin was expressed as a percentage of basal intensity (basal=baseline $\Delta\Psi_m$ - $\Delta\Psi_m$ after FCCP).

2.7 Statistical analysis

All statistical analyses were performed using GraphPad Prism version 6.00 for Windows/Mac (GraphPad Software, La Jolla California USA, www.graphpad.com). For comparison of means of two groups, parametric student t-test was used and statistical significance expressed as * $p < 0.05$; ** $p < 0.01$. For comparison of means of $>$ two groups, a bonferroni post-hoc analysis was used after a one-way analysis of variance (ANOVA). Unless otherwise stated, experiments were

performed at least three times and data presented as mean \pm standard error of the mean (S.E.M.).

Chapter 3:

Mitochondrial mutations in CMT2

3.1 Introduction

3.1.1 A role for mitochondria in neurodegenerative diseases

As seen in Chapter 1, an essential process in the maintenance of neurons is the provisioning of ATP, which will maintain the neuronal plasma membrane potential. As mitochondria are the main source of ATP, correct mitochondrial function is crucial for efficient axonal transport of all cargoes (Schon et al., 2011). Since the central and peripheral nervous systems have intense metabolic requirements and are particularly ATP dependent, any deficit in energy generation can have catastrophic effects on neural functioning. It has already been shown that mitochondrial dysfunction plays a relevant role in the pathogenesis of neurological and neuromuscular diseases such as CMT (Palau et al, 2009) and apart from the dysfunction of mitochondrial dynamics that can lead to CMT, impaired mitochondrial function, communication with other organelles and mitochondrial turnover can lead to neurodegenerative diseases such as Parkinson's disease (PD),

spinocerebellar ataxias (SCA), HSP, Huntington's disease (HD), Amyotrophic lateral sclerosis (ALS) and progressive epilepsy (Zsurka et al., 2013).

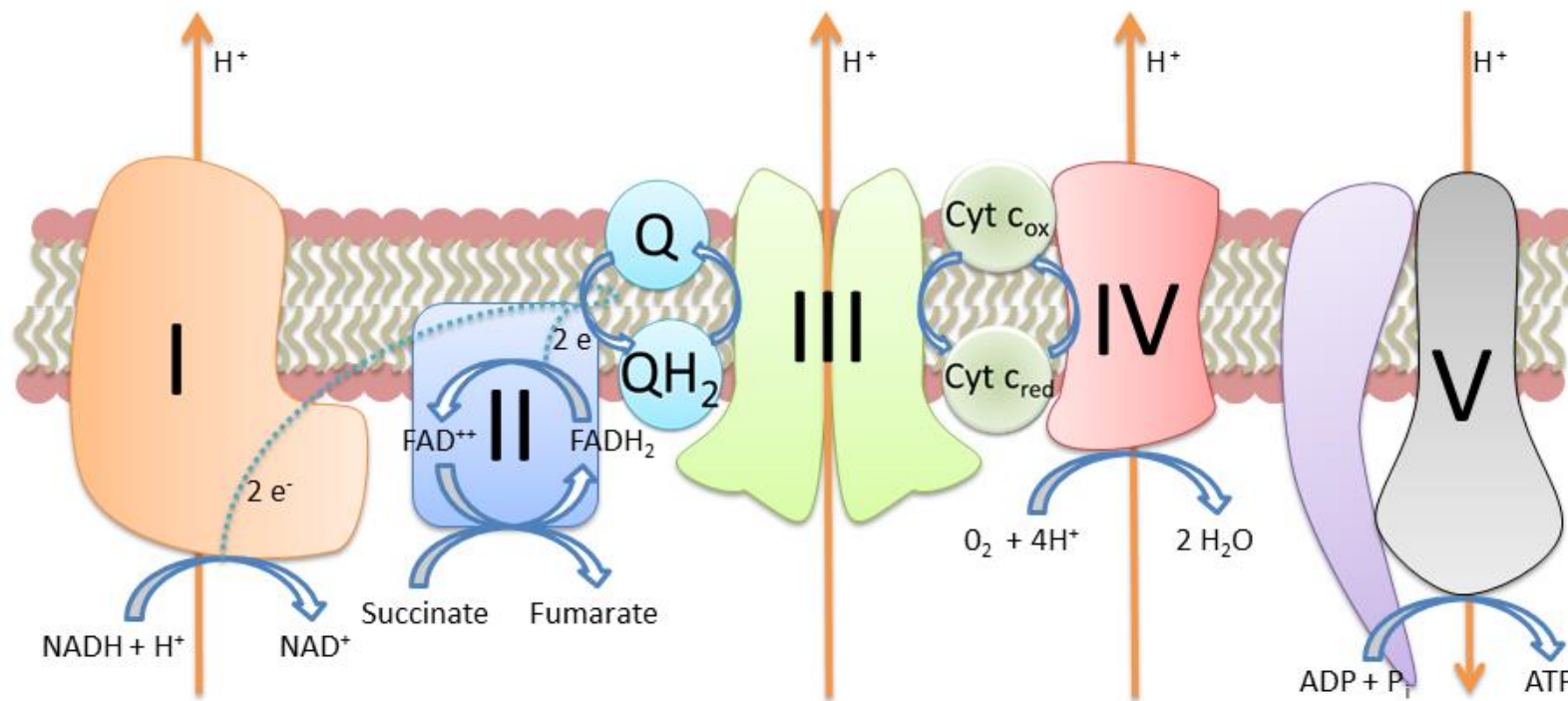
3.1.2 The oxidative phosphorylation system

The oxidative phosphorylation system (OXPHOS) is a set of biochemically linked multisubunit complexes (complexes I to V) and two electron carriers (ubiquinone/coenzyme Q and cytochrome c) that, together with the tricarboxylic acid (TCA) cycle, provides a mechanism for the production of ATP through a proton gradient (Fig. 3.1). The complexes form an electron transport chain (ETC) in the inner mitochondrial membrane, where complexes I-IV reduce molecular oxygen to water by the sequential transfer of electrons, called oxidative phosphorylation. These redox reactions release energy to form a proton gradient across the inner mitochondrial membrane that will catalyse the formation of ATP from ADP and inorganic phosphate by the ATP synthase or respiratory chain complex V (Capaldi et al., 1994; Nijtmans et al., 1995).

Complex I is the first enzyme in the ETC and is responsible for the oxidation of NADH by transferring electrons to ubiquinone, a lipid soluble electron carrier embedded in the lipid bilayer of the inner mitochondrial membrane. It is made of 45 proteins of which seven are encoded by the mitochondrial genome. This enzyme consists of three different domains and is also known as NADH-coenzyme Q oxidoreductase. The dehydrogenase domain will transfer two electrons from reduced Nicotinamide Adeninedinucleotide (NADH), oxidizing it to NAD⁺, via Flavin mononucleotide (FMN) to iron sulphur clusters. In the hydrogenase domain, these will reduce ubiquinone to ubiquinol. This electron transfer is coupled to the transfer of 4 protons in the transporter domain from the inner membrane of the matrix to the intermembrane space (Lenaz et al., 2006; Fato et al., 2008). Complex I can be inhibited by more than 60 different families of compounds, one of which is rotenone, regularly used as an inhibitor of complex I in mitochondrial membrane imaging.

Complex II, also known as Succinate-Q oxidoreductase, consists of four subunits and is the only complex in the ETC that lacks subunits encoded by the mitochondrial genome. It is also the only enzyme that plays a role in both the ETC and the TCA cycle, linking the two essential energy-producing processes of the cell.

Intermembrane space



Mitochondrial matrix

Figure 3-1 The oxidative phosphorylation system in the inner mitochondrial membrane. Cyt c= Cytochrome c; FAD= Flavine Adeninedinucleotide; NAD= Nicotinamide Adeninedinucleotide; Q= Ubiquinone; QH₂= Ubiquinol.

As part of the TCA cycle, complex II oxidises the metabolite succinate to fumarate in the mitochondrial matrix by transferring the electrons to flavin adenine dinucleotide (FAD), resulting in the formation of FADH₂. The two electrons generated will enter the ETC by passing them on to three Fe-S clusters and cytochrome b and subsequently transforming ubiquinone to ubiquinol in the mitochondrial inner membrane (Cecchinni, 2003; Kluckova et al., 2013).

Complex III is composed of 11 subunits; cytochrome b is encoded by mitochondrial DNA, with the remainder of the subunits being encoded by nuclear DNA genes. This enzyme is a dimer, with each subunit complex containing the 11 protein subunits, an iron-sulfur cluster and three cytochromes: one cytochrome c₁ and two b cytochromes. Also known as Q-cytochrome c oxidoreductase, this complex will catalyse the transfer of electrons from reduced ubiquinone to cytochrome c and will utilise the energy to translocate protons from the mitochondrial matrix to the intermembrane space, adding to the proton gradient (Berry et al., 2000; Barel et al., 2008).

Complex IV is the last complex of the ETC, also known as cytochrome c oxidase. This complex contains three mitochondrial encoded subunits and ten nuclear encoded ones and has a complicated structure that includes two copper-containing redox centres, and two cytochromes, aa₃, containing heme a moieties. It catalyses the oxidation of cytochrome c and the reduction of oxygen by transferring electrons to the terminal electron acceptor oxygen, reducing it to water. This will again contribute to the proton gradient (Calhoun et al., 1994).

Human F₀F₁-ATP synthase (Complex V of the oxidative phosphorylation system) couples the synthesis of ATP from ADP and inorganic phosphate with the passage of protons from the intermembrane space to the matrix (Noji et al, 2001; Jonkheere et al., 2012) (Fig. 3.2). This complex is comprised of 16 subunits, of which 14 are encoded by the nuclear genome and two by nucleotides 8527-9207 of the mitochondrial genome (*ATPase 6* and *ATPase 8*). Complex V is a massive structure consisting out of a ‘stalk’ - the F₀ particle – that is embedded in the mitochondrial membrane and forms the proton channel, and a ‘head’ - the F₁ particle – as the site of ATP synthesis. During ATP synthesis, protons are transferred through the

channel, causing rotation of the F1 particle, which condenses ADP and inorganic phosphate to form ATP.

3.1.3 Mutations in the OXPHOS genes in patients with peripheral neuropathy

Peripheral neuropathies have been linked to mutations in the OXPHOS genes; however, the neuropathy is rarely the presenting or predominant clinical manifestation of the disease. In contrast, patients presenting with mutations in nuclear-encoded mitochondrial genes such as *MFN2* or *GDAP1* typically present with an isolated peripheral neuropathy.

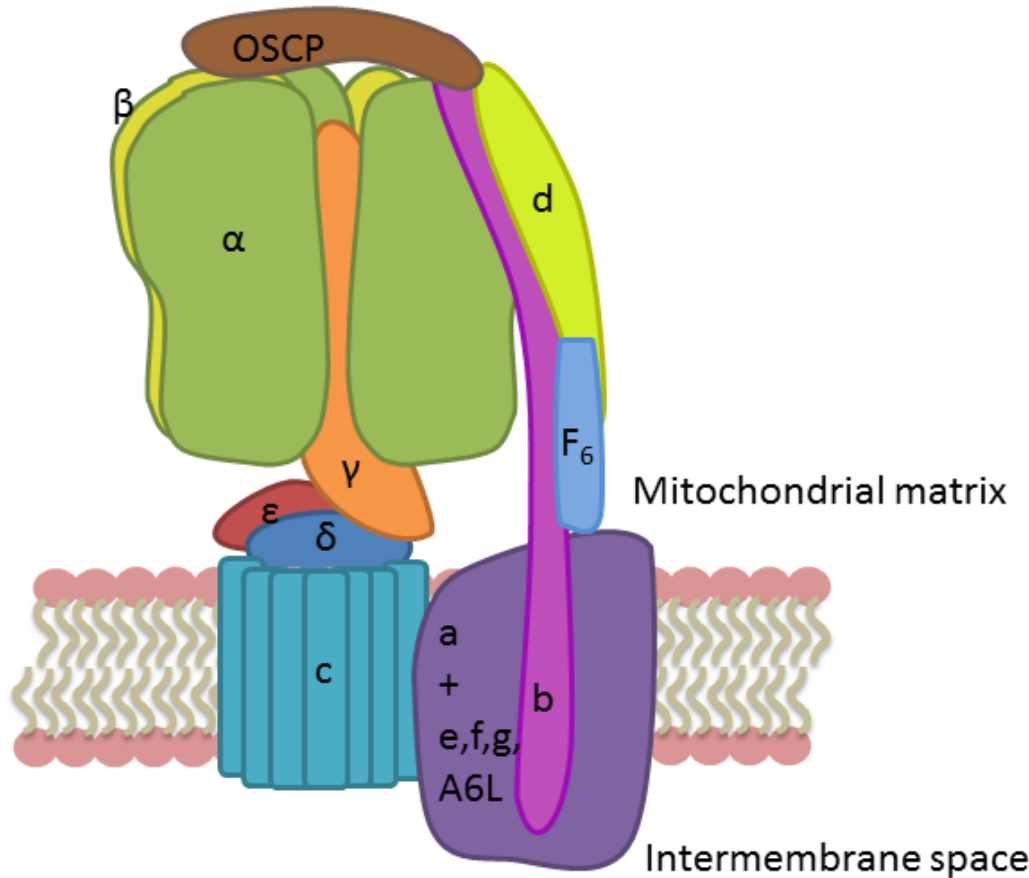


Figure 3-2 The human ATP synthase. F1 is composed of three copies of each of subunits α and β , and one each of subunits γ , δ and ε , forming the central stalk. F0 consists of a subunit c-ring and one copy each of subunits a, b, d, F6 and the oligomycin sensitivity-conferring protein (OSCP). Subunits b, d, F6 and OSCP form the peripheral stalk which lies to one side of the complex. A number of additional subunits (e, f, g, and A6L), all spanning the membrane, are associated with F0.

In the scope of this thesis, we investigated an extensive family with mitochondrial disease and axonal neuropathy in which the index case presented with a pure motor neuropathy in childhood evolving into motor-predominant CMT2 in later life and found a pathogenic missense mutation m.9185T>C in *ATPase 6*, encoding the ATP6 subunit of the mitochondrial ATP synthase (OXPHOS complex V). This segregated with disease in affected members of the pedigree.

3.1.4 Mutations in ATP synthase

Mutations in respiratory chain complex V are known to cause Leigh syndrome or Neurogenic muscle weakness, Ataxia and Retinitis Pigmentosa (NARP) (Holt et al., 1990; Rahman et al., 1996; De Coo et al., 1996). In our study, we found two mutations in the gene encoding for respiratory chain complex V, located on the mitochondrial genome: m.9185T>C, substituting a leucine for a proline and m.8993T>C, causing the same AA-substitution. The presence of these mutations confirms the link between mitochondrial dysfunction and neurodegeneration and the importance of this system in CMT.

In order to examine the prevalence of this mutation and the importance of other variants in the mitochondrial genome, I investigated a large number of patients with CMT2, HMN and HSAN for mutations in the *ATPase 6* gene and the partially overlapping *ATPase 8* gene, the only other mitochondrially encoded subunit of complex V of the respiratory chain. Since the overall phenotype in the CMT2 patient was a severe axonal neuropathy, a number of CMT1 patients was included, to examine whether this mutation could influence the severity of the neuropathy.

3.1.5 Mitochondrial genetics in humans

Following the endosymbiotic theory, mtDNA is derived from the circular genomes of the bacteria that were engulfed by the early ancestors of today's eukaryotic cells. This separate evolutionary origin gives rise to some distinct features that distinguish nuclear from mitochondrial DNA.

Each mitochondrion present in human cells will contain several copies of the circular, covalently closed, double-stranded mitochondrial DNA. This results in the presence of 100-10,000 separate copies of mtDNA per cell. There are no histones or any other proteins associated with mitochondrial DNA and the genes contain no introns. As a consequence of this lack of protective histones and the highly oxidizing

environment there is a much higher rate of mutations than nuclear DNA (Wei et al., 1998; Sigurgardottir et al., 2000).

The mitochondrial genome

The mitochondrial genome encodes for 37 genes and contains around 16,600 base pairs. These genes encompass mitochondrial ribosome subunits, transfer RNAs and subunits of the ETC. Twenty-eight out of 37 are located on the mitochondrial heavy-strand (H-strand), so called due to its high content of guanine. The opposing light strand (L-strand), mainly consisting of cytosines, encodes the remaining nine genes. For replication and transcription, the mitochondrial DNA relies on a set of nuclear gene products, after having lost the self-provisional qualities it had as a prokaryote. The genetic code is, for the most part, universal, with few exceptions: mitochondrial genetics includes some of these. For most organisms the "stop codons" are "UAA", "UAG", and "UGA". In vertebrate mitochondria "AGA" and "AGG" are also stop codons, but not "UGA", which codes for tryptophan instead. "AUA" codes for isoleucine in most organisms but for methionine in vertebrate mitochondrial mRNA (Barrell et al., 1979).

Inheritance of mitochondrial variants

In contrast to nuclear DNA, mitochondrial DNA gets passed on to future generations by maternal inheritance only. An oocyte will carry around 100,000- 1,000,000,000 mtDNA copies, whilst a spermatozoid will only carry 100-1000 copies, which will be degraded by ubiquitination (Sutovsky et al., 1999).

An important concept in mitochondrial inheritance is the existence of the genetic bottleneck. Only a fraction of the mtDNA copies in the germ-cell precursor are amplified to generate the approximately 105 mtDNA copies present in the mature oocyte. During maturation, this specific subpopulation of genomes will be rapidly replicated. Depending on which oocyte will be fertilised, this can result in different populations of mtDNA in the offspring. In the presence of mutated mtDNA, a different mutant load can be found between family members (Taylor et al., 2005).

Recent evidence also suggests a higher selectivity against nonsynonymous changes in protein-coding genes, resulting in a reduction of mutations in following generations. Differences have been found between different sites of mutations, resulting in levels that cause no phenotype at a lower level but can cause a disease-

like phenotype at higher levels (Taylor et al., 2005; Stewart et al., 2008; Samuels et al., 2010).

Mitochondrial diseases

Several disorders affecting the nervous system, the muscles, or both are caused by mutations (acquired or inherited) in mitochondrial DNA or in nuclear genes that code for mitochondrial components; these may be collectively called mitochondrial diseases. Mitochondrial abnormalities have been found in several neurodegenerative disorders, in multiple sclerosis and in an increasing number of axonal inherited neuropathies (Chinnery, 2010).

Mitochondrial diseases take on unique characteristics both because of the way the diseases are inherited and because mitochondria are so critical to cell function. Along with regulation of apoptosis, mitochondria also modulate cell pathogenesis by means of energy production, heme synthesis, heat production, reactive oxygen species (ROS) generation, and calcium buffering. Patients with mitochondrial diseases typically present with multi-system involvement, due to the critical importance of ATP for all the organ systems. Primary symptoms can range from seizures and liver failure, to cerebellar ataxia and myopathy. In the case of peripheral neuropathies, these can either manifest as primary or additional features and NCS usually point towards a predominantly axonal sensorimotor polyneuropathy (Chinnery, 2010).

Since every cell in the human body has several copies of the mtDNA, mutations residing within the mtDNA can exist in a homoplasmic state, where all the mtDNA molecules are either wild type or mutated, or in a heteroplasmic state, where varying levels of mutated and wild type mtDNA can coexist in one single cell.

The vast majority of mtDNA mutations require high levels of mutated mtDNA necessary before a phenotype is observed in cells. The threshold effect is suggested to result from a loss of wild type mtDNA molecules, and below a critical level of wild type mtDNA, a functional defect within a cell is likely to be obtained (Lax et al, 2011). As mentioned before, mitochondrial DNA is only transferred by the ovule during the impregnation, which means that mitochondrial diseases will show a

pattern of maternally inherited syndromes. Since the precursor cells for the ovule only replicate a limited amount of mitochondria, which are randomly distributed, different ovules encompass a range of mutant mtDNA levels, causing offspring to have variable disease severity (Taylor et al., 2005).

Leigh Syndrome

The pathogenic mutations found in our group of patients, m.9185T>C and m.8993T>C, are known to cause Leigh syndrome and NARP. Leigh syndrome is an early-onset progressive neurodegenerative disorder with a characteristic neuropathology consisting of focal, bilateral lesions in one or more areas of the central nervous system, including the brainstem, thalamus, basal ganglia, cerebellum, and spinal cord. The lesions are areas of demyelination, gliosis, necrosis, spongiosis, or capillary proliferation. Clinical symptoms depend on which areas of the central nervous system are involved, but often include hypotonia, spasticity, movement disorders, hypertrophic cardiomyopathy, cerebellar ataxia, and peripheral neuropathy. Onset of disease is typically between 3 to 12 months, frequently following a viral infection (Dahl, 1998; Thorburn et al., 2003).

Leigh syndrome is a progressive disease, often with poor prognosis. Death occurs usually within the first decade of life, frequently due to respiratory failure due to brain stem lesions or cardiac failure. No effective treatments have been established so far and management of the disease mainly includes education and support for the patients and their family, whilst monitoring progression of neurologic, ophthalmologic and cardiologic features. Seizures, dystonia, acidosis, cardiomyopathy and other complications are treated separately when appropriate (Koene et al., 2011).

A high genetic heterogeneity exists between patients with Leigh syndrome and transmission can be X-linked recessive, autosomal recessive or mitochondrial (DiMauro et al, 1996), though approximately 30% of all Leigh syndrome is mtDNA-associated (Rahman et al, 1996). Patients with Leigh syndrome caused by a mtDNA mutation are often referred to as having “maternally inherited Leigh syndrome” (MILS) (Ciafaloni et al., 1993).

Apart from mutations in the *ATPase6* gene, Leigh syndrome can also be caused by mutations in eleven additional mitochondrial encoded genes. Genetic testing is usually initially performed in muscle tissue to look for the two most common mutations in the *ATPase 6* gene (m.8993T>G and m.8993T>C). If negative, whole mitochondrial genome screening is performed.

NARP

NARP (Neurogenic muscle weakness, Ataxia, and Retinitis Pigmentosa) is characterised by proximal neurogenic muscle weakness with sensory neuropathy, ataxia, pigmentary retinopathy, seizures, learning difficulties and dementia (Holt et al., 1990). Other clinical features include short stature, sensorineural hearing loss, progressive external ophthalmoplegia, cardiac conduction defects (heart block) and a mild anxiety disorder (Santorelli et al., 1997). Ataxia and learning difficulties often present in early childhood and patients can be relatively stable for many years. Similar to Leigh syndrome, management consists of treatment for individual manifestations (Koene et al., 2011).

The T-to-G transversion (m.8993T>G) is most common in NARP, but a T-to-C transition (m.8993T>C) has also been described. Together they account for up to 50% of NARP patients. Individuals with moderate levels (~70%-90%) of the m.8993T>G mutation present with the NARP phenotype, while those with mutant loads above 90% have maternally inherited Leigh syndrome (Fig. 3.3). Individuals with levels lower than 60% will be asymptomatic. The transition is a less severe mutation than the transversion, and virtually all symptomatic individuals have mutant loads of more than 90% (Thorburn et al, 2011). Patients with the T>C mutation tend to present with milder symptoms but a higher frequency of ataxia (Fujii et al., 1998).

For most mtDNA mutations, it is difficult to distinguish a simple correlation between genotype and phenotype not only because of the difference in heteroplasmic levels of mtDNA. The clinical expression of a mtDNA mutation is also influenced by the pathogenicity of the mutation itself, the variation in mutant load among different tissues, and the energy requirements of brain and other tissues, which may vary with age (Thorburn et al, 2011).

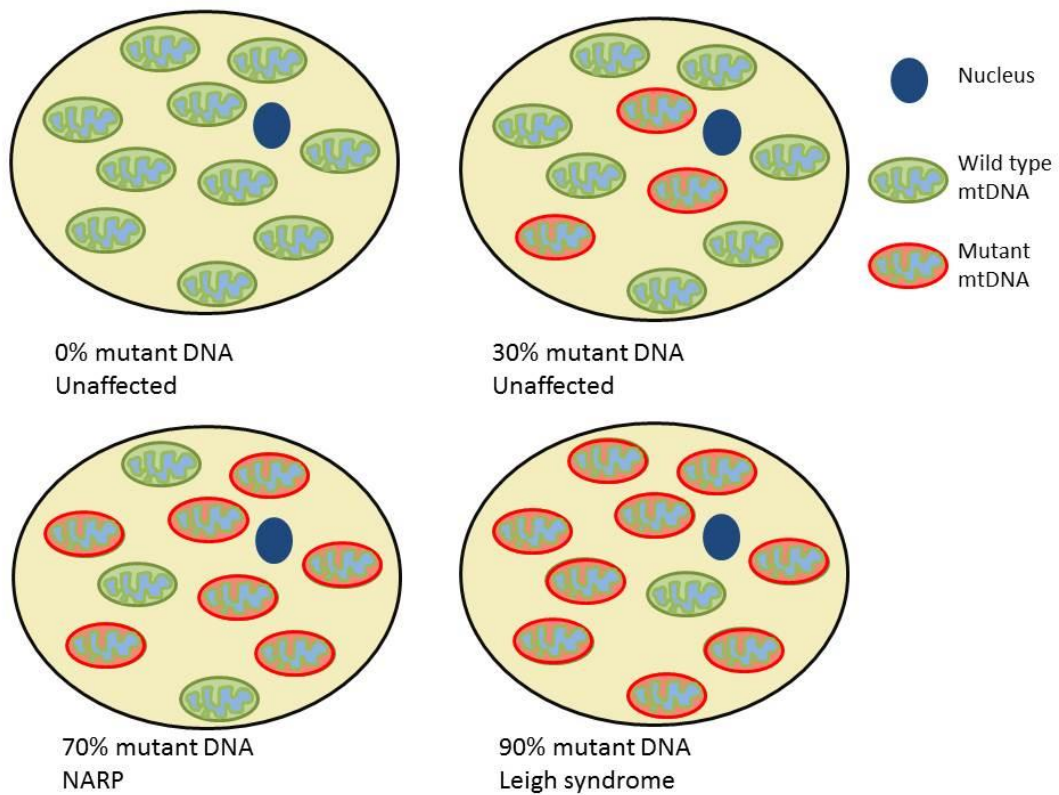


Figure 3-3 Genotype-phenotype correlation for the m.8993T>G transversion.

Since this phenotype-genotype correlation is very important in mitochondrial diseases, I performed a quantitation of the mutant load for several individuals in this thesis to investigate whether this could have an influence on the severity of the neuropathy in our cohort of patients.

In contrast to Leigh syndrome, no additional genes have been reported to cause NARP. However, one paper recently stated that mutations in the mitochondrially encoded *MT-TL2* gene result in an overlapping phenotype of Myoclonic epilepsy with ragged red fibres (MERRF) and NARP in one patient (Martin-Jimenez et al., 2012).

3.1.6 Structural results of mutations in the ATPase 6 gene

In humans, the mitochondrially encoded *ATPase 6* and *8* genes together with the nuclear-encoded *ATPase 9* form the F0 membrane-spanning portion of the ATPase complex. Membrane topology of Subunit 6, also known as subunit a, suggests the presence of six transmembrane domains. The fourth transmembrane helix of subunit 6 (Atp6p) is juxtaposed with the first transmembrane helix of subunit 9 and serves as

a proton pump. The m.8.993T>C mutation replaces the highly conserved leucine residue of subunit 6 that resides opposite an essential glutamate residue of subunit 9 to a proline residue and thus interferes with the energy-driven ATP synthesis. Studies in yeast have shown a 40-50% decrease in the rate of ATP synthesis in the mitochondria of the mutant yeast strain, due to a less efficient incorporation of the Atp6p region, modified by the m.8993T>C mutation (Kucharczyk et al., 2009). The m.9.185T>C mutation results in a leucine to proline change in the fifth transmembrane helix adjacent to the outer membrane. The leucine residue at position 220 is a well conserved residue in all animal species (Kaneko et al., 1993) and the substitution of a very poor alpha-helix former, proline, for a good alpha-helix-former, leucine, may make the fifth transmembrane structure unstable or distorted in configuration and thus interfere with the proton pump. This is the third substitution of a Leucine to a Proline in the suggested transmembrane helix that is known to cause Leigh Syndrome (Castagna et al, 2007).

3.2 Results

3.2.1 Genetic screening of the ATPase 6 and ATPase 8 genes resulted in a mutation frequency of 1.4%

Standard PCR reaction was performed to amplify the overlapping ATPase 6/8 genes in a cohort of 673 patients. Of those patients, the majority (40.6%) was diagnosed with CMT2, and HMN and HSAN in respectively 172 (25.6%) and 133 (19.8%) of the patients. 93 (13.8%) patients were diagnosed with CMT1 and were primarily screened to examine whether mutations in the mitochondrial DNA could be a modifying factor for the demyelinating phenotype. All patients with CMT2 were negative for mutations in *MFN2*. The majority of patients with CMT2 were also screened for mutations in *MPZ*, *HSPB1*, *HSPB8*, *TRPV4*, and *GJB1* where appropriate. Patients with dHMN were negative for mutations in *HSPB1*, *HSPB8*, and *TRPV4*, and selected patients were negative for mutations in *BSCL2* and *GARS*.

Mutations in the *ATPase 6* gene that are known to cause Leigh Syndrome were detected in five individuals diagnosed with CMT2. As mentioned before, the investigation of an extensive family with mitochondrial disease and axonal neuropathy in which the index case presented with a pure motor neuropathy in

childhood evolving into motor-predominant CMT2 in later life resulted in the discovery of a pathogenic missense mutation m.9185T>C in *ATPase 6*. This mutation was detected in three further unrelated probands by our genetic screening. Considering 275 CMT2 index cases were analysed, the representing frequency for this specific mutation in the *ATPase 6* gene results in a percentage of 1.4% amongst CMT2 patients.

No pathogenic variants were found in patients with dHMN, HSAN or CMT1, and no pathogenic mutations in *ATPase 8* were found in either of the groups. The m.8993T>C mutation, which substitutes a leucine for proline, was found in one patient diagnosed with CMT2. When looking at the chromatographs of the four patients with the m.9185T>C mutation, a clear difference can be observed between patients with a heteroplasmic mutant load and patients with a homoplasmic (or high heteroplasmic) load (Fig. 3.4).

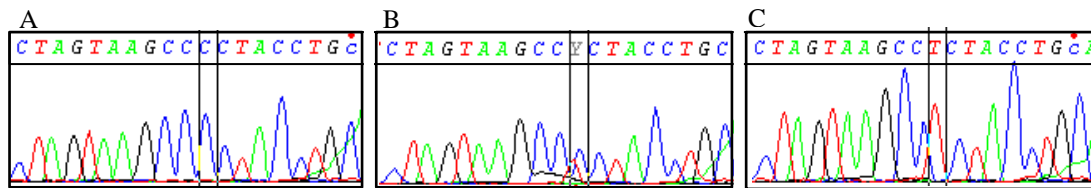


Figure 3-4 Sequencing results for the m.9185T>C variant. A: Homoplasmic wild type; B: heteroplasmic wild type/mutant; C: homoplasmic mutant.

3.2.2 Segregation analysis and the use of heteroplasmy investigation

Segregation analysis of these mutations all showed the presence of the pathogenic mutation in the affected cases. Three of these probands were part of a large family, creating the opportunity to compare the percentages of heteroplasmy with the severity of the phenotypes and the sequencing results. Different tissue samples were used to compare the mutant load in the different organs. This was mainly performed to analyse whether blood samples could be representative of muscle samples, to reduce the need of muscle biopsy.

3.2.3 Family A

The first family consisted of four generations, with three generations of affected individuals (Fig. 3.5). Blood samples were available for seven members of the

family, while muscle samples were provided for three members. The index case also provided a urine sample.

Clinical details of family A are compatible with a diagnosis of motor-predominant CMT2

The index case (Patient III-5) presented in the first decade with recurrent falls and foot drop at age 6 after normal early development. Electrophysiologically, the neuropathy was a pure motor neuropathy/neuronopathy, however, sensory signs have since developed, making the diagnosis clinically compatible with motor-predominant CMT2. Recent clinical examination at age 21 showed distal muscle wasting of the legs, pes cavus, and clawing of the toes. Muscle strength was normal in the upper limbs with mild proximal lower limb weakness and moderate distal lower limb weakness. Ankle jerks were absent. Plantar responses were extensor. Pinprick sensation was normal, but vibration detection was reduced to the knees.

Extra clinical features present in Family A suggesting mitochondrial involvement

Apart from a pure motor neuropathy in all affected patients and minor sensory involvement in patient III-5, several patients also suffered from learning difficulties, sensorineural hearing loss and retinal degeneration. Two patients died due to sepsis at the ages of 9 (Patient IV-1) and 16 (Patient III-2). This type of rapid decompensation is distinctive for Leigh syndrome, suggesting mitochondrial involvement. The neuropathy was particularly severe in 2 adults with wheelchair dependence in the third decade (patients II-3 and III-1).

Genetic analysis of family A indicate a homoplasmic m.9.185T>C mutation

After mitochondrial DNA sequencing the homoplasmic presence of the m.9185T>C mutation was revealed, which segregated in the whole family. This causes a missense change from leucine to proline at amino acid position 220 of the ATP6 protein (Leu220Pro). Affected individuals all presented with a mutant load of 100% in blood, whereas unaffected family members had lower levels of mutant load. The mutation was also quantified in two muscle samples and one urine sample, which showed an equivalent mutant load of 100% (Fig. 3.5).

Blue native gels of Family A show abnormalities in comparison to controls

Blue native gels for complex V of the respiratory chain were also performed elsewhere for three of the patients (Patients III-2, III-3 and IV-2). These both showed

reduced activity as well as impaired assembly of the complex in muscle samples (results not shown).

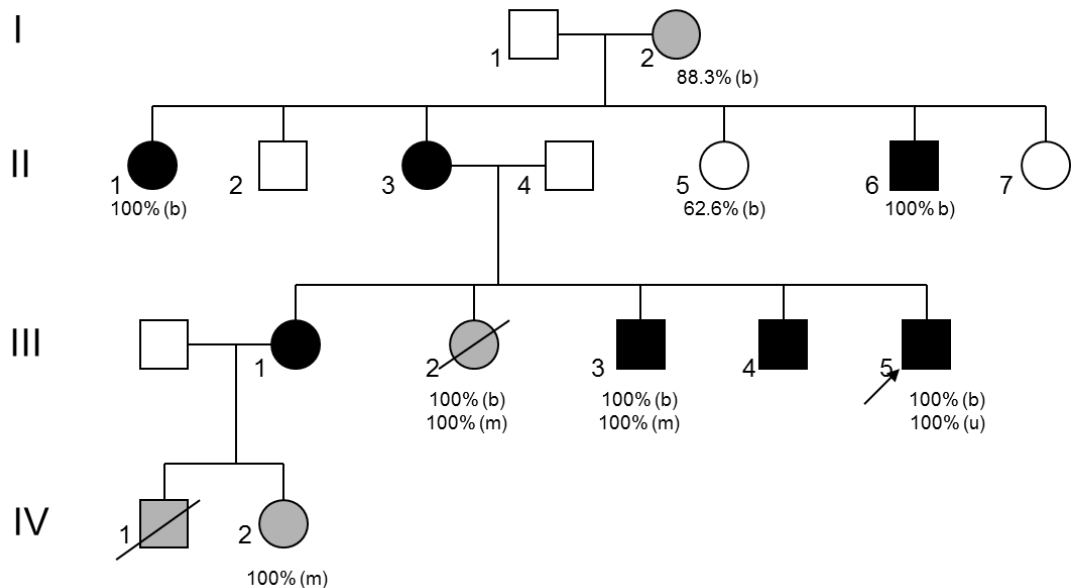


Figure 3-5 Pedigree of Family A. Black symbols specify patients with CMT2, light grey symbols specify patients with unknown clinical status. Arrow indicates index patient. b = blood; m = muscle; u = urine.

3.2.4 Family B

Clinical details of Family B show several generations with CMT2 and individuals with solely Upper Motor Neuron signs

The second family has a history of four generations presenting with CMT2 (Fig. 3.6). Patients presented in their first or second decade with typical features of inherited neuropathy, following a gradually progressive clinical course but experienced rapid decline in mobility in their fifth and sixth decades with wheelchair dependence from unaided walking over a 5-year period. Electrophysiological studies in patient III-9 pointed towards a pure motor neuropathy at age 29, but repeated studies at a later age showed sensory involvement, characteristic of CMT2. Generation III also included two individuals who displayed upper motor neuron (UMN) signs without a peripheral neuropathy.

Heteroplasmy analysis showed a difference in the mutant load between patients with CMT2 and individuals with UMN signs

Restrictive enzyme analysis suggested a mutant load of 100% in all patients of Family B characterised with CMT2, whereas both of the patients with UMN signs

had a mutant load between 70-80%. The index patient (III-9) also had a skin and muscle biopsy, both showing the same level of mutant DNA.

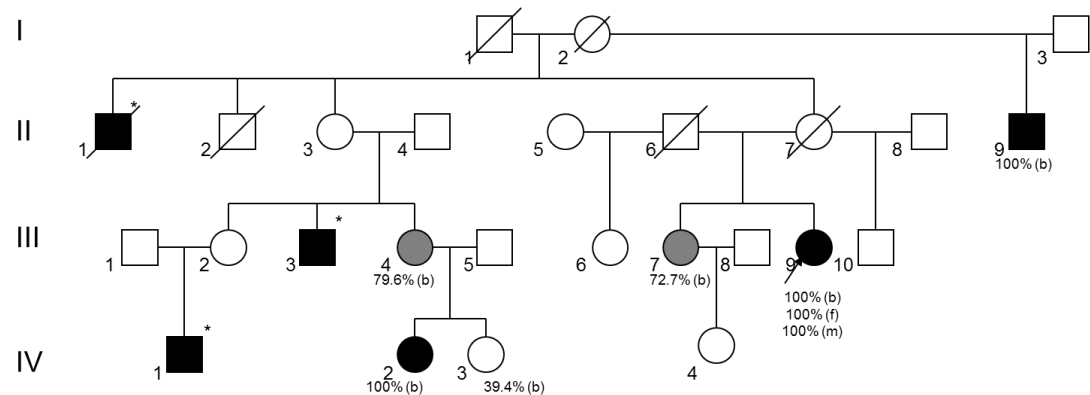


Figure 3-6 Pedigree of family B. Black symbols represent patients with CMT2, dark grey symbols represent individuals with upper motor signs. Arrow indicates the index patient. b = blood; f = fibroblasts; m = muscle. Asterisks indicate affected individuals that were not examined locally.

Blue native gel of the index patient of Family B shows abnormalities in comparison with controls.

Blue native gel of patient III-9 suggested a reduced activity of complex V in comparison with controls (results not shown).

3.2.5 Family C.

Clinical details of Family C are consistent with CMT2

The third family consisted of three generations of affected individuals (Fig. 3.7). Patient III-16 had NCS compatible with a sensorimotor axonal neuropathy, whilst studies in patient IV-2 showed a pure motor neuropathy. Patient IV-2 also presented with learning difficulties, behavioral problems, and wheelchair dependence by early adulthood. Patient III-16 had motor-predominant CMT2 with pyramidal tract signs and proximal muscle weakness, which developed in later life.

A history of insulin-dependent diabetes mellitus existed in the family, presenting in both generation II and III. This was not seen in patients with CMT2 and appeared to come from the father's side of the family.

Heteroplasmy analysis showed different levels of mutant load in the whole family

Both patients characterised had a mutant load of 100%. Two individuals in the family (III-5 and IV-1) had an unknown clinical status and had a mutant load of respectively 75% and 45%.

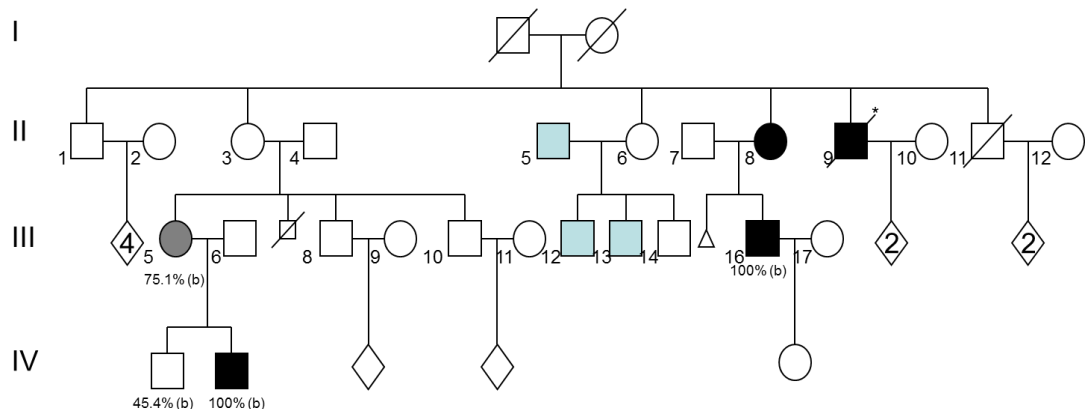


Figure 3-7 Pedigree of Family C. Black symbols represent patients with CMT2, light grey symbols represent individuals with unknown clinical status, blue symbols represent individuals with Insulin-dependent diabetes melitus. b = blood. Triangles with numbers indicate multiple individuals with unknown gender; small square with slash = still birth; small triangle with slash = miscarriage. Asterisks indicate affected individuals that were not examined locally.

3.2.6 Sporadic case

Clinical details indicate a sensorimotor axonal neuropathy

The fourth patient presenting with the m.9185T>C mutation appeared to be a sporadic case in the family, suggesting a de-novo mutation (Fig. 3.8). He presented in the first decade and was characterised with sensorimotor axonal neuropathy, confirmed by NCS. EMG showed proximal and distal lower limb denervation with no evidence of myopathy. DNA of the parents was not available for sequencing.

Heteroplasmy content showed levels lower than 100%

Chromatographs indicated a heteroplasmic content of mutant DNA. Restrictive enzyme digest resulted in a mutant load of 92%.

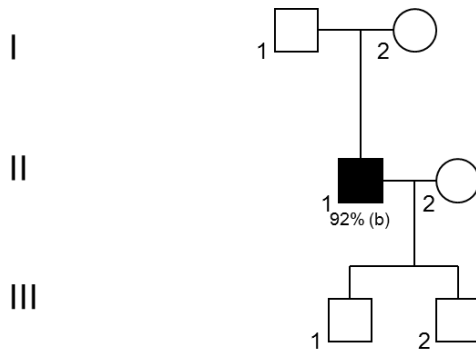


Figure 3-8 Pedigree of the sporadic case.

Black symbols specify patients with CMT2.

b = blood.

3.2.7. Estimating pathogenicity of unknown variations in the mitochondrial genome

Since the mitochondrial genome consists of numerous variations, a list of steps has been followed to exclude non-pathogenic variations amongst all the variants found in our cohort of patients (See appendix I). Mitochondrial DNA has few regulatory sequences; therefore all synonymous or non-coding variations were excluded, together with known polymorphisms. Subsequently, variations were entered into four separate databases of control individuals, available online or internally. The largest database, mitowheel, consists of 3735 human mtDNA sequences (Zsurka, Gábor and Csordás, Attila; MitoWheel, visualizing the human mitochondrial genome. Available from Nature Precedings, 2009). Variations found in more than five control individuals were excluded. Other databases used were: mtDB (Ingman et al., 2006), HmtDB (Rubino et al., 2012) and the NHNN database (Internal database). Variations found in fewer than five controls, but associated with haplotypes or proven to be non-pathogenic were also excluded.

Mutation	# Patients	Diagnosis	Conservation	# Controls
m.8381A>G: Thr-Ala	1	CMT2	Changed to I in monkey and elephant	2
m.8516T>C: Trp-Arg	1	CMT2	Conserved in all species	1
m.8605C>T: Pro-Ser	2	CMT2	Changed to Q in 1 Dormouse	1
m.8828A>G: Asn-Ser	1	CMT2	Conserved in all species	
m.9025G>A: Gly-Ser	2	CMT2 + HSAN	Conserved in all species	1

Table 3-1 Possible mutations amongst variants found in the *ATPase 6/8* genes in the mitochondrial genome. Mutation in bold was found in heteroplasmic levels in one patient.

Additionally, the conservation of basepairs was analysed by using the mtSNP database search (Fuku et al., 2005). Only variations with high conservation remained. This elimination led to a list of five possible mutations (Table 3-1). The m.8605C>T mutation was found in two CMT2 patients, one with seemingly heteroplasmic levels of the mutation.

3.3 Discussion

We identified five patients with mutations in the *ATPase6* gene. In our genetically undefined cohort of CMT2 patients, this results in a prevalence of 1.8% harbouring a mutation in the *ATPase 6* gene. Considering only one out of four patients with CMT2 receives a molecular diagnosis, this is a notable result. Several lines of evidence support the indication that this mutation is the cause of the phenotype.

3.3.1 Clinical details

All patients were seen by experienced clinicians and were considered to have a CMT2 phenotype based on clinical and electrophysiological parameters. Each of the pedigrees are compatible with a maternal lineage, however patients were never tested for mutations in this gene since they had isolated involvement of the peripheral nerves. Since there are four different families with the same mutation, the question arises if these families are related. While screening the families for mutations, polymorphisms were found in two of the four families, indicating these families are not related.

3.3.2 Pattern of disease severity

Three out of four patients were homoplasmic for the mutant DNA, the remaining patient had a mutant load of 92%. The pattern of variable disease severity matching with the levels of heteroplasmy is characteristic for diseases caused by mutations in the mtDNA. The consistency of mutant load in the different tissue samples implies a redundancy for skin or muscle biopsies, since heteroplasmy could be estimated with blood samples only. This is only demonstrated in patients with a mutant load of 100%, so caution is needed when applying this to patients with a less severe phenotype. To evaluate whether the presence of extra symptoms relates to the heteroplasmic content in other tissues, mutant load characterisation in post mortem brain tissue and peripheral tissue would be desirable.

Considering all of the CMT2 cases with a mutant load between 92% and 100% had predominantly motor axonal neuropathy, it implies that all affected individuals with neuropathy present with levels higher than 92% of mutated DNA. Whether all of the patients truly have 100% mutated DNA is not guaranteed, as we have to allow for the detection level of the method. Reverse restriction enzyme experiments, in which wild type DNA was cut rather than mutant DNA could rule out the presence of any wild type DNA present.

According to the levels of mutated DNA, patients could be broadly subdivided in four clinical groups (Fig. 3.9): group 1, affected individual with symptoms and signs of predominantly motor axonal neuropathy (100–92% mutant load); group 2, affected individuals with clinical symptoms and signs of UMN involvement without neuropathy (91%–80% mutant load); group 3, asymptomatic individuals with upper motor neuron (UMN) signs detectable on examination only (79%–64% mutant load); and group 4, unaffected individuals (<64% mutant load). Patient I-2 from the first family does not seem to fit in this classification, since she had a mutant load of 88%, without clinical features. However, this patient has never been examined and therefore cannot be excluded as a potentially affected individual.

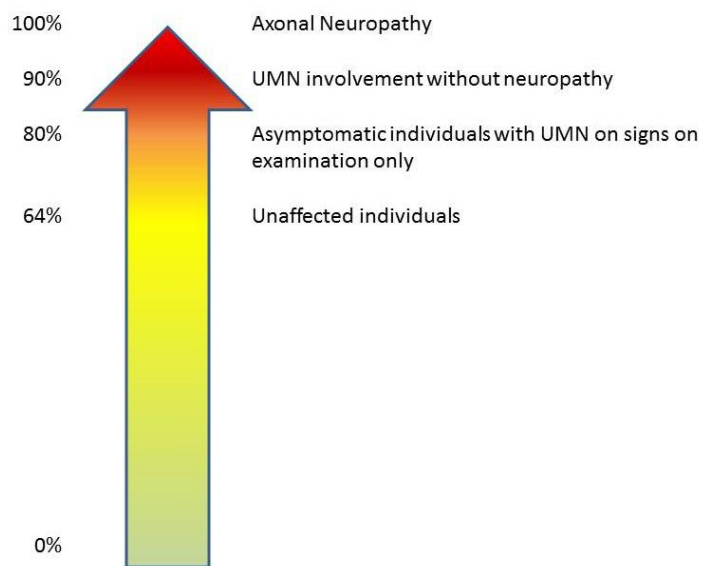


Figure 3-9 Correlation between heteroplasmic content of mutant DNA and severity of the disease.

These cut-off percentages are very characteristic for mitochondrial diseases, supporting the pathogenicity of mutations in *ATPase6* in CMT2 disease. To correctly

estimate the boundaries between the different phenotypes, more patients with different loads of mutant DNA need to be characterised, but estimations can be made.

3.3.3 Blue native gels

The use of an *E.coli* model for the m.9185T>C mutation in previous studies indicates a 70% decrease in ATP synthetic ability (Ogilvie and Capaldi, 1999), and studies in fibroblasts have shown a decrease of ATPase activity in patients with Leigh syndrome (Castagna et al., 2007). Similarly, in this study, the effects of the c.9185T>C mutation on complex V were studied in 4 different patients originating from 2 different families. These all showed impairment in the assembly and stability of the complex and/or the activity of the enzyme. This data supports the pathogenicity of the c.9185T>C mutation and indicates that this mutation is important in mitochondrial dysfunction, adding to the role of mitochondria in CMT2 disease.

The identification of the m.8993T>C mutation in a patient with CMT2 also adds supportive evidence for pathogenicity of mutations in the *ATPase 6* gene. This mutation is not as extensively studied as the more common m.8993T>G mutation, which produces a more severe phenotype in mitochondrial diseases. BN-page has previously been used to prove the pathogenicity of the c.8993T>G mutation, where an impaired assembly and activity of the enzyme indicates the deleterious effects of the mutation. The same studies were done for the m.8993T>C mutation in this study, which only showed a substantial decrease of ATP synthesis in fresh muscle biopsies of patients and not in fibroblasts cell cultures. Unfortunately, no muscle tissue was available for this patient.

3.3.4 Explanation for the phenotypic spectrum is unknown

Since these mutations are also known to cause Leigh syndrome and NARP, other factors influencing the phenotype must be present, although the exact relationship between phenotype and genotype still has to be explained. The existence of modification factors could explain this broad phenotype spectrum, but this requires further research. Considering this is the first mitochondrial gene associated with a pure neuropathy, sequencing of the whole mitochondrial genome would be

appropriate to investigate whether more mutations in mitochondrial genes can be associated with neuropathy.

3.3.5 Guidelines for mutational analysis in patients with CMT2

With the emergence of next generation sequencing and whole exome or genome sequencing, a decision has to be made whether it is worth screening for mutations in the mitochondrial DNA as well. Although most patients presented with a typical CMT2/dHMN phenotype, mutations in *ATPase6* should be particularly considered in the following cases: 1) an evolving clinical phenotype from a pure motor to a motor-predominant axonal neuropathy in the third and fourth decades; 2) early proximal lower limb muscle involvement despite mild distal weakness; 3) multisystem involvement in the patient or relatives; 4) UMN signs in affected or asymptomatic relatives; 5) rapid clinical decompensation in affected individuals after viral or septic illness.

3.3.6 Cohort study

After exclusion of non-pathogenic mutations, five possible mutations remained. These cannot be excluded with the pre-existing information available. One way to determine if these mutations are pathogenic would be to measure the *ATPase* activity in vitro, by the use of blue native gels, but this could not be performed in the time available.

Mutation	#Patients	Diagnosis	Conservation	#Controls
m.8605C>T: P-S	1	CMT2	Changed to Q in Dormouse	1
m.8828A>G: N-S	1	CMT2	Conserved in all species	
m.9025G>A: G-S	2	CMT2 + HSAN	Conserved in all species	1

Table 3-2 Variants of unknown significance found in the *ATPase 6* gene in our cohort.

Since mitochondrial DNA is very prone to variations, it is expected that most of these mutations will be polymorphisms. Considering the absence of definitely pathogenic mutations in the *ATPase 8* gene, we only focused on the variants found in the *ATPase 6* gene (Table 3.2).

The familial history of the m.8605T>C variant showed a pattern of paternal inheritance, which makes it highly unlikely that this is the causative mutation for the phenotype, unless two different causes of disease are present in one family. One

patient with CMT2 had a novel variant m.8828A>G, causing a missense change from asparagine to serine at amino acid position 101 of the ATP6 protein (Asn101Ser). Unfortunately, there was no muscle tissue available from the patient for BN-PAGE; thus, the potential pathogenic nature of this variant remains uncertain. The m.9025G>A variation was also of particular interest, and since additional information did not exclude this variation from our list of possible mutations, this variation was checked for ATPase activity using blue native gel. However, no abnormalities were found.

To conclude, mutations in the *ATPase6* gene in patients with CMT2 add to the expanding evidence for the involvement of mitochondria in axonal neuropathy and suggest the mitochondrial genome should be screened for mutations in patients with axonal neuropathy.

Chapter 4

Candidate gene screening in patients with CMT2

4.1 Introduction

4.1.1 Expanding clinical spectrum of known disease genes

Due to the phenotypically heterogeneous nature of CMT, a significant amount of genetic overlap can be found between subtypes of CMT. As genetic testing becomes more widely available, mutations in one single gene have been found to cause multiple phenotypes and different modes of inheritance; for example, mutations in *HSPB1* can cause CMT2 and dHMN in both an autosomal dominant and autosomal recessive manner. Genetic advances such as WES and WGS in recent years have broadened the phenotype of CMT and related neurodegenerative disorders (Gess et al., 2014; Robusto et al., 2014; Liu et al., 2014; Mathis et al., 2014; Schabutti et al., 2014; Azzedine et al., 2013). Not only can an entire new phenotype be found for the same gene, but broadening the already known phenotype can be beneficial to the understanding of disease pathways.

FIG4

CMT4J is a rare subtype of demyelinating CMT, responsible for ~20% of recessive Charcot–Marie–Tooth disease and 0.4% of all Charcot–Marie–Tooth disease. It is caused by recessive mutations in the phosphoinositide phosphatase *FIG4* gene, and characterised by childhood onset with accelerated proximal and distal weakness and muscle atrophy in both proximal and distal muscles. Examination may reveal decreased response to touch, pin prick, or vibration distally (Zhang et al., 2008). The first mutations in the *FIG4* gene were found in the ‘pale tremor’ mouse model, presenting with a multi-organ disorder with neuronal degeneration in the central nervous system, peripheral neuronopathy and diluted pigmentation, caused by an insertion in intron 18 of *FIG4*. The first screen of *FIG4* in 95 CMT2 patients revealed four unrelated patients with recessive mutations consisting of a combination of a missense mutation p.Ile41Thr in exon 2 and a protein truncating mutation. Few mutations have been reported in *FIG4* so far, and the majority of CMT4J patients have the compound heterozygous genotype *FIG4*I41T/null that was originally described in four families and has reached an allele frequency of 0.001 in the Northern European population whilst carriers remain clinically unaffected. Homozygotes have not been observed, showing that the presence of a null mutation on the other allele is required to manifest disease (Nicholson et al., 2011). The p.Ile41Thr mutation results in an impaired interaction with VAC14, required for the stability of the protein in vivo. As a result, protein levels in mice and patient fibroblasts are extremely low. To date, 18 cases have been described with *FIG4* mutations. 17 of these had the *FIG4*I41T/null genotype. The remaining patient had a *FIG4*L17P/null genotype (Lenk et al., 2011). A recent paper in 2014 by Menezes et al. describes one of these patients as carrying the *FIG4*I41T/null genotype. However, the mother of the index patient seemed to present with a homozygous p.Ile41Thr mutation. When looking into more detail, a deletion of exon 2 was established on the other allele. This indicates that caution has to be taken in families with two affected generations that would usually be regarded as dominantly inherited forms of CMT. Other explanations can be possible, such as recessive inheritance due to three mutations segregating within the family.

Besides CMT4J, heterozygous mutations in *FIG4* have been found in patients with ALS (Chow et al., 2009) and homozygous null mutations have been shown to cause

Yunis-Varon syndrome, a severe autosomal-recessive congenital disorder affecting multiple tissues (Campeau et al., 2013). The clinical phenotype of CMT4J shows a significant amount of overlap with patients characterised with CMT4B1 and CMT4B2, due to loss-of-function mutations in *MTMR2* and *MTMR13* respectively. These overlapping clinical symptoms of CMT4B with CMT4J might result from either less [PI5P] or elevated [PI3P] or misregulation of [PI(3,5)P2].

No mutations have been found in *VAC14* and mutations in *PIKfyve* result in Fleck corneal dystrophy (FCD), a rare autosomal dominant disease characterised by numerous tiny, dot-like white flecks scattered in all layers of the corneal stroma. Most patients are asymptomatic with normal vision, although photophobia has been reported in a small subset (Li et al., 2005).

The FIG4 protein removes the 5-phosphatase from the low-abundance signalling phosphoinositide [PI(3,5)P2], which is localised on the cytoplasmic surface of vesicles of the endosome/lysosome pathway. As mentioned in Chapter 1, [PI(3,5)P2] is one of the lowest abundant phosphoinositols present, making it difficult to study. Concentration of [PI(3,5)P2] is tightly regulated by the PAS complex, containing the PIKfyve, Vac14 and FIG4 proteins in mammals, in which PIKfyve functions as a kinase. Interestingly, activation of PIKfyve requires catalytic activity of FIG4, resulting in a tight coordination between synthesis and turnover of [PI(3,5)P2]. There is a significant role for this complex in an amount of pathways, such as the traffic of cell surface receptors to lysosomes, ion channel function or exocytosis (McCartney et al., 2014). Besides this, [PI(3,5)P2] also serves as a precursor for [PI5P]. This requires the presence of proteins with 3-phosphatase activity such has MTRMRs. MTMR2, another protein mutated in CMT4B1, acts on the same substrate as FIG4 but with opposing effects. It is suggested that an imbalance of [PI(3,5)P2] might be at the basis of the excessive myelin growth and hypermyelination (Vaccari et al., 2011). However, there are still alternative hypotheses that indicate generation of [PI5P] by PIKfyve (Shisheva, 2012).

In mice, the imbalance of [PI(3,5)P2] leads to accumulation of enlarged vesicles derived from the endosome/lysosome pathway in fibroblasts and neurons, similar to the vesicle accumulation that can be seen in fibroblasts from a patient with CMT4J

(Chow et al., 2007; Zhang et al., 2008; Ferguson et al., 2009). Pale tremor mice also exhibit impaired autophagy with accumulation of p62/ubiquitin-positive inclusion bodies in astrocytes and neurons (Ferguson et al., 2009). The original mouse model, consisting of a homozygous insertion in intron 18 of *FIG4* has been shown to survive for 4–6 weeks and exhibits extensive spongiform neurodegeneration in brain and peripheral ganglia, as well as loss of large diameter-myelinated neurons in sciatic nerve (Chow et al., 2007). A severe reduction in protein levels in comparison with the transcript level can be observed and is thought to originate from the protein instability caused by impaired interaction of the mutant protein with VAC14. This result was also confirmed in patient fibroblasts. A transgenic model expressing the CMT4J variant *FIG4I41T* on a *FIG4* null background was later developed and exhibits dose-dependent rescue of mutant phenotypes, including neurodegeneration in the brain and dorsal root ganglia, and myelination of the sciatic nerve (Lenk et al., 2011).

Disease onset in patients varies widely from early childhood to the sixth decade, but so far no correlation with the mutation spectrum has been found. Proximal weakness in patients with CMT4J can be used to distinguish from typical CMT that is predominantly distal. Most patients show asymmetric weakness and in several cases trauma, such as a fall, can trigger the initial symptoms or cause a period of rapid progression. There is major reduction of motor nerve conduction velocity affecting both upper and lower extremities with frequent progression to severe amyotrophy. Sensory findings are uniformly less severe than motor findings but can progress to total loss of sharp sensation and reduced joint position sense with sensory nerve action potentials being reduced and becoming unobtainable with time. Most patients are also areflexic and few have shown signs of cranial nerve involvement. Neurophysiologic studies show severe combined axonal and demyelinating neuropathy, with major reduction of motor nerve conduction velocities, much slower than expected from denervation alone and often showing a decrease in amplitude (Chow et al., 2007; Zhang et al., 2008; Nicholson et al., 2011).

EMG shows evidence of active and chronic denervation, including fibrillation potentials, positive sharp waves and reduced recruitment patterns. Sites of muscle atrophy correspond to the sites of weakness. Sural nerve biopsies show loss of large-

diameter myelinated fibres, onion bulb formations, and progressive loss of axons in most patients.

Chronic inflammatory demyelinating polyradiculopathy (CIDP) typically presents acutely, often with a patchy, non-homogeneous, predominantly motor neuropathy with associated demyelinating features on nerve conduction studies. Rapid progression of weakness in a single limb usually suggests an acquired inflammatory neuropathy like CIDP. It is becoming more recognised that patients who were previously thought of having an inflammatory neuropathy such as CIDP are being diagnosed with CMT (Houlden et al., 2009; Michell et al., 2009); hence we screened a cohort of 35 patients in this study with an early onset demyelinating neuropathy and distal motor neuropathy/neuronopathy for mutations in the phosphoinositide phosphatase *FIG4*. Cases were selected where the disorder was progressive and asymmetrical, as these would normally be interpreted as CIDP in comparison with the more symmetrical pattern expected from inherited neuropathies.

C9orf72

Two separate studies simultaneously reported the discovery of a GGGGCC repeat expansion in the first exon and promotor region of the *C9orf72* gene in families with genetic linkage to chromosome 9p21 and a phenotype of FTLD-ALS (DeJesus-Hernandez et al., 2011; Renton et al., 2011). Amyotrophic lateral sclerosis (ALS) and frontotemporal lobar degeneration (FTLD) are two fatal neurodegenerative diseases without effective therapies. ALS is the most frequent motor neuron disease and is characterised by the degeneration of upper and lower motor neurons, leading to muscle weakness, spasticity and atrophy. FTLD is a common cause of early onset dementia, resulting from the degeneration of frontal and temporal lobes, and encompasses a group of disorders distinguished clinically by abnormalities in behaviour, language and personality. Both are part of a spectrum of disorders that have overlapping clinical, pathological and genetical features (Verma et al., 2014). After screening the appropriate cohorts, it was shown that the GGGGCC repeat is the most frequent genetic cause of both conditions. Further research found *C9orf72* expansions in patients with Parkinson's disease (PD) (Lesage et al., 2013), progressive supranuclear palsy (Origone et al., 2013), ataxic syndromes and corticobasal degeneration (Lindquist et al., 2013). Most controls possess either 2,5 or

8 repeats on each allele, as does the non-expanded allele in patients whilst the disease allele has more than 400 repeats, usually up to 2000. The maximum number of repeats in controls was estimated at 25-30 repeats, depending on the study. Since the expansion repeat exceeded the upper detection limit of the assay in two of the studies, a minimum length of 60 repeats was suggested (DeJesus-Hernandez et al., 2011; Renton et al., 2011; Gijselinck et al., 2011). A classification was suggested with repeats under 30 being non-pathogenic, repeats between 30 and 60 possibly pathogenic and repeats over 60 definitely pathogenic. More research is being performed on the grey zone below 60 repeats, where the number of repeats is not clearly pathological, but outside the typical range of healthy control repeat size. In rare cases, there have been reports of repeat lengths lower than 30 segregating in families (Gomez-Tortosa et al., 2013; Millecamps et al., 2012), even though these numbers have also been found in controls in other studies (Ratti et al., 2012; Simon-Sanchez et al., 2012; Beck et al., 2013). Different disease mechanisms have been suggested which include toxicity induced by repeat-containing RNAs forming nuclear RNA foci that interact with various RNA-binding proteins causing transcriptome defects, RAN-translation of the *c9orf72* transcript leading to accumulation of RAN proteins in cytoplasmic aggregates in affected brain regions or decreased mRNA expression leading to loss of C9orf72 function (Gendron et al., 2014). Whilst the exact mechanism of pathogenicity is not yet known, studies indicate the clue can be found with repeat-containing RNAs. The normal function of C9orf72 has only recently begun to be elucidated and co-expression studies suggest it might be involved in ubiquitin-dependent protein degradation (Bieniek et al., 2013), whilst others suggest a role in endosomal trafficking due to colocalisation with Rab proteins implicated in autophagy and endocytic transport such as Rab7, also implicated in CMT. Since CMT is also a neurodegenerative disorder, it was questioned whether the disease mechanism could stretch as far as being the cause for peripheral neuropathies.

4.1.2 Frequency of genetic subtypes

Dealing with a genetically heterogeneous disease has the consequence that new genes will be discovered continuously and the search can seem never-ending. The majority of these genes are found in few families with a very specific phenotype and estimations of the frequency of the genetic subtypes are difficult to make. These

frequencies can also differ significantly depending on the population and can demonstrate a founder effect in different ethnic groups. In the event new genes are discovered by other research groups, screening appropriate cohorts to estimate the frequency of the gene and diagnose some of the patients present in the in-house databases is a good opportunity and can provide a useful tool for clinicians to determine which genes to screen first.

In a large study by Saporta et al including 787 CMT patients, it was estimated that 67% of CMT patients receive a genetic diagnosis, and out of these 92% has either the *PMP22* duplication or mutations in *PMP22*, *MPZ*, *GJB1* or *MFN2* (Saporta et al., 2011). The same percentage was established in a study by Murphy et al in 425 patients with CMT (Murphy et al., 2012). A more recent study by DiVincenzo et al estimated the amount to be 94,9% of genetically diagnosed patients (DiVincenzo et al., 2014). All other genetic subtypes accounted for less than 1-3% of the total CMT patients with a genetic diagnosis, depending on the study (Saporta et al., 2011; Murphy et al., 2012). Whilst only 1.8% of patients with CMT1 were left without a genetic diagnosis in the study in Detroit, the study in London reported a genetic diagnosis in 80% of CMT1 patients. For CMT2, 34.5% of patients in Detroit and 25,2% of patients in London received a genetic diagnosis, indicating there are still multiple genes to be discovered in axonal CMT.

HINT1

In 2012, Zimon *et al.* reported a new gene called Histidine triad nucleotide-binding protein 1 (*HINT1*) in which loss-of-function mutations cause an axonal neuropathy with neuromyotonia in 33 families. Neuromyotonia is a rare neuromuscular disorder that can either be acquired, paraneoplastic or hereditary. It results from hyperexcitability of peripheral motor nerves, characterised by spontaneous muscular activity at rest (myokymia), impaired muscle relaxation (pseudomyotonia), and contractures of the hands and feet. In hereditary cases it usually has an onset in late childhood or early adulthood. The authors stated a frequency of 11% for mutations in *HINT1* in patients with autosomal recessive or sporadic CMT.

HINT1 is a 126 amino acid protein that is ubiquitously expressed and functions as a homodimeric purine phosphoramide and lysyl-adenylate generated by lysyl-tRNA

synthetase (LysRS) (Chou et al. 2007). HINT1 is also a member of the evolutionarily conserved family of histidine triad proteins that acts as a haplo-insufficient tumour suppressor, participating in several apoptotic pathways (Weiske et al, 2006). Eight different mutations were originally described to cause the same phenotype of axonal neuropathy with neuromyotonia (Zimon M et al., 2012). The most prevalent mutation is the p.Arg37Pro, with a later study in Czech patients showing a presence of 95% (Laššuthová et al., 2015). The same study reports a significant under-recognition of neuromyotonia in patients, with only three out of 19 patients with neuromyotonia being characterised before molecular diagnosis. Most patients described with mutations in *HINT1* come from eastern-European countries, suggesting a founder-effect (Zhao et al., 2014; Caetano et al., 2014).

Yeast complementation assays resulted in reduced viability or no growth of the transformed strains, due to protein instability. Lymphoblast cultures of patients showed negligible expression of the HINT1 protein due to post-translational degradation. How this leads to neurodegeneration has not been established yet but transcriptional regulation and/or RNA metabolism have been implied (Zimon et al., 2012). The original study was performed in a cohort with predominantly eastern European patients with autosomal recessive or sporadic CMT. To examine the frequency of mutations in *HINT1* in the UK population, a cohort with predominantly recessive CMT2 was selected from the cases available at Queen Square for this study.

SCN9A

Pain disorders can be severe, debilitating conditions, which affect almost 10% of the worldwide population. Currently, treatment of these disorders remains unsatisfactory (Lampert et al, 2010). The most essential nociceptive or pain-signalling sensory neurons are located in the dorsal root ganglia (DRG) and trigeminal ganglia and constitute the peripheral entry point of the pain pathway. When stimulated, these neurons produce a series of action potentials, allowing information about the external sensory world to be transmitted to the brain. Injury to these neurons causes them to become hyperexcitable, thus giving rise to abnormal, unprovoked spontaneous action potentials or pathological bursting, which results in chronic pain (Fisher et al, 2010). Two distinct phenotypes involving chronic pain are caused by gain-of-function

mutations in *SCN9A*, while loss-of-function mutations have been found in patients with a congenital insensitivity to pain (CIP). Despite *SCN9A* mutations having been a long-established cause of pain disorders, we screened a cohort of our patients for mutations in the gene. A large number of *SCN9A* mutations have been reported in this highly polymorphic gene, but little estimation has been made about how frequently mutations occur in these disorders. For example, a study in 19 patients with pain disorders resulted in a positive result in *SCN9A* in only two of the patients (Klein et al., 2013).

Inherited erythromelalgia is characterised by episodic symmetrical red congestion, vasodilatation and burning pain of the feet and the lower legs, mostly provoked by exercise, long standing or exposure to warmth. Relief could be obtained with cold (Michiels et al, 2005). The severity of this disorder can progress with age, and the symptoms may extend over a larger bodily area and become constant (Mandell et al, 1977). In the absence of an underlying cause (such as myeloproliferative diseases or as a side effect of medication), it is referred as 'Primary erythromelalgia', which is known to be an autosomal dominant disorder (Fisher et al, 2010).

Paroxysmal extreme pain disorder, also known as familial rectal pain, is characterised by paroxysms of rectal, ocular, or submandibular pain with flushing (Fertleman et al, 2006). These pain attacks start as early as infancy and are accompanied by autonomic manifestations such as skin flushing. The severity of pain is worst in the lower part of the body and can be triggered by bowel movements or probing of the perianal area. Attacks can also be accompanied by tonic nonepileptic seizures, bradycardia, and/or apnea, which appear to be more common in infancy and young children. The cause for the seizure-like activity and cardiac symptoms is not well understood (Fisher et al, 2010).

Why IEM patients experience pain in the feet and hands, triggered by warmth, while PEPD patients experience pain in the perianal area, triggered by rectal stimuli, perimandibular and/or periocular pain, is not currently known (Fisher et al, 2010).

In the case of loss-of-function mutations in *SCN9A*, which produce truncated, nonfunctional proteins (Fisher et al, 2010), the resulting phenotype is congenital insensitivity to pain (CIP). Patients display painless burns, fractures, and injuries of

the lips and tongue and were reported never to have felt pain in any part of the body in response to any injury or noxious stimulus. Other sensory modalities are preserved and the remainder of the patients' central and peripheral nervous systems are intact by report. Patients did not appear to exhibit any autonomic or motor abnormalities, and reportedly had normal tear formation, sweating ability, reflexes, and intelligence. (Fisher et al, 2010).

Voltage-gated sodium channels are important in the generation and conduction of action potentials. These are integral membrane proteins and are comprised of a large α -subunit, which forms the voltage-sensitive and ion-selective pore, and smaller auxiliary β -subunit(s) that can modulate the kinetics and voltage dependence of channel gating (Catteral et al, 2000). There are 9 isoforms known of the sodium-channel α -subunit (Nav1.1–Nav1.9), each with a unique central and peripheral nervous system expression profile. These different sodium channels share a common structure but are encoded by different genes and manifest distinct voltage-dependent and kinetic properties (Catteral et al, 2005). All α -subunits share the same general structure of six transmembrane segments (S1 to S6) present in each of four domains (DI to DIV), which are connected by intracellular peptide linkers. Voltage-gated sodium channels are members of the P-loop channel superfamily, which also includes voltage-gated potassium and calcium channels.

The voltage sensors in these channels are formed by the S1 to S4 transmembrane segments in every domain, while the walls of the permeation pathway are formed by the S6 helices. S4 is characterised by a series of positive gating charges that are crucial for sensing changes in the membrane potential (Lampert et al, 2010).

Nav1.7, Nav1.8, and Nav1.9 are the sodium channels known to be expressed neuronally. They are preferentially expressed in DRG and trigeminal ganglia neurons, most of which are nociceptive. The Nav 1.7 channel is expressed in almost all DRG neurons at various levels while the Nav1.8 and Nav1.9 channels are primarily expressed in small DRG neurons that include nociceptors (Fisher et al, 2010). Although Nav1.3 channels are not expressed above background levels in adult DRG neurons, the Nav1.3 channel has been shown to be upregulated in DRG neurons following injury. Therefore, along with the Nav1.8 and Nav1.9 channels, Nav1.3 has been suggested to play a role in neuropathic pain (Black et al, 1999). The

various voltage-dependent sodium channels present in these neurons can not only be differentiated by their gating kinetics and voltage dependence, but also by their sensitivity to the voltage-gated sodium-channel blocker tetrodotoxin (TTX) (Drenth et al, 2007). The Nav1.8 and Nav1.9 channels can be distinguished from the Nav1.7 channel by their resistance to TTX (Dib-hajj et al, 1999), while the Nav1.7 channel produces a rapidly activating and inactivating current that is sensitive to submicromolar levels of TTX. Here, we will focus on the first of the α -subunits, Nav1.7, because of its critical role in pain sensation.

Nav1.7 is encoded by *SCN9A*, a 113.5-kb gene comprising 26 exons. The coding region accounts for 1977 amino acids, which are organised into the typical structure of four domains each with six transmembrane segments. This particular sodium channel is predominantly expressed in the dorsal root ganglion neurons and sympathetic neurons (Toledo, 1997). The large majority of DRG neurons that express this channel are pain sensing (nociceptive), suggesting a role for Nav1.7 in the pathogenesis of pain.

Nav1.7 is characterised by slow transition of the channel into an inactive state when it is depolarised, even to a minor degree, a property that allows these channels to remain available for activation with small or slowly developing depolarisations. Thus, Nav1.7 acts as a “threshold channel” that amplifies small, subtle depolarisations such as generator potentials, thereby bringing neurons to voltages that stimulate Nav1.8, which has a more depolarised activation threshold. Nav1.8 then produces most of the transmembrane current responsible for the depolarising phase of action potentials (Renganathan et al, 2001). In this regard, Nav1.7 is proposed as a molecular gatekeeper of pain detection at peripheral nociceptors (Waxman, 2007).

A number of *SCN9A* gene point mutations are associated with human genetic pain disorders. Mutations causing a loss of function of Nav1.7 have been found in individuals with CIP. Conversely, 22 distinct mutations of Nav1.7 causing a gain of function have been found in individuals suffering from the pain syndromes IEM and PEPD. All 14 CIP-inducing mutations identified so far introduce a stop codon, which leads to premature protein truncation. The majority of patients are

homozygous, although some are compound heterozygotes with two different mutations, one on each allele. Mutations for IEM and PEPD on the contrary, are all missense mutations. The 13 mutations described for IEM were all identified as mutations located in highly conserved regions, while the substituted amino acids in PEPD lie in channel sections essential for fast inactivation, namely the linker between domains III and IV containing the IFM sequence motif that constitutes the inactivation particle and the inactivation particle receptor site (Lampert et al, 2010).

4.1.3 Mouse models as an example to screen new genes

Apart from accumulating additional knowledge about already known genes, further data can also be extracted by comparison with already known genes in animal models. The discovery of new animal models which are phenotypically similar to existing models or resemble the phenotype in patients invoke the need to screen relevant patient groups, to investigate whether these could also result in disease in humans. For most cases, animal models were generated after the discovery of the gene, but a handful of mouse models have been described with motor neurodegeneration where initially there was no causal gene known. Examples of this are the motor neuron degeneration 2 (*mnd2*) mouse (Jones et al., 1993) or the motor neuron disease (*mneu*) mouse (Miyata, 1983). Over the years, some of these cases were solved by finding the causative gene such as for the neuromuscular degeneration (*nmd*) mouse (Cox et al., 1998), the peripheral motoneuronopathy (*pmn*) mouse (Martin et al., 2002) and the legs at odd angles (*loa*) mouse (Hafezparast et al., 2003). In these three examples, patients were found with mutations in the same genes, leading to a similar phenotype.

Through collaboration with the MRC functional genomics unit in Oxford, a mutation in the ADP-ribosylation factor-like protein 1 (*ARL1*) gene was found in a mouse mutant. This mutation caused a progressive tremor and loss of fibres in the nerves, which points towards demyelination. *ARL1* is known to be localised on the trans-golgi and has been proposed to have a function in both exocytosis and in retrograde traffic from endosomes (Lowe et al., 1996). In this context, myelin biogenesis and maintenance is a complex process involving coordinated exocytosis, endocytosis, and cytoskeletal dynamics. Faults in the myelin protein trafficking and/or turnover could lead to demyelinating neuropathies in humans (Scherer et al., 2008).

In the same pathway, a mutation in the *ARL6ip1* gene was found in-house in a family with spasticity, neuropathy and mental retardation. This gene has previously been suggested as a HSP candidate gene, as a homozygous frameshift variant was found in a large family with the disease (Novarino et al., 2014). *ARL6ip1* encodes a membrane protein found in the ER, implicated in the formation of ER tubules. A zebrafish knockdown resulted in a phenotype of both touch-induced and spontaneous locomotion behaviour, as previously reported for other HSP candidate genes (Fassier et al., 2010). In combination with the results from the mouse model, the presence of mutations in two genes of the same pathway leading to neurodegeneration encouraged us to screen different cohorts for mutations in these genes.

4.2 Results

4.2.1 FIG4

Primer sequences were obtained from the lab of Prof. Timmerman in Belgium and in the selected cohort of 35 patients, one case was found to be a *FIG4* compound heterozygote carrying the previously reported p.Ile41Thr missense mutation and the protein truncation mutation p.Lys278YfsX5 (Fig. 4.1). A further nine variants were found in the cohort, six of which were intronic (Table 4.1). All but one were present in a high frequency in the EVS server database. One novel variant, c.289+5G>A, was predicted to affect the splicing site by spliceport. However, since CMT4J is a recessive disease, the presence of an additional mutation is required. Investigation showed no extra variants in this patient.

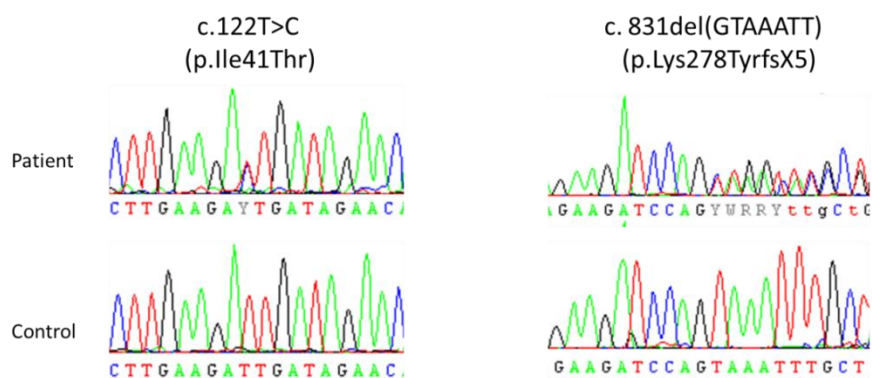


Figure 4-1 Electropherograms of compound heterozygous mutations found in *FIG4*.

Variants	dbSNP No	Info
c.67-7T>C	rs56378532	Intronic
c.289+5G>A		Intronic
c.647-18C>A	rs2273752	Intronic
c.877-54_877-50delTCATT	rs57291908	Intronic
c.1948+3A>G	rs10499054	Intronic
c.1961T>C	rs9885672	High frequency
c.2180+63G>T	rs9384723	Intronic
c.2559G>A	rs1127771	Synonymous
c.*29G>A	rs10659	High frequency

Table 4-1 Variants found in the *FIG4* gene.

Clinical details

A 26-year old man diagnosed with a congenital hypomyelinating neuropathy (CMT1), with early onset progressive weakness in all 4 limbs, was referred to clinic with rapid development of a wasted left arm over a period of 2 years. Following normal pregnancy and delivery, he had walked late at 26 months of age. He was the youngest of four brothers in a non-consanguineous Scottish family with no family history of neuromuscular disease. Both parents previously had normal clinical and neurophysiological examinations. In early childhood, progressive weakness, starting distally and advancing proximally, was observed. At 13 years of age, he started using a wheelchair and he became completely wheelchair dependent following a fracture of the left femur at 22 years of age. Two years prior to presentation, he developed rapidly progressive distal weakness of the left upper limb that progressed proximally. The left hand has been left functionally useless, whilst before there was only mild symmetric weakness and function was preserved function in both hands. No improvement was seen despite a 5-day course of 500 mg methylprednisolone.

On examination, he had a wasted, flaccid clawed left hand with wrist drop. There was no movement on finger extension or in the intrinsic muscles of the left hand and strength at the elbow, wrist and the intrinsic muscles of the left hand was lower than the right hand. There was mild weakness of hip flexion. He was areflexic. Vibration sense was normal in the right hand, reduced to the metacarpophalangeal joint in the left hand, and to the costal margins bilaterally in the lower limbs. Proprioception was

reduced to the right metacarpophalangeal joint, left wrist, and knees bilaterally. Sensation for pinprick was reduced to the wrist and ankles bilaterally.

Due to the rapidly progressive distal weakness of the left upper limb and the lack of a response to anti-inflammatories, a neoplastic cause was also suspected, particularly involving the left brachial plexus. An MRI of both brachial plexuses was normal and a T1 weighted MRI of the left upper limb at latest presentation demonstrated fatty infiltration of muscles, more marked distally, with sparing of biceps compared with triceps (Fig. 4.2).

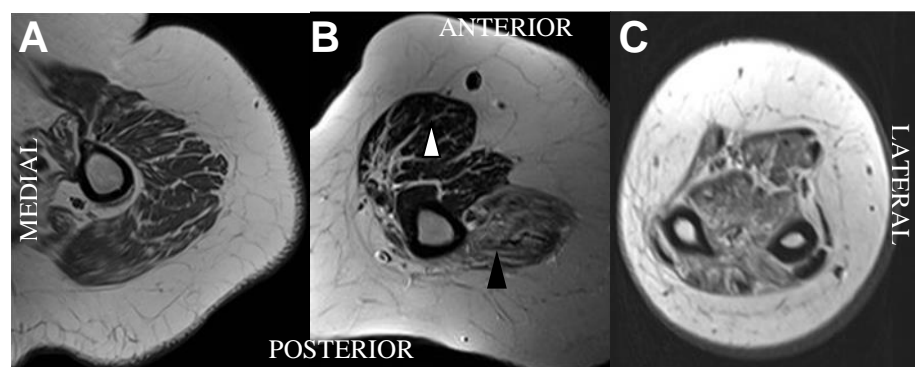


Figure 4-2 MRI of the patient. At the level of the upper humerus (A) there are streaks of fat infiltration in deltoid muscle. At the level of the lower humerus (B) there is extensive fat infiltration of triceps (black arrowhead) with less infiltration in biceps (white arrowhead). In the forearm (C) there is extensive fat infiltration of all muscle compartments. Image orientation is the same for all images.

Nerve conduction studies were performed at the age of 13 years, 19 years and at the latest presentation at age 26 years (Table 4.2). These showed a demyelinating neuropathy with dispersed proximal responses and a fall in the conduction velocity in the right median nerve from 16 m/s to 4 m/s over 6 years. In the latest studies, there was a significant asymmetry in the CMAP, with low amplitudes in the right median and ulnar nerves, and absent amplitudes on the left. There was evidence of conduction block in the right median nerve.

The most recent EMG showed no spontaneous activity and wide polyphasic units firing at high rates in relative isolation, consistent with severe chronic denervation, in the right triceps, right first dorsal interosseous (FDIO), left deltoid, left biceps, left triceps, and left extensor digitorum communis muscles. EMG of the left FDIO

showed frequent fibrillations and positive sharp waves and no motor units under voluntary control. A sural nerve biopsy was performed at 14 years of age and showed a severe demyelinating neuropathy with complete absence of large regularly myelinated axons in the resin semi-thin section and electron microscopy (Fig. 4.3).

	13 years	19 years	26 years
Motor conduction			
Median (R)			
DML	7.6 ms	12.0 ms	9.2 ms
CMAP (Wrist)	2.3 mV	4.4 mV	3.9 mV
CMAP (Elbow)	0.5 mV (dispersed)	2.4 mV (dispersed)	unobtainable
CV	16 m/s	4 m/s	
Median (L)			
CMAP (Wrist)			absent
Ulnar (R)			
DML	6.8 ms	7.6 ms	15.6
CMAP (Wrist)	1.4 mV	1.3 mV	0.7 mV
CMAP (Elbow)	unobtainable	unobtainable	0.4 mV (dispersed)
CV			4 m/s
Ulnar (L)			
CMAP (Wrist)		absent	absent
Posterior Tibial (R)			
CMAP (Ankle)	absent		
Common Peroneal (R)			
CMAP (Ankle)	absent		
Sensory conduction			
Median (Right)	absent	absent	
Ulnar (Right)	absent	absent	
Radial (Right)		absent	
Median (Left)			absent
Ulnar (Left)			absent
Sural (Right)	absent		

Table 4-2 Nerve conduction studies at ages 13,19 and 26. L = Left; R = Right; DML = distal motor latency; CMAP = compound muscle action potential; CV = conduction velocity.

There were relatively frequent large and medium-sized thinly myelinated fibres surrounded by concentric layers of Schwann cell profiles in keeping with onion bulbs. Several axons within the onion bulbs were devoid of myelin sheaths. No inflammation was present.

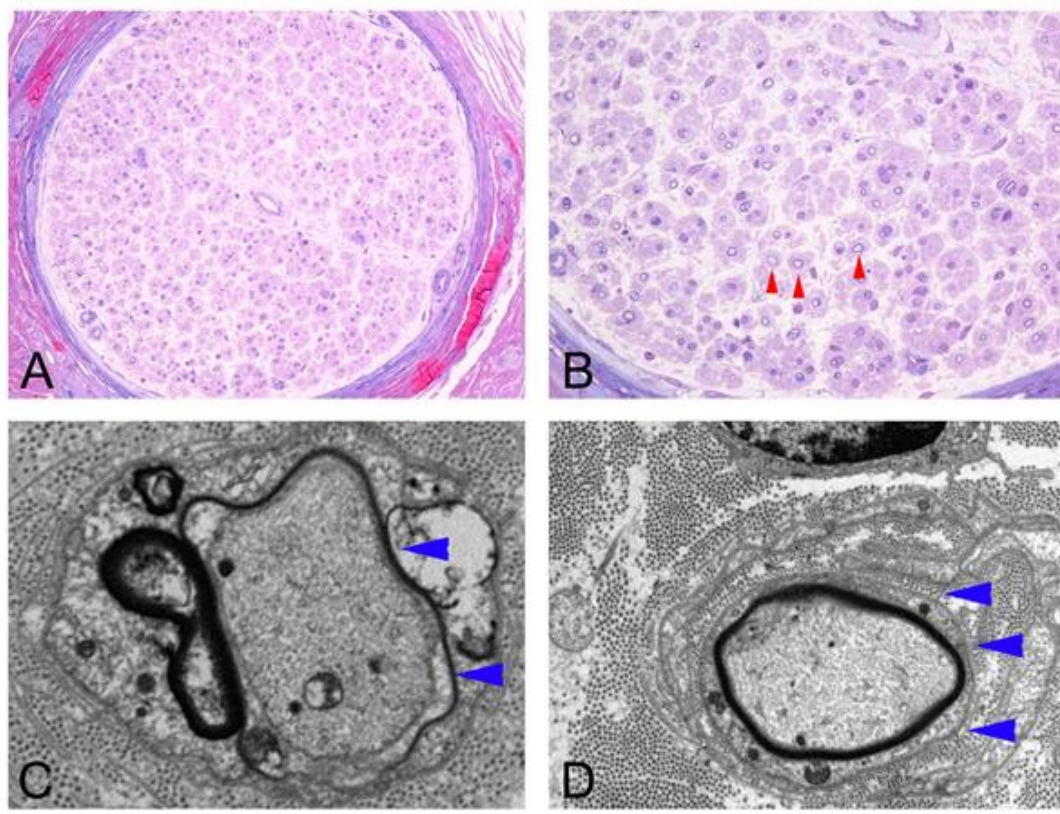


Figure 4-3 Sural nerve biopsy at age 14 years. (A and B) Semi-thin resin sections, stained with methylene blue azure – basic fuchsin. One single fascicle with absent large normally myelinated fibres and frequent large thinly myelinated fibres surrounded by concentric Schwann cell profiles (red arrowheads). (C) Electron microscopy showing demyelinating fibres losing their myelin sheath (blue arrowheads) (D) Electron microscopy showing frequent onion bulbs consisting of concentric multilayers of Schwann cell processes (blue arrowheads). The Schwann cell processes within the onion bulbs are separated by densely packed collagen bundles. Scale bar: 200 μ m (A), 100 μ m (B), 2.5 μ m (C), 5 μ m (D).

4.2.2 *C9orf72*

A cohort of 185 dHMN patients was screened for the repeat expansion in *C9orf72*. No patients presented with a pathological repeat expansion that was significantly over the threshold. Different amounts of repeats were found in the cohort with the longest repeat length consisting of 17 repeats, found in two patients (Fig. 4.4).

Whilst the pathogenic cut-off for the repeat expansions remains debatable, repeat sizes of 17 are commonly found in controls and are regarded as non-pathogenic.

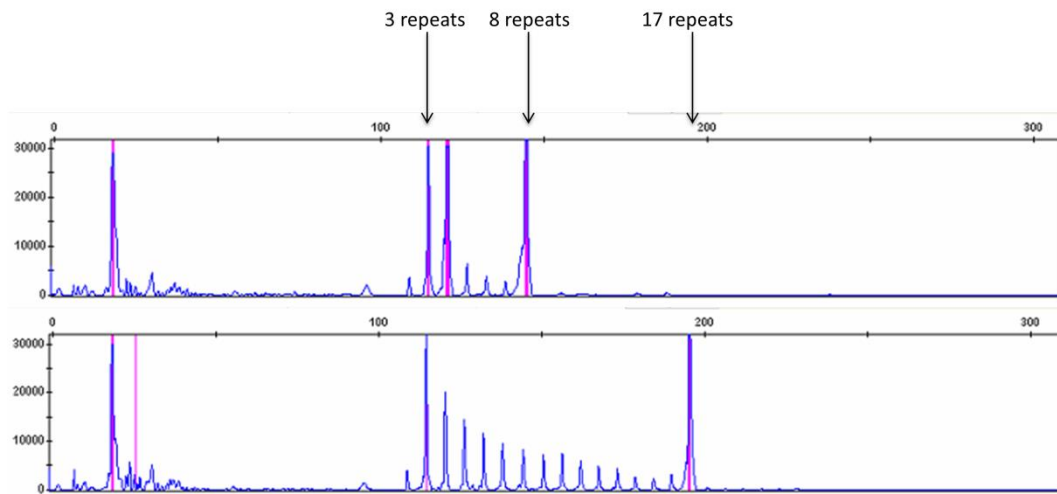


Figure 4-4 Example of fragment analysis in *C9orf72*. Upper panel = control. Lower panel = CMT2 patient. A repeat size of 17 repeats was found, which has been shown to be non-pathogenic.

4.2.3 *HINT1*

We investigated a cohort of 127 patients with predominantly recessive CMT2, but no mutations in the *HINT1* gene were found (Table 4.3).

Phenotype	#Patients
CMT2	84
Intermediate CMT	15
CMT1	2
Unclassified CMT	4
CMT2 plus	7
CMT1 plus	2
dHMN	11
HSAN	2

Table 4-3 Phenotype for the 127 patients analysed for mutations in the *HINT1* gene.

In the whole cohort, four variants were found, two of which were intronic and two synonymous; all were present in the EVS at a high frequency (Table 4.4). A cohort of 33 samples with CMT2 of Spanish origin was investigated by Dr. Alex Horga, a fellow PhD student, which also resulted in no pathogenic variants (In press).

Variants	dbSNP No.	Info
c.57T>C	rs4696	Synonymous
c.111+37T>G	rs2278060	Intronic
c.159G>A	rs199716973	Synonymous
c.216+37T>C	rs17165688	Intronic

Table 4-4 Variants found in the *HINT1* gene.

4.2.4 *SCN9A*

Three patients with CIP and twelve patients with IEM were selected for screening of *SCN9A* (Table 4.5).

Cases	Sex	Diagnosis	Clinical features
1	F	CIP	AR neuropathy, lack of sensation hands and feet, parents are cousins
2	F	CIP	CIP, AR neuropathy, very early onset, lack of distal sensation mainly to pain.
3	M	IEM	Stinking, painful and bright red feet felt to be consistent with erythromelalgia.
4	F	CIP	Neuropathy, pain loss distally.
5	F	IEM	Facial flushing provoked by heat, wheat and spicy food. Episodes associated with burning dysesthesia. Episodic bilateral facial aedema. Onset age 13.
6	F	IEM	FH of narcolepsy and pes cavus. Small fibre neuropathy. Painful feet with redness. Checking for mutations in SPTLC and RAS7.
7	F	IEM	Arms and face associated with face pain and headache.
8	M	IEM	Painful neuropathy. Redness and discolouration. Negative for SPTLC1.
9	F	IEM	Painful feet and cold feet.
10	F	IEM	Familial neuropathy. Pain and numbness.
11	M	IEM	Painful erythromelalgia and redness.
12	F	IEM	Episodic pain + redness in feet.
13	M	IEM	History of pain & redness - episodic - both feet. Some improvement with carbamazepine.
14	M	IEM	Painful erythromelalgia and redness.
15	F	IEM	Sister also affected. Very painful neuropathy with erythema.

Table 4-5 Patient cohort for the screening of *SCN9A*.

No known mutations were found in either of the two groups. However, 18 intronic and 15 coding variants were found, seven of which were synonymous (Table 4.6). No further investigations were made for the intronic variants, since none of them were located close to a splice site. Out of seven synonymous variants, only one was novel, which was not located anywhere close to a splice site hence no further investigations were made. Seven out of eight coding, nonsynonymous variants were prevalent in the EVS and ExAc databases. The remaining novel variant was the c.4645T>C (p.Trp1549Arg) missense variant in patient no.9, suffering from IEM with painful and cold feet (Fig.4.5). This variation is situated in the S2 transmembranous segment of domain four and changes tryptophan 1549 to arginine. So far, no other mutations have been found in any of the S2 segments. Few mutations, causing either CIP or PEPD have been found in domain four. Both PolyPhen2 as SIFT prediction programs were used, resulting in a contradicting outcome. However, prediction programs are often not very accurate, and when known *SCN9A* mutations are entered, they can also be predicted as being benign. Tryptophan 1549 is conserved amongst higher species and the change of an aromatic aminoacid to a negative would suggest that this might be a pathogenic mutation.

Synonymous changes		Coding nonsynonymous	
c.174G>A	rs6432901	c.684C>G	rs71428908
c.444A>G	rs9646771	c.2971G>T	rs4369876
c.1119T>C	rs13414203	c.3329G>A	rs74401238
c.1266A>G	rs13402180	c.3448T>C	rs6746030
c.1287T>A	rs6747673	c.4612T>C	rs202084411
c.3642C>A	rs77144869	c.4645T>C	
c.4812G>T		c.4741+16T>A	rs10180721
		c.5725A>G	rs3750904

Table 4-6 Coding changes found in the *SCN9A* gene.

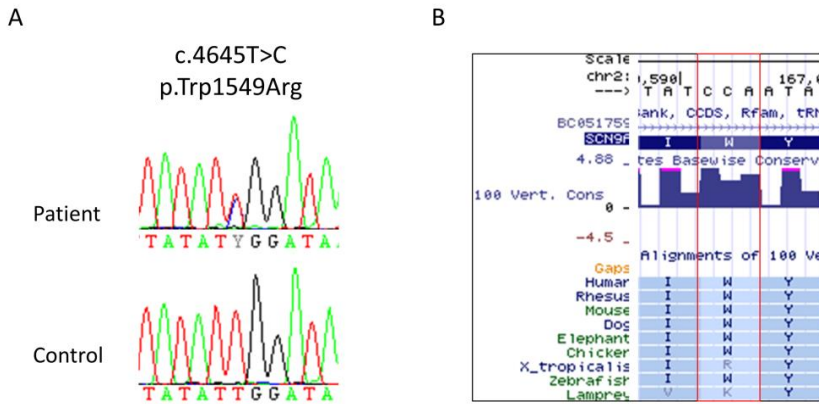


Figure 4-5 Missense variant in *SCN9A*. (A) Electropherogram of the c.4645T>C missense variant in patient 9. (B) Conservation of the tryptophan aminoacid at position 1549 in *SCN9A*.

4.2.5 *ARL1* and *ARL6ip1*

Screening of *ARL1*

A cohort of 35 patients with CMT1 was selected for screening of *ARL1*, but no coding variants were found. Five variants were found outside the coding regions, with four of them located deep in the introns of the gene (Table 4.7). The last variant was located three base pairs from the stop codon but showed a high prevalence in the EVS database.

Variants	dbSNP no
c.1-82G>C	rs76432489
c.225-58T>G	rs17500203
c.336+74A>G	
c.337-18A>G	rs73159756
c.*3C>A	rs201219157

Table 4-7 Variants found in the *ARL1* gene.

Screening of *ARL6ip1*

45 patients with a CMT2 phenotype were selected for screening of *ARL6ip1*. Results showed three intronic variants and one coding, synonymous variant present in the EVS database (Table 4.8).

Variants	RS no
c.36+104delC	rs141868228
c.170+12A>T	rs17663173
c.204C>T	rs138748723
c.409-18T>C	rs71382566

Table 4-8 Variants found in the *ARL6ip1* gene.

4.3 Discussion

4.3.1 *FIG4*

Multiple reports have shown cases of patients with CMT and mutations in *GJB1*, *SH3TC2* or *SPTLC1* mimicking CIDP by showing asymmetric or proximal weakness (Houlden et al., 2006; Houlden et al., 2009; Michell et al., 2009). When combined with a progressive course and a poor response to treatment, the possibility of CMT might arise. The presence of a proximal and asymmetric weakness and rapid deterioration of strength in a single limb in our patient suggested the presentation of CIDP with an underlying genetic neuropathy, which would have been expected to improve with immunosuppressant medication. However, two compound heterozygous mutations in the *FIG4* gene were found resulting in the *FIG4* I41T/K278YfsX5 genotype. One patient has been described with the same genotype before, and has also been treated with immunosuppressant medication (Nicholson et al., 2011). He had been diagnosed with Dejerine-Sottas syndrome at age 5 and progressed to wheelchair dependence over a period of 30 years, then developed a rapidly progressive weakness of his left arm at age 41. Sural nerve biopsy also showed features of onion bulbs and extensive loss of large diameter myelinated fibres. Improvement with corticosteroids was not sustained, and there was no response to intravenous immunoglobulin.

This leads to the conclusion that compound heterozygous mutations in *FIG4* can be a rare cause of Charcot-Marie-Tooth disease where initially inflammatory demyelinating neuropathy is suspected. Early onset and progressive proximal and distal weakness in a single limb with chronic denervation changes on EMG are clinical clues that could suggest the diagnosis.

4.3.2 *C9orf72*

There was an absence of *C9orf72* repeat expansions in the dHMN cohort screened, which helped to define the spectrum of *C9orf72* expansion-associated neuropathology. Repeats above 60 are normally considered pathologic; repeat sizes between 30-60 remain debatable as intermediate alleles and their significance has not been clarified yet. The longest repeat size found in our cohort was 17 repeats, regarded as being non-pathogenic. Therefore it could be concluded that repeat expansions in *C9orf72* are highly unlikely to be responsible for a CMT phenotype.

4.3.3 *HINT1*

The original report by Zimon et al. stated a frequency of mutations in *HINT1* of 11%, which could not be replicated in our study. Only 33 families with a very specific phenotype were originally screened in the paper, explaining the high frequency. It is remarkable that even in a large cohort of more phenotypically heterogeneous CMT2, no mutations were observed. This suggests that mutations in *HINT1* might not be as frequent as stated in CMT and predominantly occur in families presenting with a specific phenotype of axonal neuropathy and neuromyotonia. Screening of a Spanish cohort resulted in the same negative results and together with the observation that from a total of 73 patients with *HINT1*-related neuropathies reported to date, 59 (81%) are from the Czech Republic, Austria, Serbia, Bulgaria and Turkey, the presence of a founder-effect is highly likely. This geographical distribution together with mutation distribution and haplotype studies suggests the presence of founder effects that may explain the prevalence of the disorder in those areas. *HINT1*-related neuropathies are not widely distributed but mostly confined to specific European populations, although additional studies are needed to confirm this observation. This conclusion underlines the importance of considering the ethnic background of a patient when screening for mutations in neuropathy-related genes.

4.3.4 *SCN9A*

Only one potentially pathogenic variant was found in the 15 patients with pain disorders. This patient was seen in clinic only once and was diagnosed with a small fibre painful neuropathy at late onset in adulthood. She had no family history and is now in her seventies. Unfortunately, the patient did not return for further clinical investigation and DNA from the family was not available for segregation. Whilst the

prediction programs were contradictory, the absence of the mutation in controls and the relatively high conservation indicate the potential pathogenicity of the variant. None of the other patients with CIP or IEM showed any possible pathogenic variants in the exons of the *SCN9A* gene and will be investigated further for mutations that could explain the phenotype.

4.3.5 *ARL1* and *ARL6ip1*

Although no mutations were found in our cohort for the *ARL1* or *ARL6ip1* genes, this does not rule out these genes as causative genes for peripheral neuropathies. The presence of a progressive tremor and loss of fibres in the nerves in mutated mice indicates demyelination and further studies in undiagnosed families with similar phenotypes might reveal mutations in these genes.

4.3.6 *Overall discussion*

Recent advantages in next-generation sequencing have dramatically changed the process of Mendelian disease gene identification. Past identification of Mendelian disease genes was carried out by Sanger sequencing, with candidate genes being selected due to resemblance of genes in similar diseases, predicted protein function being relevant or positional mapping pointing to a genomic region. The rise of next generation sequencing techniques has resulted in a move from the use of Sanger sequencing for a general search of causative genes towards more targeted resequencing. There is no longer a need for complex and time-consuming processes for gene-identification and in the future, more advanced techniques will become faster and more affordable, leading to the disappearance of single gene testing. In the meantime, diagnostic guidelines are used to target specific genes in undiagnosed families or cohorts.

Chapter 5

Whole exome sequencing

5.1 Introduction

5.1.1 Previous ways to identify disease genes

Historically, before the use of mapping information, the discovery of pathogenic mutations in genes started with position-independent methods based on the knowledge of the gene product. Approaches ranged from the generation of a cDNA expression library out of amino acid information, animal models or detection of repeat expansions in the case of anticipation of disorders along generations. When techniques such as linkage analysis became available to estimate the approximate chromosomal location, positional cloning techniques were used to identify the causal gene. Clones were established for the whole of the candidate region and a transcript map was used to identify all genes within the candidate region. This list of genes was further prioritised by appropriate expression pattern, function, or homology to a relevant paralogous or orthologous gene. In rare cases, chromosomal abnormalities such as translocations or deletions provided an alternative method of localising a disease gene. Mutation screening, restoration of the normal phenotype in vitro or production of a mouse model of the disease were used to demonstrate the likeliness of a candidate gene as disease locus.

5.1.1 Discovering new genes with the use of whole exome sequencing

The recent shift from traditional Sanger sequencing and linkage analysis to high-throughput next-generation sequencing methods has revolutionised gene discovery and diagnostics for Mendelian and complex diseases, and exome sequencing has already been proven to be a useful tool in the discovery of new Mendelian disease genes. In more than 85% of the cases, mutations associated with known Mendelian diseases are located in protein-coding exons (Bamshad et al., 2011). Therefore, exome sequencing may be an efficient tool for the identification of novel mutations/genes in patients with diseases such as CMT2. While there are still some challenges to overcome, using this technique is on the whole advantageous. In the first two results sections, focus will be on two examples where interesting candidate genes were found and pursued with functional experiments. However, in the majority of cases, identifying one specific candidate gene has been proven to be difficult. Most of the remaining undiagnosed CMT families are small and only few ways to narrow down the list of candidate genes are possible. Even in larger families this raises a problem. The remaining result sections will go through the challenges of finding a new gene with the help of exome sequencing and some of the open questions that it results in.

5.1.2 The usage of linkage analysis in combination with whole exome sequencing

Although exome sequencing is an extremely useful technique, one of the disadvantages when performed on two distant relatives such as cousins is that it can give up to thousands of shared nonsynonymous variants. Different filters can be used to narrow down these lists of variants, but one highly useful technique is linkage analysis (Fig. 5.1). Several generations with multiple affected and unaffected individuals are necessary to give power to this technique. These affected and unaffected family members are used to map the fragments of the genome that are shared only by the affected patients and not by the unaffected members of the family. Only variants that are present in linkage areas could be causing the disease. This could narrow down the list of possible variants significantly, but for diseases where there is a high risk of incomplete penetrance, this is not the optimal technique to use. In CMT2, there are only few cases that have shown reduced penetrance in families with *MFN2* or *TRPV4* mutations (Nicholson et al., 2008; Berciano et al.,

2011), meaning we can safely assume no pathogenic variants will be excluded when using a model with 90% penetrance.

5.1.3 Prioritizing variants to find a favourable candidate gene

Even though linkage analysis can significantly reduce the candidate gene list, additional methods are necessary to decide on a specific candidate gene (Fig. 5.1). First of all, synonymous variants and variants with a segmental duplication coefficient higher than 0.96 will be excluded. Of the remaining variants, those that have a minor allele frequency higher than 0.5% in the public databases will also be omitted. As few genes in CMT2 show incomplete penetrance, variants that are novel and have not been found in any of the publicly available databases will be prioritised. Providing there are no mutations in the known CMT2 genes, variants in genes that have been implicated in other neurological diseases can be excellent candidates. Recent research has shown the expansion of phenotypes associated with genes is becoming increasingly more common. In the event that none of the variants are located in pathogenic genes, a selection can be made of genes specifically expressed in the PNS, or with functions related to known pathogenic mechanisms in CMT2. Evidence of genetic or functional interactions with known CMT2 genes can also shortlist candidates. This usually results in a reduced list of potential candidates.

5.1.4 The ubiquitous variants of unknown significance

For many, if not all, novel missense mutations, there can be little data on which pathogenicity can be based. A range of bioinformatics tools are available to predict or estimate the influence of a variant by looking at the evolutionary conservation, the consequences on structural conformation, and many others.

Whilst these tools can be useful to prioritise the most likely candidate gene, their predictive power is highly variable and does not lead to definitive conclusions. Due to the genotypically heterogeneous character of CMT, the functions of known pathogenic genes are extremely divergent; meaning functional testing of candidate genes will rarely have a precursor amongst the known genes. This results in the development of individual functional tests to prove the pathogenicity of novel variants, a time-consuming and often difficult task.

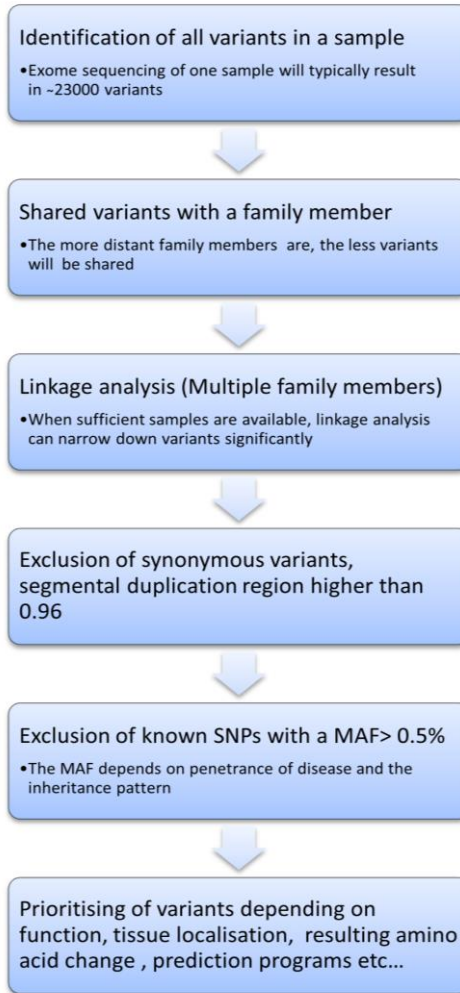


Figure 5-1 Exome sequencing workflow, starting from the return of the data to the choice of a candidate gene.

Similarly, it can be as challenging to prove a variant is benign as it is to prove it is pathogenic. This will result in the presence of variants of unknown significance that can only be ruled out over time. As more next-generation sequencing data will become available, fewer variants will be considered novel and clinical and molecular research will categorise variants as convincingly benign or pathogenic. However, caution has to be taken with publicly available data. The increase in NGS data will identify rare variants previously considered as rare to be polymorphisms, but at the same time will return more novel variants that result from the normal mutation rate. It should be anticipated that the existence of novel mutations will persist and will remain challenging.

5.2 Results

5.2.1 Success rate of exome sequencing in rare diseases

In our centre, exome sequencing was performed in 31 probands and 22 relatives with CMT. Out of these, 24 cases were familial and 7 were sporadic. In three of the probands, mutations were located in known genes. One probable pathogenic genetic variant was identified in a novel gene in one pedigree, and two definite pathogenic variants were found in two unrelated pedigrees in novel genes. Whilst analysis is still in progress, preliminary results suggest a success rate of 6/31 (19%) of exome sequencing for the detection of known or novel variants in inherited neuropathies (unpublished data). Published data by several groups can range from a success rate of 10-71% (Gilissen et al., 2012; Need et al., 2012; Gahl et al., 2012; de Ligt et al., 2012; Choi et al., 2012). This immense range results from differences in the exome sequencing approach. Studies with a high success rate have a higher turnover of mutations in known pathogenic CMT genes, resulting from a more diagnostic approach. Depending on the phenotype of the family and the centre of research, exome sequencing can be a more cost-efficient way to find the genetic diagnosis, especially when families are less well-characterised.

5.2.2 Family D

The index case (Patient IV-1, Fig. 5.2) was a 24 year-old patient who had normal birth and normal milestones. From the age of 2 he had frequent falls, lower limb wasting and a tendency to turn over his ankles and high arches. Slowly progressive distal wasting and weakness of the lower limbs and sensory loss in the feet followed. During examination, he was unable to stand unaided from sitting and had a positive Gower's manoeuvre. He was unable to stand on heels or toes and walked with a slightly stiff gait. Tone was increased in the lower limbs, with no clonus. Distal wasting was present in both the upper and lower limbs. He was areflexic. Sensory examination showed pin prick reduction in the fingers and to the proximal half of the calf bilaterally; vibration sense was present at the knees and proprioception was normal.

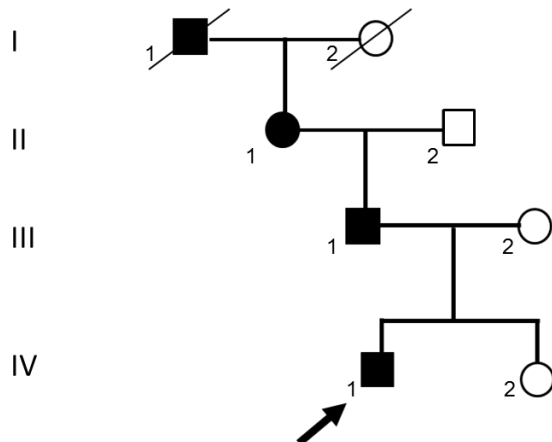


Figure 5-2 Pedigree of CMT2 family D. The index case is indicated with an arrow. Black symbols represent individuals with CMT2.

NCS revealed an axonal sensorimotor neuropathy affecting the lower limbs only. EMG showed a neurogenic pattern with proximal and distal lower limb muscles affected equally. Central motor conduction times to the lower limbs were mildly prolonged. Lateral vastus muscle biopsy showed angular atrophic fibres, grouping of type I and III fibres consistent with denervation and reinnervation. Respiratory chain enzyme analysis showed reduction of complex I 0.077 (ratio 0.104 – 0.268), II 0.032 (ratio 0.040 – 0.204), IV 0.008 (ratio 0.014 -0.034).

The father of the index case (Patient III.1; Fig. 5.2) was 56 and has worn shoes with ankle support since the age of 15. He complained of occasional cramps and could run until the age of 48. Neurological examination showed minimal wasting of intrinsic muscle of the hands and tibialis anterior. He had mild distal weakness in the upper and lower limbs. Reflexes were normal except ankle reflexes which were absent. Plantars were extensor. Sensory examination showed reduced pinprick to mid foot and mid palm bilaterally, reduced vibration sense to ankles, normal proprioception. NCS was consistent with an axonal sensory and motor neuropathy. EMG showed denervation changes in upper and lower limb muscles again equally involving proximal and distal muscles.

The grandmother (Patient II.1; Fig. 5.2) was an 88 year old woman who had been diagnosed with Charcot-Marie-Tooth disease at the age of 49. She recalled being unable to stand on her toes in her 20s and walking “flat footed”. She began to use a stick at the age of 50 and her walking slowly deteriorated over the years and she

became wheelchair-bound in her 70s. In her 50s she developed symptoms in her upper limbs with hand fine movements difficulties. She developed hearing loss at the age of 78. Neurological examination showed intrinsic hand muscles and proximal and distal wasting in the lower limbs. She had moderate distal weakness in the upper limbs, mild proximal weakness in the lower limbs and severe distal lower limb weakness. She was areflexic. Sensory examination showed reduction of pin prick to the knees; vibration sense was absent in the lower limbs. Proprioception was normal. NCS showed a severe axonal motor and sensory peripheral neuropathy. EMG showed denervation in upper and lower limb muscles again with proximal and distal muscles being equally affected. The neurophysiological findings were similar to those demonstrated in her son and grandson.

Overall, the phenotype in this family was consistent with an axonal sensor and motor neuropathy, however, the index case was much more severe in comparison to the father and grandmother.

The discovery of a candidate gene

Sequencing of the index patient at a diagnostic level returned negative results for *PMP22*, *MPZ*, *GJB1*, *MFN2*, *TRPV4*, *HSPB1*, *HSPB8*, *GDAP* and *BSCL2*. He was also negative for common point mutations and large scale rearrangements of mitochondrial DNA in the muscle, and for common mutations in the nuclear encoded DNA polymerase gamma (*POLG*) and *PEO1* genes. Full mitochondrial genome sequencing of muscle from the index patient identified a homoplasmic m.12241delC deletion in *tRNA serine* 2 (Fig. 5.3). This single base pair deletion was heteroplasmic (63%) in the mother's blood. This variant has not been previously described and is located at a highly conserved nucleotide suggesting it may be pathogenic. Mitomap shows the presence of this variant in six samples out of 26,851; all located within different haplotypes, but no phenotypic data was available. Considering the difference in severity between the index case and the father and grandmother, the presence of this deletion in both index case and mother questions whether this might be an influencing factor on the phenotype of the index patient. This deletion is located in the T-stem of the tRNA Ser (AGY), in a short c-stretch, containing five G-C base pairs (Fig. 5.3). The m.12241 position is highly conserved amongst species, but depending on the nomenclature, this variant can also be

referred to as m.12239delC, a location that is much less conserved and is deleted in many species (Sprinzl et al., 1998). However, whilst other tRNA genes have shown to be more affected by mutations, only six mutations in the MT-TS2 are known to cause disease. These were associated with chronic intestinal pseudo-obstruction with myopathy and ophthalmoplegia, diabetes mellitus with deafness and retinitis pigmentosa with progressive sensorineural hearing loss, MELAS-like phenotype, and non-syndromic hearing impairment (Cardaioli et al., 2011).

To find the causative variant, exome sequencing in the index patient, father and grandmother revealed novel variants in several genes which could explain the phenotype. In collaboration with Professor Zuchner's lab in Miami, the candidate list was narrowed down to 34 possible candidates by a strict filtering approach for segregation of nonsynonymous heterozygous variants using the Genomes Management Application (GEM.app) software (See appendix II), one of them being the trafficking protein, kinesin binding 2 (*TRAK2*) gene.

Trafficking protein, kinesin binding 2

TRAK2, also known as Grif1 or Milton in *drosophila*, is a member of the molecular complex that links mitochondria to kinesin motors and is known to associate with *MFN2* (Glater et al., 2006; Misko et al., 2010), making it a suitable candidate to explain the phenotype, considering the lower activities of the complexes in the electron transport chain. *TRAK2* is a 913-amino acid protein that was originally identified as a GABA_A receptor-trafficking protein called GABA_A receptor interacting factor-1 (GRIF-1) (Beck et al., 2002). It was renamed *TRAK2* in 2006 after studies showed it is a kinesin adaptor protein, part of the *TRAK* family of kinesin adaptors (Brickley et al., 2005; Smith et al., 2006). This family consists of two members, *TRAK1* and *TRAK2*. Both bind to the cargo binding domain of kinesin-1 heavy chains to connect the motor protein and the cargo. One well-established cargo in this context is the mitochondria.

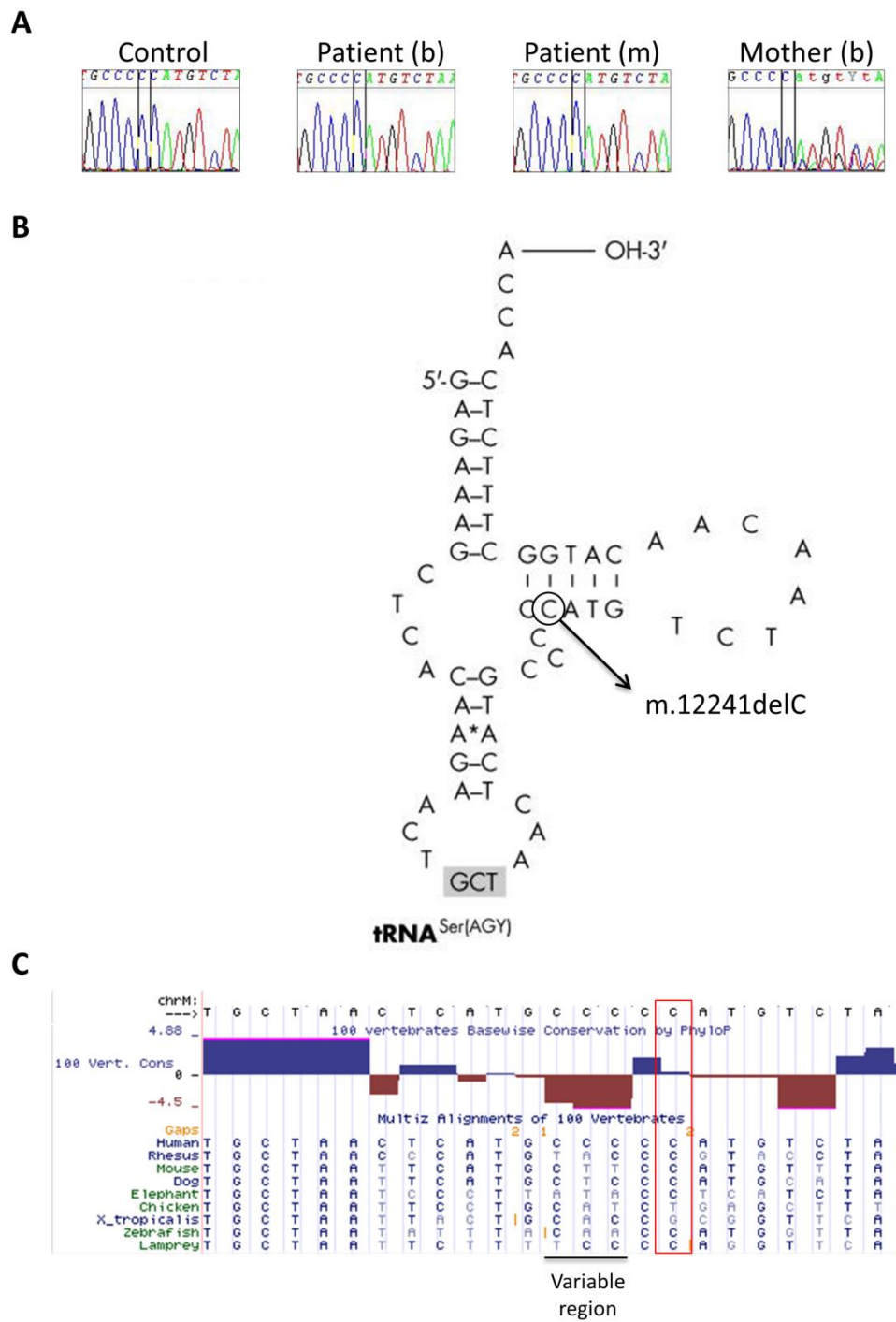


Figure 5-3 (A) Electropherograms of the m.12241delC variant in the blood and muscle of the index patient and blood of the mother (III.2) in comparison with a control. b = blood; m = muscle (B) Localisation of the m.12241delC frameshift variant in *tRNA serine* 2 (C) Conservation of the basepair amongst different species.

Both TRAK1 and TRAK2 associate with the outer mitochondrial membrane GTPase protein Miro, facilitating mitochondrial transport (MacAskill et al., 2009; Brickley et al., 2011). Recent studies show that TRAK2 preferably binds to Dyenin/dynactin and is more abundantly expressed in dendrites. These differences in preference follow from their distinct conformations; TRAK2 adopts a folded conformation through an association between its NH₂ and COOH termini, which inhibits the binding to kinesin-1 in low concentrations (Van Spronsen et al., 2013).

The implications of mutations in TRAK2

The transport of mitochondria is particularly vital in neurons because of their extended processes, and the disruption of mitochondrial transport is correlated with neurodegenerative diseases (Hollenbeck et al., 2005). So far, neither TRAK1 nor TRAK2 have been implicated in disease. Knockdown studies in hippocampal neurons show a decreased mitochondrial mobility in the TRAK1 shRNAi transfected cells, but no difference was found in TRAK2 shRNAi transfected cells (Brickley et al., 2011).

In reference to CMT2, interaction between MFN2 and TRAK1/2 has been shown to mediate mitochondrial transport. CMT2A mutants result in an increased pause time and slower movement velocities in both anterograde and retrograde directions, similar as to what has been seen in the TRAK1 shRNAi transfected cells. Results suggest this occurs by affecting the functionality of the molecular adaptor complex that links mitochondria to kinesins and not by disrupting the formation, since the interaction is still present (Misko et al., 2010). With *MFN2* being the most common gene in CMT2, *TRAK2* presents as an interesting candidate gene to explain the phenotype in this family. Exome sequencing in our index patient revealed a novel variant in the *TRAK2* gene, c.682C>T (p.Arg228Ter), which introduces a stop codon. This variant is located at a conserved location, part of a 297 amino acid stretch encoding a coiled-coil domain that shows high similarity to the Huntington-associated protein-1 (HAP1). This protein is also a GABA_A receptor β subunit interacting protein, similarly to TRAK2 (Kittler et al., 2004). HAP1 also functions as a kinesin adaptor protein, suggesting that this variant might affect the binding with kinesin (Twelvetrees et al., 2010).

Genetic screening of patients with CMT2 revealed two unrelated probands with variants in TRAK2

Genomic DNA sequence analysis in a specifically selected cohort of 48 patients with CMT2 identified two different novel missense variants in two separate patients that were screened for variants in *TRAK2*: c.416G>A (p.Arg139Gln) in exon 5 and c.2099G>T (p.Ser700Ile) in exon 13 (Fig. 5.4). Neither was detected in 5250 controls. Polyphen2 predicted c.416G>A to be damaging, contrasting the benign prediction of SIFT. The latter variant was predicted to be possibly damaging by both programs. Whilst the conservation of the c.416G>A variant is conserved over species and it is also located in the HAP1 homologous region, this is not the case for the c.2099G>T variant. Familial segregation analysis in the first patient revealed that the p.Arg139Gln variant was not present in the unaffected mother of the patient. DNA for the father was not available. The p.Ser700Ile variant in the second patient was found in the father of the patient, who was unaffected. This indicates that this variant is a polymorphism and not the cause of disease. Collaborators in Miami later on discovered an additional patient that presented with a CMT2 phenotype and a nonsense variant in the *TRAK2* gene. However, this variant was also present in the non-affected father. The presence of a nonsense variant in this gene in a non-affected individual strongly suggests the variant found in our index case is not pathogenic and a hypothesis of haploinsufficiency would not be valid. Preliminary functional studies were already performed before this variant was found and will be discussed below.

Clinical details of the patient with the c.416G>A missense variant in the TRAK2 gene

A 51 year-old male developed lower back pain at the age of 39. Two years later he developed numbness in his left leg. At the age of 43 he underwent L5/S1 discectomy and at that time he noticed wasting of the left calf. Over the years he had progressive wasting, weakness and sensory loss in the left leg and he noticed involvement of the right leg. His parents were not consanguineous; the mother was clinically examined and was unaffected and the father and one sibling were reportedly unaffected, although they were unavailable for examination. On neurological examination he walked with a bilateral foot drop and could not stand on toes or heels. He had distal wasting of the lower limbs, more pronounced on the left side. He had normal strength in the upper limbs and distal weakness in the lower limb.

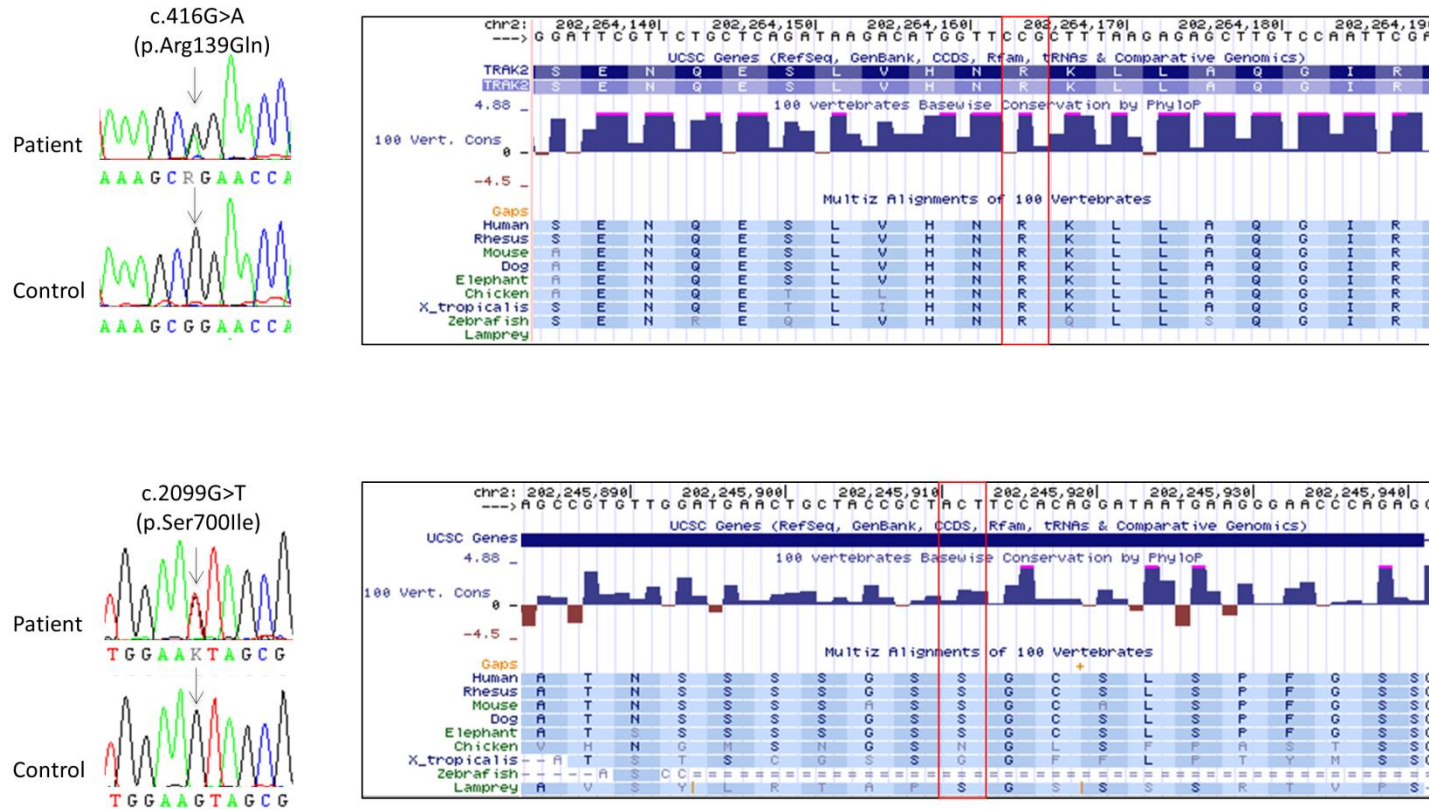


Figure 5-4 Electropherograms and conservation of the novel missense variants found in the CMT2 patient cohort.

Triceps and knee reflexes were brisk, ankle jerks were absent and all other reflexes were present. Plantars were downgoing. Sensory examination showed decreased pin prick up to the distal half of the calf bilaterally. Vibration sense was reduced at the knees and proprioception was normal. Nerve conduction studies demonstrated length-dependent axonal peripheral neuropathy with predominant sensory involvement.

Nonsense-mediated decay is present in fibroblasts of patients with variants in TRAK2

PCR analysis of the extracted mRNA indicated degradation of the mutated mRNA by the nonsense-mediated decay (NMD) pathway rather than the production of truncated proteins. Figure 5.5 shows that the mRNA level of the mutated codon was found to be significantly lower than the WT codon, indicating NMD. This occurs by selectively degrading mRNA transcripts that contain premature termination codons (PTCs) from nonsense and frameshift mutations. Two different analysing programs were used to analyse the sequence, with different calling thresholds. The seqscape program did call the variant, whilst sequencher did not pick up the signal.

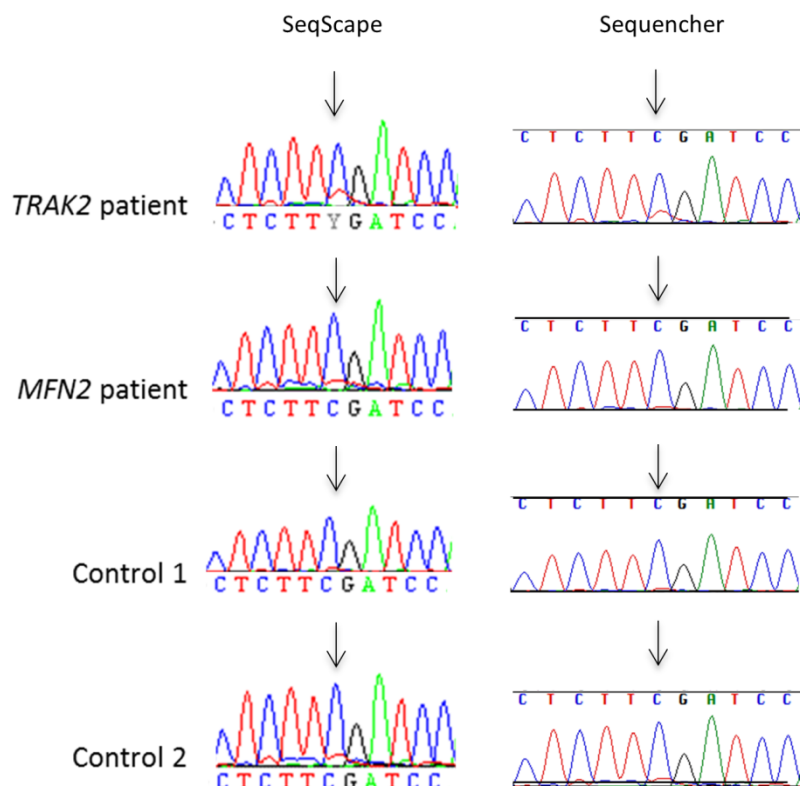


Figure 5-5 cDNA analysis of the nonsense variation in *TRAK2*. The variant is not present, indicating NMD.

Subcellular localisation of TRAK2 in patient fibroblasts is normal

In collaboration with the lab in Miami, localisation experiments were performed. COS7 cells were transfected with wild type and mutant c.682C>T *TRAK2*. This resulted in aggregation in puncta of the truncated TRAK2 in the nucleus (Fig. 5.6).

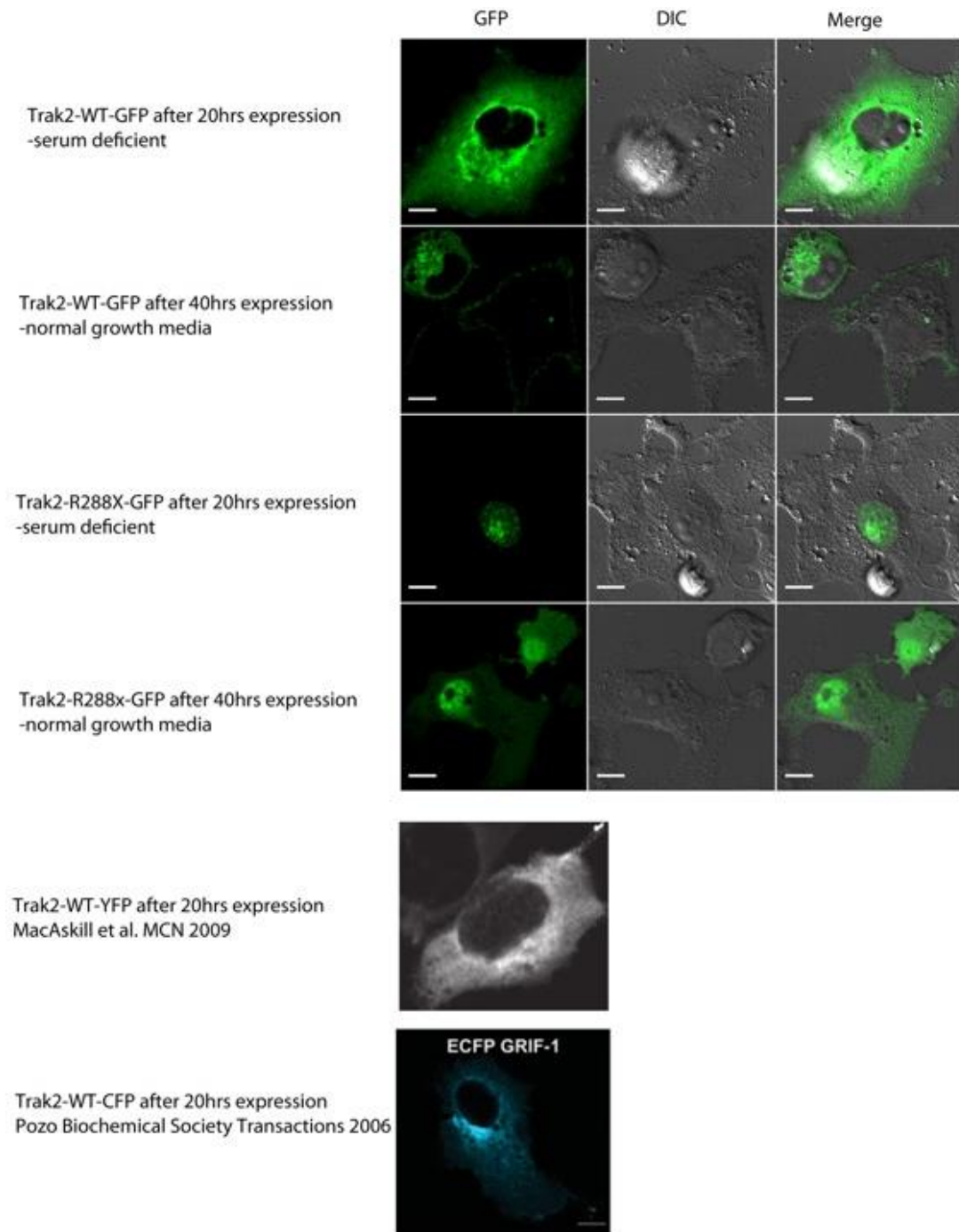


Figure 5-6 Localisation experiments of TRAK2 in transfected COS7 cells, experiments performed in Miami.

To investigate whether the nonsense variant also affected the localisation of the endogenous protein, experiments were performed in patient fibroblasts. However, immunocytochemistry showed no morphological differences between the cultured fibroblasts from patient and controls (Fig. 5.7). The subcellular localisation of the TRAK2 protein remained the same in all the different cell lines and no puncta were present in the patient cell lines.

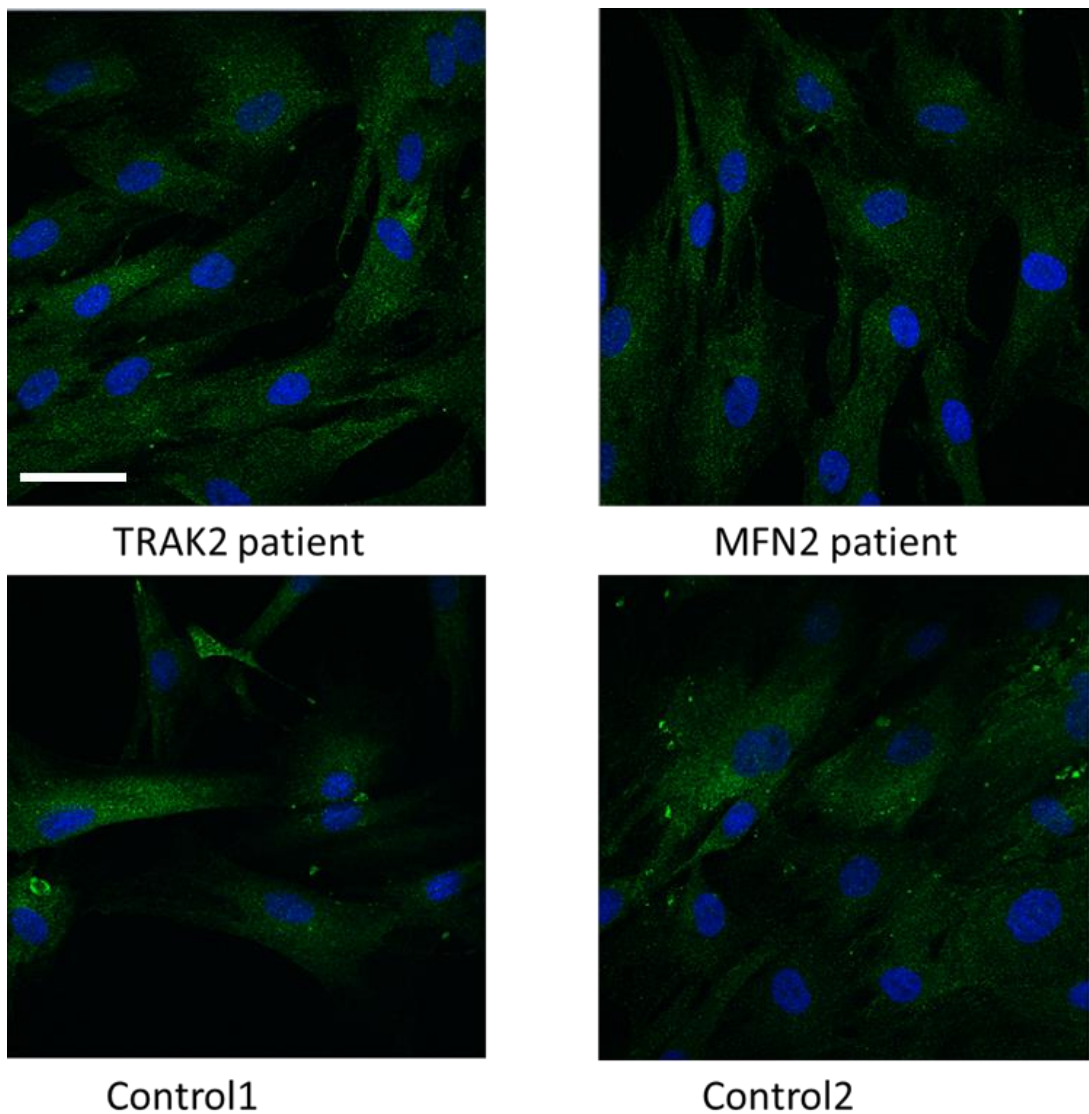


Figure 5-7 Localisation of TRAK2 in patient fibroblasts in comparison with a MFN2 patient and two controls. Scale = 49 μ m. Green: TRAK2; Blue: 4',6-diamidino-2-phenylindole (DAPI) staining for the nucleus. No difference in clustering of the truncated protein is found between the controls and both the TRAK2 and MFN2 mutated cell lines. TRAK2 patient = p.Arg228Ter; MFN2 patient = p.Ser249Thr.

Basal mitochondrial membrane potential in TRAK2 fibroblasts results in too variable results

The mitochondrial membrane potential ($\Delta\Psi_m$) is an important indicator of mitochondrial health. An essential player in the maintenance of this potential is the electron transport chain. Since the activities of complex I, II and IV were below average in the index patient, abnormalities in the $\Delta\Psi_m$ could elucidate the pathomechanism of this variant by examining whether it is involved in this pathway. Using TMRM as an indicator of $\Delta\Psi_m$, we investigated patient fibroblasts for abnormalities in comparison with other CMT2 patients and controls, but no significant differences between the cell lines were found (Fig. 5.8-5.9). Due to the high variance within the different fibroblasts and between the different controls, even after repeated experiments, it was difficult to draw any conclusions out of these results.

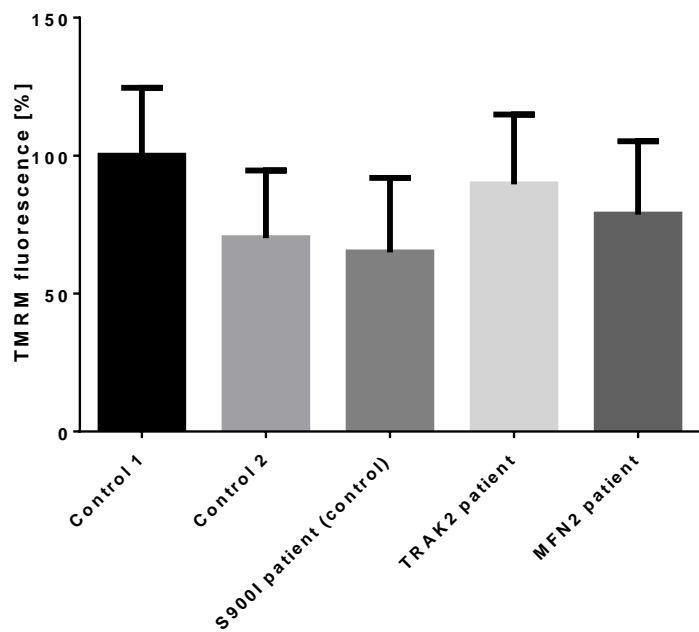


Figure 5-8 Percentage of mitochondrial membrane potential of patient fibroblasts and MFN2 positive control in comparison with normal control fibroblasts. Results are standardised against control 1. Statistical significance across groups was analysed using one-way analysis of variance and Bonferroni's post hoc test to compare all data groups, but no significance was found.

The mitochondrial membrane potential is maintained by the mitochondrial respiratory chain

In order to examine the mechanism of maintenance of $\Delta\Psi_m$, a series of mitochondrial toxins were applied to observe their effects on $\Delta\Psi_m$. Application of oligomycin, an inhibitor of the F1F0-ATPase, induced no response or a slight hyperpolarisation in all the cell lines as proton entry through the ATP synthase was constrained. This implies that the $\Delta\Psi_m$ is still maintained by the mitochondrial respiratory chain. Application of rotenone, which inhibits complex I, occasionally showed depolarisation after addition, but this was observed with the same frequency in controls and patients. Complete depolarisation was estimated by addition of the mitochondrial uncoupler FCCP. No significant differences between the cell lines were observed. These results are in contrast with the initial screening that showed a decreased activity of complex I. However, activity levels were only slightly below average and repeated experiments showed borderline-low complex I and IV activities, within normal limits.

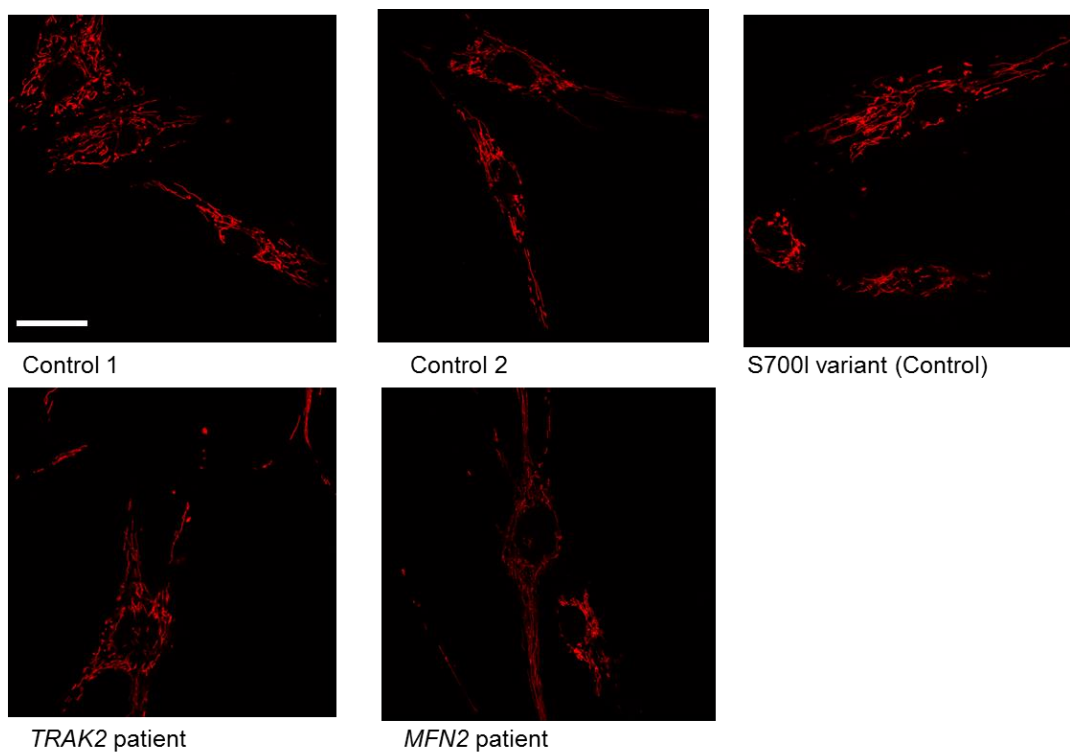


Figure 5-9 Confocal images of the mitochondrial membrane potential of patient fibroblasts in comparison with a MFN2 positive control and normal control fibroblasts. No significant difference was found. Scale = 36 μ m. TRAK2 patient = p.Arg228Ter; MFN2 patient = p.Ser249Thr.

TRAK2 discussion

The index patient presented with a nonsense p.Arg228Ter variant in the TRAK2 gene, which segregated in the family. Since the presence of a nonsense mutation could lead to NMD, this was investigated. mRNA analysis showed NMD was present, leaning towards a pathogenic mechanism of haploinsufficiency. Functional analyses were performed to look at the cellular localisation and the mitochondrial membrane potential, but these were too variable to draw any conclusions. It is important to remark that a patient with a mutation in *MFN2* was used as control in these experiments. However, no remarkable changes were observed in this patient, which might indicate that using fibroblasts is not optimal for these experiments. Whilst this cell type has been used before for the purpose of mitochondrial membrane experiments (Bartolome et al., 2013), our results were too variable amongst the cell lines, so in future experiments, a different type of cell line might have to be used for estimation of the mitochondrial membrane potential in peripheral neuropathies. No optimisation to this process was made, due to the discovery of an additional patient with a nonsense variant that was also present in the non-affected father, clearly undermining the hypothesis of haploinsufficiency. Together with the lack of functional data pointing to an effect of the variant in the *TRAK2* gene, evidence to prove the pathogenicity of this variant is weak.

The discovery of a new candidate gene

Several possible pathogenic variants still remained that could be causing this disease. In collaboration with Prof. Zuchner's lab in Miami, experiments were later performed to investigate a frameshift in the neurofilament, heavy polypeptide (*NEFH*) gene: c.3010_3011delCA, resulting in a stop loss and the addition of 40 extra aminoacids at the C-terminal end of the protein: p.Asp1004fs*56. After screening exome data of 322 families, one extra family with another heterozygous frameshift in *NEFH* was found. Segregation analysis identified the presence of the variant in all four affected siblings whilst the unaffected sibling and the father did not have the variant. Further functional experiments are still ongoing in the lab of Professor Zuchner regarding the pathogenicity of this gene.

The phenotype of the index patient is more severe than his relatives. In cases like this, the presence of a genetic modifier can partially explain the variability observed.

The m.12241delC variant, located in the mitochondrial *tRNA Serine 2* gene and only present in the index patient and not in the father or grandmother, highlights the possibility of mitochondrial mutations acting as genetic modifiers for disease, especially within families. However, this variant is located in a variable domain, and pathogenicity has not been proven.

5.2.3 Family E

Despite most of the research being focused on patients with an isolated neuropathy, in some cases the axonal neuropathy can be part of a more generalised disorder. Knowing the cause of disease in these cases could help us clarify the presence of the neuropathy and the mechanism underlying the molecular basis of pathology.

Clinical details of family E

For this part of the study, exome sequencing was performed by one of our collaborators on a consanguineous family with four affected individuals (Fig. 5.10). The patients presented with a spastic diplegic/quadriplegic cerebral palsy, intellectual disabilities and axonal neuropathy. The parents of the affected children were asymptomatic, with normal intellectual and adaptive functioning, without neuromotor findings. One sibling was unaffected (Fig. 5.10, II-4)

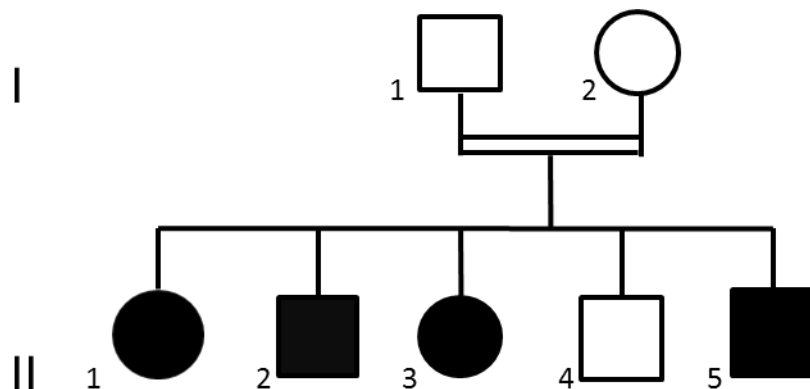


Figure 5-10 Pedigree of family F

The discovery of a candidate gene

Filtering was performed by Michael Kruer's lab in Sanford. Five interesting homozygous candidates were identified within the chromosome 10 autozygous regions that were found. Only two of these segregated in the family: Adducin 3 (*ADD3*) and ATP-binding cassette, subfamily C, member 2 (*ABCC2*).

Mutations in *ABCC2* cause a metabolic disease called Dubin-Johnson syndrome. This is a well-characterised autosomal recessive disorder that leads to episodic jaundice and conjugated hyperbilirubinemia in times of metabolic stress (Wada et al., 1998). Considering this protein is mainly expressed in the canalicular part of the hepatocyte and functions in biliary transport and mutations have never been associated with a neurological phenotype, the novel variant (p.Ser1342Tyr) identified in this gene was not investigated any further. Episodic jaundice was observed in affected family members and could be accounted for by the homozygous variant in this gene. Most likely, this variant co-segregates with the gene responsible for the neurologic phenotype, residing within the same haplotype block.

The other variant found was in the *ADD3* gene c.1100G>A; p.Gly367Asp, and this was the variant focused on during research on this family.

y-adducin

Adducin is a ubiquitously expressed protein that was first identified as an erythrocyte membrane-associated protein with calmodulin binding activity (Gardner et al., 1986). Further experiments indicated that it is located at the spectrin-actin junctions and binds to spectrin-F-actin complexes, promoting binding of spectrin to F-actin. It exists as a tetramer, formed out of either α/β or α/γ heterodimers, with *ADD3* encoding for the γ -subunit. The p.Gly367Asp mutation in the γ -subunit is localised in the oligomerisation domain, between subunits 335-436, responsible for the binding with the α -subunit (Dong et al., 1995; Hughes et al., 1995; Y Matsuoka et al., 1999). *ADD3* functions as an in vivo substrate for protein kinase A and C (PKA/PKC) and phosphorylation by PKA, but not PKC, reducing the affinity of spectrin-F-actin binding. Rho-kinase also phosphorylates α -adducin, resulting in an enhanced interaction of α -adducin with actin filaments in vitro (Kimura et al., 1998).

The implications of mutations in y-adducin

Thus far, inherited forms of spastic quadriplegic cerebral palsy have been known to be caused by the Kn motif-and ankyrin repeat domain-containing protein 1 (*KANK1*) protein, which contributes to the regulation of actin polymerisation. This results from a deletion of approximately 225 kb, encompassing the *KANK1* gene. Deletions were transmitted from unaffected fathers to affected children in an apparently maternally imprinted inheritance pattern. This means that *KANK1* is expressed in healthy individuals who carry the deletion on the maternal allele and a

normal paternal allele, whereas in the affected individuals who are carriers of the paternal deletion and a normal maternal allele, expression is repressed (Lerer et al., 2005). Due to the role of ADD3 in the binding of Spectrin-F-actin and the importance of KANK1 in the dynamics of the cytoskeleton, impaired adducin function may lead to abnormalities of the dynamic cytoskeleton as a pathogenic mechanism contributing to cerebral palsy and therefore makes an interesting candidate gene.

Although the p.Gly367Asp variant was predicted to be benign by Polyphen 2, SIFT categorised it as pathogenic and conservation of this residue was conserved over all species (Fig. 5.11). Considering its location in the oligomerisation domain, it could be hypothesised that this variant will affect the function by impairing the binding with the α -subunit.

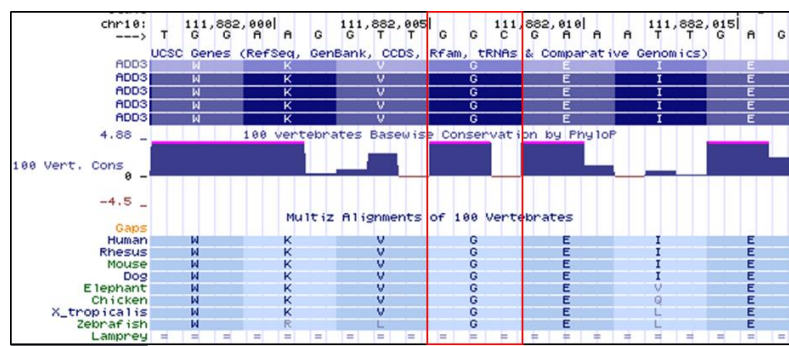


Figure 5-11 Conservation of Glycine 367 in γ -adducin.

Genetic analysis of the ADD3 gene revealed no mutations in ADD3 in a cohort of CMT2 patients

A cohort of 172 patients with CMT2 was screened for mutations in only exon 9 of *ADD3*, while 96 patients were screened for mutations in the whole of the 16 exon gene. No mutations were found in any of the exons of the *ADD3* gene in the cohort of CMT2 patients. Since the index patient presented with cerebral palsy as the main symptom, this is not surprising and indicates mutations in the *ADD3* gene are unlikely to result in an isolated axonal neuropathy.

Studies in patient fibroblasts indicate a loss of function mechanism

As most of this work was done in collaboration with the Kruer lab in Sanford, the majority of experiments were performed there. Results showed that fibroblast lysates have an impaired actin capping activity in the mutant, comparable to a siRNA

knockdown of the *ADD3* transcript, suggesting the p.Gly367Asp variant serves as a loss-of-function mutation. Co-localisation of the γ -subunit with the α -subunit of adducin showed a small decrease in the affected fibroblasts, suggesting an effect on the heteromer formation despite adequate protein levels of each isoform. Both proliferation and migration of cells were significantly increased in patient cell lines compared to controls. Morphologically, mutant fibroblasts demonstrated a lack of neurite-like processes as compared to wild type fibroblasts, consistent with the role of γ -adducin in controlling process outgrowth (Kruer et al., 2013).

Endocytosis investigation showed no significant difference between control and patient cell lines

Previous experiments by Torielli et al in 2008 showed that mutations in α -adducin result in a reduced overall endocytotic activity in cells transfected with the mutant form, associated with a lower internalisation rate of transferrin. Since mutations in genes causing CMT2 (e.g. *DNM2*) also impair clathrin-mediated receptor endocytosis (Bitoun et al., 2009), additional experiments were performed by me to investigate the effects of this mutation on the endocytotic pathway.

Transferrin labelled with Alexa-Fluor 488 was used to estimate the uptake of transferrin in fibroblast cell lines, indicating the overall endocytotic activity. The expression of mutated human γ -adducin reduced the average slope of uptake (2.187 ± 0.6063 mean intensity/volume) compared with wild type adducin cells (2.862 ± 0.5509 mean intensity/volume). However, this was not significant (Fig. 5.12).

High variability in repeated experiments was present amongst the different cell lines, especially in patient cell lines (Fig. 5.13). Punctate structures were present in both the patient and control cells after 30 minutes, as can be seen in representative images for an incubation time of 20 and 30 minutes, shown in Figure 5.14.

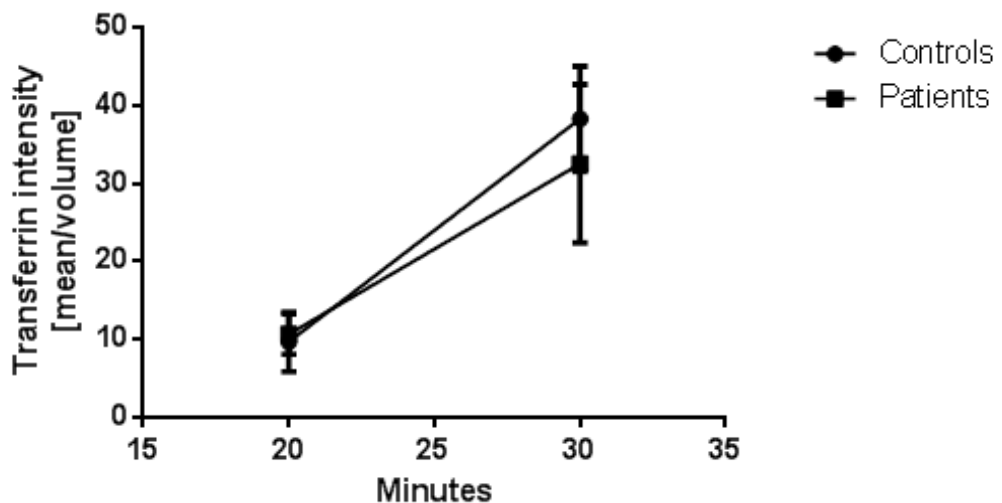


Figure 5-12 Time course of transferrin internalisation in controls (•) and patients (▪) fibroblast cell lines. • = Control fibroblasts (n = 2; 2.862 ± 0.5509 mean intensity/volume) ▪ = Patient fibroblasts (n = 3; 2.187 ± 0.6063 mean intensity/volume). Statistical significance across groups was analysed using GraphPad Prism version 6.00 but no significance was found.

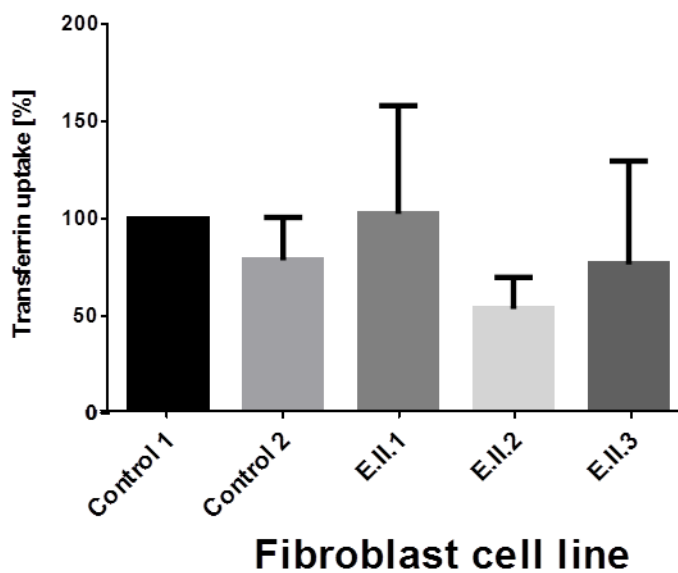


Figure 5-13 Transferrin intensity in the different fibroblast cell lines. Results are standardised against control 1. Statistical significance across groups was analysed using one-way analysis of variance and Bonferroni's post hoc test to compare all data groups, but no significance was found.

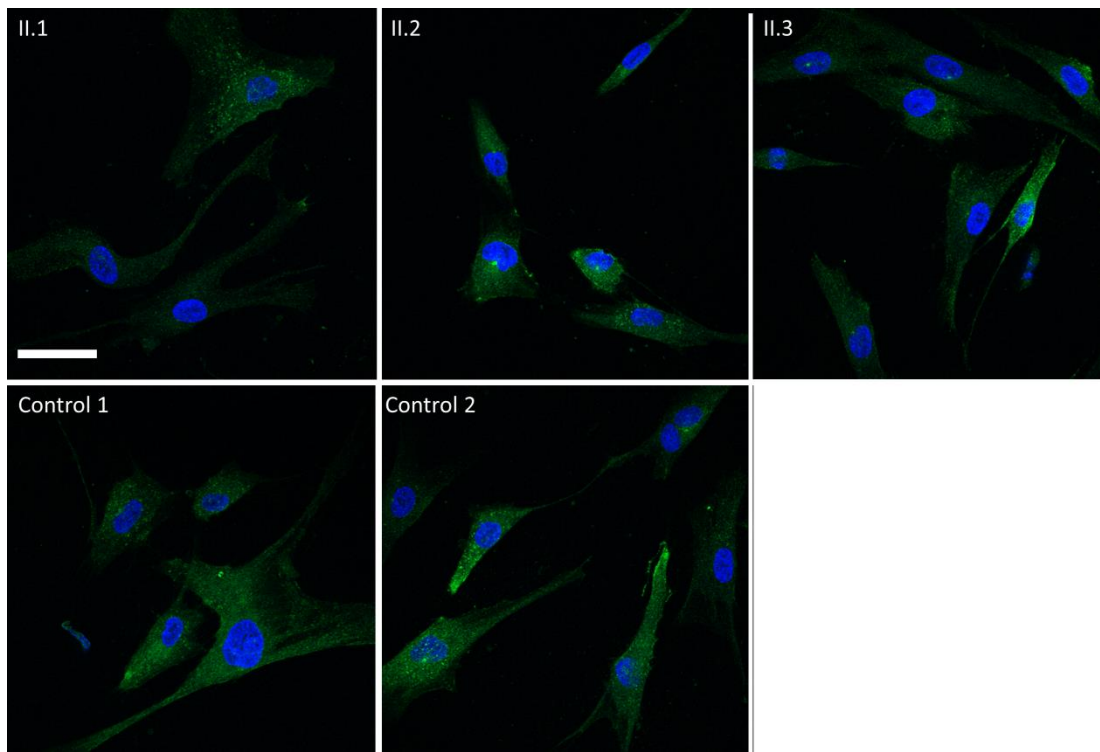


Figure 5-14 Representative confocal images for the uptake of transferrin in human fibroblasts after an incubation period of 30 minutes. Scale bar = 49 μ m. Green = Transferrin; Blue = DAPI staining for the nucleus.

Basal mitochondrial membrane potential and response to mitochondrial toxins in ADD3 patient fibroblasts

PKC has been suggested to associate with mitochondria and alter the mitochondrial membrane potential, especially in the oxidative stress response (Li et al., 1999; Majumder et al., 2001). Considering the presence of a mitochondrial cluster of genes mutated in CMT, it was questioned whether this part of the pathway could be causing the axonal neuropathy in the patients and mitochondrial membrane potential experiments were performed accordingly.

With the use of TMRM dye, the mitochondrial network was investigated in fibroblast cell lines of controls and patients. Figure 5.15 shows representative images of all the different cell lines, to compare the physiology of the mitochondrial network. The network was less outstretched in the diseased cell lines, especially II.1, but this was not consistent in all the patient cell lines.

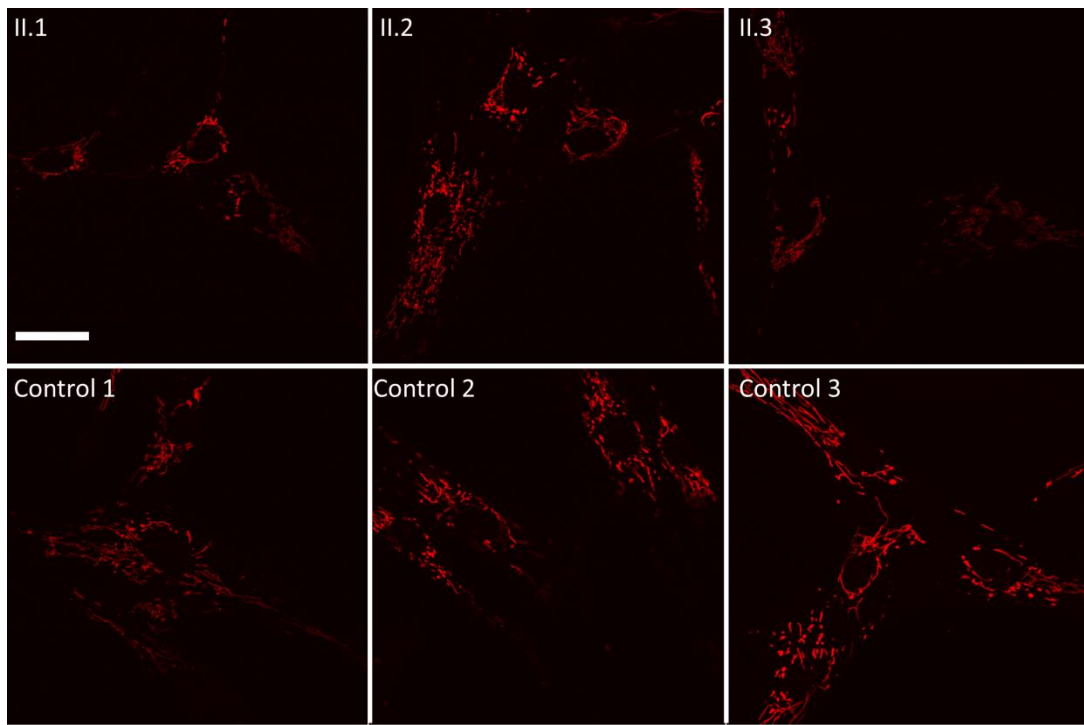


Figure 5-15 Physiology of the mitochondrial network in patient and control fibroblasts. No significant differences were found. Scale = 36 μ m.

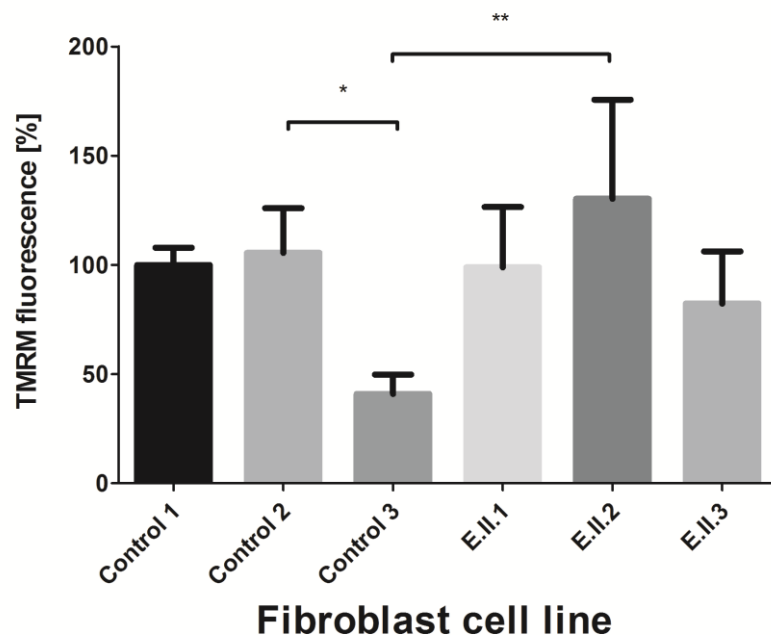


Figure 5-16 Mitochondrial membrane potential in the different fibroblast cell lines. Results are standardised against control 1. Statistical significance across groups was analysed using one-way analysis of variance and Bonferroni's post hoc test to compare all data groups, but was only found with control 3 in comparison with control 2 and E.II.2.

As was the case in patients with the *TRAK2* variants in subchapter 5.2.1, no significant difference was observed between patient and control cell lines with the use of the TMRM dye in patients with *ADD3* mutations (Fig. 5.16). High variability was found between the different cell lines and no conclusions could be drawn.

By adding toxins, depolarisation after addition of oligomycin or complete depolarisation after addition of rotenone could occasionally be observed in both patient and control cell lines, but these results were not consistent. We could hypothesise that the mitochondrial membrane potential is still maintained by the mitochondrial respiratory chain, since the depolarisation occurred in both controls and patients and there were no significant consistent differences between the different cell lines.

Discussion

Previous experiments have already shown that abnormalities in the dynamic cytoskeleton, process outgrowth or protein trafficking can be linked to hereditary forms of cerebral palsy. In this study, a homozygous p.Gly367Asn mutation in *ADD3* was found in a family with four children with spastic diplegic/quadriplegic cerebral palsy and intellectual disability. Experiments performed by the Kruer lab in Sanford indicated that this mutation impaired the heterodimer/heterotetramer formation, disrupting cellular actin polymer growth. Changes have been observed in process extension, cell migration, and proliferation.

As part of this study, statistical analysis were performed to investigate whether there was a significant difference in the uptake of transferrin by endocytosis, but no differences were found between control and patient cell lines. This indicates that the pathomechanism is in all probability not originating from this pathway. However, the use of fibroblasts as a cell model has to be questioned, since this is not the main tissue of disease. The original study investigating endocytosis made use of transfected HEK293 cells, resulting in an overexpression model. It can be asked whether the significance of these results would also be seen at normal physiological levels of mutated α -adducin. To answer this, endocytosis experiments would have to be repeated in patient related tissues from α -adducin patients. By clarifying the role of adducin in cerebral palsy further, an explanation for the axonal neuropathy in

these patients might be uncovered; however, this is not the major focus of this thesis and further experiments were not implemented.

Whilst investigation of the mitochondrial membrane potential was also performed in these cell lines, as with the use of fibroblasts in the TRAK2 fibroblasts, the results were too variable to draw any conclusions, adding to the observation that fibroblasts might not be the optimal cell type to use.

In one of the patients, a more condensed network could be observed, but whether this is because of a fault in the network or whether the cell size was significantly smaller, we cannot conclude from this data. This was not consistently detected in all patients and repeated measurements or further experiments to compare the size of the mitochondrial network with the cell size were not performed.

5.2.4 Family F

Exome sequencing was performed in a family with AD inheritance consisting of three generations with eleven affected and one suspected affected family member out of 26. DNA was available for six affected, four unaffected and the one suspected affected member (Fig. 5.17; Individuals with DNA in bold). Exome sequencing was performed on two distant cousins (Fig. 5.17; Patients III-1, III-11) while linkage analysis was performed on four affected and three unaffected members (Fig. 5.17; Individuals II.2, III.1, III.2, III.4, III.5, III.8, III.11). Exome sequencing alone resulted in 7427 nonsynonymous variants shared between the two patients. With a cut-off MAF $\leq 0.5\%$ in the public databases, this was reduced to a list of 80 variants.

Linkage analysis was performed twice with a different subset of SNPs and resulted in five linkage regions (Fig. 5.18). All of these regions resulted in a maximum lod score of 2 and cut-offs were chosen at the zero intersection. Of the remaining 17 chromosomes, eight had a lod score below -2 over the whole chromosome and could be excluded based on the linkage analysis (See appendix III). Using these linkage areas, the candidate gene list was reduced to 16 variants. By comparing these variants to internal databases, three could be excluded as artefacts from the exome sequencing process, whilst two other variants were located in highly polymorphic genes. The remaining eleven variants were all investigated by Sanger sequencing for

which eight did not segregate in the family, one could not be confirmed with Sanger sequencing and the remaining two were present in the EVS database (Table 5.1). The MAF $\leq 0.5\%$ cut-off is mainly used to assure no pathogenic variants might be missed, and the presence of 22 control individuals with the same variant highly suggests the eukaryotic translation initiation factor 2D (*EIF2D*) gene will not be responsible for the phenotype. Similarly, since incomplete penetrance is not expected in patients with dHMN, having nine control individuals with the same variant highly questions the pathogenicity of the missense variant in the acyl-coa synthetase, bubblegum family, member 1 (*ACSBG1*) gene. During the write-up of this project, the ExAc Browser, consisting of exome data of 60,706 unrelated individuals sequenced as part of various disease-specific and population genetic studies, was also made publicly available and both variants were present in respectively 218 and 68 individuals, suggesting non-pathogenicity.

However, segregation analysis had already been performed and the latter variant segregated in the family, but was not present in the member with suspected disease status. This individual was last seen at age 16 and has not been officially diagnosed with dHMN. Unless found in other patients with a similar phenotype, follow-up of this gene will not be performed. As the implementation of linkage analysis returned no pathogenic variants in the linkage areas and lod scores were not higher than 3, the list of all nonsynonymous shared heterozygous variants was re-analysed to confirm no pathogenic variants were missed. However, none of the variants outside the linkage areas that were not present in any of the public databases or in our internal database segregated in the family (Table 5.2).

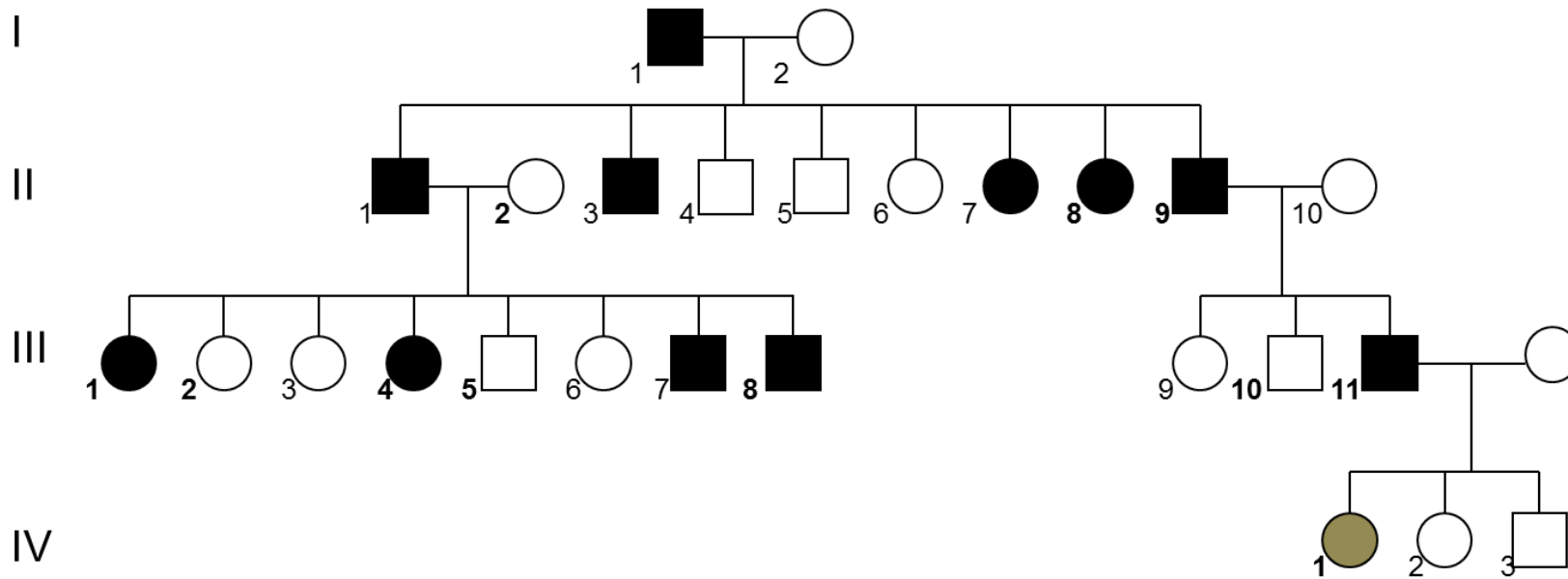
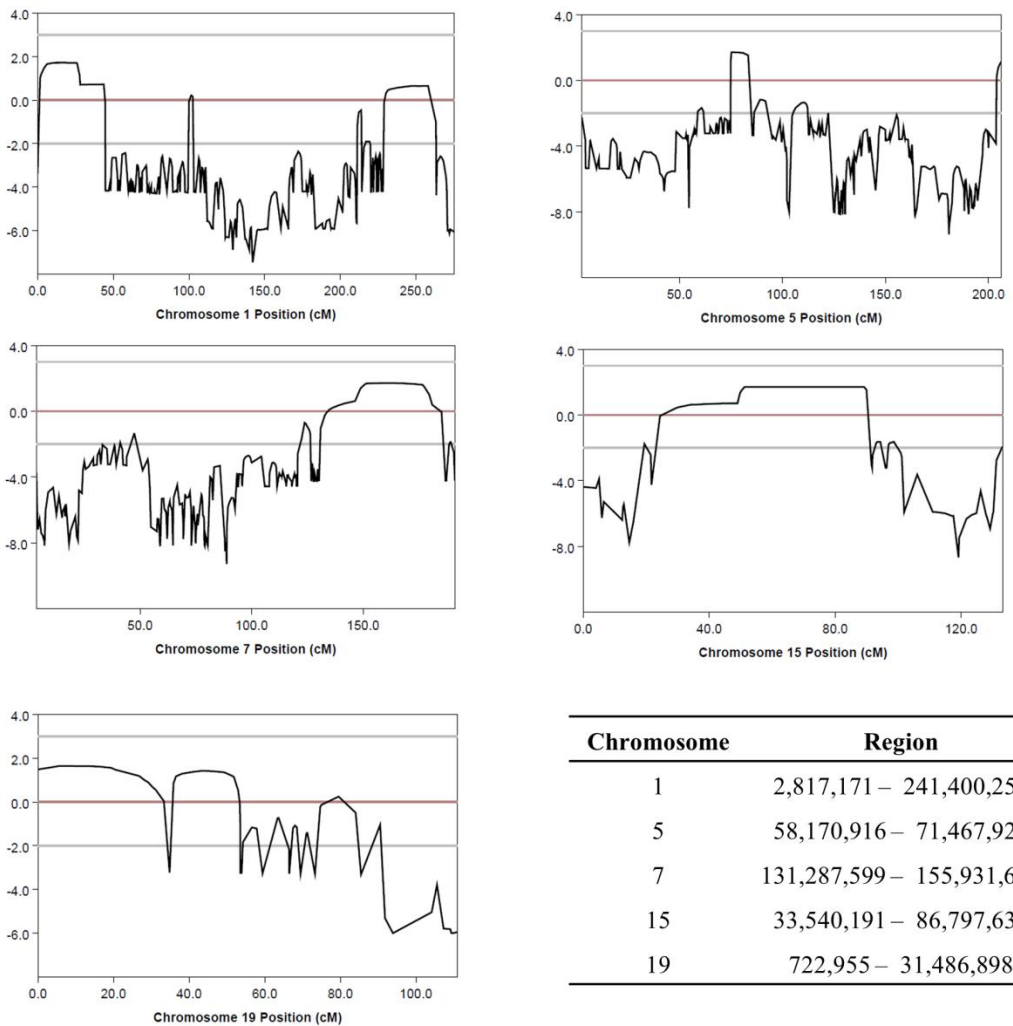


Figure 5-17 Pedigree of Family F. Black symbols represent patients with CMT2, grey symbols represent individuals with unknown clinical status.



Chromosome	Region
1	2,817,171 – 241,400,254
5	58,170,916 – 71,467,920
7	131,287,599 – 155,931,611
15	33,540,191 – 86,797,634
19	722,955 – 31,486,898

Figure 5-18 Linkage areas of family F located on chromosomes 1,5,7,15 and 19.

Gene	Exonic Function	X1000g - 2012	SIFT	PolyPhen2	Mutation	GERP	OMIM	Signature	Status
					Taster	score			
PRDM16	nonsynonymous	NA	D	NA	D	3.5	605557	1_3342158_G_A	Doesn't segregate
CLSTN1	nonsynonymous	NA	B	B	B	4.39	611321	1_9809615_C_T	Doesn't segregate
LCE1F	nonframeshift substitution	NA	NA	NA	NA	NA	612608;6 12605	1_152749038_GTGGTGG_GCTGC TGCAGCTCTGGGGTGGTGG	Doesn't segregate
KIF14	nonsynonymous	0.0023	B	D	D	2.7	611279	1_200574499_T_C	Doesn't segregate
EIF2D	nonsynonymous	5.00E-04	B	B	B	5.37	151625	1_206772388_T_C	Present in 218 genotypes in ExAC Browser
NUP205	nonsynonymous	NA	NA	B	B	3.04	NA	7_135290962_C_T	Doesn't segregate
PDIA4	nonsynonymous	NA	D	D	D	4.18	NA	7_148718180_C_G	Doesn't segregate
RYR3	nonsynonymous	NA	NA	NA	NA	NA	180903	15_34030702_G_A	Doesn't segregate
SPTBN5	nonsynonymous	NA	NA	NA	NA	NA	605916	15_42169056_G_A	Doesn't segregate
ACSBG1	nonsynonymous	0.0014	B	D	D	5.02	NA	15_78475108_T_A	Present in 68 genotypes in ExAC Browser
ADAMTS7	frameshift insertion	NA	NA	NA	NA	NA	605009	15_79058195_-CCTGGGT	Not present in sanger sequencing

Table 5-1 List of eleven candidate genes for Family F within the linkage areas. NA = Not applicable; B = Benign; D = Damaging

Gene	Exonic Function	X1000g	SIFT	PolyPhen2	Mutation	GERP	OMIM	signature	Status
		2012		Taster	score				
ACOT12	Nonsynonymous	NA	B	B	B	-5.32	NA	5_80626728_T_C	Doesn't segregate
SNRPC	nonframeshift insertion	NA	NA	NA	NA	NA	603522	6_34725662_-_CTT	Doesn't segregate
TBP	nonframeshift deletion	NA	NA	NA	NA	NA	608964; 600075	6_170871097_GCAGCAGCA	CAG-stretch
ASCL1	nonframeshift insertion	NA	NA	NA	NA	NA	100790	12_103352208_-_CAG	CAG short stretch
RFX4	Nonsynonymous	NA	B	D	D	5.55	603958	12_107109277_A_G	Doesn't segregate
CCDC63	Nonsynonymous	NA	B	B	B	-7.23	NA	12_111336781_C_A	Doesn't segregate
GPC5	NA	NA	NA	NA	NA	NA	602446	13_92050913_AGGCGGCG GC GG CGG CGG CAGTGG_-	Intronic
YY1	nonframeshift deletion	NA	NA	NA	NA	NA	600013	14_100705803_CCA_-	Present in 57 genotypes in ExAC Browser
SPATA22	NA	NA	NA	NA	NA	NA	NA	17_3374975_CA_-	Spermatogenesis gene
MX1	Nonsynonymous	NA	B	B	B	-1.4	147150	21_42830594_G_A	Doesn't segregate
HLA-H	frameshift deletion	NA	NA	NA	NA	NA	NA	6_29857237_G_-	Known pseudogene

Table 5-2 List of novel variants outside the linkage areas in family F. NA = Not applicable; B = Benign; D = Damaging

5.2.5 Family G

Family G was originally seen in Brighton Hospital 13 years ago and was referred to our clinic after a couple of years. There were seven affected patients in four generations with an AD inheritance pattern. DNA was available for four affected and six unaffected family members (Fig. 5.19; Individuals in bold). Exome sequencing was performed on four family members at different time points along the project, resulting in only three exomes with high quality results (Fig. 5.19; Patients I.2, II.2, III.2). As patient II.2 did not add any value to the analysis of shared exomes, only data of patients I.2 and III.2 were used. This resulted in 13472 shared variants amongst those two individuals, out of which 71 were nonsynonymous heterozygous variants with a MAF $\leq 0.5\%$. Interestingly, when comparing the data of all three patients, only 68 shared variants were found. This indicates that even though coverage was sufficient, not all variants might have been called with this technique and caution is necessary.

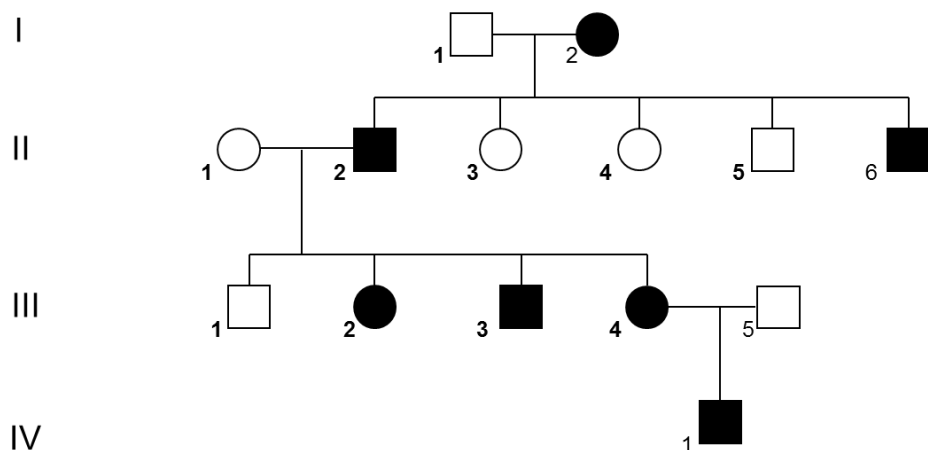
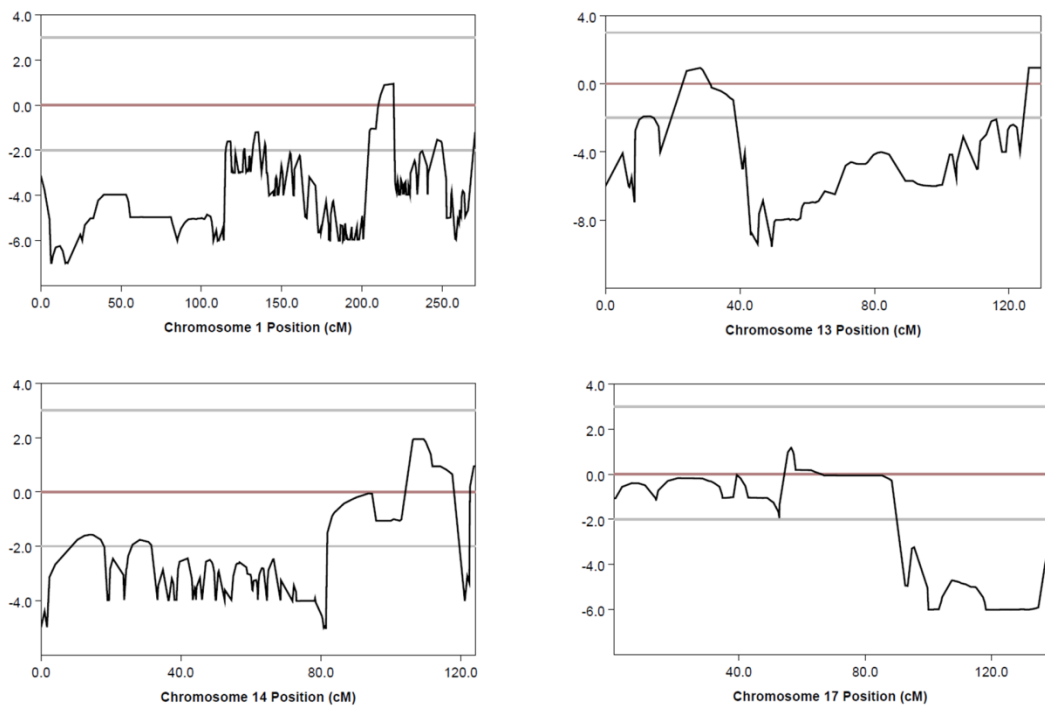


Figure 5-19 Pedigree of Family G. Black symbols represent patients with CMT2.

Repeated linkage analysis in all affected and unaffected members resulted in six small linkage areas on four different chromosomes that only reached a lod score of 1 (Fig. 5.20). Out of the 71 variants, only one was present in the linkage area, a missense variant in exon 8 of the tryptophanyl-tRNA synthetase (*WARS*) gene: c.818A>T (p.Asp273Val). Considering the involvement of tRNA-synthetases in the pathomechanism of CMT, *WARS* would be an excellent candidate gene. However, segregation analysis indicated the presence of this variant in individual II-5, who is unaffected, suggesting this is not the causative variant.



Chromosome	Region
1	213,524,310 – 215,930,045
13	30,515,303 – 32,213,374
	113,336,423 – end
14	97,523,495 – 101,877,270
	104,464,550 – end
17	30,941,678 – 35,910,985

Figure 5-20 Linkage areas of Family G located on chromosomes 1,13,14 and 17.

Of 71 original nonsynonymous heterozygous variants with a MAF $\leq 0.5\%$, there are still 34 shared novel variants between the two patients outside the linkage areas that could qualify as a candidate gene (Table 5.3). Of these, only one segregated. This variant in the WD repeat domain 48 (*WDR48*) gene is located on one of the chromosomes that was originally excluded due to the LOD score being below -2 (See appendix IV) and results in a c.797C>G variant in exon 9. This will change the polar, uncharged proline 266 to a positively charged arginine. In a recent report by Novarino et al., a homozygous 3 bp-deletion was identified in this gene in a patient with spastic paraplegia (Novarino et al., 2014). This variant (c.1879_1881delAAG) resulted in the deletion of a glutamic acid at position 628 (p.Glu628del).

Gene	Exonic Function	X1000g	SIFT	PolyPhen2	Mutation	GERP	OMIM	signature	Status
		2012			Taster	score			
KCNA10	nonsynonymous	NA	D	B	B	1.91	602420	1_111061292_G_A	Not present in Sanger sequencing
WDR77	nonsynonymous	NA	NA	P	B	2.99	603270;	1_111991772_G_A	Not present in Sanger: C-stretch
							611734		
CTTNBP2NL	nonsynonymous	NA	B	P	B	5.72	NA	1_112998758_G_A	Doesn't segregate
ITGA10	nonsynonymous	NA	B	D	B	4.5	604042	1_145538779_C_T	Doesn't segregate
CNST	nonsynonymous	NA	B	B	B	1.8	NA	1_246829025_A_G	Doesn't segregate
DHX57	nonsynonymous	NA	B	D	D	5.24	NA	2_39042757_G_A	Doesn't segregate
MTERFD2	nonsynonymous	NA	D	P	B	-3.35	NA	2_242039227_G_A	Doesn't segregate
WDR48	nonsynonymous	NA	B	B	D	5.56	612167	3_39119698_C_G	Segregates
ZNF167	nonsynonymous	NA	B	B	B	3.63	NA	3_44612019_G_A	Doesn't segregate
RPL29	nonframeshift	NA	NA	NA	NA	NA	601832	3_52027880_- _GGGCCT	Doesn't segregate
ITIH3	nonsynonymous	NA	NA	NA	NA	NA	146650	3_52836502_G_T	Doesn't segregate
FLNB	nonsynonymous	NA	D	D	D	4.28	603381	3_58083678_C_T	Doesn't segregate
RP1	nonsynonymous	NA	D	B	B	-1.78	180100;	8_55539000_A_G	Doesn't segregate
							603937		
SLC10A5	nonsynonymous	NA	B	D	B	5.57	NA	8_82606490_A_C	Doesn't segregate
COL14A1	nonsynonymous	NA	B	D	B	4.17	120324	8_121243810_A_G	Doesn't segregate
NSMCE2	frameshift	NA	NA	NA	NA	NA	NA	8_126194426_T_-	Doesn't segregate
	deletion								
CSNK2A1	nonsynonymous	NA	B	B	B	4.89	115440	20_467035_C_T	Doesn't segregate
DYRK4	frameshift	NA	NA	NA	NA	NA	609181	12_4719356_A_-	Doesn't segregate

	deletion								
MLL2	nonsynonymous	NA	NA	NA	NA	NA	602113	12_49447305_G_A	Doesn't segregate
LMBR1L	nonsynonymous	NA	D	D	D	5.38	610007	12_49491774_A_C	Doesn't segregate
KRT85	nonsynonymous	NA	B	B	B	4.58	602767	12_52761167_A_T	Keratin gene
SRGAP1	nonsynonymous	NA	B	D	B	4.21	606523	12_64472790_G_A	Doesn't segregate
PPTC7	nonframeshift	NA	NA	NA	NA	NA	609668	12_111020757_CCG_-	Doesn't segregate
	deletion								
PABPC3	nonsynonymous	NA	D	B	B	0.935	604680	13_25671466_A_G	Doesn't segregate
PABPC3	nonframeshift	NA	NA	NA	NA	NA	604680	13_25670424_AAG_-	Doesn't segregate
	deletion								
WARS	nonsynonymous	NA	D	P	D	4.5	191050	14_100808907_T_A	Doesn't segregate
PIF1	nonsynonymous	NA	D	D	D	4.99	610953	15_65110540_T_A	Doesn't segregate
C15orf37	nonframeshift	NA	NA	NA	NA	NA	NA	15_80215177_CAG_-	Intronic + present in EVS server
	deletion								
KRTAP9-1	nonsynonymous	NA	NA	NA	NA	NA	NA	17_39346629_A_G	Keratin gene
KRT33B	stopgain	NA	NA	NA	A	4.18	602762	17_39522769_C_A	Keratin gene
KRT17	frameshift	NA	NA	NA	NA	NA	148069	17_39780702_-C	Keratin gene
	insertion								
RRBP1	nonsynonymous	NA	NA	NA	NA	NA	601418	20_17639816_T_G	Not present in Sanger sequencing - Repetitive stretch
RRBP1	nonsynonymous	NA	NA	NA	NA	NA	601418	20_17639786_T_G	Not present in Sanger sequencing - Repetitive stretch
XKRX	nonsynonymous	NA	B	NA	B	2.99	300684	X_100183238_A_G	Doesn't segregate

Table 5-3 Shared, novel, nonsynonymous variants in family G. NA = Not applicable; B = Benign; D = Damaging; P = Probably damaging.

c.1879_1881delAAG was found in one patient who presented with hypertension, nystagmus, increased patellar but absent achilles tendon reflexes, mild learning disabilities and peripheral neuropathy, labelled by the authors as spastic paraplegia-60 (SPG60). Whilst this has been characterised as recessive inheritance, the presence of peripheral neuropathy in this patient suggests this might be the causative variant in the family. This is supported by the presence of the missense variant in only one person out of 60,706 available in the ExAc Browse. The most recent update of Polyphen-2 predicts this variant to be possibly damaging, whilst the SIFT prediction categorises it as benign. Conservation of this amino acid is preserved over all representative species (Fig. 5.21).

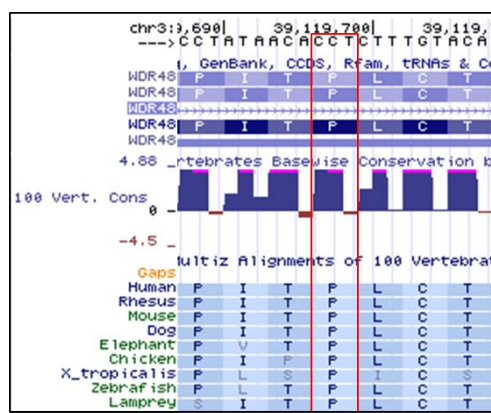


Figure 5-21 Conservation of Proline 266 in the *WDR48* gene.

WDR48 forms stable complexes with deubiquitinating enzymes in the endosomal sorting complexes, is required for enzymatic activity and is linked to lysosomal trafficking (Park et al., 2002). Defects in the endosomal-lysosomal pathways have been recurrently linked to inherited neuropathies such as CMT, suggesting a possible pathogenic role for variants in *WDR48*. Mice models of the gene resulted in embryonic lethality in homozygous mouse; heterozygous mice were smaller and showed defects in skeletal development (Park et al., 2013). No functional studies were performed due to lack of a second family with potential pathogenic variants in this gene, but *WDR48* will be treated as a candidate gene in the future.

5.2.6 Family H

The following family had a history of AD dHMN in four generations and contained nineteen affected family members out of 42. DNA was available for six affected and one unaffected members (Fig. 5.22; Individuals in bold).

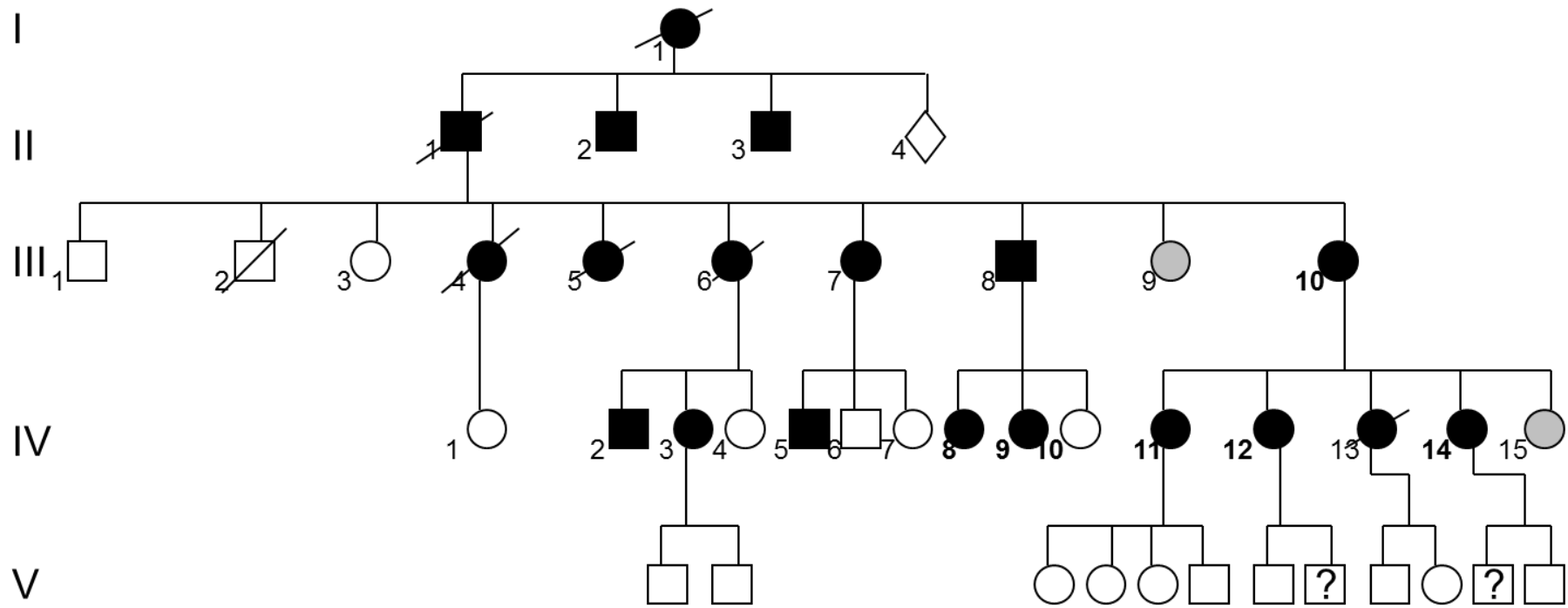


Figure 5-22 Pedigree of Family H. . Black symbols represent patients with CMT2, grey symbols represent individuals with unknown clinical status.

Exome sequencing was performed on two cousins and all the available DNA samples were used for linkage analysis (Fig. 5.22; Patients IV.8, IV.11). After analysis of the data, 5792 shared, nonsynonymous, heterozygous variants remained. Filtering these variants by examining their presence in the public databases and the segment duplication coefficient reduced the list to 196 possible pathogenic variants. As this family was already screened for the relevant genes for dHMN, no mutations in known pathogenic genes were expected to be found. However, a mutation in the *HSPB1* gene was discovered (c.544C>G). This is the third mutation affecting the same amino acid, with both c.544C>T and c.545C>T having been reported before (Kijima et al., 2005, Evgrafov et al., 2004). This gene was originally sequenced in these patients and no mutation was present, so sample confusion was suspected. Linkage analysis resulted in a linkage area on chromosome 7 that overlapped with the *HSPB1* gene hence Sanger sequencing was repeated twice, which resulted in the presence of the mutation in only one of the runs. This was traced back to a 4-bp insertion in intron 2 on the same allele as the missense mutation in exon 3. This was captured as part of the exon 3 PCR and occurs in an extremely G/C rich region as an insertion of a GGTG within a short repeat sequence. The addition of the extra 4 bp into this repeat might cause preferential amplification of the wild type allele and provide an explanation for missing the missense mutation in diagnostic sequencing. These results were repeated on diagnostic levels to provide the family with a genetic diagnosis.

5.2.7 Family I

A small family presented with seven individuals characterised with AD CMT2 over four generations. DNA was available for four affected and one unaffected member (Fig. 5.23; Individuals in bold). Exome sequencing was performed on two cousins and the daughter of one of the cousins (Fig. 5.23; Patients III.2, III.4 and IV.1), which resulted in 11197 shared variants. After analysis, 30 shared nonsynonymous heterozygous variants with a MAF $\leq 0.5\%$ were present. Of those, 19 were novel variants. After comparison with the in-house database, a candidate list of 12 genes was created (Table 5.4). Of these, three genes segregated in the family, with only the nonsense variant present in 15 individuals in the ExAc Browser database. One of the missense variants was located in the Repulsive guidance molecule, domain B (*RGMb*) gene – also known as DRAGON (Samad et al., 2004).

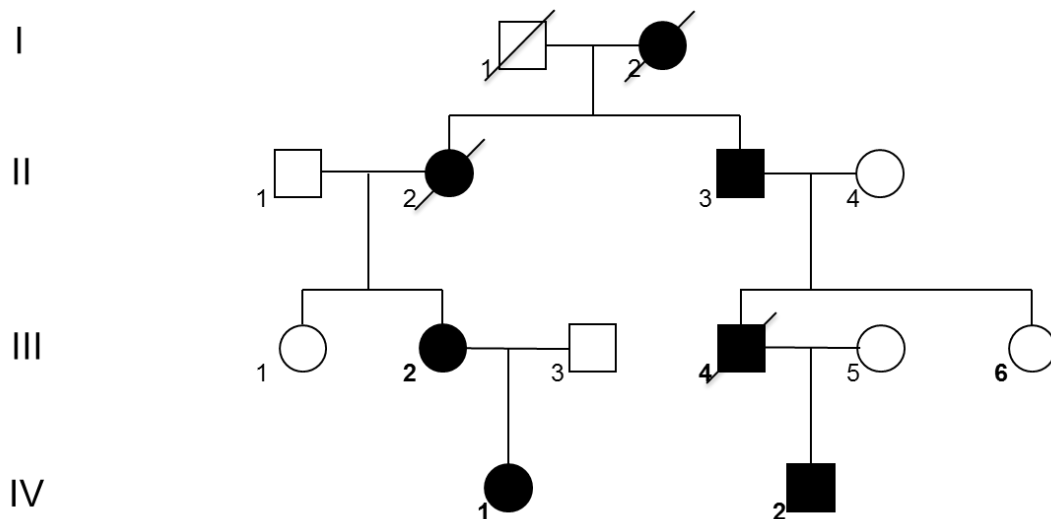


Figure 5-23 Pedigree of family I. . Black symbols represent patients with CMT2.

The c.979G>A variant (p.Gly327Ser) is located in a conserved domain (Fig. 5.24), with the glycine aminoacid being conserved over multiple species. Both SIFT and Polyphen predicted this variant to be pathogenic and no presence in controls was found. *RGMb* is a glycosylphosphatidylinositol-anchored member of the repulsive guidance molecule family, which is expressed early in the developing nervous system, and has been identified as a factor important for neuronal adhesion in DRG neurons by homophilic interactions (Samad et al., 2004). All repulsive guidance molecules were characterised as bone morphogenetic protein (BMP) co-receptors that enhance BMP signalling (Samad et al., 2005) and it has been suggested *RGMb* is directly involved in the suppression of IL-6 expression through the p38 MAPK and Erk1/2 pathways (Xia et al., 2011). This variant segregated in all DNA samples of the family but no second family was found when we screened a cohort of 250 CMT2 patients for mutations. Another missense variant was located in the *MORC2* gene. *MORC2* has an ATPase-dependent chromatin remodelling function and has been speculated to be involved in DNA transcription (Li et al., 2013). Recent studies have implied the involvement of *MORC2* in human cancers (Wang et al., 2010; Tuupanen et al., 2014) by efficiently integrating growth factor signalling with DNA repair processes (Li et al., 2013). The variant found in the family results in the change of a highly conserved negative aspartic acid to a neutral asparagine (Fig. 5.24). Whilst this is located in a conserved area, it is not part of a functional domain. Both PolyPhen and SIFT predict this variant to be pathogenic and no presence in controls was found. This variant segregated in the family but no further

investigations were made and both *RGMb* and *MORC2* will be regarded as a candidate gene in future. Lastly, the deletion of a G in the *IDE* gene will result in a frameshift in the first exon of the gene, leading to a stopcodon instead of Leucine. However, this variant is present in 12 alleles in the EVS server and 15 in the ExAc Browser, resulting in prioritisation of the two other variants.

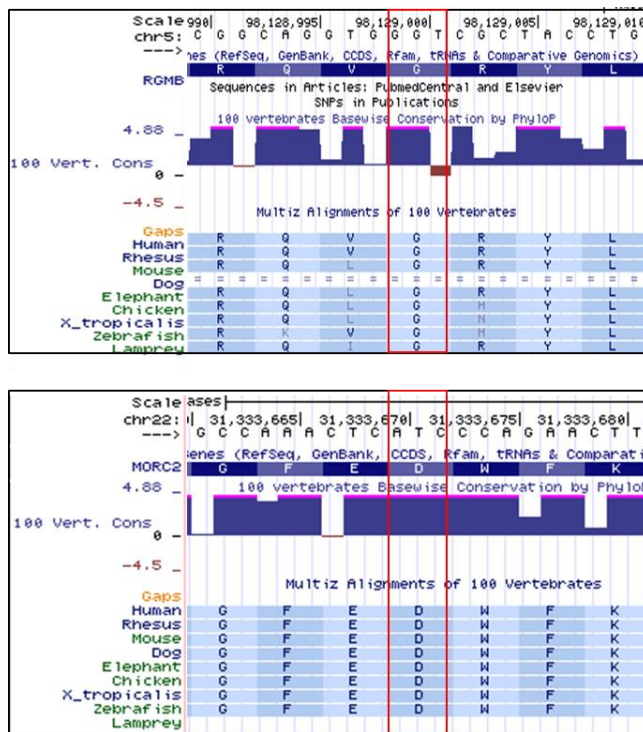


Figure 5-24 Conservation of the variants in the *RGMb* (upper frame) and *MORC2* (lower frame) genes.

During the write-up of this thesis, one of the family members (III.2) was seen in clinic again and mentioned the possible affected status of family member III.6. This patient will be brought into clinic to establish the correct clinical status, which might result in different candidate genes.

Gene	Exonic Function	X1000g	SIFT	PolyPhen2	Mutation	GERP	OMIM	signature	Status
		2012			Taster	score			
NADK	nonframeshift insertion	NA	NA	NA	NA	NA	611616	1_1684375_-_CTC	Not present in sanger sequencing
RGMB	nonsynonymous	NA	B	NA	NA	NA	612687	5_98128999_G_A	Segregates
DIP2C	nonsynonymous	NA	B	D	D	5.5	611380	10_428681_C_G	Doesn't segregate
IDE	stopgain	NA	NA	NA	NA	NA	146680	10_94333764_G_-	Segregates
PRSS23	nonsynonymous	NA	B	B	B	4.75	NA	11_86519328_G_A	Doesn't segregate
MGA	nonsynonymous	NA	B	NA	NA	NA	NA	15_41991118_G_T	Doesn't segregate
EPB42	nonsynonymous	NA	NA	NA	NA	NA	177070	15_43494077_C_T	Doesn't segregate
PSMD8	nonsynonymous	NA	B	NA	NA	NA	NA	19_38865459_C_T	Doesn't segregate
FAM71E1	nonsynonymous	NA	D	B	B	-2.67	NA	19_50971037_A_G	Doesn't segregate
ADRA1D	nonsynonymous	NA	B	B	D	3.81	104219	20_4228848_C_T	Doesn't segregate
TGM2	nonsynonymous	NA	B	D	B	2.3	190196	20_36789956_C_T	Doesn't segregate
MORC2	nonsynonymous	NA	B	D	D	5.37	NA	22_31333672_C_T	Segregates

Table 5-4 Shared, novel, nonsynonymous variants in family I. NA = Not applicable; B = Benign; D = Damaging.

5.2.8 Family J

A small family presented with AD HSAN in three generations (Fig. 5.25). DNA was available for five family members and exome sequencing was performed on patients II.1 and III.3. This resulted in 14313 variants shared between the two patients. After exclusion of synonymous variants or those with a frequency over 0.5%, a list of 55 shared variants was produced. Of these, 30 were novel variants of which six segregated in the DNA samples available for the family (Table 5.5).

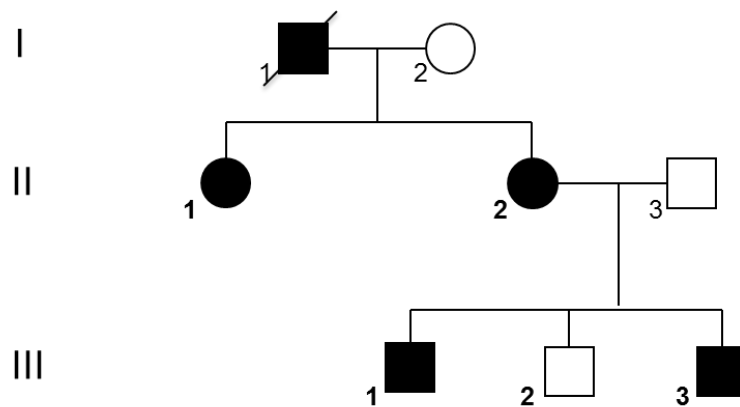


Figure 5-25 Pedigree of Family J.

The variants were located in the following six genes: *FAM126A*, *CNTRL*, *GOLGA2*, *SSTR5*, *TBC1D24* and *PKMYT1*. The missense variant in *SSTR5* could be found in 144 individuals in the ExAc Browser, indicating its polymorphic nature. Whilst the missense variant in *PKMYT1* was found in six individuals, suggesting non-pathogenicity, all the other variants were found in three or fewer individuals.

The most interesting variation in the context of HSAN is in the family with sequence similarity 126, member a (*FAM126A*) gene. Recessive mutations in this gene have been found in patients with congenital cataract, progressive neurological impairment and diffuse myelin deficiency, characterised as HCC (Zara et al., 2006; Ugur et al., 2008). All patients showed slowly progressive pyramidal and cerebellar dysfunction, muscle weakness and wasting predominantly in the lower limbs and most of them became wheelchair bound. Clinical features suggested *FAM126A* as essential for proper myelination in both the central and peripheral nervous system.

Gene	Exonic Function	1000g	SIFT	PolyPhen2	Mutation	GERP	OMIM	Signature	Status
		2012			Taster	score			
CDK11A	nonframeshift insertion	NA	NA	NA	NA	NA	176873; 116951	1_1647900_-_TTCTTT	Not present in sanger sequencing
NADK	nonframeshift insertion	NA	NA	NA	NA	NA	611616	1_1684375_-_CTC	Not present in sanger sequencing
DENND4B	nonframeshift substitution	NA	NA	NA	NA	NA	NA	1_153907278_CCTGC TGCT...	Long Q stretch
RIF1	nonsynonymous	NA	B	B	NA	-3.33	608952	2_152322348_T_C	Doesn't segregate
FANCD2	nonsynonymous	NA	D	D	D	5.11	227646; 227650	3_10107554_C_G	Doesn't segregate
MAGI1	nonframeshift substitution	NA	NA	NA	NA	NA	602625	3_65425560_TCTGCT GCTGCT...	Long Q stretch
FAM126A	nonsynonymous	NA	D	B	B	3.71	610531	7_22985650_G_A	Segregates + Present in 1 genoptye in the ExAc browser
AC118759.1	nonsynonymous	NA	NA	NA	NA	NA	NA	7_100549592_T_A	Mucin gene
AC118759.1	nonsynonymous	NA	NA	NA	NA	NA	NA	7_100549787_C_T	Mucin gene
MUC3A	nonsynonymous	NA	NA	NA	NA	NA	NA	7_100552535_G_A	Mucus gene
TRBV5-6	nonsynonymous	NA	NA	NA	NA	NA	NA	7_142131832_C_T	Not present in sanger sequencing
PCSK5	nonsynonymous	NA	NA	NA	NA	NA	600488	9_78790136_T_C	Not present in sanger sequencing
CNTRL	nonsynonymous	NA	D	P	B	5.11	605496	9_123912532_T_C	Segregates
GOLGA2	nonsynonymous	NA	B	B	D	-3.08	602580	9_131022937_C_T	Segregates + Present in 3 genotypes in the ExAc browser

MUC6	nonsynonymous	NA	NA	NA	NA	NA	158374	11_1016890_G_A	Mucin gene
MUC2	nonframeshift insertion	NA	NA	NA	NA	NA	158370	11_1092623_-_AAC	Mucin gene
C14orf23	nonframeshift insertion	NA	NA	NA	NA	NA	NA	14_29261307_-_CAA	Doesn't segregate
DICER1	nonframeshift deletion	NA	NA	NA	NA	NA	606241	14_95563003_CTC_-	Doesn't segregate
SSTR5	nonsynonymous	NA	D	P	B	4.52	182455	16_1129218_C_T	Segregates + Present in 144 genotypes in the ExAc browser
TBC1D24	nonsynonymous	NA	NA	NA	B	0.0379	NA	16_2550330_C_T	Segregates
PKMYT1	nonsynonymous	NA	B	B	B	2.37	602474	16_3024281_C_T	Segregates + Present in 6 genotypes in the ExAc browser
AC009113.1	nonsynonymous	NA	NA	NA	NA	NA	NA	16_89299807_A_G	No gene there
RRBP1	nonsynonymous	NA	NA	NA	NA	NA	601418	20_17639786_T_G	Not present in Sanger sequencing - Highly repetitive stretch
OGFR	nonsynonymous	NA	B	NA	B	-3.64	606459	20_61444633_G_A	Doesn't segregate
IGLV5-45	nonsynonymous	NA	NA	NA	NA	NA	NA	22_22730696_C_T	Doesn't segregate
IGLV5-45	nonsynonymous	NA	NA	NA	NA	NA	NA	22_22730702_A_G	Doesn't segregate
IGLV5-45	nonsynonymous	NA	NA	NA	NA	NA	NA	22_22730788_G_A	Doesn't segregate
IGLV5-45	nonsynonymous	NA	NA	NA	NA	NA	NA	22_22730800_A_C	Not present in Sanger sequencing
FAM155B	nonframeshift deletion	NA	NA	NA	NA	NA	NA	X_68725197_CTG_-	Deletion in CTG stretch, present in EVS server on different location

Table 5-5 Shared, novel, nonsynonymous variants in Family J. NA = Not applicable; B = Benign; D = Damaging; P = Probably damaging.

To date, six families have been found with mutations in this gene, five of which were splice site defects and one was a missense mutation, resulting in lower levels of the protein (Zara et al., 2006). The c.C1124T (p.Pro375Leu) missense variant in family J resulted in a substitution of proline to a leucine, both nonpolar amino acids. This variant has only been found in one allele in the ExAc browser, which does not exclude it from being pathogenic. In multiple species, a threonine can be found on position 375 instead of a proline, indicating that the amino acid is not conserved (Fig. 5.26). Whilst SIFT predicts the substitution to be benign, Polyphen2 is contradicting. Considering the prevalence of multiple segregating genes, this has not been taken forward.

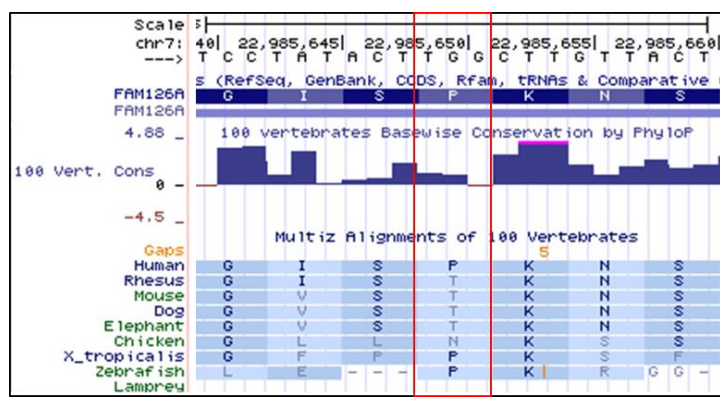


Figure 5.26 Conservation of the variant in the *FAM126A* gene.

5.2.9 Family K

Once again in collaboration with Professor Zuchner's lab in Miami, exome sequencing was performed on one patient of a complex family to identify mutations in known CMT genes (Fig. 5.27). A list of 93 candidates was established by the lab in Miami, incorporating several interesting candidate genes (See Appendix V). After careful clinical evaluation the phenotype resembled a lower SMA phenotype, which is characteristic for mutations in *DYNC1H1*. This brought up a c.1502G>C (p.Arg501Pro) variant in the Bicaudal D homolog 2 (Drosophila) (*BICD2*) gene as a potential cause for the disease. *BICD2* is an adaptor protein interacting with the dynein-dynactin motor complex, facilitating trafficking of cellular cargos that are critical to motor neuron development and maintenance. After confirming the segregation of this variant in the family, 39 more cases with a similar phenotype were screened for mutations in this gene by me.

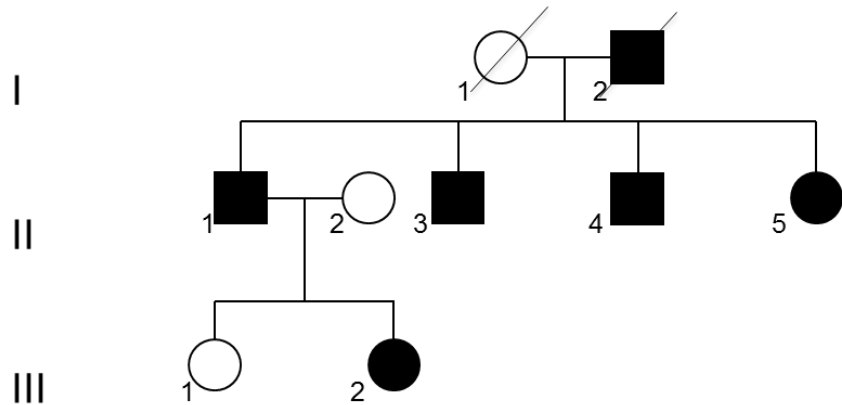


Figure 5-27 Pedigree of Family K.

One more patient was found with a mutation in this gene: c.565A>T (p.Ile189Phe) (Fig. 5.28). This was a de novo case where the unaffected parents did not carry the mutation. Both of the patients presented with autosomal-dominant congenital SMA (DCSMA) and upper moto neuron signs (UMN). In collaboration with other centres, four more DCSMA (+UMN) or HSP families were found with mutations in this gene. Functional studies performed by Dr. Alex Rossor showed a higher affinity of the mutated proteins to the dynein-dynactin complex, resulting in altered cellular trafficking processes. Simultaneously, two more groups published their studies on mutations in *BICD2* in patients with DCSMA, adding five separate families to the original six (Neveling et al., 2013; Peeters et al., 2013).

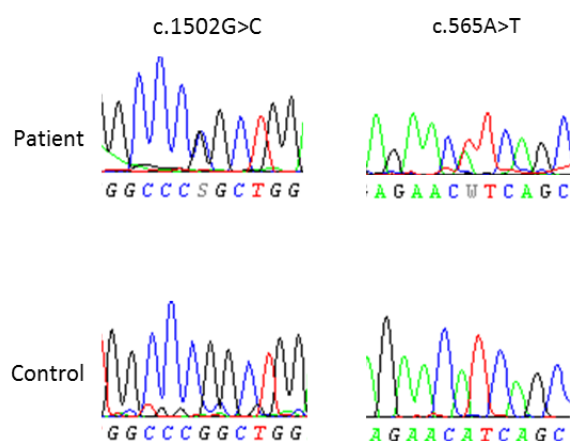


Figure 5-28 Electropherograms of mutations in *BICD2*.

As stated before, *BICD2* is an adaptor protein interacting with the dynein-dynactin motor complex and the small ATPase RAB6, thereby facilitating the trafficking of key cellular cargos such as mRNA, Golgi, and secretory vesicles. Transfected cells showed a higher binding affinity between *BICD2* and the Dyenin-Dynactin complex

when mutated. One study showed accumulation of BICD2 in the perinuclear region for one mutation, colocalised with RAB6, potentially decreasing anterograde trafficking of secretory vesicles to the plasma membrane (Oates et al., 2013). However, opposite results were obtained in the study by Peeters et al., showing decreased colocalisation with RAB6A for two other mutations. It is not clear whether the alterations in BICD2 lead to gain-of-function or dominant-negative loss-of function effects, nonetheless it can be concluded *BICD2* mutations are linked to SMA with dominant inheritance.

5.2.10 Family L

In collaboration with Dr. Wilson Marques from Brazil, exome sequencing was performed on one index patient from a large family with CMT2 and HMN. This was initially performed to examine known pathogenic mutations. When no such mutations were found, two additional family members were sequenced. Surprisingly, a known pathogenic mutation in the *MFN2* gene was found in these two patients: c.494A>G. Re-examination of the raw data files of the index patient revealed this area was covered but the mutation was only present in 1 out of 60 reads (Fig. 5.29). Sanger sequencing indicated this mutation in all patients, resulting in an explanation for the observed phenotype.

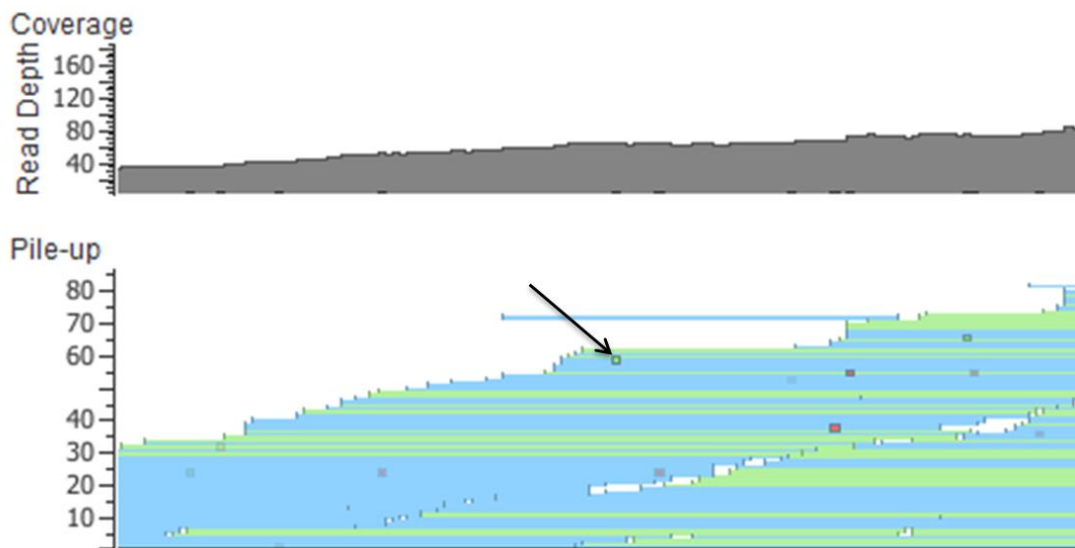


Figure 5-29 Coverage of the *MFN2* variant in the original exome sequencing. The mutation was only present in 1 out of 60 reads.

5.3. Discussion

Exome sequencing was performed in several families resulting in a pathogenic gene in five families. Previously pathogenic genes were discovered after performing exome sequencing in two undiagnosed families.

In family H, diagnostic guidelines had already indicated the possibility of mutations in the *HSPB1* gene but Sanger sequencing of the gene showed negative results. However, during analysis of the exome data, a c.544C>G variant in this gene was found, resulting in a novel mutation of Proline 181 to Alanine. Previous reports have stated mutations changing the same exact Proline to both Serine or Leucine in patients, indicating the pathogenicity of mutations in this amino acid. Initial Sanger sequencing of *HSPB1* in the index cases did not call this variant due to a 4-bp insertion in intron 2 on the same allele, leading to a preferred amplification of the wild type allele and masking the pathogenic variant. This requires caution whilst screening for mutations in *HSPB1* in undiagnosed families with CMT. Previous families screened for mutations in *HSPB1* were repeated with new primers to investigate whether pathogenic mutations were missed, but no further mutations were found.

In family L, a known pathogenic mutation in *MFN2* was found. Exome sequencing to look for pathogenic mutations in the index case resulted in no positive hits, leading to additional exome sequencing in two more family members. This showed a c.494A>G variant that has been found in two previous families with axonal neuropathy, one of them sporadic and one familial case. This variant was only called in 1 out of 60 reads of the exome sequencing of the original index case and subsequently was not listed in the variant file. Segregation analysis confirmed the presence of the variant in the four generation family, reaffirming the pathogenic status of the variant in the family.

In addition to the known pathogenic genes, three novel genes were suggested as pathogenic cause for the disease in three separate families. In family D, a nonsense variant in the *TRAK2* gene was initially pursued and haploinsufficiency was suspected to result in an axonal neuropathy. However, the presence of an additional

patient with a nonsense variant which also occurred in the unaffected father quickly undermined this hypothesis and together with the lack of functional data, evidence was low to establish *TRAK2* as the causative gene. The focus of investigation was shifted to a frameshift variant in the *NEFH* gene that resulted in a stop-loss and the addition of 40 extra aminoacids. Functional experiments are ongoing by our collaborators in Miami in cell lines and zebrafish models to investigate the pathogenicity of the variant.

In Family E, a homozygous missense mutation in the *ADD3* gene was the primary candidate to explain the phenotype of spastic diplegic/quadriplegic cerebral palsy, intellectual disabilities and axonal neuropathy. Functional investigation of fibroblasts performed by the Kruer lab indicated a loss of function mechanism of the mutation by impairing heterodimer/heterotetramer formation and disrupting the regulation of cellular actin polymer growth. Genetic forms of cerebral palsy are rare and the lack of an additional family indicates the rarity of mutations in *ADD3*. Since no further mutations were found in patients with an isolated peripheral neuropathy, chances are low that variants in this gene will be causative for isolated inherited neuropathies.

The last novel pathogenic gene was originally found in one family with three generations of DCSMA (Family K). Due to the well-characterised phenotype, highly resembling patients with mutations in *DYNC1H1*, an interactor protein, *BICD2*, was pursued as a candidate gene. Five more families were found and functional investigations showed altered cellular trafficking processes. Five further families were found at the same time by two other groups, indicating the importance of mutations in *BICD2* in patients with DCSMA and upper motor signs.

Within the remaining four families, the candidate gene list could not be narrowed down to one likely pathogenic gene with the information available. This ensued in a shorter list of probable pathogenic genes that will require the presence of an additional family or other indications towards pathogenicity before further investigations will be performed. Several mutations will only be found in one or two families and pathogenicity can still be questioned. This has to be addressed by performing functional experiments and extensive studies of the influence of the variant. However, functional work cannot be performed on all possible variants due

to time limitations, so genetic proof regarding pathogenicity is desirable before further steps are undertaken.

Whilst exome sequencing has provided a huge step forward in the discovery of pathogenic variants in genes, the enrichment steps involved lead to non-uniform coverage, generating both 'hot spots' with too much coverage and regions with too little coverage and low reading depth. One way to counteract this is the use of whole genome sequencing, which does not require an enrichment step, resulting in a more uniform coverage of the genome. This will also cover intronic regions and possible deletions that might have been missed with the use of whole exome sequencing since the longer reads available for whole genome sequencing allow for better determination of copy number variations, rearrangements and other structural variations. While previously, exome sequencing provided a significantly lower-cost and less time consuming option, whole genome sequencing has begun to close in on the price advantage, slowly moving the field from exome to genome. It could still be advocated that whole exome sequencing requires lower data storage costs and quicker, cheaper and easier data analysis, since the reads only focus on ~2% of the genome in comparison to 5% to 98% of the genome. There is also a better chance of interpreting variants in a meaningful way due to a better characterisation of the coding region of the genome, which promotes whole exome sequencing as a first approach. The work in this chapter demonstrates the benefit of the use of the whole-exome sequencing in genetic diagnosis; however, the limitations of the methodology have also been highlighted.

Chapter 6

Genetic and functional analysis of *IGHMBP2*

6.1 Introduction

6.1.1 Spinal Muscular Atrophy with Respiratory distress 1

In 1974, Mellins et al reported two unrelated cases of spinal muscular atrophy 1 with respiratory distress as first manifestation. In cases with SMA1, patients typically present with proximal weakness before they suffer from respiratory failure; patients with SMARD1 present with diaphragmatic paralysis very early on in disease and develop predominantly distal limb involvement (Bertini et al., 1989; Grohmann et al., 2001; Grohmann et al., 2003; Kaindl et al., 2008). In 2001, a study by Grohmann et al. linked patients with SMARD1 to mutations in *IGHMBP2*.

Disease onset is normally within the first few weeks after birth and patients rarely survive the first decade (Rudnik-Schöneborn et al., 2004; Messina et al., 2012). The oldest patient reported to date is a 20 year old man with infantile-onset SMARD1, compound heterozygous with the following mutations: c.1082T>C (p.Leu361Pro) and c.1144G>A (p.Glu382Lys). He presented with distal weakness and respiratory

failure associated with diaphragmatic elevation at 4 months of age and has been ventilator-dependent since. Later on, he developed a length-dependent progressive sensory-motor neuropathy associated with loss of sensation, muscular denervation and atrophy. Cognitive testing was limited but revealed intellectual disability and some tongue fasciculations were present; otherwise, his cranial nerves were normal (Pierson et al., 2011).

SMARD1 patients with mutations in *IGHMBP2* can present with varying clinical outcomes. The most dramatic disease progression happens within the first year of life, resulting in loss of independent breathing and muscle strength. Whilst prognosis is poor, a heterogeneous clinical course with marked differences in the disease outcome can be observed in the later years, ranging from not being able to communicate to breathing independently in the first decade of life. Clinical scores at the age of three months showed a positive correlation with the clinical outcome in the later years. When expressed in an in vitro recombinant system, patients with more favourable outcomes tend to have mutations that retain residual enzymatic activity (Eckart et al., 2012). However, severity does not only depend on the mutations and can vary within families. For example, in a family with two siblings with an identical compound heterozygous combination of a stop mutation and a missense mutation in exon 10 of the *IGHMBP2* gene, one presented with a phenotype of typical infantile onset with respiratory insufficiency whilst the other sibling had motor regression from the age of 19 months with respiratory impairment only starting from the age of 7 years (Joseph et al., 2009).

Nerve conduction studies and electromyography

NCS are used for the determination of the peripheral nerve function, resulting in markedly reduced motor conduction velocities, particularly in the legs, and a very marked reduction or loss of the compound muscle action potential. Studies of the sensory fibres showed similar results, but much milder. EMG revealed a denervation pattern only in distal muscles initially. Abnormal EMG results of the diaphragm, showing denervation often with little abnormality in the intercostal muscles, are typical in SMARD1. The severity of the initial presentation can be easily obtained by the compound muscle action potential of the m. abductor hallucis longus, presenting

an easily obtained parameter against which prognosis and progress might be judged (Pitt et al., 2003).

Pathological findings

Small anterior roots are typically observed in the spinal cord of SMARD1 patients, with the remaining motor neurons showing dissolution of the Nissl bodies in the cell body. Due to the presence of both atrophy of the anterior roots and primary degeneration of the cell bodies, dying-back and dying-forward mechanisms are both suggested to be involved. Accumulation of neurofilaments, ubiquitination and apoptosis are also frequently observed (Grohmann et al., 1999). Sural and tibial nerves of patients showed typical signs of axonal degeneration, the presence of tomacula and myelin loops and endoneurial fibrosis, but a normal structure of unmyelinated axons. A considerable variation of myelin thickness and areas with a reduced number of axons is observed, especially the thick myelinated fibres, resulting in small myelinated fibres and fascicular areas. Wallerian degeneration and marked axonal atrophy with hypo-and hypermyelination were prominent in motor and sensory neurons, but no signs of demyelination were present. Signs of active axonal degeneration are present but no evidence of regeneration (Pitt et al., 2003; Diers et al., 2005). Together these features are suggestive of abnormalities in myelination, caused by mutations in *IGHMBP2*. This could be caused through primary Schwann cell dysfunction or as a secondary outcome due to impaired interactions between the axons and Schwann cells. In the neuromuscular junctions of SMARD1 patients, terminal axons were absent, subsynaptic clefts were reduced and no motor end plates could be found in the diaphragm. Skeletal muscle sections showed neurogenic atrophy and inactivity without fibre grouping (Diers et al., 2005). Ultrastructural analysis of the muscle nuclei showed aberrant heterochromatin reorganisation and distorted nuclear-envelope continuity with the formation of granular chromatin blebs, abnormalities that were also found in the nuclei of Schwann cells and are often seen in laminopathies (Jedrzejowska et al., 2014). These suggest an initial anterior horn cell degradation accompanied by myelination abnormalities, followed by degeneration of axons and their endings at the endplate.

6.1.2 Immunoglobulin mu binding protein 2 protein

Structure

Human IGHMBP2 consists of 993 amino acids and contains an RNA/DNA helicase domain, an R3H, single-stranded nucleic acid-binding domain and a zinc finger domain (Fig. 6.1). The gene encodes a helicase superfamily member that binds a specific DNA sequence from the immunoglobulin mu chain switch region and has been classified as a member of the Upf1-like group within helicase superfamily 1 (SF1) (Fukita et al., 1993; Jankowsky, 2011). Also in this group of Upf1-like proteins are Upf1 and Senataxin (Bhattacharya et al., 2000; Chen et al., 2006; Fairman-Williams et al., 2010). Senataxin encodes a 302.8-kD protein implicated in a type of motor neuronopathy called ALS4 and ataxia with neuropathy called ataxia-oculomotor apraxia type 2 (Chen et al., 2004; Suraweera et al., 2009). The overlap in homology suggests that DNA/RNA helicase dysfunction may play an important role in the development of different types of neuropathy. The signature of this group of proteins is a DEAD box-like helicase/ATPase domain consisting of seven to nine canonical motifs, including the Walker A and B motifs, involved in ATP binding and hydrolysis (Cordin et al., 2006; Lim et al., 2012).

Residues 638–786, including the R3H domain of IGHMBP2 at the C-terminal end, were identified as a segment that specifically binds 5'-phosphorylated, guanine-rich, single-stranded DNA (ssDNA) sequences (Fukita et al., 1993). Not only is the R3H domain involved in nucleic acid-binding, it also provides a surface area that could be involved in yet unknown protein-protein interactions (Liepinsh et al., 2003).

Function

The structure of the protein together with the observation that immunoprecipitates of IGHMBP2 showed an affinity to single-stranded DNA and an unwinding activity on partially double-stranded DNA (Molnar et al., 1997), suggests a potential role of IGHMBP2 in replication or transcription of DNA. Research by Guenther et al. in 2009 identified IGHMBP2 as a 5'-3' helicase, unwinding DNA and RNA duplexes with 5' overhangs in an ATP-dependent manner. IGHMBP2 has an almost exclusive localisation within the cytoplasm of the cell, where it co-localises with components of the translation machinery as part of ribonucleoprotein complexes by interacting with the large and the small ribosomal subunits (Guenther et al., 2009).

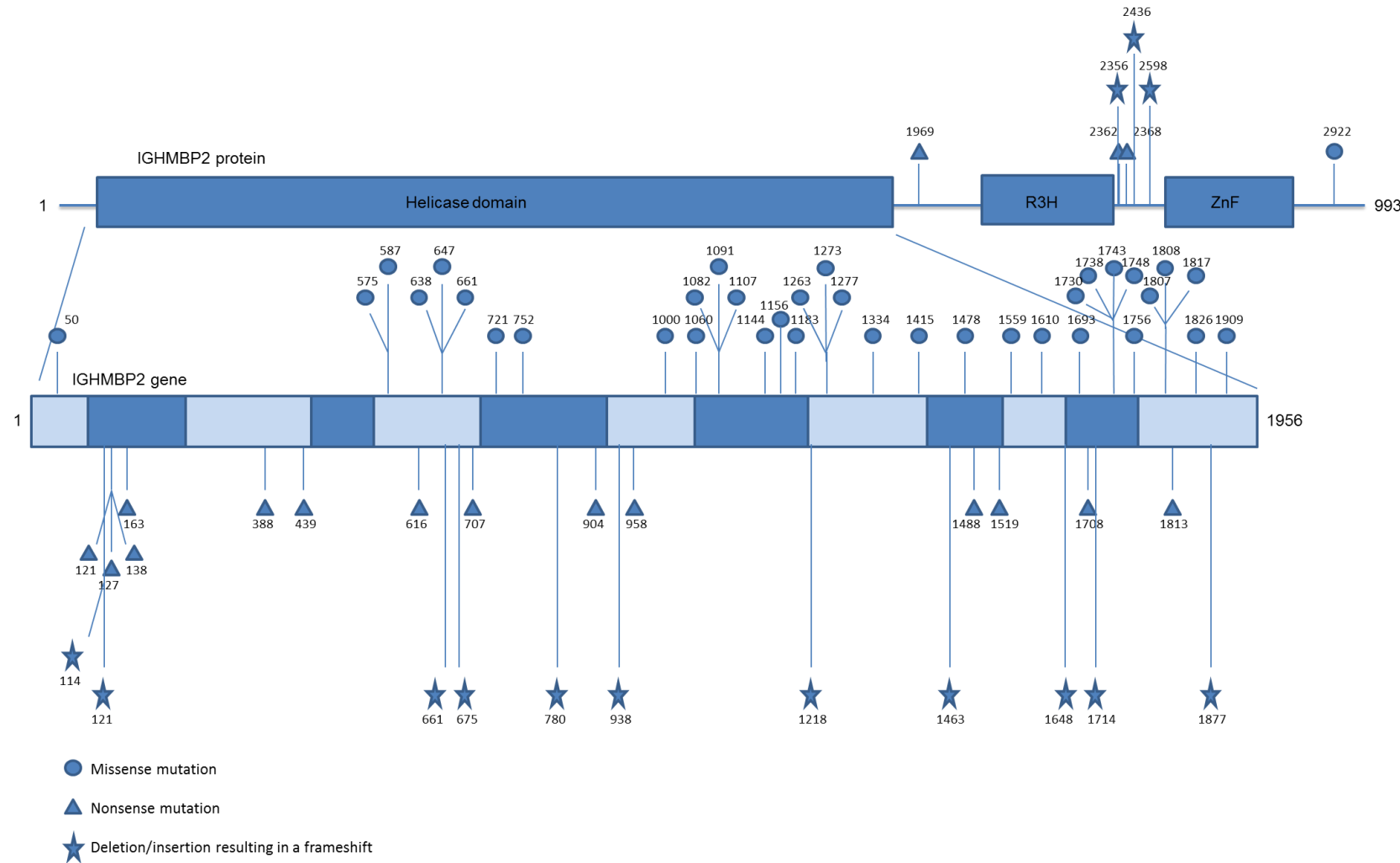


Figure 6-1 Location of all missense, nonsense and frameshift mutations in the structure of *IGHMBP2*.

Effect of mutations in IGHMBP2

Mutational analysis of mutations in *IGHMBP2* that lead to SMARD1 showed that either the unwinding capacity or the ATPase activity of the protein was affected or severely reduced steady-state protein levels were detected *in vivo*. None of the mutations affect ribosomal association. Several mutations residing in the helicase domain were studied, most of them affecting both the ATPase and the unwinding activity of the protein. Three exceptions were found so far: p.His213Arg, p.Thr491Ile and p.Asp565Asn. For the latter, only the unwinding activity was affected, whilst the other two mutations retained both unwinding and ATPase activity. One of these, p.Thr491Ile, was studied in patient lymphoblastoid cell lines and showed a lower steady-state protein level.

It has been suggested that a retained residual enzymatic activity correlates with a more positive disease outcome and might delay disease progression or manifestation age, but this was done in a very small sample size. Since most of these patients are compound heterozygotes, the exact contribution of each mutation to the phenotype cannot be assessed (Guenther et al., 2009; Eckart et al., 2012). Quantification of the steady-state protein levels in five patients with either juvenile or infantile onset and different combinations of mutations revealed significantly lower levels in all five patients in comparison with controls or heterozygous carriers. Significantly lower steady-state protein levels were observed in the infantile patients in comparison with the juvenile onset patients. Heterozygous carriers of mutations all showed lower steady-state protein levels, ranging between 50-80% of the controls, depending on the mutation.

Whilst most mutations in *IGHMBP2* are located within the helicase domain, few mutations have been found outside of this domain. In most cases, the disease-causing mutations outside the helicase domain result in the generation of mRNA with a premature stop codon. Only one missense mutation outside the helicase domain has been reported so far: c.2922T>G (p.Asp974Glu), in combination with an in-frame deletion in exon 12 (Grohmann et al., 2003). So far, 76 mutations have been reported to cause SMARD1, 53 of which are missense/nonsense mutations and 15 deletions/insertions causing a frameshift (Fig. 6.1). Other causes of disease consist of

splicing mutations, gross deletions or genomic rearrangements (not depicted in figure).

6.1.3 *nmd* mouse

The *nmd*^{2J} mouse is a spontaneous autosomal recessive mouse mutant caused by loss of function of the *IGHMBP2* gene due to a splice donor mutation (Cox et al., 1998). Nmd mice showed greatly reduced levels of the *IGHMBP2* protein and a severe loss of spinal cord motor neurons before onset of clinical symptoms. This was followed by axonal degeneration in corresponding nerves and loss of axon terminals at motor endplates at the final stages of disease. Signs of respiratory distress are only developed clinically at the later stages and no significant reduction in axon numbers of phrenic nerves was observed in mice of 14 weeks old. Myopathic alterations such as large numbers of regenerating muscle fibres and occasional muscle fibre necrosis were found in 8-week old mice (Grohmann et al., 2004). Transgenic expression of *IGHMBP2* cDNA prevented primary motor neuron degeneration, while restoring the normal axonal morphology and density in nmd mice. However, these mice developed a previously unobserved cardiac and skeletal myopathy, with the cardiomyocyte degeneration being much more severe than the myopathy observed in the skeletal muscle fibres, suggesting these might have a higher requirement for *IGHMBP2*. Whilst there have been no reports of cardiomyopathy in SMARD1 patients, cardiac arrhythmia has been described in several infants (Pitt et al., 2003; Grohmann et al., 2003).

Modifiers of disease

When first described, it was observed that 25% of the (B6-*nmd*^{2J} X CAST/EiJ)F2 *nmd*^{2J}/ *nmd*^{2J} mice were very mildly affected concerning the neurogenic atrophy and paralysis (Cox et al., 1998) This was attributed to a single locus on chromosome 13 containing the *Mnm*^C gene. Further analysis narrowed the effect down to one single BAC rescue clone of 166 kb within the *mnm* modifier, encompassing the *ABT1* and *Zfp322a* genes, six tRNA genes and one noncoding EST. This genetic modifier did not restore the splicing defect in nmd mouse, nor did it have an influence on the protein levels (de Planell-Saguer et al., 2009). Whether it affects either the *IGHMBP2* protein directly, or rather contributes to the survival of motor neurons independently, remains to be determined. Interestingly, Co-IP experiments have shown an interaction between *IGHMBP2* and *ABT1*, a factor in pre-ribosomal RNA

processing and maturation of ribosomes (de Planell-Saguer et al., 2009). As mentioned before, there is a high intra- and interfamilial heterogeneity in age of onset or severity of symptoms in SMARD1 patients, which implies the existence of a modifier gene, but none have been identified so far. ES-derived motor neuron cultures have been developed from both wild type and mutant mice with or without this modifier region, aiming to elucidate the molecular pathway responsible for the difference in severity (Van der Pol et al., 2013).

6.1.4 Treatment and management

SMARD1 is a severely disabling disorder with a very poor prognosis. All patients require ventilation early on in life and few reach the stage of being able to sit unsupported. No treatment options are available and focus lies on management of the disease. A long-term observational study of patients who survived on permanent ventilator support showed that most patients are well-integrated into their environments and two thirds are able to attend kindergarten or school (Eckart et al., 2011). Considering the rarity of these patients, most centres only have few SMARD1 patients under their care and international collaboration is necessary to establish a uniform standard for genotype/phenotype relations and provide updates on relevant clinical and research information (Van der Pol et al., 2013).

6.1.5 Future directions

Stem cells

Neuronal stem cell (NSC) and neuronal precursor transplantation in *nmd* mice have shown to result in a longer survival and improvement of the phenotype (Corti et al., 2006, 2009). Transplantation of human derived iPSC-derived NSCs significantly improved the neurological phenotype and the survival of the *nmd* mice, although not sufficiently enough to rescue to *nmd* phenotype. Molecularly, upregulation of genes involved in chromatin organisation, cytoskeletal function, and neurogenesis was observed in transplanted mice in comparison to untreated mice as well as downregulation of genes involved in excitatory amino acid toxicity and oxidative stress (Simone et al., 2014). Co-cultures of NSCs with murine and human motor neurons exhibited a neuroprotective effect by producing neurotrophic factors that inhibit both GSK-3 and HGK kinases. Motor neuron survival improved and an increased neurite length and growth cone size was observed in SMARD1 iPSC-

derived motor neurons (Simone et al., 2014). Not only could iPSC derived from affected patients be a more valuable model for testing therapeutic strategies next to results from the animal model, the combination of cell transplantation with an effective drug therapy might ultimately lead to clinically significant results in patients.

Gene therapy

Gene therapy in mouse models of SMA has shown positive results, increasing life expectancy from 27 to 340 days, preventing motor neuron death, complete correction of motor function and rescue of the weight loss phenotype close to normal (Dominguez et al., 2011). Recent findings have shown systemic administration of AONs to restore *SMN2* splicing rescues the phenotype more efficiently than intraventricular administration, leading to the targeting of motor neurons by intravenous administration with a self-complimentary adeno-associated virus 9 (scAAV9) vector (Duque et al., 2009; Hua et al., 2011; Van Meerbeke et al., 2011). Research for SMA is advancing to the stage of AAV9 vector-based gene therapy trials in human patients. This appeals for similar studies in the nmd mouse model with scAAV9 vector supported *IGHMBP2* gene therapy.

Insulin-like growth factor 1 (IGF-1)

IGF1, also known as somatomedin C, plays an important role in the developmental process of neurons, promoting peripheral neuron survival and inducing regeneration (Gao et al., 1999). Recent studies in the *Nmd^{2J}* mice identified a systemic IGF1 deficit in blood serum, which could be compensated by treating mice with subcutaneous injections of Polyethylene glycol-coupled IGF1. This resulted in improvement of the motor deficits, an 84% reduction of spontaneous activity in the gastrocnemius muscle and a slight gain of CMAP amplitude. PEG-IGF1 treatment markedly ameliorated or even prevented the myopathic pattern of pathology seen in the gastrocnemius and diaphragm muscles but did not rescue motor neuron and motor axon loss (Krieger et al., 2014). Studies in the *pmn* mouse showed positive effects on spinal motor neuron survival when a 3-fold higher dose of PEG-IGF1 was applied but these could not be replicated in the *Nmd^{2J}* mice due to fatality of the higher dose (Jablonka et al., 2011). Molecular studies suggest that the beneficial effect of PEG-IGF1 in striated muscle is mediated through the Akt/p70^{S6K} signalling pathway, adjusting muscle differentiation and protein biosynthesis via the PI3

kinase/p70^{S6K}/mTOR pathway. Recombinant human insulin-like growth factor 1 (rhIGF1) (Mecasermin) is already a Food and Drug Administration-approved drug for the long-term treatment of growth failure in children with severe primary IGF-I deficiency (Backeljauw et al., 2012) and was recently used in a phase 1 trial for rett syndrome (RTT), a severe X-linked neurodevelopmental disorder associated with mutations in *MECP2*, to evaluate the safety, tolerability and pharmacokinetic profiles of IGF-1 in 12 patients (Khwaja et al., 2014). This ameliorated certain breathing and behavioural abnormalities and was well tolerated; suggesting PEG-IGF1 could be a reasonable candidate as a therapeutic compound in SMARD1 patients.

6.2 Results

6.2.1 Clinical details of two siblings with CMT2

In line with the previous chapter, exome sequencing was performed in a recessive family with two siblings in their 40's, affected with axonal neuropathy (Family M). Clinical and neurophysiological examination of both parents was normal and family history was otherwise unremarkable. Both sisters presented at age 3 and 6 years with toe walking and slowly progressive distal lower limb wasting and weakness. Hand involvement subsequently developed. There were no sensory symptoms. Disease course was similar in both siblings until early in the third decade of life. At that time, the oldest sibling developed right shoulder pain radiating down her right arm followed by anisocoria and cranial neuropathies of the right XI and XII nerves, but no significant abnormalities were observed on brain MRI, PET scan and ENT examinations. Neurological examination at the age of 25 disclosed asymmetrical pupils reacting normally to light and accommodation with no ptosis, right-sided atrophy and weakness of the tongue, and mild weakness of the right trapezius and sternocleidomastoid muscles. Electromyography of the right tongue, trapezius, and sternocleidomastoid muscles showed chronic neurogenic changes. There was no suggestion of myopathy. Sensory examination was normal, but NCS showed absent sensory responses in upper and lower limbs, and absent motor responses from the median, common peroneal and posterior tibial nerves. Overall, the neurophysiological pattern was consistent with a motor and sensory axonal polyneuropathy and XI and XII right cranial neuropathies.

During the last examination of the siblings at 42 and 38 years of age, both of them worked for the government, were still active, able to drive, and used a stick to walk with silicon ankle foot orthosis. Examination of the index case at age 42 revealed bilateral foot drop, distal weakness and wasting in the upper and lower limbs, with mild proximal lower limb weakness. Reflexes were absent and there was sensory loss in the feet and hands. Cranial nerves were normal apart from a wasted tongue. There were no respiratory problems. Chest X-ray and sleep study was normal, nerve conduction studies indicated an axonal neuropathy and a nerve biopsy showed an axonal neuropathy. Her sister had almost identical but milder clinical features, and examination findings at the age of 38 years revealed bilateral foot drop, severe distal weakness and wasting in the upper and lower limbs, with mild proximal lower limb weakness, areflexia and minor sensory deficits. There were no respiratory problems and an axonal neuropathy was seen on nerve conduction studies.

6.2.2 Exome sequencing revealed a mutation in the IGHMBP2 gene

17p11.2 chromosome region rearrangements were not detected and sequence analysis of *MPZ*, *PMP22*, *GJB1*, *MFN2* and *GDAP1* showed no pathogenic variants. Exome sequencing was performed and analysis of the results detected two compound heterozygous mutations in the immunoglobulin helicase μ -binding protein 2 (*IGHMBP2*) gene. Mutations in this gene have been previously described to cause Spinal Muscular Atrophy with Respiratory Distress 1 (SMARD1) (Grohmann et al., 2001). Exome sequencing revealed a nonsense 5' mutation (c.138T>A, p.Cys46Ter) and a 3' frameshift mutation in the last exon of the gene (c.2911_2912delAG, p.Arg971Glufs*4). The mother and father were heterozygous for the c.138T>A and c.2911_2912delAG mutations, respectively. The nonsense mutation has been found before in a patient with SMARD1, in combination with a frameshift insertion in exon 12: c.1649insC (Grohmann et al., 2003). At the time of discovery, the deletion was regarded as a novel mutation, not present in the 1000 genomes database, the exome variant server (EVS) of 6500 individuals, or our in-house exome database of 480 clinically and neuropathologically normal controls. More recent updates show the presence of this variation in the online servers. Considering the recessive nature of the disorder, the presence of carriers in the population has to be taken into account. Verifying the pathogenicity of the deletion is a vital step to take this gene forward in the context of CMT2. Seeing there is a substantial difference in the

severity of the diseases, an explanation as to why this occurs in CMT2 would lead to a better understanding of the pathways in which *IGHMBP2* is involved and how difference in genotype can establish a difference in phenotype.

6.2.3 Genetic screening

As an initial approach, Sanger sequencing was performed in 260 CMT2 patients with suggestive or possible recessive inheritance. Five extra patients from four families were found with compound heterozygous mutations in the *IGHMBP2* gene (Table 6.1, Families N-Q). Segregation analysis in families N-P revealed the consistent presence of one variant in each parent (Fig. 6.2). Further analysis of collaborator data revealed three families with compound heterozygous mutations and one with a homozygous mutation (Table 6.1, Families R-U). In two extra families, only one heterozygous mutation could be identified (Table 6.1, Families V, W). For these two families, MLPA for *IGHMBP2* did not show any deletions. This brings the total to fifteen CMT2 patients with mutations in *IGHMBP2* (Table 6.1). Both of the mutations initially seen in the index patients were independently found in other patients (Table 6.1, Families O and S).

6.2.4 Clinical details

All families with CMT2 and *IGHMBP2* mutations showed an autosomal recessive pattern of inheritance (Table 6.2). All fifteen patients presented in their first decade with difficulty walking and distal weakness of predominantly the lower limbs. Upper limb involvement developed soon after. The phenotype consists of slow progression involving lower limbs more than upper limbs and predominantly motor involvement. Sensory involvement was mild glove and stocking and electrophysiology indicated a sensory and motor axonal neuropathy in all cases. At the latest examination, all had moderate to severe weakness in both upper and lower limbs, pinprick and vibration sense was normal for most patients or reduced below wrist/ankle and reflexes were absent. Neurological examination showed proximal weakness in the older cases but after 40 years of disease. None of the cases had respiratory compromise, recurrent chest infections or previous ventilator assistance or sleep apnea. Results of the forced vital capacity test in four patients ranged from 25-95% of normal. Out of fifteen patients, six are currently wheelchair-bound and one further case had wasting of the tongue, comparable to the index patients. Extensive clinical details were available for two patients, who were seen locally.

Family	Ethnicity	Sex	Diagnosis	Age at onset	Current age	Protein change	Nucleotide change
M	English	Female	CMT2	7 years	42 years	p.Cys46Ter + p.Arg971Glufs*4	c.138T>A + c.2911_2912delAG
M	English	Female	CMT2	6 years	38 years	p.Cys46Ter + p.Arg971Glufs*4	c.138T>A + c.2911_2912delAG
N	English	Male	CMT2	5 years	23 years	p.Cys46Ter + p.Arg971Glufs*4	c.138T>A + c.2911_2912delAG
O	Serbian	Male	CMT2	2 years	14 years	p.Cys46Ter + p.Phe202Val	c.138T>A + c.604T>G
O	Serbian	Female	CMT2	2 years	15 years	p.Cys46Ter + p.Phe202Val	c.138T>A + c.604T>G
P	Pakistani	Female	CMT2 + Trisomy 21	7 years	20 years	p.Pro531Thr + p.Val580Ile	c.1591C>A + c.1738G>A
Q	English	Male	CMT2	4 years	15 years	p.Ser80Gly + p.Cys496Ter	c.238A>G + c.1488C>A
R	Vietnamese	Female	CMT2	3 years	39 years	p.Arg605Ter + p.His924YTyr	c.1813C>T + c.2770C>T
S	USA	Female	CMT2	6 years	10 years	p.Trp386Arg + p.Arg971Glufs*4	c.1156T>C + c.2911_2912delAG
T	Polish	Female	CMT2	4 years	28 years	p.990_994del (Hom)	c.2968_2980del (Hom)
U	Italian	Female	CMT2	1 years	12 years	p.Val373Gly + p.Ala528Thr	c.1118T>G + c.1582G>A
U	Italian	Male	CMT2	1 years	6 years	p.Val373Gly + p.Ala528Thr	c.1118T>G + c. 1582G>A
V	Korean	Male	CMT2	5 years	41 years	p.Asn245Ser (Het)	c.734A>G (Het)
W	English	Male	CMT2	7 years	20 years	p.Arg605Ter (Het)	c.1813C>T (Het)
W	English	Female	CMT2	10 years	18 years	p.Arg605Ter (Het)	c.1813C>T (Het)

Table 6-1 List of all patients with CMT2 and mutations in *IGHMBP2*.

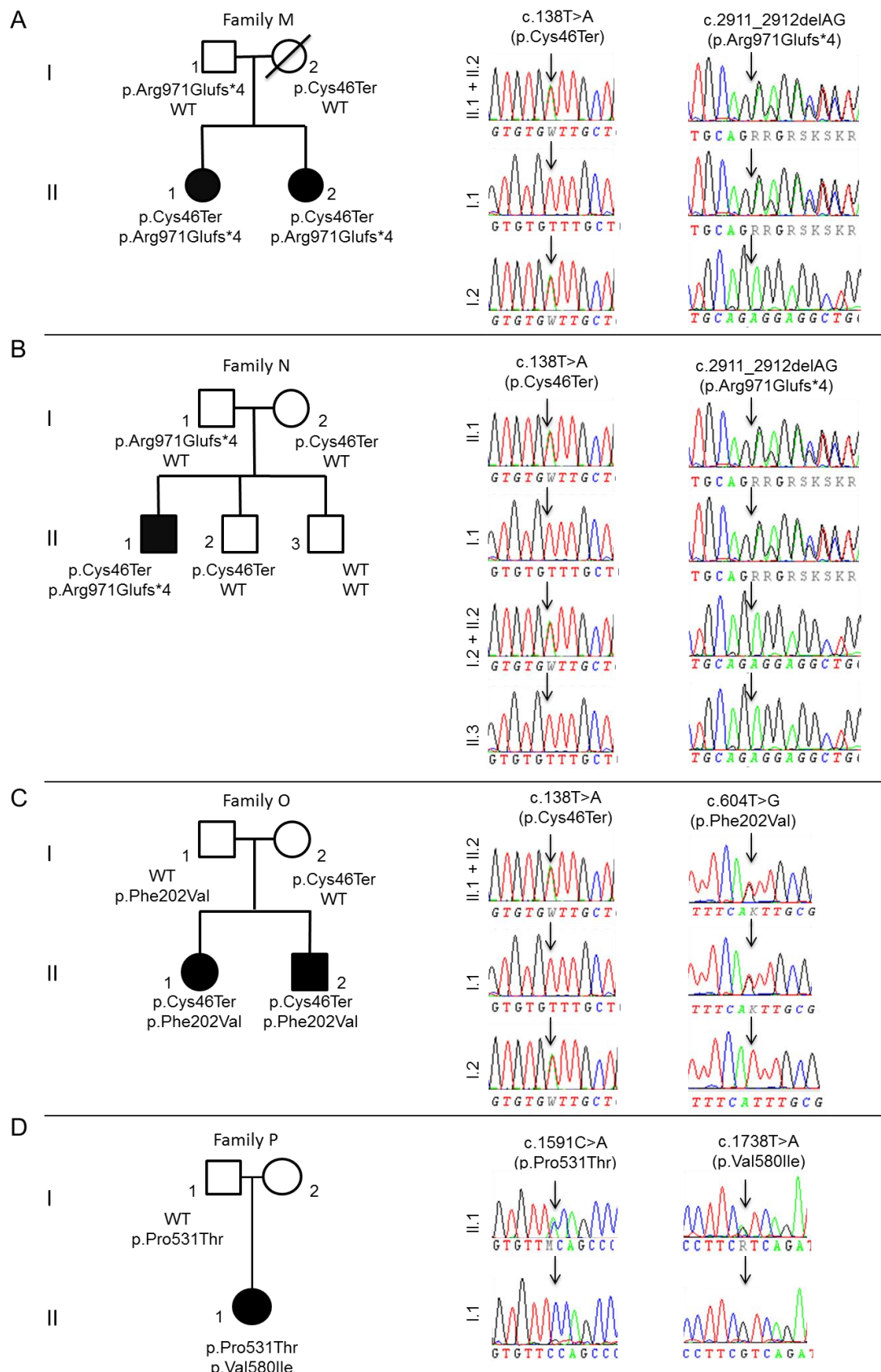


Figure 6-2 Electropherograms of the segregation analysis in families A-D.

Individual	1	2	3	4	5	6	7	8	9	10	12	13	11	14	15
Family no.	M	M	N	O	O	P	Q	R	S	T	U	U	V	W	W
Sex/age (y)	F/43	F/40	M/23	M/14	F/15	F/19	M/15	F/39	F/10	F/28	F/12	M/6	M/41	M/20	F/18
Ethnicity	English	English	English	Serbian	Serbian	Pakistani	English	Vietnamese	USA	Polish	Italian	Italian	Korean	English	English
Mutation	p.Cys46Ter + p.Arg971 Glufs*4	p.Cys46Ter + p.Arg971 Glufs*4	p.Cys46Ter + p.Arg971 Glufs*4	p.Cys46Ter + p.Phe202 Val	p.Cys46Ter + p.Val580Ile	p.Pro531Thr + p.Cys496Ter	p.Ser80Gly + p.His924Tyr	p.Arg605Ter + p.Arg971 Glufs*4	p.Trp386Arg + p.Arg971 Glufs*4	p.990_994Fs (Hom)	p.Val373Gly + p.Ala528Thr	p.Val373Gly + p.Ala528Thr	p.Asn245Ser (Het)	p.Arg605Ter (Het)	p.Arg605Ter (Het)
Age at first symptoms	7 y	6 y	<5 y	<2 y	<2 y	<10 y	4 y	<3 y	6 y	4 y	1y	1y	5 y	7y	10y
First symptom/s	Toe walking, high stepping gait	Toe walking, hand and leg weakness	Difficulty walking, foot drop	Delayed milestone, hypotonia	Delayed walking	Hypotonia, foot drop	Foot drop	Delayed motor milestone s	Foot drop, high stepping gait	Hand weakness difficulty walking	hand fingers flexion foot weakness	bilateral equino-varus foot	Gait difficulty	Foot drop, clumsiness	Feet deformity
Weakness ^a															
UL	+++	+++	++	+++	+++	+++	++	+++	N	++	+++	+	+	++	+
LL	+++	+++	++	+++	+++	+++	++	+++	++	+++	+++	++	++	++	+
Pinprick ^b															
UL	N	N	+	N	N	n/a	n/a	N	N	+	+	n/a	+	N	N
LL	+	N	+	N	N	n/a	n/a	N	N	n/a	+	n/a	+	N	N
Vibration ^c															
UL	N	N	N	N	N	n/a	n/a	N	N	n/a	n/a	n/a	++	N	N
LL	+	N	+	N	N	n/a	n/a	N	N	n/a	n/a	n/a	++	N	N
Reflexes															
UL	Abs	Abs	Abs	Abs	Abs	Abs	n/a	Abs	+	+/-	Abs	abs	abs	N	N
LL	Abs	Abs	Abs	Abs	Abs	Abs	n/a	Abs	Abs (AJ)	Abs	Abs	abs	abs	AJ	+-
Bulbar involvement	No (rhomboid-shaped tongue)	Wasted tongue	No	No	No	Wasted tongue	n/a	No	No	No	No	No	No	No	No

Individual	1	2	3	4	5	6	7	8	9	10	12	13	11	14	15
Family no.	M	M	N	O	O	P	Q	R	S	T	U	U	V	W	W
Respiratory problems/ Respiratory support	No	No	No	No	No	No	No	No	No	No	No	No	No	No	No
Musculo-skeletal deformities	Equinus foot deformity	Equinus foot deformity	Feet deformity (surgery)	Lumbar hyper-lordosis, scoliosis	Lumbar hyper-lordosis	Lumbar hyper-lordosis,	No	Varus feet hip problems	Achilles tendon contracture	Scoliosis	Achilles tendon contractures, scoliosis	Achilles tendon contractures	Thenar muscle atrophy (right>left), Pes cavus	Equinus foot deformity (surgery)	Equinus foot deformity (surgery)
Overall maximal function	Independent ambulation	Independent ambulation	Independent ambulation	n/a	n/a	Independent ambulation	n/a	n/a	n/a	n/a	Independent ambulation	Walking with support	FDS(3), CMTNS(19), 9 hole peg test (23.3 sec)	Independent ambulation	Independent ambulation
Walking aids	AFO	AFO (past)	n/a	WC	WC	WC	AFO	WC since 16	AFO	WC	WC since age 5 years	Bilateral support	AFO	AFO+Crutches	No
Other features	n/a	Wasted right shoulder and lower cranial nerves	n/a	n/a	Without other features	Trisomy 21 mosaicism	Small focus of increased signal in right cerebellar hemisphere (brain MRI)	n/a	McCune Albright syndrome (unconfirmed)	Obese	Marked worsening during febrile illness	No	Sensory ataxia	Without other features	Without other features

Table 6-2 Clinical features of all patients with CMT2 and *IGHMBP2* mutations. AFO = ankle foot orthosis; n/a = not available; LL= lower limbs; UL = upper limbs; WC = wheelchair. a Weakness: N normal; +4> distal muscles; ++ proximal weakness (knee flexion and extension, elbow flexion and extension or above). b Pinprick and vibration sensation: N normal; + reduced below wrist/ankle; ++ reduced below knee/elbow; +++ reduced at or above elbow/knee. c Reflexes: N normal/present; ++ brisk; +++ brisk with extensor plantars; +/- = present with reinforcement; abs = absent; abs (AJ) = absent ankle jerks only

Family N

A 16-year-old male presented with a longstanding history of upper and lower limbs weakness. Early during development he was noted to drag his feet when walking and underwent several operations to his feet since the age of 5 years. He then gradually developed slowly progressive weakness of his lower legs and subsequently of his hands. Examination at the age of 17 years showed significant distal upper and lower limb muscle wasting, weakness of first dorsal interosseus and abductor pollicis brevis muscles, no movement below the ankles, absent reflexes and abnormal sensation in his fingers and lower legs. Nerve conduction studies at age 16 years revealed absent sensory responses in upper and lower limbs, and absent motor responses from the median, common peroneal and posterior tibial nerves. Right ulnar nerve distal CMAP amplitude was 5.7 mV with conduction velocity of 45 m/s. Electromyography of proximal limb muscles showed no significant abnormalities. The neurophysiological pattern was consistent with a motor and sensory axonal polyneuropathy.

Family P

An 18-year-old female was born to non-consanguineous parents in Pakistan. She presented with seizures secondary to hypocalcaemia at the age of 3. She was noted to be hypotonic and dysmorphic and diagnosed with trisomy 21 mosaicism. During childhood, she exhibited developmental delay, bilateral foot drop and limb contractures. On examination at the age of 11 years, she had lumbar hyperlordosis, severe walking difficulty and was able to stand only for one minute without support. There was distal muscle wasting and weakness in her lower limbs and to a lesser degree in her hands. Reflexes were absent and the remainder of the examination was unremarkable. Forced vital capacity was 1.35 L (57% of predicted) but she had difficulty in performing the test. At the age of 18 years, she used a manual wheelchair for outdoor mobility. Sensation was difficult to assess. Neurophysiology at the age of 14 years was consistent with an axonal neuropathy with no recordable motor units from tibialis anterior and extensor digitorum brevis muscles. There were denervation changes in extensor digitorum communis and tongue. Neurophysiology at the age of 20 years confirmed both motor and sensory involvement.

6.2.5 Mutation spectrum

Three families (five patients) carried the c.138T>A nonsense mutation in combination with either a c.2911_2912delAG deletion, causing a p.Arg971Glufs*4 frameshift in the last exon (Family M and N), or a novel c.604T>G (p.Phe202Val) variant (Family O). The remaining eight families either had two missense mutations (Families P,U), a missense mutation in combination with a truncating mutation (Families Q-S) – one of which had the same c.2911_2912delAG deletion as the index family (Family S) – a homozygous truncating mutation (Family T) or one heterozygous missense mutation (Families V,W). Most of these mutations were located in the helicase domain of the protein, apart from the c.2911_2912delAG and c.2968_2980delGAGAGGGGGACGT truncating mutations in the last exon of the gene and the c.2770C>T missense mutation in the zinc finger domain (Fig. 6.3). This is consistent with the observation that in SMARD1, the majority of disease-causing mutations are found within the helicase domain and those that are found outside this domain often result in the generation of mRNAs with premature stop codons. Of all mutations in this cohort, five have been found before in SMARD1 patients. Nine are novel variants, seven of which are missense mutations. Looking at a selected subset of 9 species, representing the 100 species available at the UCSC browser, conservation of these variants is highly preserved. The only exception is the p.Pro531Thr variant, found in family P (Fig. 6.4). This variant is only preserved in the rhesus monkey and the dog. In the other species, proline has changed to Glutamine or Lysine. This results in a respectively polar or positively charged amino acid instead of a non-polar one. When looking into more detail, the proline is preserved over most primates, with gorilla and bushbaby being the exception (Fig. 6.5). Both of these result from a mutation in the second aminocacid of the codon, whilst the variant found in the patient results from changing the first aminoacid of the codon. The conservation score of this particular aminoacid has been determined at 2.61818 by using the PhyloP program, an incorporated function of the genome browser, indicating the conservation and acceleration of this amino acid is more preserved than the average.

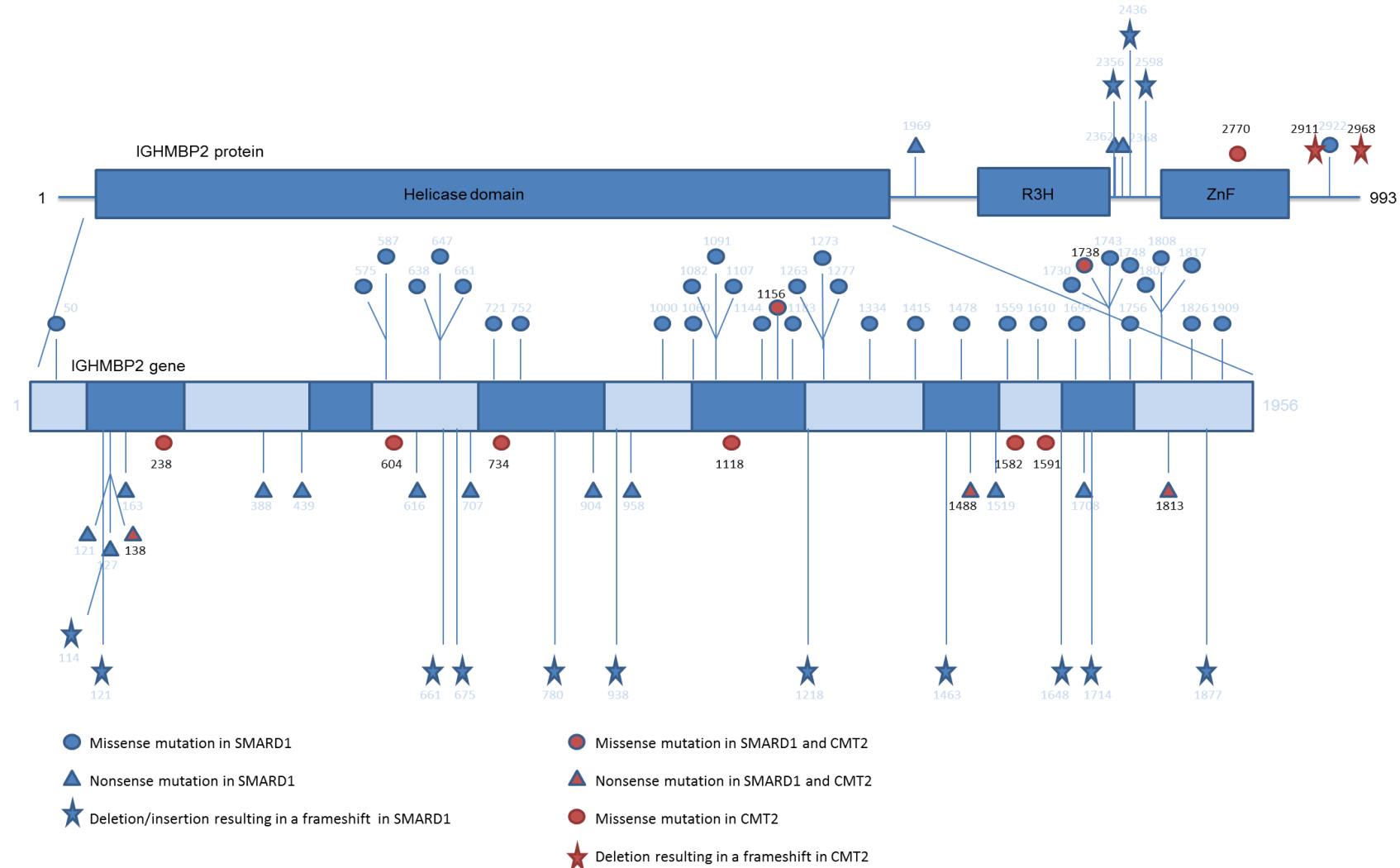


Figure 6-3 Localisation of the newly found mutations in *IGHMBP2* in CMT2 patients in comparison with the already known pathogenic mutations in SMARD1 patients.

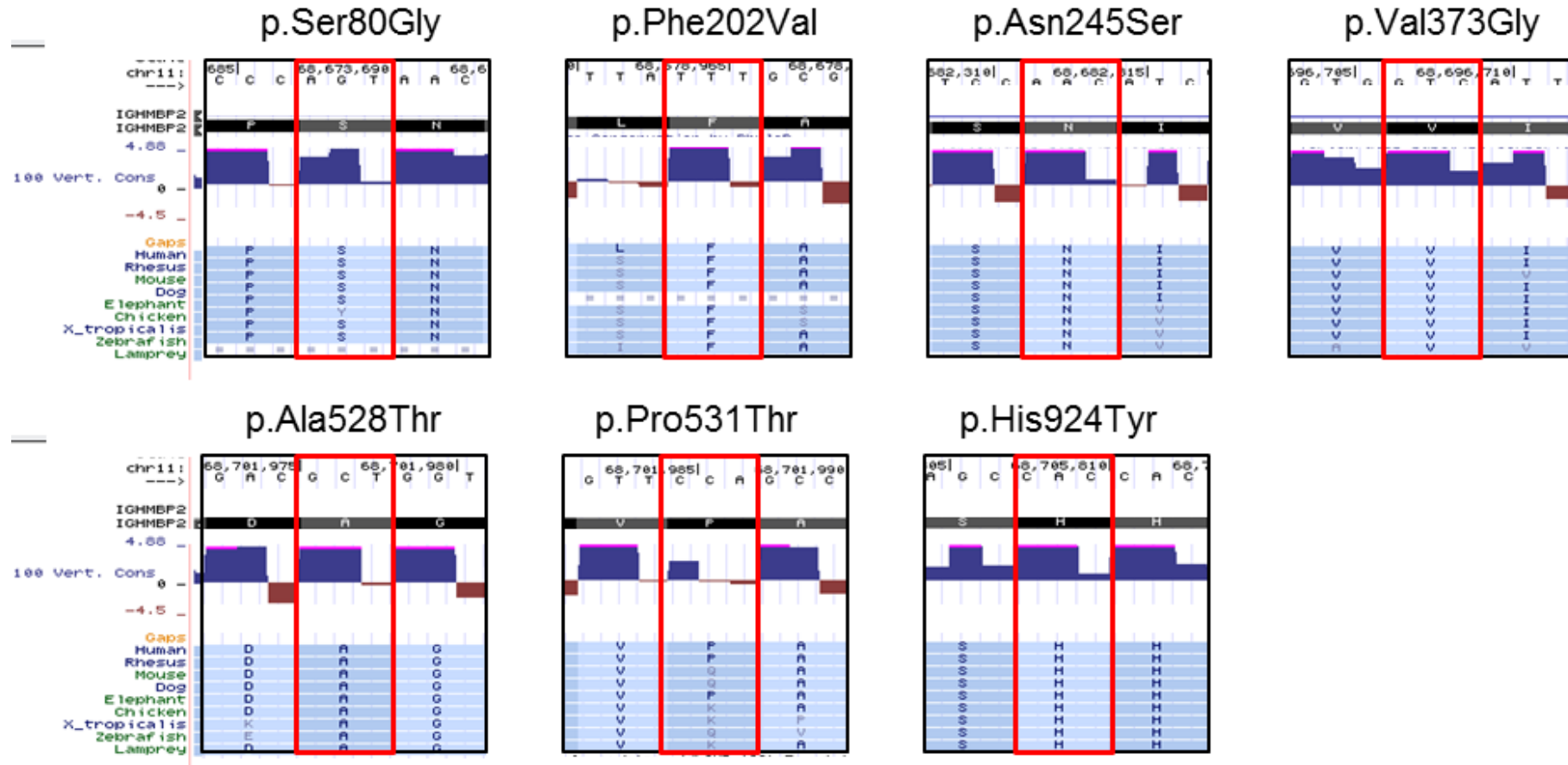


Figure 6-4 Conservation of the novel variants found in *IGHMBP2*. All variants are well conserved over species apart from the p.Pro531Thr variant.

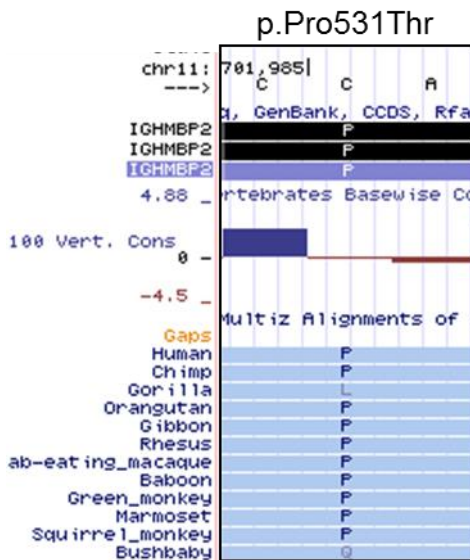


Figure 6-5 Conservation of Proline 531 of *IGHMBP2* in primates.

6.2.6 Localisation of the missense mutations within the structural domains of *IGHMBP2*

Whilst nonsense and frameshift mutations will likely result in the loss of functional protein due to nonsense-mediated decay or truncated proteins, the mechanism of disease for missense mutations in *IGHMBP2* is less clear. Depending on the localisation in the structure, missense mutations could interfere with the function of the protein or result in accumulation of aberrant proteins. Misfolded or mislocalised proteins can interact inappropriately with other cellular factors to cause toxicity. In Family O, the novel p.Phe202Val variant is part of an α -helix in domain 1A, but not central to the protein structure (Fig 6.6 E). In family P, the known severe pathogenic variant p. Val580Ile lies near a β -strand in the core of domain 2A and interacts with Ser539 on a neighbouring strand to stabilise the RecA-like fold. Mutating a valine to a isoleucine, which has a longer side chain, likely disrupts the formation of the β -sheet and hence destabilises domain 2A. The other variant in this family, the novel p.Pro531Thr, lies in a loop region and is exposed to the solvent region on the protein surface. The side chain of the residue does not interact with neighbouring residues and will likely have a milder phenotype (Fig. 6.6 A). Similarly, the novel p.Ser80Gly variant in family Q lies in a loop region of domain 1B but its side chain does not interact with any neighbouring residues (Fig. 6.6 E).

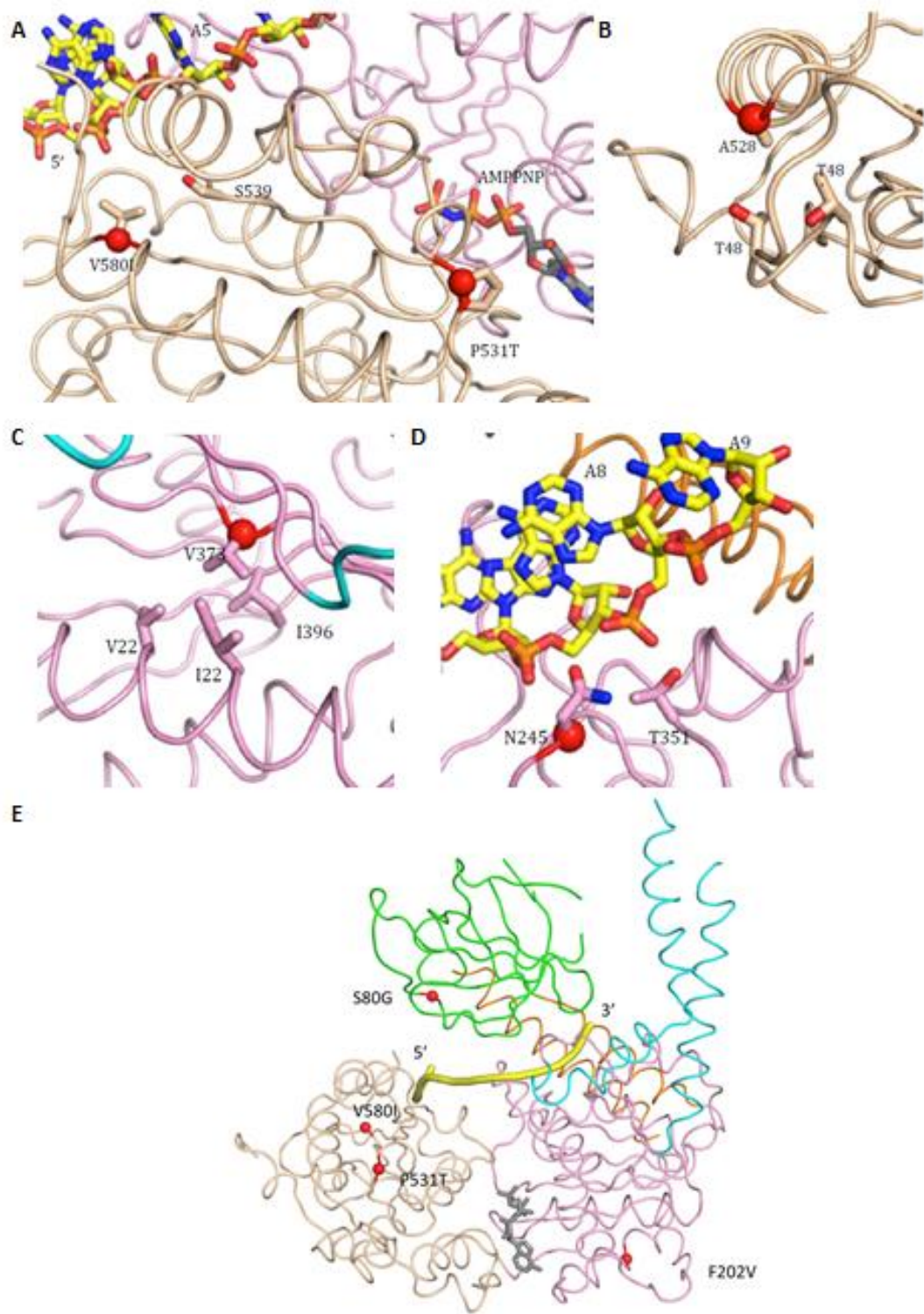


Figure 6-6 Mapping of the missense mutations of families O, P, Q, U, V and W on to the IGHMBP2 structure. All the missense mutations are mapped onto the structure of hIghmbp2-RNA (PDB code: 4B3G) with the C α atoms of the mutated residues shown as red spheres. AMPPNP (in grey) is modelled by superposition of the structure of hIghmbp2-RNA with that of human Upf1 Δ CH-AMPPNP (PDB code:2GJK). The bound ssRNA is shown as yellow tube. (A) Missense mutations in Family P (B and C) Missense mutation in Family U. (D) Missense mutations in Families V and W.(E) Mutations in family O,P and Q.

In family S, a known pathogenic missense variant (p.Trp386Arg) replaces a hydrophobic residue to a positively charged residue, resulting in protein instability due to the loss of some favourable van der Waals contacts with neighbouring hydrophobic residues. The other missense mutations p.Val373Gly and p.Ala528Thr in family U are also predicted to cause protein instability, resulting in loss of functional protein (Fig. 6.6 B and C). Lastly, the only heterozygous mutation in families V, p.Asn245Ser, targets a conserved residue in motif Ia that forms important interactions with the phosphate backbone of RNA. Mutating it to a serine residue could affect the interaction with RNA since the serine side chain is shorter and lacks the amide group (Fig. 6.6 D).

6.2.7 Haplotyping

To investigate the relationship of the three CMT2 families with the p.Cys46Ter mutation (Families M, N and O), five highly polymorphic microsatellite markers closest with respect to the *IGHMBP2* gene were genotyped, the distance between the outer markers measuring 5.5 cM (Table 6.3). Haplotype analysis was performed on the five affected patients and their respective unaffected family members to investigate a common founder. A shared haplotype, spanning 1.2cM (only 2/5 markers) and containing the p.Cys46Ter nonsense mutation, was found in all three families, suggesting families are not closely related. In families M and N, only one marker was shared on the allele with the AG deletion in the last exon. This is the closest marker, located 0.1 cM from the gene.

Microsatellite marker name	Chromosome location	Distance from <i>IGHMBP2</i>
D11S1889	11:67313143-67313325	1.51 cM (1,357,985 bp)
D11S4178	11:68189108-68189359	1.12 cM (481,951 bp)
IGHMBP2	11: 68671310-68708067	0 cM
D11S4113	11:68765634-68765859	0.1 cM (57,567 bp)
D11S4095	11:69268159-69268361	1.09 cM (560,092 bp)
D11S4139	11:70504269-70504461	3.97 cM (1,796,202 bp)

Table 6-3 Polymorphic microsatellite markers used for the haplotyping of the nonsense and frameshift mutations in *IGHMBP2* in families M, N and O. cM = centimorgan

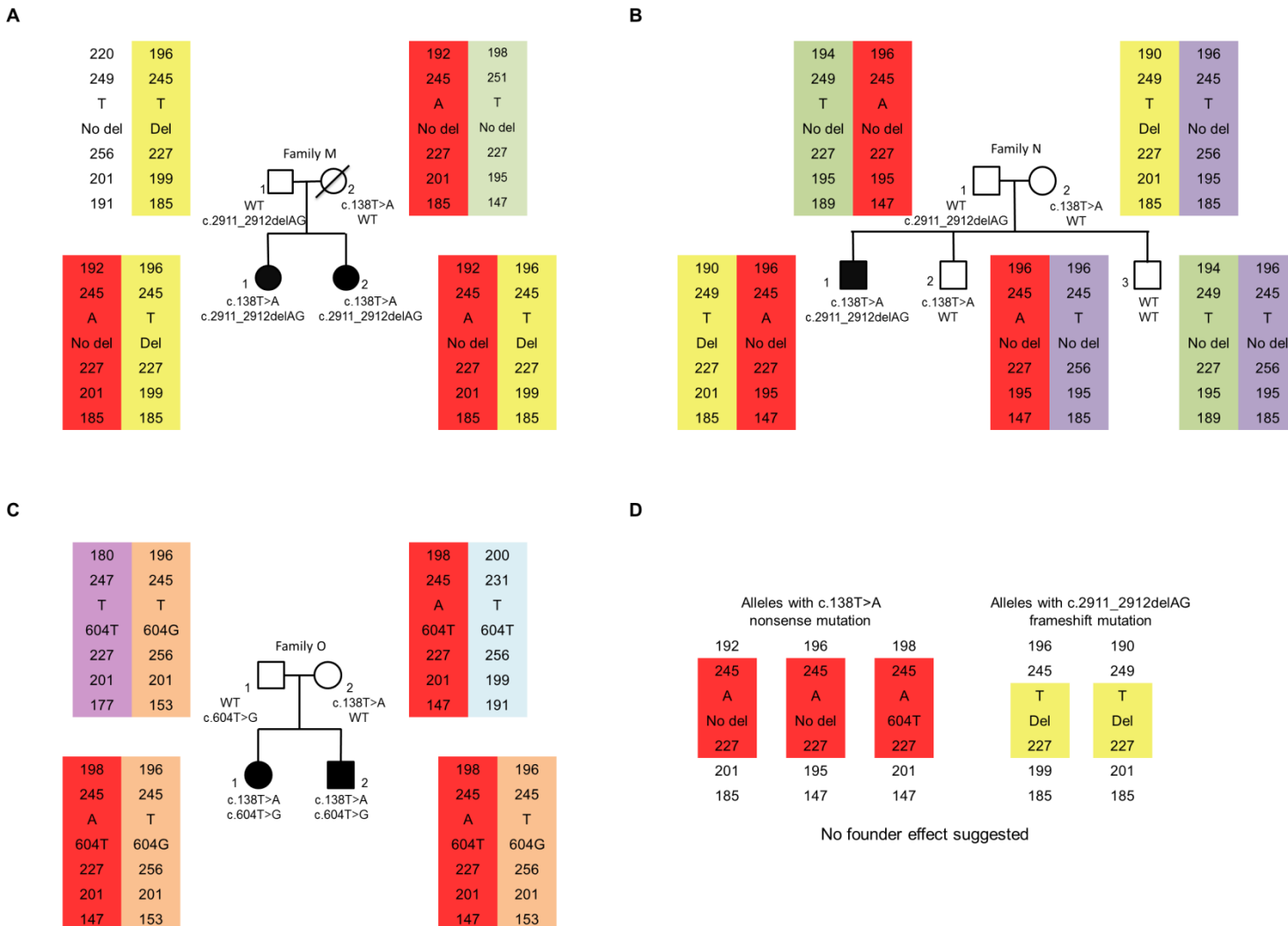


Figure 6-7 Haplotyping results for families M, N and O. (A) Pedigree of family M (B) Pedigree of Family N (C) Pedigree of family O (D) Markers that were shared between the three families for the c.138T>A mutations or the two families for the c.2911_2912delAG.

6.2.8 mRNA analysis of *IGHMBP2* nonsense mutations

The presence of a nonsense-mutation is highly suggestive of nonsense-mediated decay. This was investigated by isolation of the mRNA of patient fibroblast and lymphoblastoid cell lines. Patient and carrier cell lines of families M and N were used to determine whether the p.Cys46Ter nonsense mutation, caused by the transversion of a thymine to an adenine at position 138 of the coding DNA, was still present. Both in fibroblasts and lymphoblastoid cell lines of carriers and patients, the nonsense mutation was still present at the mRNA level, suggesting NMD had not been activated. Since the p.Arg971Glufs*4 frameshift is located in the last exon of the gene, we would not expect nonsense-mediated decay to occur.

To determine whether this lack of NMD is specific for the p.Cys46Ter nonsense mutation, two fibroblasts lines from SMARD1 patients with heterozygous or homozygous frameshift mutations were also investigated. Both the homozygous deletion at position 292 and the heterozygous deletion at position 1632 were still present in the mRNA, suggesting that *IGHMBP2* is somehow protected from NMD, leading to truncated proteins. In collaboration with Professor Horvath at the University of Newcastle, cDNA analysis was also performed to investigate the presence of the nonsense mutation in family W. This showed the stop mutation as hemizygous, suggesting a deletion on the other allele (Fig. 6.8).

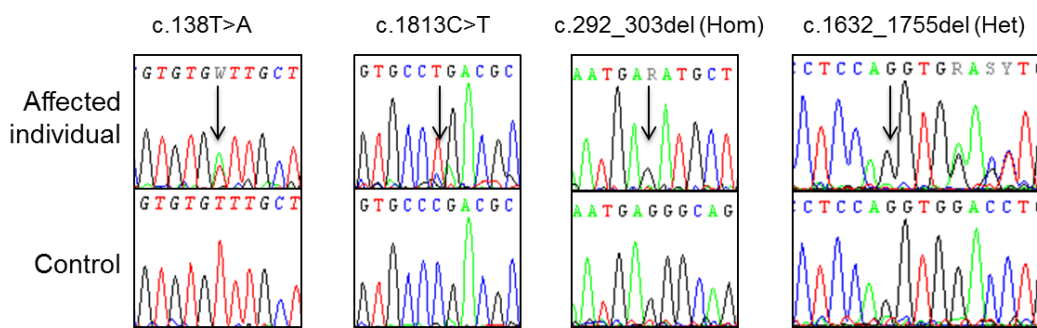


Figure 6-8 Sequence electropherograms of the c.138T>A mutation in the mRNA of lymphoblasts and fibroblasts of CMT2 individuals and carriers, the c.1813C>T mutation in fibroblasts of CMT2 individuals, and frameshift mutations in fibroblasts of SMARD1 individuals. The nonsense mutations are still present in the mRNA of both affected individuals and carriers in comparison with mRNA from a non-mutation control, indicating NMD is not present. The same is observed for the frameshift mutations in the SMARD1 fibroblasts in comparison with mRNA from a non-mutation control, indicating there is no NMD.

6.2.9 Subcellular localisation of IGHMBP2 in patient fibroblasts

Considering nonsense-mediated decay is not activated, nonsense mutations such as p.Cys46Ter will result in shorter, truncated proteins. It was hypothesised these might lead to mislocalisation of the protein or the formation of aggregates. However, immunocytochemistry experiments in selected fibroblasts of a CMT2 patient, carrier and SMARD1 patient showed no significant difference with those from controls (Fig 6.9). In all cell lines the protein is mainly present in the cytoplasm and spread throughout. Actin staining was also performed to look at the overall structure of the cell. The intensity of the fluorescence was not measured, since levels of the protein were established via western blot in the next section (6.2.10).

6.2.10 Protein levels of IGHMBP2 in patient fibroblasts

A previous paper by Guenther et al. in 2008 investigated the levels of the steady-state IGHMBP2 protein in the lymphoblastoid cell lines of three patients with an infantile onset and two patients with juvenile onset at 3.5 or 4.3 years. These were compared with three of their parents, carriers for one heterozygous mutation, and 3 controls. It was observed that infantile onset patients had lower residual levels of the protein than juvenile onset patients and all were significantly lower than controls. Whilst lymphoblastoid cell lines have been shown to reflect the changes of the protein levels in the spinal cord of mice, making it a valuable cell model to study the effects on the protein level in patients, immortalisation can be quite costly and time consuming. As an alternative, patient-derived fibroblast cell lines were initially used to investigate the protein levels in CMT2 and SMARD1 patients in comparison with carriers and controls, to evaluate whether this would be a valid cell type to use.

Fibroblasts were available for families M, N and patients of families O and P. These were compared with three controls, one SMA control with a mutation in *SMN* and three SMARD1 patients (Table 6.4). Due to the generosity of Professor Utz Fisher, the original 481 antibody used in the paper was obtained. However, using different buffers and different running conditions, a working protocol could not be established in the fibroblast cell lines and only resulted in background bands without the observation of a band at the right weight (Fig. 6.10 A). Different cell lines such as lymphoblastoid cell lines were used, since the original experiments were performed in that specific cell type, but no usable results could be acquired (Fig. 6.10 B).

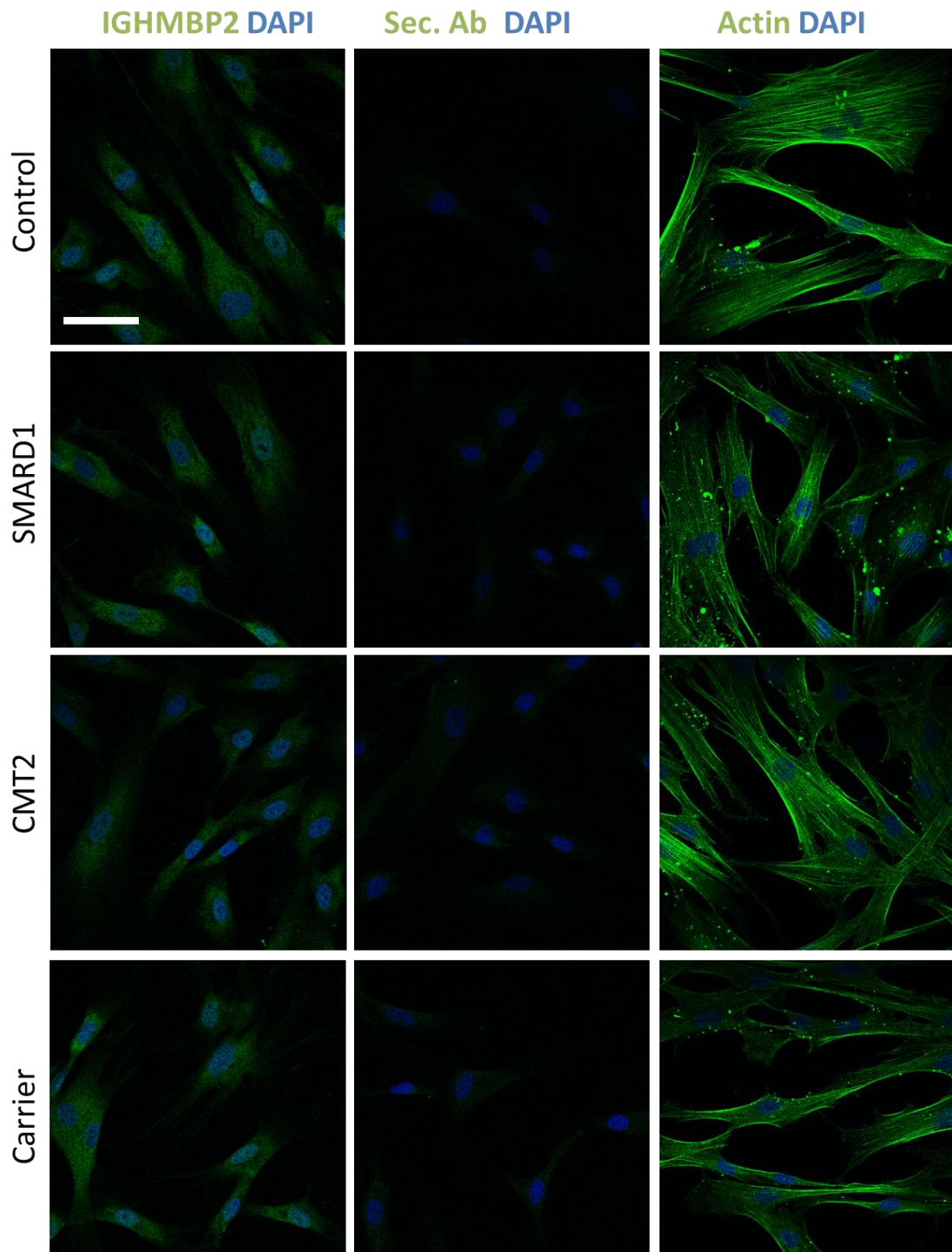


Figure 6-9 Localisation of the IGHMBP2 protein in fibroblasts. Scale bar = 58.00 μ m. Green: IGHMBP2; Blue: 4',6-diamidino-2-phenylindole (DAPI) staining for the nucleus. Green last column: Actin; No difference in clustering of the truncated protein is found between the control and both the affected individuals and the carrier. A negligible background can be observed with the staining with the secondary antibody only. The overall structure of the cells is similar, as indicated by actin. SMARD1 = p.Gly98Fs; CMT2 = p.Cys46Ter + p.Arg971Glufs*4; Carrier = p.Arg971Glufs*4.

Patient	Family no.	Sex/Age	Fibroblasts	LCL	Phenotype	Mutation
1	M	F/41	M. II.1		CMT2	p.Cys46Ter + p.Arg971Glufs*4
2	M	F/38	M. II.2	M. II.2	CMT2	p.Cys46Ter + p.Arg971Glufs*4
3	N	M/23	N. II.1	N. II.1	CMT2	p.Cys46Ter + p.Arg971Glufs*4
4	O	M/14	O. II.1		Severe CMT2	p.Cys46Ter + p.Phe202Val
5	O	F/15	O. II.2		Severe CMT2	p.Cys46Ter + p.Phe202Val
6	P	F/19	P. II.1		CMT2	p.Pro531Thr + p.Val580Ile
Carrier 1	M	M/72	M. I.1	M. I.1	Unaffected carrier	p.Arg971Glufs*4
Carrier 2	N	M/57	N. I.1	N. I.1	Unaffected carrier	p.Cys46Ter
Carrier 3	N	M/21	N. II.2	N. II.2	Unaffected carrier	p.Cys46Ter
Unaffected Sibling	N	M/19	N. II.3	N. II.3	Unaffected	
Carrier 4	N	F/54	N. I.2	N. I.2	Unaffected carrier	p.Arg971Glufs*4
SMARD1 1		<1y	S1		SMARD1	p.Gly98Fs
SMARD1 2		<1y	S2		SMARD1	p.Gln544Fs + p. Arg637Cys
SMARD1 3			S3	S3	SMARD1	p.His213Arg
SMARD1 4				S4	SMARD1	c.2611+1G>T
Control 1		F/54	C1		Unaffected	
Control 2		M/9	C2		Unaffected	
Control 3		F/39	C3		Unaffected	
Control 4		Unknown	C4		SMN1	

Table 6-4 List of all the available fibroblast and lymphoblast cell lines in the IGHMBP2 project.

This urged the use of a commercial available antibody, IGHMBP2, clone mAb11-24 (Millipore), which was tested in different cell lines. This resulted in a much higher quality blot and was used throughout all further western blot experiments (Fig. 6.10 C). Initially only HEK and SY5Y cell lysates showed a clearly distinguishable band, indicating the overall protein content loaded for fibroblast cell lines needed to be heightened, due to low expression in this tissue. Initial experiments were performed in triplicate with nine different fibroblast cell lines and showed a consistent lower steady-state protein level in the SMARD1 patients (0-12%) in comparison with the

CMT2 patients (15-20%) when standardised against 2 controls. This hypothesis was not followed by the SMARD1 fibroblast cell line S3, which was obtained from Dr. Katja Von Au in Germany. However, lymphoblasts of S3 were also available and are studied in a further section, showing negligible amounts of protein. One carrier cell line was available and showed 42% of steady-state protein levels in comparison with controls (Fig. 6.10 D and E). Multiple more fibroblast cell lines were obtained from patients, carriers and controls, leading to a total of 17 fibroblast cell lines. Multiple rounds of optimisation were required before establishing a protocol returning qualitative results.

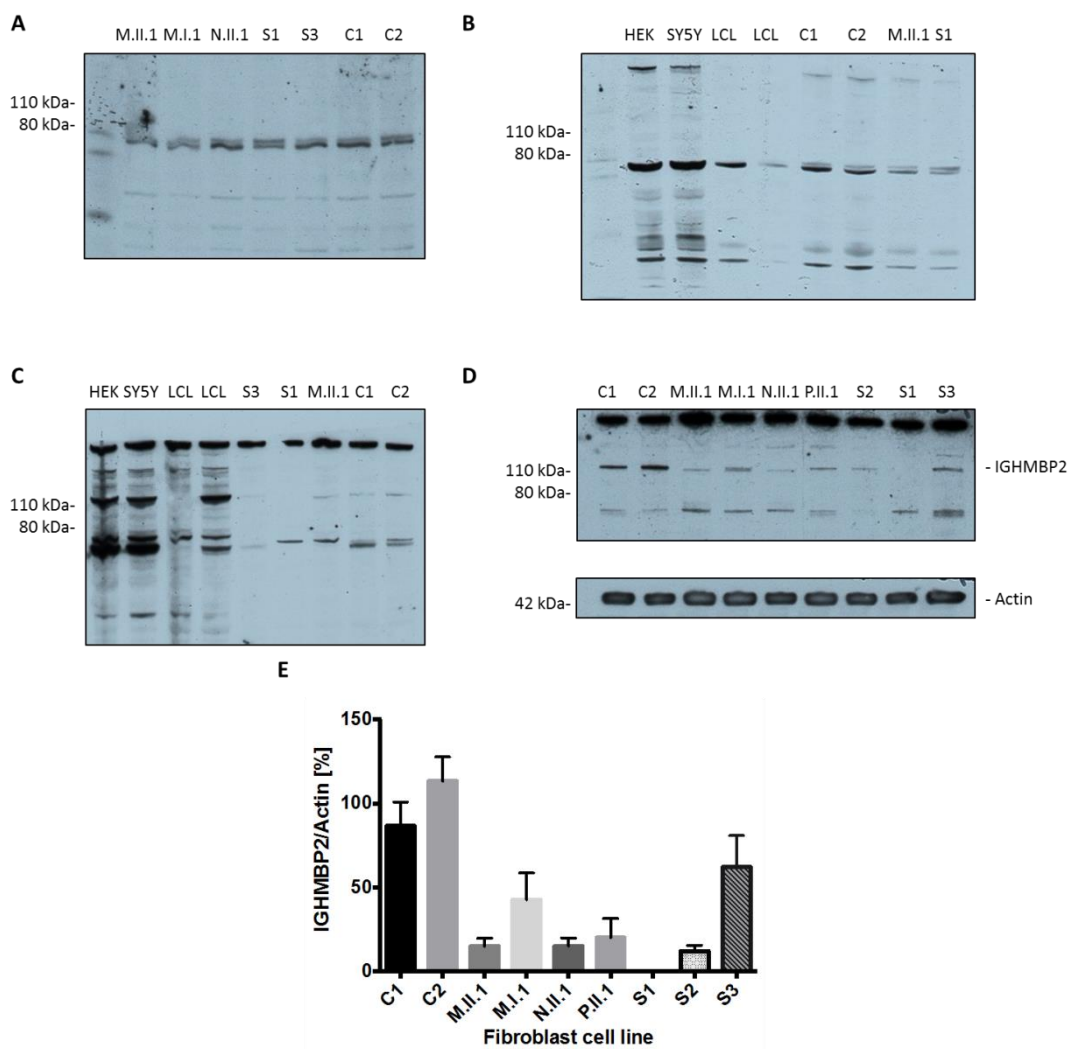


Figure 6-10 Comparison of the different antibodies for IGHMBP2 in different cell types. (A) 481 antibody in fibroblasts (B) 481 antibody in different cell lines (C) mAb11-24 antibody in different cell lines (D) Representative western blot for the triplicate staining of mAb11-24 in fibroblasts (E) Percentages of steady-state protein level in fibroblast cell lines standardised against two controls.

Whilst performing these experiments, a major bacterial infection issue arose in the tissue culture facilities being used. This instigated a severe delay of experiments and untrustworthy results. Cell lysates from infected cell lines were still being used and exhibited similar behaviour as healthy cell lines, with results indicating the same trend as previous experiments. However, results were not used before cell lines were completely eradicated from bacterial infections. Interestingly, when performing western blot on infected cell lines, a different protein pattern could be observed with the Ponceau staining, suggesting this might influence the protein levels of multiple proteins (Fig. 6.11).

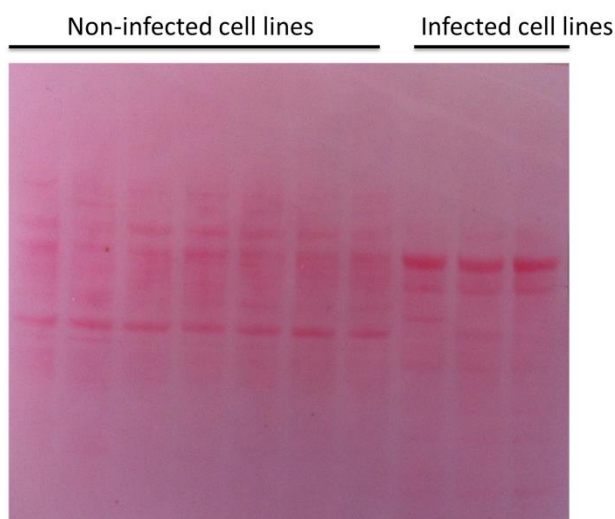


Figure 6-11 Ponceau staining of different fibroblast cell lines during a period of bacterial infections in the tissue culture labs.

Bacterial analysis showed a contamination with the *Achromobacter* bacteria, which had been identified before as a cell culture contaminant (Gray et al., 2010). Even though blast searches excluded the presence of an identical protein sequence that would be recognised by the IGHMBP2 antibody, shorter sequences with an 82% identity can be found in *Achromobacter* bacteria. Together with the uncertainty of the influence of the infection on different pathways in fibroblast cultures, results from potentially affected cell lines were not used for analysis. After taking the appropriate measures against future infections, experiments were repeated in triplicate in cell lines clear from infections. High variability could be observed within the different carriers, and it is noteworthy that those were the main cell lines affected by the bacterial infection (N. I.1; N.I.2; N.II.2; N.II.3). However, a trend

could be observed for lower steady-state protein levels in carriers than controls, but higher than in patients (Fig. 6.12). An example of the variability between different blots can be seen in figure 6.13, where two blots with the same samples, harvested and processed on different days, are depicted. Especially samples C3, C4 and P.II.1 vary on these blots, even though the same amount of whole cell protein content was loaded.

In the three individuals with the combination of the p.Cys4Ter and p.Arg971Glufs*4 variants, an extra band was detected between 70–80 kDa. This band was not detected in any other affected individuals, carriers or controls (Fig. 6.14). With the help of online tools, the molecular weight of the truncated protein resulting from the p.Cys46Ter variant was estimated at 52 kDa, whereas the p.Arg971-Glufs*4 frameshift results in a protein of 109 kDa. In previous experiments by Guenther et al, physicochemical properties of the wild type protein were investigated in comparison with the p.Thr493Ile variant, known to cause SMARD1. Western blot showed a degradation band at 75 kDa that was primarily present in the p.Thr493Ile transfected cells and comprises the N-terminal amino acid residues 1–674. Similar to this variant, the p.Cys46Ter variant or the p.Arg971Glufs*4 frameshift in these individuals could alter the physicochemical properties of the protein and results in a degradation product at 75 kDa. Because neither of the carriers with either the p.Cys46Ter and p.Arg971Glufs*4 variant show a band at this molecular weight, it could be hypothesised that the lower levels of functioning protein in the compound heterozygous individuals activate a feedback mechanism that preserved any residual truncated protein.

During optimisation of the protocol, an incident occurred where two cell lines, kept in a different incubator, were stressed for a period of 48h due to a failure of the incubator that resulted in low CO₂ pressure. Only one of the cell lines survived and protein lysate was run with the same protocol. Results showed a band ~20 kDa higher than the original protein, indicating the stress-response might have had an influence on IGHMBP2 (Fig. 6.15). This was not comparable to the phosphorylation or ubiquitination pattern normally observed in cell lines, where a smear of multiple bands are visible. Unfortunately, further inquiries could not be made due to lack of time after bacterial infections.

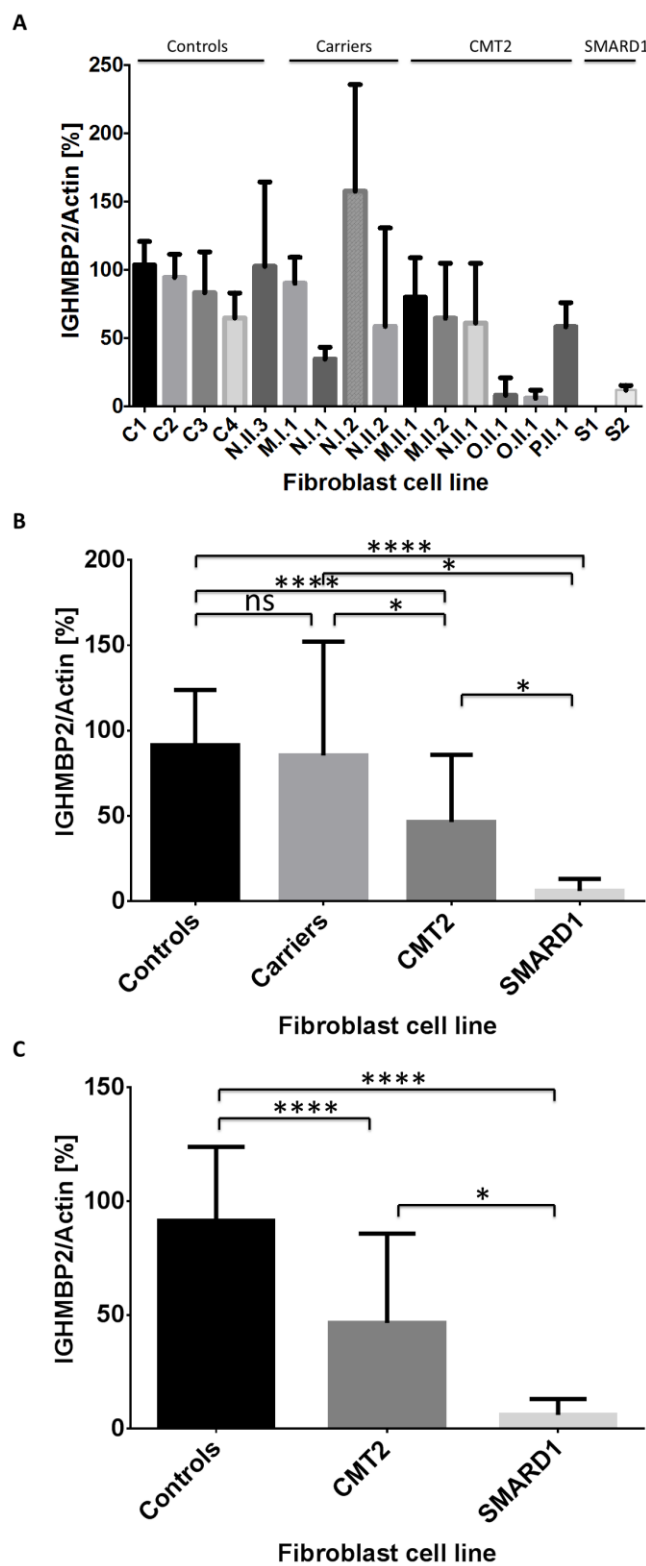


Figure 6-12 Steady-state protein levels of IGHMBP2 in fibroblast cell lines. (A) IGHMBP2 levels in all 17 cell lines. (B) IGHMBP2 levels grouped according to disease status. (C) IGHMBP2 levels compared for the two patient groups against the controls. Statistical significance across groups was analysed using one-way analysis of variance and Bonferroni's post hoc test to compare all data groups.

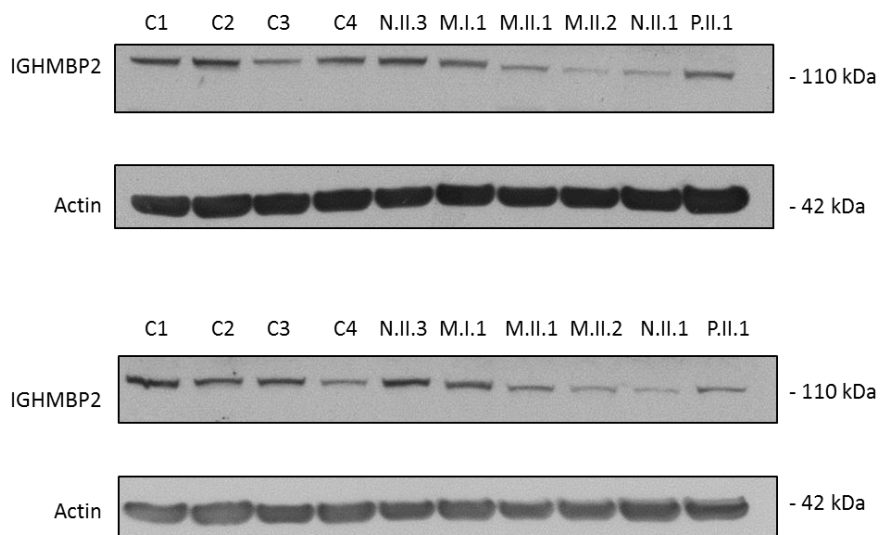


Figure 6-13 Western blot results for 2 sets of identical samples, harvested and processed on different days. Variability in protein levels can be observed in various samples, such as Controls 3 and 4.

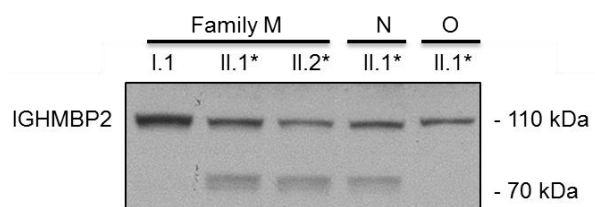


Figure 6-14 Existence of a degradation band around 70–80 kDa in individuals with CMT2 and a combination of the p.Cys46Ter and p.Arg971Glufs*4 mutations.

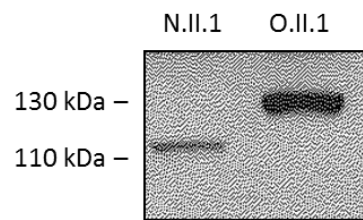


Figure 6-15 Western blot showed the presence of an extra band at ~130 kDa in fibroblasts under stressful conditions.

6.2.11 Protein levels of *IGHMBP2* in lymphoblastoid cell lines

Matching experiments were replicated in nine available lymphoblastoid cell lines, encompassing two CMT2 patients, four carriers, one control and two SMARD1 patients (Table 6.4). Whilst the levels in the carriers were variable, the difference between CMT2 and SMARD1 patients was highly significant, with levels of the SMARD1 patients not being detectable with the technique used, even when higher protein content was loaded (Fig. 6.16). Levels were standardised against one control, resulting in a percentage between 25-50% for CMT2 patients.

6.2.12 *IGHMBP2* expression studies

Expression of *IGHMBP2* was estimated by reverse transcriptase polymerase chain reaction using gene-specific primers against cDNA generated from tissue-specific RNA as compared to the housekeeping gene *GAPDH* in eighteen different body tissues, with moderate expression in fibroblasts and lymphoblastoid cell lines in comparison with the brain and other high-expression level tissues (Fig. 6.17). Within the brain, *IGHMBP2* expression was assessed in 10 regions of the normal human brain, using data from human post-mortem brain tissue from the UK Human Brain Expression Consortium (Trabzuni et al., 2011). The highest expression levels were detected in the cerebellum, followed by the cortex. According to data from the Human Brain Transcriptome (HBT) project, mRNA expression of the *IGHMBP2* gene shows an increase in the cerebellar cortex after birth, whilst other brain regions show a small decrease (Fig. 6.18). However, *IGHMBP2* gene expression levels seem to be constant throughout life in the six brain regions that were assessed in humans during development.

6.2.13 mRNA levels of *IGHMBP2* in fibroblasts

Initial experiments in the paper by Guenther et al. showed slightly elevated levels of *IGHMBP2* mRNA in both infantile and juvenile patients. To investigate whether there were any significant differences between CMT2 patients and carriers/controls, mRNA levels were estimated with the SYBR green method in the original 9 fibroblast cell lines. Both *GAPDH* and *HPRT1* were used as reference genes.

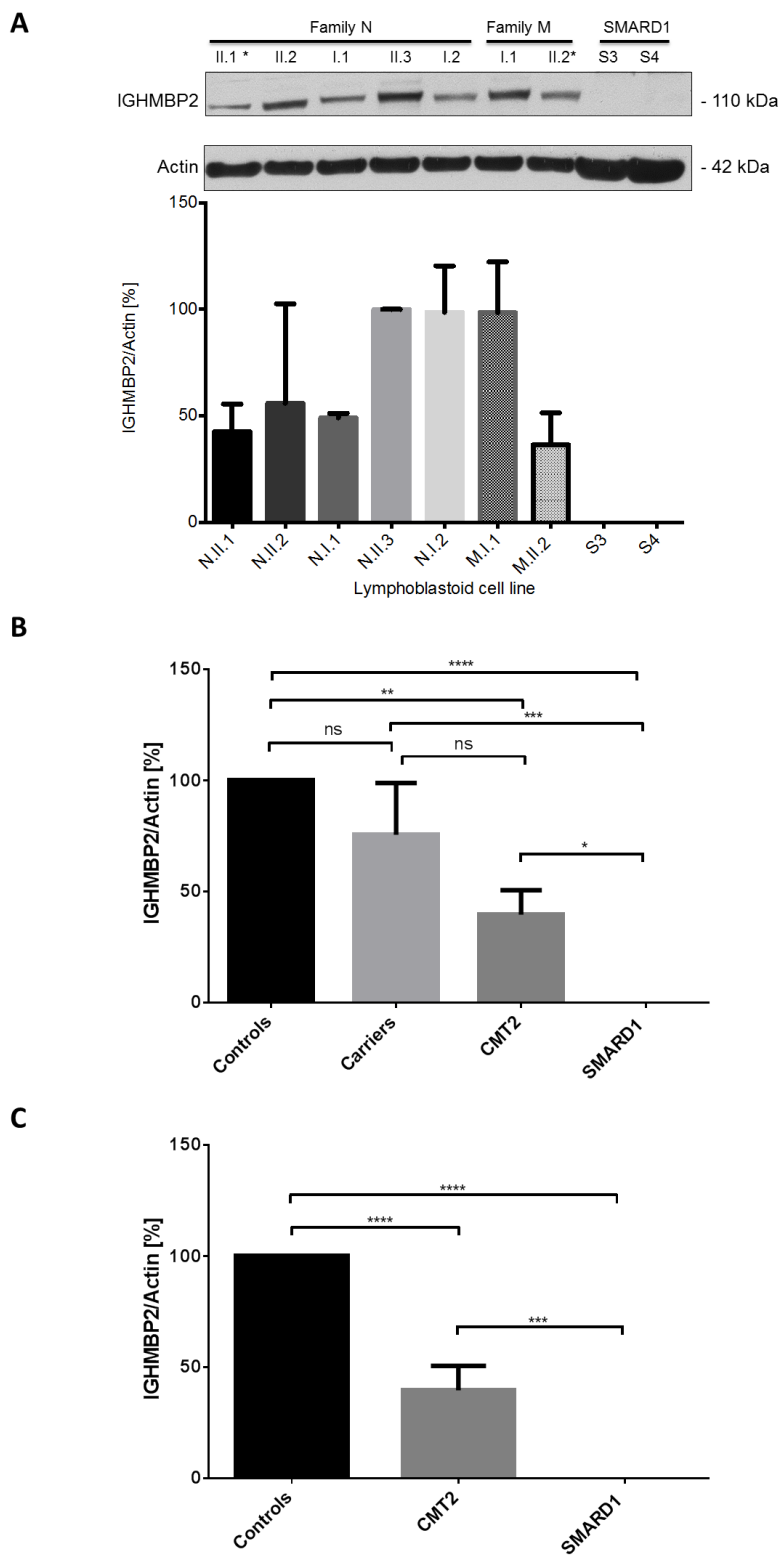


Figure 6-16 Steady-state protein levels in lymphoblastoid cell lines. (A) IGHMBP2 levels in all 9 cell lines. (B) IGHMBP2 levels grouped according to disease status. (C) IGHMBP2 levels compared for the two patient groups against the controls. Statistical significance across groups was analysed using one-way analysis of variance and Bonferroni's post hoc test to compare all data groups. * = Affected individuals with CMT2.

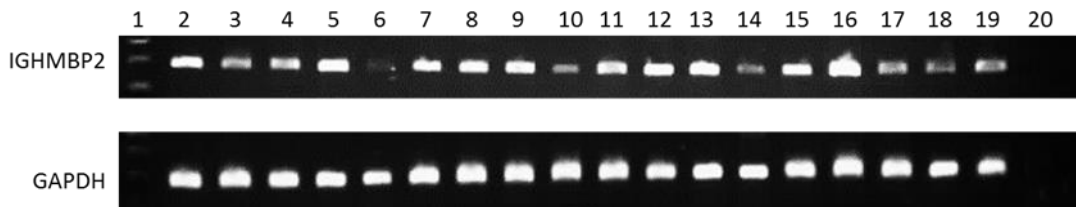


Figure 6-17 Expression of IGHMBP2 (top row) in various human tissues as compared to the housekeeping gene GAPDH (bottom row). Expression of IGHMBP2 is ubiquitous, with a moderate expression in fibroblasts (18) and lymphoblastoid cell lines (19), used in experiments, 1 = ladder; 2 = Thrachea; 3 = Thyroid; 4 = Prostate; 5 = Skeletal muscle; 6 = Spleen; 7 = Small intestine; 8 = Thymus; 9 = Lung; 10 = Placenta; 11 = Kidney; 12 = Adipose tissue; 13 = Brain; 14 = Oesophagus; 15 = Colon; 16 = Heart; 17 = Liver; 18 = Fibroblasts; 19 = Lymphoblastoid cell lines; 20 = no cDNA control. Expression was determined using gene-specific primers against cDNA generated from tissue-specific RNA in the FirstChoice Human Total RNA Survey Panel (Life Technologies, Carlsbad, USA).

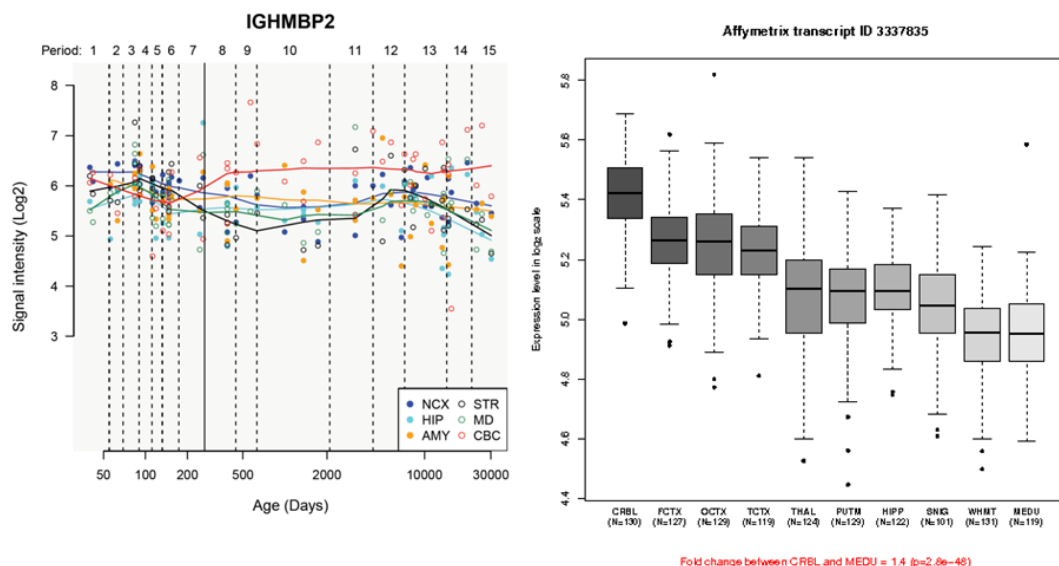


Figure 6-18 mRNA expression levels in different tissues at different stages of life. Left: Data from the Human Brain Transcriptome (HBT) project (<http://hbAtlas.org/>), CBC: the cerebellar cortex, MD: mediodorsal nucleus of the thalamus, STR: striatum, AMY: amygdala, HIP: hippocampus, NCX: 11 areas of the neocortex. Right: Data from the UK Brain Expression Consortium (<http://caprica.genetics.kcl.ac.uk:51519/BRAINEAC/>). Regional brain distribution of *IGHMBP2* mRNA expression in the normal human brain was determined using microarray analysis of human post-mortem brain tissue from the UK Human Brain Expression Consortium (Trabzuni et al, 2011). CRBL: cerebellum, FCTX: frontal cortex, HIPP: hippocampus, MEDU: medulla, OCTX: occipital cortex, PUTM: putamen, SNIG: substantia nigra, TCTX: temporal cortex, THAL: thalamus, WHMT: white matter.

Since the expression levels of *IGHMBP2* are constant throughout life, results from all fibroblast cell lines were compared regardless of age. The $\Delta\Delta Ct$ method was used

to normalise the target amount in the sample against either *HPRT1* or *GAPDH* to make a relative quantification, using the average of the unaffected sibling control fibroblasts as a calibrator in the following formula:

$$\Delta\Delta Ct = (Ct_{\text{target}} - Ct_{\text{reference}})_{\text{calibrator}} - (Ct_{\text{target}} - Ct_{\text{reference}})_{\text{sample}}$$

One pilot study with a limited amount of cell lines was originally performed, to investigate whether viable results could be obtained for larger scale experiments. Unfortunately, bacterial infection delayed the cultivation of the required fibroblasts so significantly that the experiments could not be performed again in triplicate. Results were variable when comparing the two reference genes but a trend could be seen towards a higher level of mRNA expression in the SMARD1 in comparison with the CMT2 patient fibroblasts. Apart from patient M.II.1, all patients had elevated levels of mRNA in comparison with controls, as previously indicated in the paper by Guenther et al (Fig. 6.19).

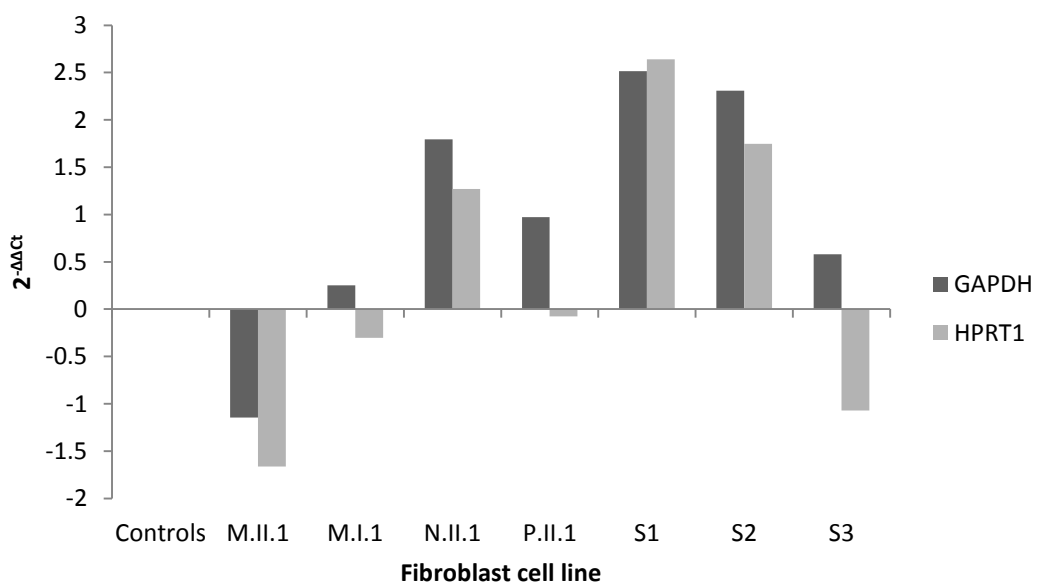


Figure 6-19 mRNA expression levels of *IGHMBP2* in fibroblast cell lines. The $\Delta\Delta Ct$ method was used to normalise the target amount in the sample against either *HPRT1* or *GAPDH*. Apart from patient M.II.1, all patients had elevated levels of mRNA in comparison with controls.

6.2.14 mRNA levels of *IGHMBP2* in lymphoblasts

Matching experiments were performed in all available lymphoblastoid cell lines and repeated three times for both *HPRT1* and *GAPDH*. Experiments were originally performed on a Corbett Rotor-gene machine, but had to be completed on the Stratagene/Agilent MX3000P due to problems with the sealing function of the machine. High variation was found in between the repeated runs, as shown by the error bars, and no significant difference was found between controls, carriers, CMT2 or SMARD1 patients (Fig. 6.20). No further investigations were made, due to lack of time.

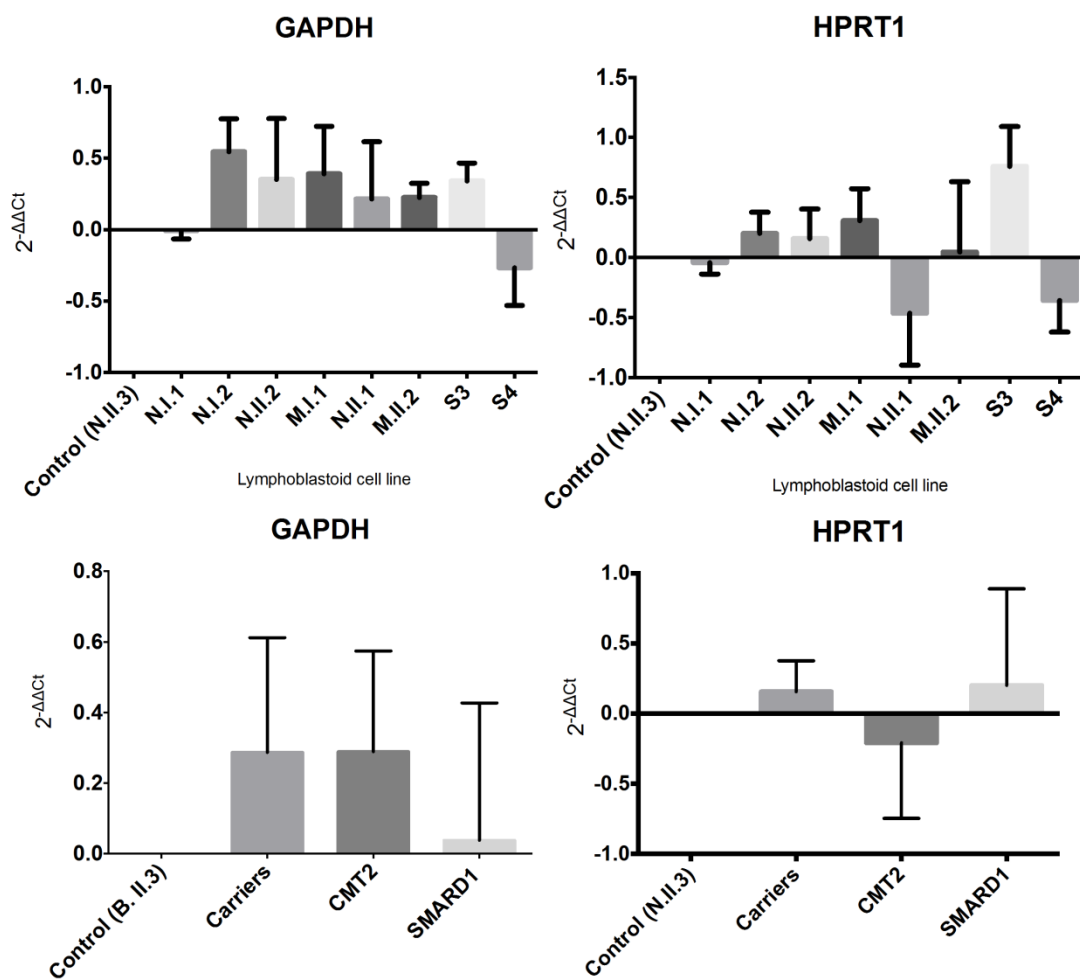


Figure 6.20 mRNA expression levels of *IGHMBP2* in lymphoblastoid cell lines. The $\Delta\Delta Ct$ method was used to normalise the target amount in the sample against either *HPRT1* or *GAPDH*. No significant difference was found between controls, carriers, CMT2 or SMARD1 patients

6.2.15 Co-immunoprecipitation of IGHMBP2 with proteins implicated in Amyotrophic lateral sclerosis

Since SMARD1 and SMA1 have similar phenotypes, research had already been performed to investigate whether IGHMBP2 interacts with SMN or other components of the SMN complex (de Planell-Saquer et al., 2009). However, none of these proteins co-immunoprecipitated with IGHMBP2, suggesting it does not associate with the SMN complex. Given the clinical relevance between patients with motor neuron diseases such as SMARD1 and Amyotrophic Lateral Sclerosis (ALS), co-immunoprecipitation was performed to investigate interactions between IGHMBP2 and proteins mutated in ALS, such as Tar DNA-Binding protein, 43-KDa (TDP-43), Superoxide dismutase 1 (SOD1) or Fused in Sarcoma (FUS). No interaction was found for either SOD1 or FUS (Fig. 6.21), but co-immunoprecipitation results showed an interaction between IGHMBP2 and TDP-43, repeated in triplicate (Fig. 6.22). This is a novel, RNA-independent interaction. To examine whether the interaction of TDP-43 with IGHMBP2 might be involved in the pathomechanism of disease, constructs were made for the following missense mutations: p.Ser80Gly, p.Phe202Val, p.Pro531Thr and p.Val580Ile. All of these are novel, except for p.Val580Ile, which has been found as a pathogenic mutation in SMARD1 patients.

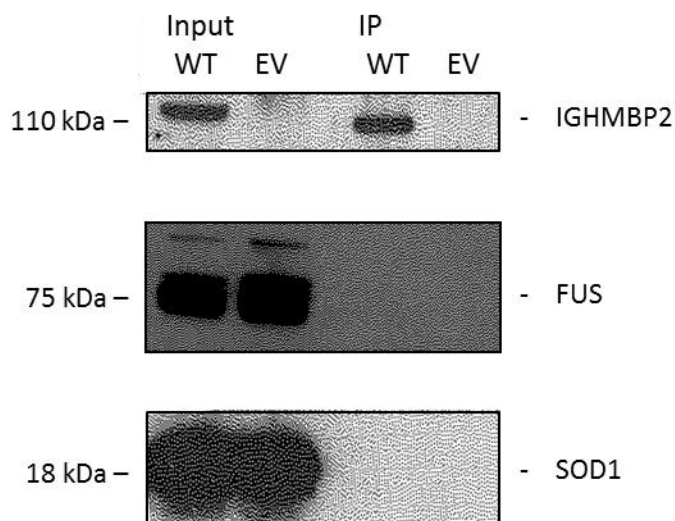


Figure 6-21 Co-immunoprecipitation experiments carried out in HEK293-T cells transfected with wild type construct of *IGHMBP2* show no interaction between IGHMBP2 and FUS or SOD1. IP = Immunoprecipitation.

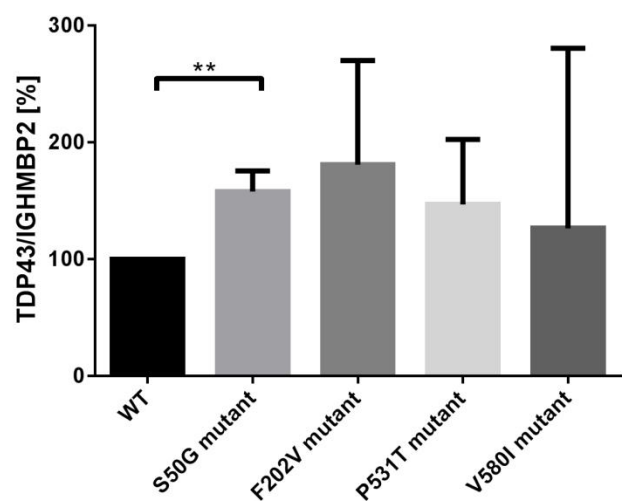
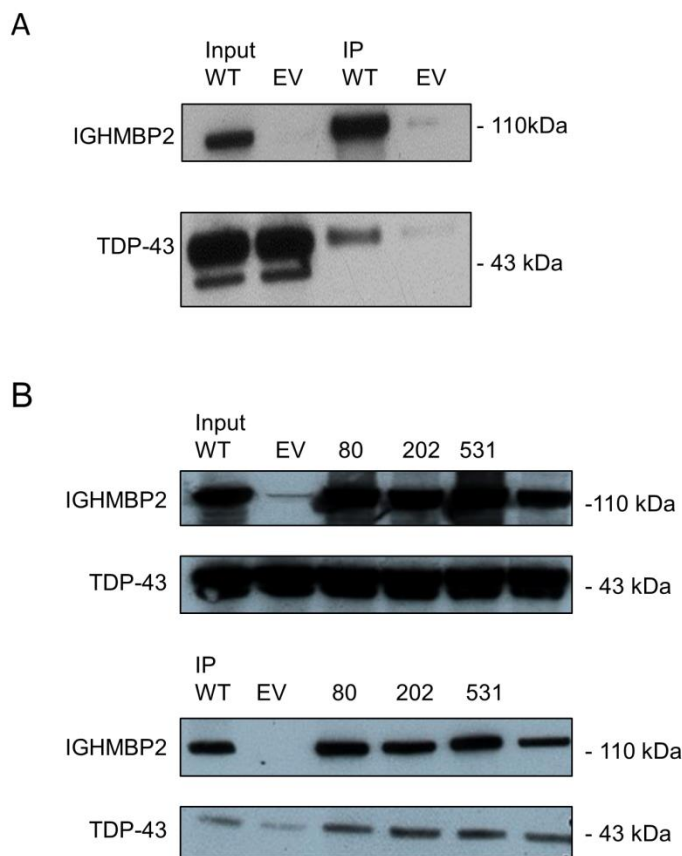


Figure 6-22 Co-immunoprecipitation experiments carried out in HEK293-T cells transfected with wild type or mutated construct of *IGHMBP2* show that TDP43 interacts with IGHMBP2. (A) Wild type and empty vector Co-IP shows an RNA-independent interaction with TDP43, (B-C) A significant stronger interaction can be observed in HEK293T cells transfected with the S80G mutant. Other mutants show a trend towards higher interaction, which was not significant. $n = 3$, ** $p < 0.01$, IP = Immunoprecipitation. Statistical analysis was performed with the unpaired t-test.

Whilst the results for the latter were variable, potentially due to the sensitivity of the technique, a trend was shown towards a greater interaction in all mutant constructs as compared to wild type. This reached significance level for the S80G mutation, with a p-value below 0.01 with the unpaired t-test. This implicates TDP-43 in the pathogenesis of *IGHMBP2* mutations, but a larger number of mutations are required to be investigated. This could not be explored in further depth due to lack of time resulting from the ongoing bacterial infections.

6.2.16 Subcellular localisation of TDP43

It is well known that cytoplasmic inclusions containing hyperphosphorylated and ubiquitinated TDP-43 are a pathological hallmark of ALS. This has both been shown in spinal cord and motor neurons of patients, the primary tissues of disease in SMARD1. Spinal cord tissue was available for one SMARD1 patient and TDP43 staining was performed, but no abnormalities could be seen on the anterior horn cells of the spinal cord (Fig. 6.23). Further investigation regarding the localisation of TDP-43 in fibroblasts of patients with CMT2 and SMARD1 was implemented, however, no differences could be observed between CMT2 or SMARD1 patients in comparison with carriers or controls (Fig. 6.24).

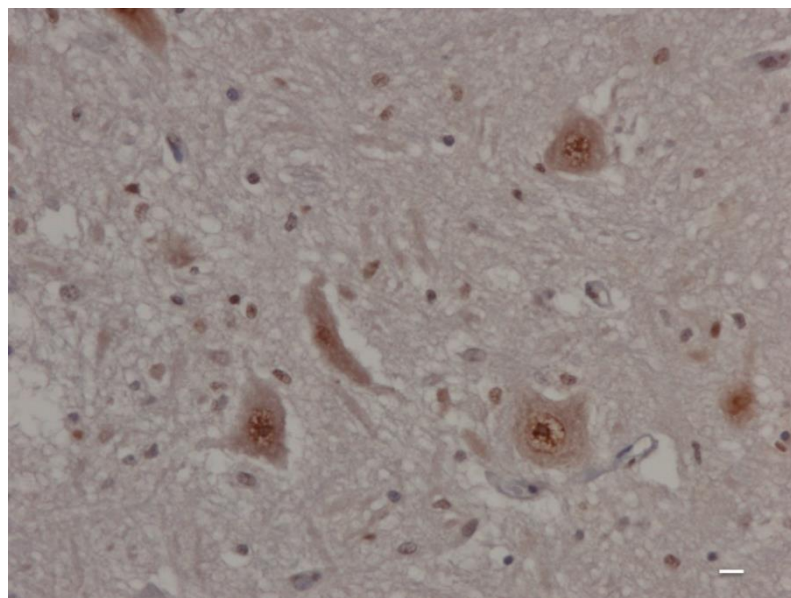


Figure 6-23 Immunostaining of TDP43 in the anterior horn cells of the spinal cord of a SMARD1 patient with mutations in *IGHMBP2*. No abnormalities could be seen. Scale = 10 μ m.

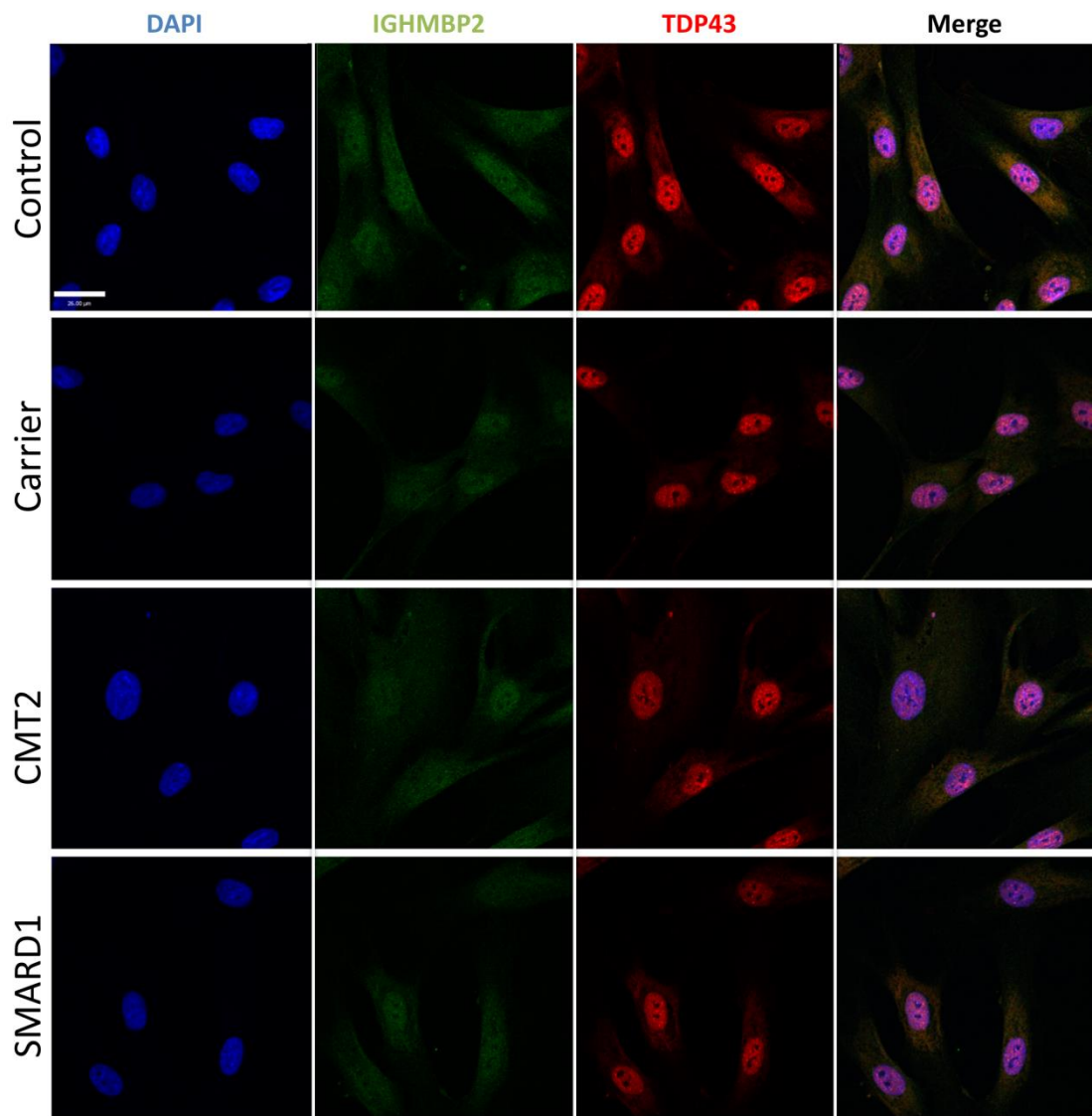


Figure 6-24 Localisation of TDP43 and colocalisation of IGHMBP2 and TDP43 in human fibroblasts. No significant difference in localisation or clustering is found between the control and both the affected individuals and the carrier for TDP43. Green: IGHMBP2; Red: TDP43; Blue: 4',6-diamidino-2-phenylindole (DAPI) staining for the nucleus. SMARD1= p.Gly98Fs; CMT2 = p.Cys46Ter + p.Arg971Glufs*4; Carrier = p.Arg971Glufs*4.

6.2.17 Colocalisation of IGHMBP2 with TDP43

To estimate the colocalisation of IGHMBP2 and TDP43, the global Pearson's correlation coefficient was calculated with the Volocity program for the different fibroblast cell lines. Whilst the difference is significant between SMARD1 and the controls, no significant difference could be found between the CMT2 and SMARD1 fibroblasts (Fig. 6.24-25).

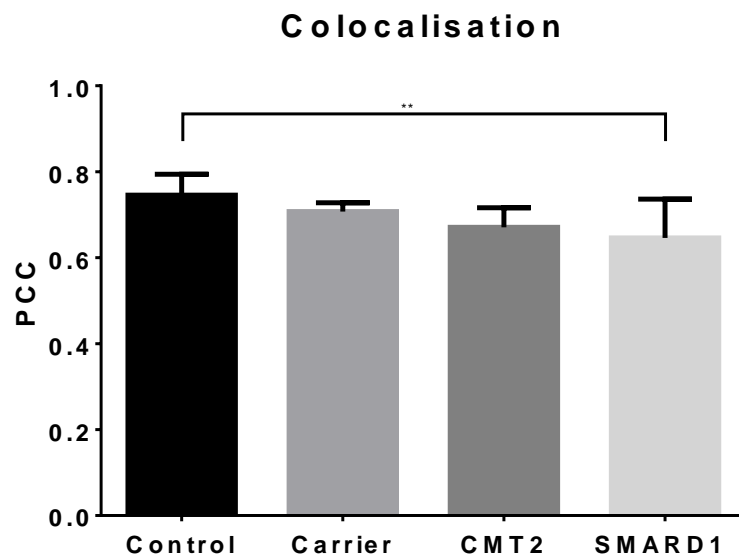


Figure 6-25 Pierson's correlation coefficient for the colocalisation of IGHMBP2 and TDP43 in different human fibroblast cell lines. Difference is significant between SMARD1 and controls, but not significant between the CMT2 and SMARD1 fibroblasts

6.2.18 Co-immunoprecipitation of IGHMBP2 with proteins implicated in CMT

Considering the novelty of IGHMBP2 in the pathogenesis of CMT, co-immunoprecipitation experiments were performed to investigate whether a link could be established with one of the already known genes in CMT. The genetic background plays an important role in the classification of the disease and is crucial to find common pathways to explain the characteristic features seen in most patients. Recently, a new gene called LAS1-like (*LASIL*) was discovered to cause a phenotype of congenital motor neuron disease with early demise due to respiratory insufficiency, showing clinical overlap with SMARD1 (Butterfield et al., 2014). *LASIL* has been implied in ribosome biogenesis, similar to IGHMBP2. Equally, due to the predominantly distal involvement in the CMT2 and SMARD1 patients, interaction with HSP27 was considered.

Lastly, since HINT1 has been shown to interact with the helicases reptin and pontin, which form a complex with IGHMBP2, it was investigated whether a direct interaction was also present. However, none of these proteins co-immunoprecipitated with the IGHMBP2 protein and so far, no direct interactions between IGHMBP2 and any other CMT2 proteins have been reported (Fig. 6.26).

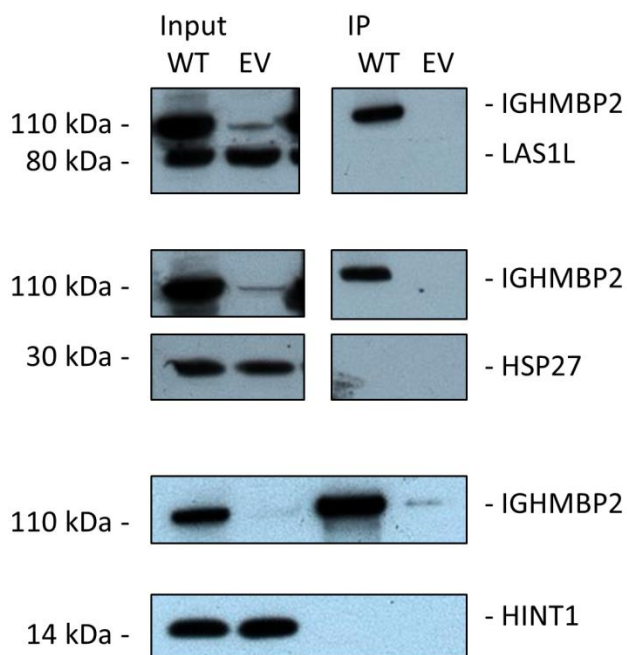


Figure 6-26 Co-immunoprecipitation experiments carried out in HEK293-T cells transfected with wild type construct of *IGHMBP2* show no interaction between *IGHMBP2* and selected proteins involved in CMT2. IP = Immunoprecipitation.

6.2.19 Visualisation of *IGHMBP2* in the CMT2 protein network

With the use of the GeneMANIA prediction server 21 (Warde-Farley et al., 2010), the presence of a network of interacting proteins known in CMT2 with *IGHMBP2* can be observed (Fig. 6.27). No direct interactions or other sorts of associations are known with any CMT2 proteins so far, but further research might elucidate additional pathways linking *IGHMBP2* to one of the already known CMT2 proteins.

6.2.20 ATPase activity of the *IGHMBP2* protein in transfected HEK cells

Not only has it been shown that mutations in *IGHMBP2* can result in severely reduced steady-state protein levels in SMARD1 patients, pathogenic mutants of *IGHMBP2* have also been tested for their enzymatic activities, such as ATPase activity and the unwinding activity. All mutations residing in or close to conserved motifs within the helicase domain resulted in an impaired enzymatic activity (Guenther et al., 2009).

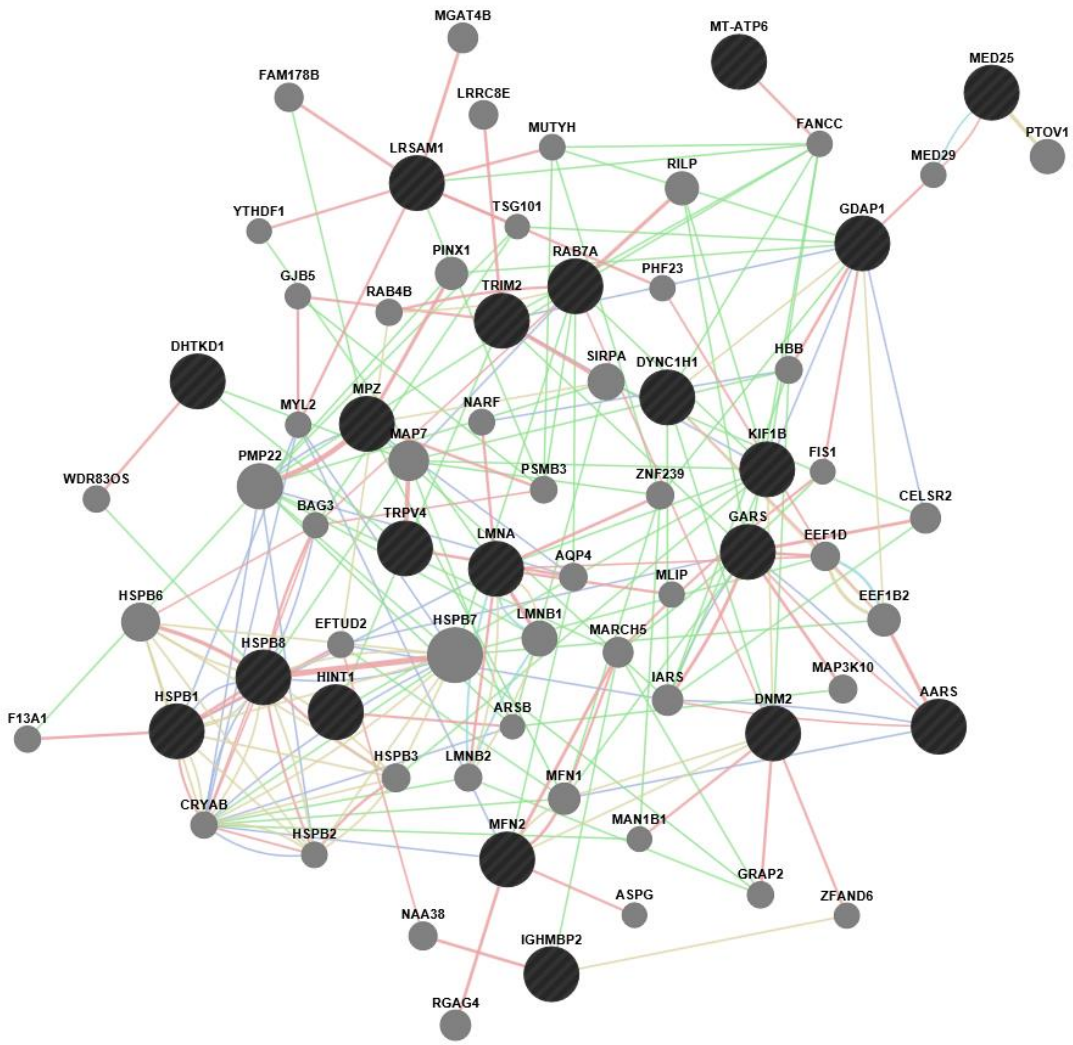


Figure 6-27 Protein network of CMT2 proteins and IGHMBP2. Different colours of lines indicate the nature of the interaction. Purple: Co-expression; Orange: Predicted; Red: Physical interactions; Green: Genetic interaction; Grey: Shared protein domains. Abbreviations for proteins can be found in Chapter 1.

One mutation, p.Thr493Ile, was not located within these domains and showed unaltered enzymatic activity. This mutation was studied previously and showed lower steady-state levels in both infantile and juvenile onset patients (Guenther et al., 2008). It was concluded that loss of enzymatic activity contributes to the pathological basis of SMARD1 and patients with a more favourable outcome retained residual catalytic activity (Eckart et al., 2011). This observation could be an explanation for the less severe phenotype of CMT2 patients with *IGHMBP2* mutations. Multiple constructs were available, but a pilot study was implemented with the wild type construct and the construct with a p.Val580Ile mutation, which has been shown to affect the activity of the protein and acted as a positive control.

Purification of the protein was accomplished by immunoprecipitation with Anti-FLAG beads. A negative untransfected control was used and coomassie blue staining and western blot were performed on IP samples to confirm purification. Different elution protocols were used to optimise the protocol. On the first attempt, only one 15 cm² dish was used and IPs were washed with a combination of 5 different washing buffers (20 mM Tris, 500-150 mM NaCl, 1-0.02% Triton X-100), decreasing in NaCl and Triton X-100 concentration. 3x Flag peptide (Sigma-Aldrich) was used to elute bound protein. However, this resulted in a complete loss of protein, most likely due to the amount of washes. Further experiments were performed with different combinations of NP40⁺ Lysis buffer without EDTA and washing buffers (Table 6.5). 3x Flag peptide (Sigma-Aldrich) was used to elute bound protein. Samples of both the eluate and the used beads were separated on a gel and stained with Coomassie blue, using different exposure settings to scan the results (Fig. 6.28). Due to the presence of background bands in condition 3 + 4, it was decided to use condition 2 for further experiments and to scale up to 3x 15 cm² dishes. These showed an enhanced purification of IGHMBP2 for the wild type construct (Fig. 6.29).

Condition	Lysis buffer	Washing buffer
1	NP40 ⁺ w/o EDTA	5 washing buffers (20 mM Tris, 500-150 mM NaCl, 1-0.02% Triton X-100)
2	NP40 ⁺ w/o EDTA	6 washes with 25 mM Tris pH 7.5, 400 mM NaCl, 1% Triton X-100
3	NP40 ⁺ w/o EDTA	6 washes with NP40 ⁺ w/o EDTA
4	NP40 ⁺	6 washes with NP40 ⁺ w/o EDTA

Table 6-5 Different buffers used for the optimisation of IGHMBP2 purification.

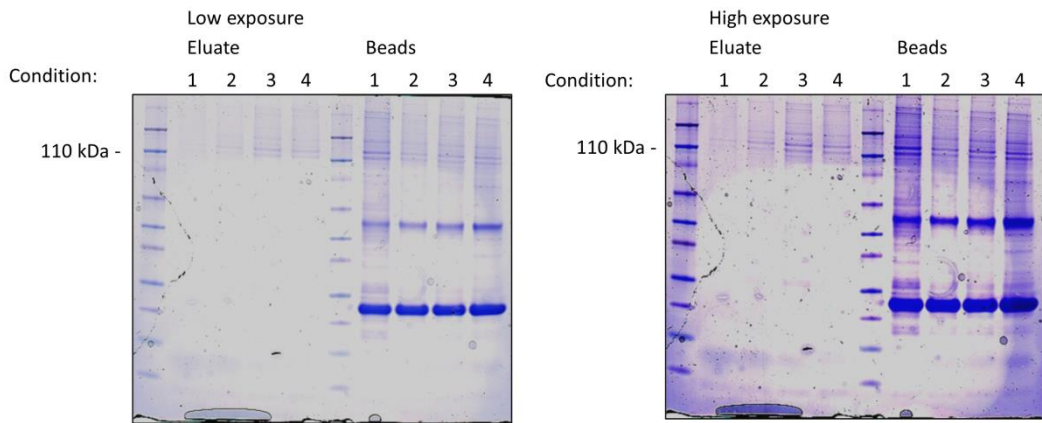


Figure 6-28 Coomassie blue staining of the different conditions for the optimisation of IGHMBP2 purification. Due to the presence of background bands in condition 3 + 4, it was decided to use condition 2 for further experiments and to scale up to 3x 15 cm² dishes.

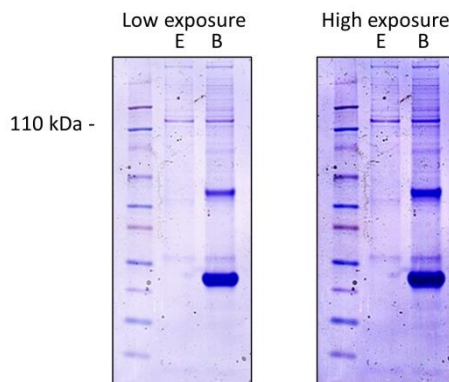


Figure 6-29 Purification of wild type-IGHMBP2 with condition 2 and 3x 15 cm² dishes. E = Eluate; B = Beads.

The same protocol was used for both the wild type, empty vector and the construct with the p.Val580Ile mutation for the ATPase assay. However, no difference could be observed between the wild type and the mutant transfected cells. The coomassie blue staining showed one extra band in all cell lines (even the empty vector), suggesting the protein was not optimally purified and other proteins are still present in the eluate. A new combination of 3 different washing buffers (20 mM Tris, 1000-200 mM NaCl, 1% triton X-100) was tried to improve the purification of the eluate in different orders, showing optimal results for condition 7 (Table 6.6 – Fig 6.30).

Condition	Buffer order
5	1-3-1-3-1-3
6	2-3-2-3-2-3
7	1-1-2-2-3-3

Buffer 1 1000 mM NaCl
 Buffer 2 400 mM NaCl
 Buffer 3 200 mM NaCl

Table 6-6 Order of different buffers used for further optimisation of IGHMBP2 purification.

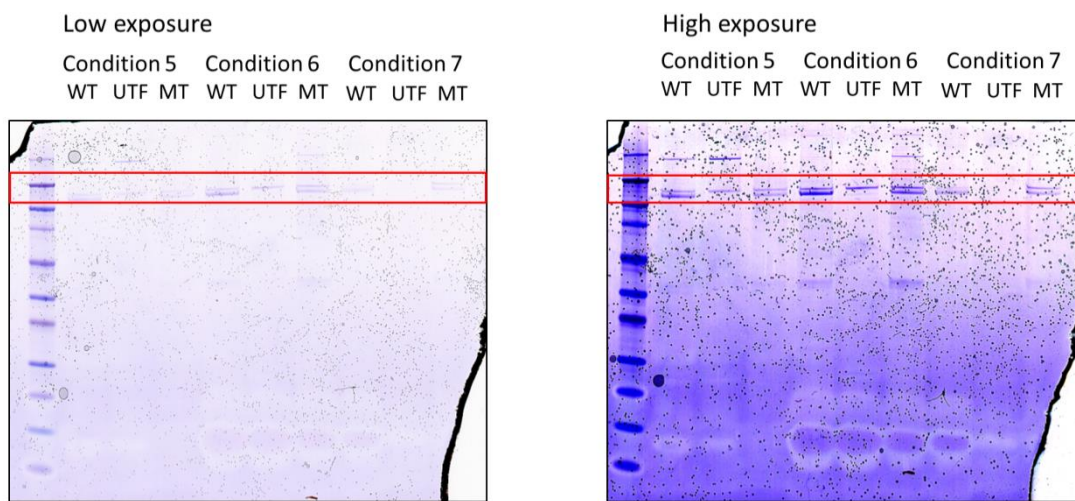


Figure 6-30 Coomassie Blue staining for the different conditions used for further IGHMBP2 purification with conditions 5,6 and 7. Condition 7 was used for further experiments. WT = Wild type; UTF = Untransfected; MT = Mutant

Coomassie blue staining showed a protein band at the expected 110 kDa in both wild type and positive control. However, when performing the ATPase assay, no hydrolysis could be observed in none of the three samples (Fig. 6.31). An extra band was still observed in all three lysates, but as this band is not present on the western blot staining for IGHMBP2, it is unlikely to be the targeted protein and is probable background. Elimination of this band with the use of various eluting conditions was not successful. Whilst purification is necessary to isolate the ATPase activity of IGHMBP2, background can be tolerated if no enzymes with ATPase activity are present. Additional to these three lysates, calf intestine alkaline phosphatase (CIP) enzyme was used as a positive control for buffer conditions of the assay. CIP was used in duplicate, once in the buffer accompanying the enzyme, once in the buffer used for the IGHMBP2 lysates. In both conditions, CIP hydrolyses ATP to ADP.

However, with the same conditions, no ATPase activity could be seen in the IGHMBP2 lysates (Fig 6.32).

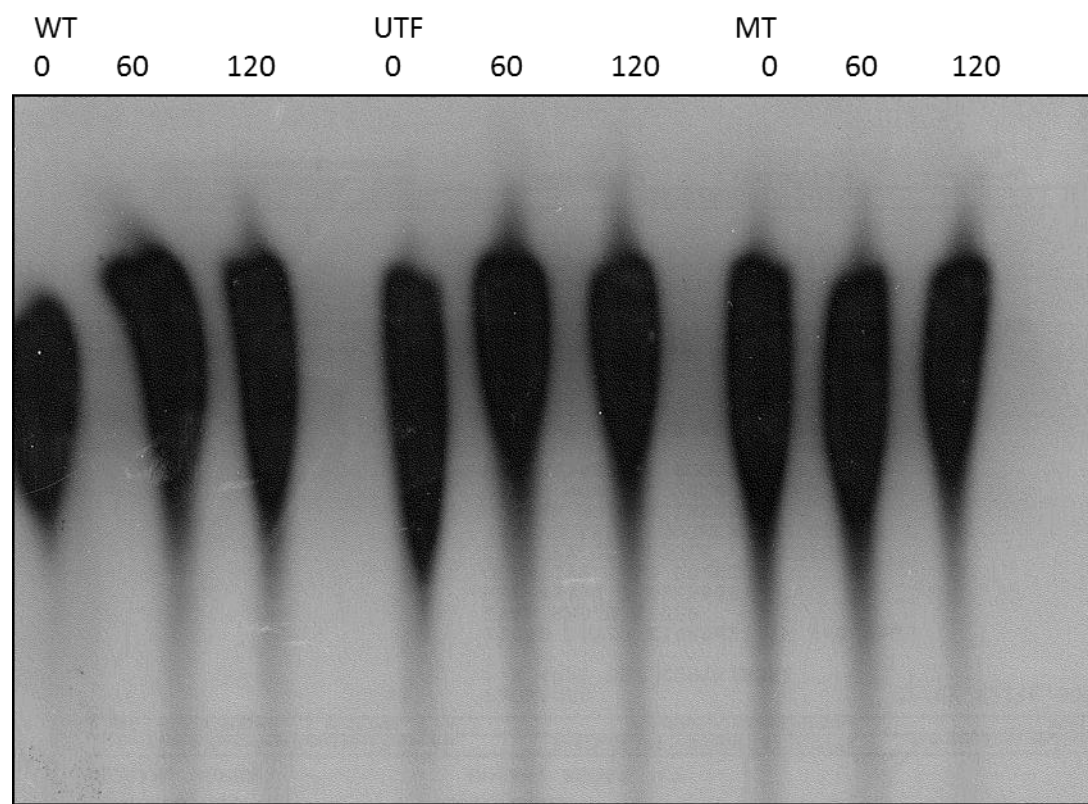


Figure 6-31 ATPase assay for different construct of IGHMBP2. No hydrolysis could be observed in any of the samples. WT= Wild type; UTF = Untransfected; MT = Mutant.

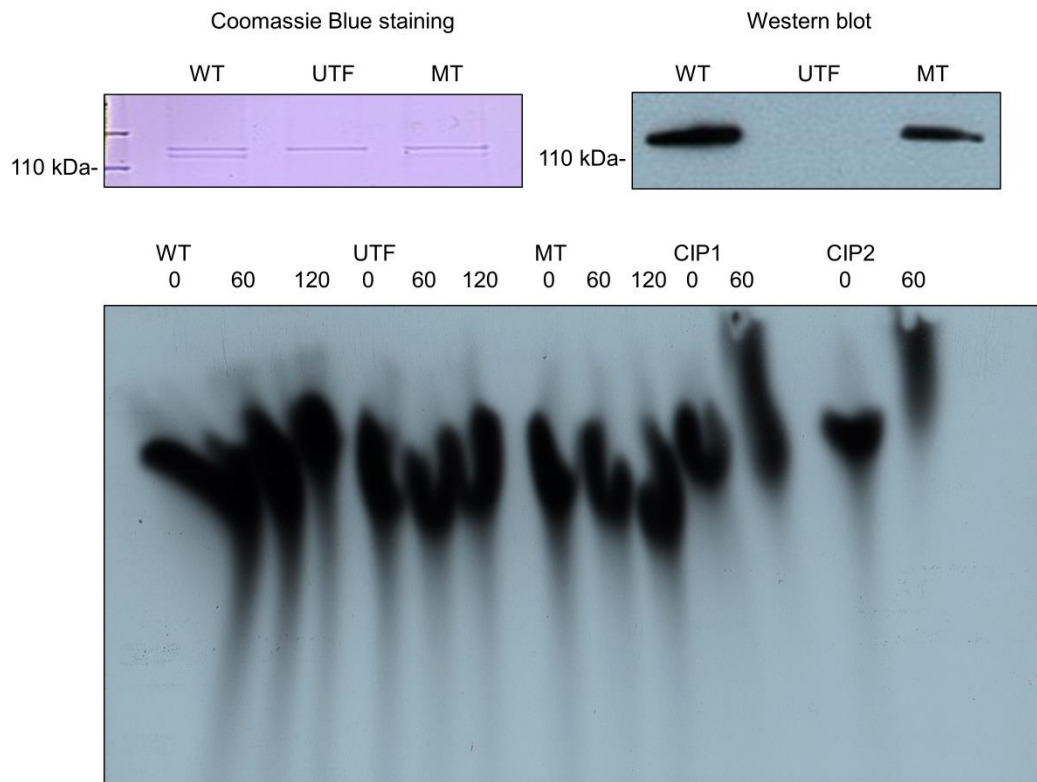


Figure 6-32 ATPase assay for different construct of *IGHMBP2* with a positive CIP control. Hydrolysis could be observed in the samples incubated with the CIP positive control, but not in the samples incubated with the different *IGHMBP2* constructs. WT= Wild type; UTF = Untransfected; MT = Mutant

6.3 Discussion

Autosomal recessive mutations in *IGHMBP2* were already implied in the pathogenesis of SMARD1. Results discussed in this chapter indicate that mutations in this gene can also be causative for CMT2. In total, eleven families were found with slowly progressive weakness, wasting and sensory loss, and an axonal neuropathy typical of CMT2, but no significant respiratory compromise. Nine families had compound heterozygous or homozygous mutations in *IGHMBP2* and two families presented with only one heterozygous variant. The 5' promoter region and the exome BAM files for sequencing coverage did not show any additional variants in these two families but *IGHMBP2* cDNA sequencing in the two affected individuals from family W disclosed the stop mutation as hemizygous, suggesting a deletion on the other allele. MLPA was performed, but no large deletions were found in the family. mRNA analysis of frameshift and nonsense mutations in SMARD1

and CMT2 patients revealed that *IGHMBP2* is not subjected to NMD, resulting in the presence of truncated proteins.

Functional investigation in 17 fibroblast and 9 lymphoblastoid cell lines failed to show any changes in the subcellular localisation or clustering of the protein; however, protein levels in CMT2 patients were significantly lower in comparison with controls and carriers, but higher than SMARD1 patient levels. This suggests that defective or truncated proteins undergo posttranslational degradation. Clinical phenotype differences are related to the *IGHMBP2* protein levels, but the small numbers require caution about whether this always correlates with the onset of disease and phenotype. Higher mRNA levels were observed in individuals with SMARD1 in previous reports but despite our best efforts only a trend towards higher mRNA levels in patients could be detected. This suggests the presence of a feedback mechanism to maintain protein homeostasis.

To elucidate the pathomechanism leading to the difference in severity between the two phenotypes, co-immunoprecipitation experiments were performed, showing interaction with TDP-43. A trend towards higher interaction with TDP-43 was observed in the mutant constructs, and the Pearson's correlation coefficient was significantly higher in SMARD1 fibroblasts in comparison with controls. Whilst no significant difference could be observed between CMT2 and SMARD1 patients, these results point towards involvement of TDP-43 in the pathogenesis of mutations in *IGHMBP2*. It should be noted that cell lines were only transfected with one missense mutation as compared to the compound heterozygous mutations present in patients. The effects of the numerous nonsense and frameshift mutations in the CMT cohort have not been established yet in transfected cell lines.

In addition to that, experiments were performed in fibroblasts and lymphoblastoid cell lines, which are not tissues primarily affected in CMT2, thus caution has to be applied when interpreting the results. Considering *IGHMBP2* mRNA is widely expressed throughout the body, it is likely that these tissues will reflect the consequences of mutations.

Unfortunately, results from the helicase assay could not be obtained, but it is highly likely that most mutations in *IGHMBP2* may lead to the dysfunction of the helicase

activity of this protein. The reduced protein levels or the abnormal IGHMBP2 protein in SMARD1 and CMT2 may impair the capacity of neurons to produce error-free mature mRNA, thus leading to neuronal degeneration. Further investigation in both CMT2 and SMARD1 patients will reveal the process responsible for the differences in severity and the lack of respiratory involvement in CMT2 patients.

Chapter 7

General conclusions

Diverse genetic and functional techniques were used in this thesis to investigate different types of inherited neuropathies. The main focus was applied to Charcot-Marie-Tooth disease, a genetically and phenotypically variable disease. After the discovery of the first CMT locus in 1982, the next 30 years of research have led to the unearthing of more than 80 disease-causing genes. Initially, these genes were identified by using genetic linkage studies, positional cloning, or candidate gene approaches. This was accelerated by the development of high-throughput techniques such as whole genome/exome sequencing and the publication of the human genome in 2001. To complicate things, mutations in the same gene can cause different CMT phenotypes at the same time as mutations in different genes may result in the same phenotype. Several genes can be grouped into pathogenic pathways involved in CMT, such as myelin biogenesis, axonal transport, mitochondrial dynamics and others discussed in the introduction. The availability of the human genome has led to the identification of mutations in genes that were not the primary functional candidates for CMT neuropathies and the discovery of novel pathways involved in CMT that did not have such evident involvement. My research has focused on the detection and subsequent investigation of new genes implicated in CMT and the expansion of the phenotypes associated with known pathogenic genes.

Mendelian inheritance patterns occurring in CMT include dominant, recessive, and X-linked and mutations in isolated patients can arise as *de novo*. In chapter 3, we discuss four CMT families with a mitochondrial inheritance pattern, caused by mutations in the *ATPase6* gene. This is the first gene in the mitochondrial genome implicated in CMT. Previously, mutations in this gene have been shown to cause Leigh Syndrome or NARP, both progressive neurodegenerative disorders. Two known pathogenic mutations were found in our cohort, leading to an overall presence of 1.1% in patients with CMT2 or dHMN. This is a moderately high percentage, considering only 25% of patients with CMT2 receive a genetic diagnosis.

So far, this is the only gene in the mitochondrial genome responsible for a CMT phenotype. In the future, *ATPase 6* sequencing should be performed in patients with an appropriate phenotype. Next-generation sequencing does not include the mitochondrial genome, meaning mutations in *ATPase 6* will be missed when performing exome sequencing in CMT families. This necessitates a highly specific characterisation of the family phenotype to prompt the screening for mutations in *ATPase 6*, discussed in chapter 3.

To elucidate the mechanism responsible for the differences in phenotype due to mutations in *ATPase 6*, additional functional experiments were undertaken. Since the mutations are identical, patient material was used to investigate the differences observed in patients. Available muscle biopsies of patients showed reduced activity and assembly of complex V, similar to previously performed experiments in patients with the NARP m.8993T>G mutation. This suggests the presence of a poorly assembled and unstable complex V holoenzyme. Some variability could be observed in both activity and assembly on BN-PAGE for patients with identical mutation loads which may be attributable to holoenzyme disassembly occurring during sample preparation. Whilst this proves the pathogenicity of the mutation in patients with an isolated neuropathy, it does not provide an explanation for why some patients harbouring homoplasmic levels of m.9185T>C develop a tissue-specific peripheral neuropathic phenotype, whereas others with similar mutant loads develop a multisystem neurologic syndrome such as Leigh syndrome. Additional factors might

increase the susceptibility of certain patients to neuropathy or protect them from a more generalised disorder, but this will require further functional studies.

In chapter 4, the focus was the nuclear genome and traditional methods were used to find causative genes for CMT. Compound heterozygous *FIG4* mutations were found in a suspected case of inflammatory demyelinating neuropathy, with a two year history of rapidly progressive weakness in a single limb. *FIG4* mutations are normally associated with progressive proximal and distal weakness but some patients may show asymmetrical rapid deterioration of strength in a single limb, mimicking inflammatory demyelinating neuropathy. This expands the already known phenotype and should alert clinicians to the possibility of *FIG4* mutations especially if there is an early onset, chronic progressive course followed by a more rapid deterioration in one limb.

Chapter 4 also reports the screening of appropriate cohorts of CMT patients for mutations in *C9orf72*, *HINT1*, *SCN9A*, *ARL1* and *ARL6ip1*, but found no definite pathogenic mutations. Cohorts consisted of a relatively small number of patients, therefore not excluding the potential presence of pathogenic variants. The frequency of mutations may be so low as to be missed in a preliminary screen. In future, traditional Sanger sequencing will gradually be replaced by next-generation sequencing which may reveal variants in the genes mentioned. Interestingly, the frequency of mutations in *HINT1* was estimated at 11% in the original paper by Zimon et al, which could not be replicated. This high frequency is likely due to a founder effect in central Europe patients with neuropathy and neuromyotonia.

In the following chapter, next-generation sequencing techniques (whole exome sequencing) were used instead of the more traditional methods to find new causative genes. Nine families were investigated and resulted in the detection of a pathogenic variant in five families out of nine. As well as two previously known pathogenic variants in *HSPB1* and *MFN2*, three probably new pathogenic genes were discovered: *NEFH* (*still being investigated*), *ADD3* and *BICD2*.

A frameshift variant near the 3' end of the *NEFH* gene was found in a family with axonal neuropathy. This led to the loss of the stopcodon and an extension of 40 additional amino acids. This potentially adds NF-H to the list of proteins interfering

with the cytoskeleton and further research is required to elucidate the exact pathomechanism.

In one family with four children with spastic diplegic/quadriplegic cerebral palsy and intellectual disability, a homozygous p.Gly367Asn mutation in *ADD3* was found. Studies in fibroblast cell lines showed an impaired actin capping activity in the mutant cell lines, implicating the involvement of the cytoskeleton in the pathomechanism of disease. Mutations in α II spectrin, a cytoskeletal protein that lines the intracellular side of the plasma membrane in eukaryotic cells, have previously been identified as a cause of epilepsy, intellectual disability and spastic quadripareisis. So have mutations in *KANK1*, which have also been implicated in hereditary cerebral palsy and play an important role in the cytoskeleton. This links hereditary forms of cerebral palsy to abnormalities of components of the dynamic cytoskeleton, as seen before in isolated inherited neuropathies.

Mutations in *BICD2* were found by three groups simultaneously in a total of eleven families with DCSMA with a pattern of muscle involvement highly similar to that seen in patients with *DYNC1H1* mutations. *BICD2* mutations resulted in an increased binding affinity between *BICD2* and the dynein-dynactin complex, therefore altering *BICD2*-mediated cellular trafficking processes. As mentioned in the introduction, several proteins involved in transporting cargo from the periphery to the cell body, such as *DCTN1* and *DYNH1C1*, have been implicated in CMT. The addition of *BICD2* to the list of pathogenic genes confirms the importance of this pathway and the impairment of *BICD2*-mediated trafficking likely leads to compromised development and maintenance of a key subset of anterior horn cells and UMNs.

For the remaining four families, shorter lists of probable pathogenic genes have been established. Whilst in most cases, candidate genes could be prioritised due to their function and segregation analysis in the family, these still require additional families or other indications towards pathogenicity before investing in functional experiments to prove pathogenicity.

Chapter 6 provides an example of functional experiments taken forward to elucidate the pathomechanism of a variant. In total, eleven CMT2 families were found with recessive compound heterozygous mutations in *IGHMBP2*, normally causing SMARD1. Western blots in fibroblast and lymphoblastoid cell lines showed lower protein levels in SMARD1 patients in comparison with CMT2 patients, suggesting the severity of the phenotype may depend on the residual levels of the protein. Co-immunoprecipitation experiments showed interaction with TDP-43, and a trend towards higher interaction in the mutant constructs was observed. The mutation spectrum in CMT2 patients showed segregating mutations as a combination of a nonsense or frameshift and fewer missense mutations, where one or both were in the last exon, escaping nonsense mediated decay and leading to a truncated and likely still active protein. Several families also presented with a combination of missense mutations. Whilst there were no CMT2 patients presenting with the same combination of mutations as SMARD1 patients, five mutations found in the CMT2 cohort were known to be pathogenic in SMARD1 cases. This suggests an extra factor influencing the severity of the phenotype. In the *nmd* mouse model, this factor is contained within the BAC-27k3 transgene, with the syntenic genomic area in humans comprising four tRNATyr genes and the activator of basal transcription 1 (*ABT1*) gene, but no variations were found in these genes in the exomes of the index patients. For future experiments, international collaboration will be essential, since most clinical centres only have few SMARD/DSMA1 patients under their care and tissue is very hard to obtain from these patients. To investigate potential biomarkers for disease severity and outcomes such as clinical scales, CMAP amplitudes and *IGHMBP2* enzymatic activity; large studies with both SMARD1 and CMT2 patients will have to be performed. Clarifying the difference in severity will be helpful to target potential therapeutic strategies.

This thesis demonstrates the progress of genetic to functional techniques involved in the discovery of new pathogenic genes. In the first chapters, more traditional methods such as Sanger sequencing were used to identify genetic variants causing CMT and genes were chosen due to their function, involvement in similar phenotypes or the presence in mouse models. In the later chapters, more advanced next generation sequencing techniques were used to explore the whole exome of one or multiple patients. In the event of novel variant discovery, further functional tests

to prove pathogenicity of the variant were required. In situ methods such as Polyphen and SIFT were used to estimate the influence of variants on traits such as the folding and functionality of the protein. Whilst being indicative, these are not decisive for the pathogenic status of a variant. Known pathogenic variants have previously been categorised as non-pathogenic and vice versa. This highlights the necessity of in vitro studies.

For the purpose of this thesis, two different types of in vitro models were used. Due to excellent transfectability, HEK293 cell lines were used as a model system for transfection experiments and DNA was condensed into positively charged particles, binding to anionic cell surface residues and brought into the cell via endocytosis. This resulted in an overexpression system with the presence of either wild type or mutated protein, helping the purification process. However, there are a few disadvantages in using overexpression models. Overexpression may influence balanced gene dosage, affecting protein folding, localisation, complex assembly and downstream regulation.

Additionally, patient-derived cell lines were used as cellular models in multiple projects to study disease-related cellular phenotypes. Due to the ease of isolation, fibroblasts are a popular cellular model to use. Fibroblast cultures can be derived from a 4-mm human skin biopsy and have a very high success rate which is important when dealing with patient-derived tissue samples. They are easy to cultivate and use, but have relatively low protein content. Whilst these are characteristic for the individual patient, the primary affected tissue consists of nerves, and results might not always be representative. As shown in chapter 4, variability in the mitochondrial membrane potential is too high in fibroblasts to draw any results. Depending on the experiment, fibroblasts can prove to be a valuable model. This also applies to the lymphoblast cell lines that were used. Human peripheral blood mononuclear cells (PBMC's) can be easily isolated from whole blood and subsequently immortalised by transformation with the Epstein Barr Virus, although the latter can be rather costly and time consuming. However, in comparison with fibroblasts, higher protein content is present and as the cells are in suspension it makes it easier to cultivate. Since the primarily affected tissue (nerve) could not be obtained, these are good alternatives for in vitro experiments. The nature of

experiments will depend on the gene of interest and, as mentioned before, the heterogeneity in genes with mutations associated with CMT results in a variety of functional tests being developed to prove pathogenicity of a variant.

Whilst chapter 4 used a more traditional approach of gene discovery, chapter 5 incorporated next-generation sequencing techniques that were less commonly used at the start of this thesis but during the three years of research became increasingly high-throughput. Initially, quality was variable and coverage was not homogeneous throughout the genome or showed very low depth. Variants could be missed and individual patients required very detailed analysis to avoid missing pathogenic variants, preventing it from being used for routine testing. Further optimisation is gradually leading to a revolution in gene discovery and diagnostics for Mendelian and complex diseases and it is predicted that exome sequencing will become a commonly used diagnostic screening tool within the next few years. Smaller families and isolated individuals previously omitted from searches based on the traditional methods will be able to be investigated, whilst only needing a minimal amount of DNA. As a highly heterogeneous phenotypic and genetic disease, CMT is an example where NGS is particularly time and cost-efficient. In a diagnostic setting, patients with a well characterised phenotype can be screened for the 17p duplication -found in two-third of patients with CMT1- and then *PMP22*, *GJB1*, *MPZ*, or *MFN2* when appropriate. However, conventional Sanger sequencing for the remaining CMT genes can be time consuming, cumbersome, expensive and unrewarding. Instead of consecutive sequencing of multiple genes, NGS can uncover mutations in all known genes simultaneously, even rare genes for which until now testing was not often available.

Even though NGS is an optimal technique for the discovery of novel genes, the heterogeneous functions and ubiquitous expression of several CMT genes and small families can make it challenging to identify the one pathogenic variant amongst a long list of variants leading to a peripheral nerve phenotype. From the ~20,000 variants typically found in a European American sample, more than 95% are already known as polymorphisms. Additionally, various filtering techniques can be used to hone in to the possible culprit gene, such as the mode of inheritance or the pedigree. Although increasingly more gene discovery research is focused on exome

sequencing, many families for which exome sequencing is performed remain without a genetic diagnosis. Only success stories will be published and whilst exome sequencing benefits from traits such as low cost, rapidity, low DNA requirements and screening of close to all coding-regions, exome sequencing in singletons and very small families still remains extremely challenging, as evidenced in Chapter 5.

Exome sequencing is more cost-efficient and less data-intensive than whole-genome sequencing and requires only 2% of the sequencing needed for an entire human genome; however, variants outside the coding region will not be covered and large indels, duplications and translocations will not be discovered. As the cost of sequencing continues to fall, a gradual movement from exome to whole-genome sequencing is occurring. Nevertheless, many pitfalls still remain. Finding the one pathogenic variant in whole-exome data can be cumbersome and this will prove to be even more difficult for whole-genome data, trying to incorporate the effect of non-coding variants. Even though challenging, the aim is a future where the genetic basis of all Mendelian traits is known, and this knowledge can be used to understand the underlying molecular basis of pathology, shifting the emphasis towards understanding disease mechanisms and genotype–phenotype relationships, providing diagnostic insight and information to patients and their families and developing improved therapeutics and improvement of human health.

In addressing to the aims of this thesis, the following conclusions can be made:

- Chapter 3: Detection of mutations in *ATPase6* in five families with CMT2 leads to an overall presence of the mutation in 1.1% in undiagnosed patients with a CMT2 or dHMN phenotype. *ATPase6* is the first mitochondrial gene responsible for an isolated peripheral neuropathy phenotype.
- Chapter 4: The CMT4J phenotype of *FIG4* mutations includes asymmetrical rapid deterioration of strength in a single limb, mimicking inflammatory demyelinating neuropathy.
- Chapter 4: There is a likely founder effect for mutations in *HINT1* in central Europe, due to the absence of mutations in UK/Spanish cohorts.

- Chapter 4: *C9orf72*, *ARL1* and *ARL6ip1* have been excluded as common causes for CMT.
- Chapter 5: We have identified three novel pathogenic genes (*NEFH* (*to be confirmed*), *ADD3* and *BICD2*), involved in the pathogenesis of CMT, spastic diplegic/quadriplegic cerebral palsy or DCSMA respectively, together with several further potential pathogenic genes involved in the pathogenesis of CMT, including: *ACSBG1*, *WDR48*, *RGMb*, *MORC2*, *FAM126A*, *CNTRL*, *GOLGA2*, *SSTR5*, *TBC1D24* and *PKMYT1*.
- Chapter 6: We have shown mutations in *IGHMBP2* to be a cause of axonal neuropathy, with significantly lower protein levels in fibroblast and lymphoblastoid cell lines of SMARD1 patients in comparison to CMT2 patients.
- Chapter 6: We have discovered a novel RNase-independent interaction between *IGHMBP2* and TDP-43, with a trend of a higher interaction for selected mutations implicated in CMT2.

Appendix I

Synonymous changes	Nonsynonymous changes	non-coding region
8248A>G: M-M: Hom (2)	8381A>G: T-A: Hom (1)	8291G>A: Hom (1)
8347A>G: L-L: Hom (1)	8388T>C: V-A: Hom (2)	8302A>G: Hom (1)
8485G>A: L-L: Het (1)	8396A>G: T-A: Het (1)	8311T>C: Hom (2)
8503T>C: N-N: Hom (4)	8461C>A: N-K: Hom (1)	8349C>T: Hom (2)
8533G>A: T-T: Hom (1)	8471C>T: P-S: Hom (1)	
8538T>C: N-N: Hom (A6) (1)	8477T>G: S-A: Hom (2)	
8545G>A: S-S: Hom (A8) (1)	8489A>C: M-L: Hom (2)	
8566A>G: Q-Q: Hom (1)	8490T>C: M-T: Hom (2)	
8572G>A: X-X: Hom (A8) (4)	8502A>G: N-S: Hom (1)	
8598T>C: I-I: Hom (2)	8516T>C: W-R: Hom (1)	
8679A>G: L-L : Hom (1)	8519G>A: E-L: Hom (4)	
8740C>T: L-L: Hom (1)	8531A>G: T-A: Hom (1)	
8754C>T: I-I: Hom (1)	8538T>C: I-T: Hom (A8) (1)	
8769A>G: T-T: Hom (2)	8545G>A: A-T: Hom (A6) (1)	
8772T>C: T-T: Hom (1)	8572G>A: G-S: Hom (A6) (4)	
8805A>G: T-T: Hom (1)	8578C>T: P-S: Hom (2)	
8820A>G: L-L: Hom (4)	8605C>T: P-S: Hom (2)	
8889T>C: I-I: Hom (1)	8619C>A: I-M: Hom (1)	
8925A>G:T-T: Hom (2)	8620C>T: P-S: Hom (1)	
8940C>T: I-I: Hom (2)	8633A>G: Y-C: Hom (1)	
8955T>C: I-I: Hom (2)	8698A>G: M-V: Het (1)	
8958C>T: I-I: Hom (1)	8699T>C: M-T: Hom (2)	
9006A>G: L-L: Hom (6)	8704A>G: M-V: Hom (4)	
9015C>T: N-N: Hom (1)	8725A>G: T-A: Hom (1)	
9042C>T: H-H: Hom (3)	8765C>T: A-V: Hom (2)	
9048T>C: I-I: Hom (1)	8794C>T: H-Y: Hom (1)	
9060C>A: T-T: Het (2)	8828A>G: N-S: Hom (1)	
9060C>T: T-T: Hom (1)	8836A>G: M-V: Hom (4)	
9061C>T: L-L: Hom (1)	8839G>A: A-T: Hom (3)	

9075C>T: T-T: Het (1)	8864T>C: V-A: Hom (1)
9078T>C: I-I: Hom (1)	8875T>C: F-L: Hom (2)
9117T>C: I-I: Hom (4)	8887A>G: I-V: Hom (2)
9120A>G: L-L: Hom (2)	8932C>T: P-S: Hom (1)
9126T>C: T-T: Hom (1)	8950G>A: V-M: Hom (2)
9168C>T: F-F: Het (1)	8974C>T: L-F: Hom (1)
9224T>C: H-H: Hom (1)	8993T>C: L-P: Hom (1)
9254A>G: W-W: Hom (7)	9025G>A: G-S: Hom (2)
9266G>A: G-G: Hom (4)	9055G>A: A-T: Hom (5)
9269C>T: A-A: Hom (1)	9067A>G: M-V: Hom (1)
9350A>G: L-L: Hom (1)	9070T>G: S-A: Hom (2)
9374A>G: Q-Q: Hom (1)	9101T>C: I-T: Hom (2)
9530T>C: P-P: Hom (1)	9139G>A: A-T: Hom (1)
9653T>C: H-H: Hom (2)	9185T>C: L-P: Hom (4)
9664A>G: G-G: Hom (3)	9210A>G: T-A: Hom (1)
9707T>C: I-I: Hom (1)	9243C>A: P-T: Hom (1)
	9288A>G: T-A: Hom (2)
	9300G>A: A-T: Hom (6)
	9325T>C: M-T: Hom (6)
	9366A>T: M-L: Hom (2)
	9438G>A: G-S: Hom (3)
	9580A>G: N-S: Hom (2)
	9664A>G: G-E: Hom (3)
	9682T>C: M-T: Hom (1)

Appendix I: List of all variants found in the *ATPase 6/8* genes in our cohort. Hom = homoplasmic; Het = Heteroplasmic; A8 = *ATPase8* reading frame; A6 = *ATPase6* reading frame; Number between brackets = number of individuals with this variant.

Appendix II

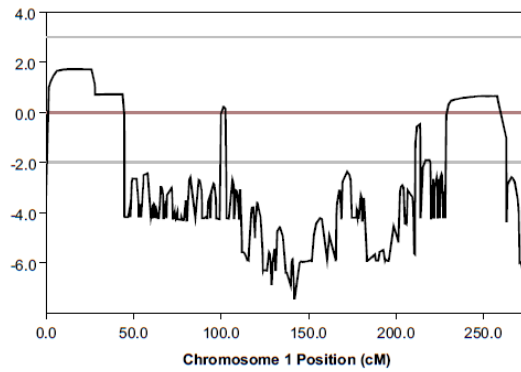
gene	OMIM	Exonic	Var	Gene	Poly	Grantham	PhastCons	GERP	Rs No.	MAF	Signature
		Function	count	count	Phen2	Score	score	Score			
ARHGAP11A		missense	1	4	D	81	1	5.04	rs140472511	0.004409	15_32921855_G_S
ATP10B		missense	3	8	D	94	0.949	-0.718	rs61734665	0.012739	5_160042903_G_K
TTC18		missense	1	2	D	68	1	5.29			10_75051751_T_K
MFF		missense	1	5	D	29	1	4.83			2_228197228_G_R
CEP110		missense	1	14	D	101	0.797	3.38	rs34344401	0.001297	9_123931891_C_Y
DENND5B		missense	1	5		10	0.988	-4.63	rs34129725	0.003106	12_31600503_T_Y
DNAH10		missense	1	16	D	81	1	5.47	rs147774367	0.002417	12_124270348_T_Y
DNAH17		missense	1	40		145	0.975	4.77			17_76440872_G_R
KIAA0232		missense	1	3	D	110	1	5.58	rs111811307	0.5	4_6826228_C_S
LIPG		missense	2	4	P	46	1	4.31	rs77960347	0.008597	18_47109955_A_R
MACF1		missense	1	20	D	99	1	5.68	rs144760259	0.002208	1_39853641_G_K
CAB39L		missense	1	2	D	180	1	4.62			13_49906202_G_R
OAS3,LOC100287897		nonsense	2	5		NA	0.854	1.88	rs61942233	0.010317	12_113403675_C_Y

gene	OMIM	Exonic	Var	Gene	Poly	Grantham	PhastCons	GERP	Rs No.	MAF	Signature
			Function	count	count	Phen2	Score	score			
ZFYVE9		missense	1	4	D	15	1	4.45			1_52759319_C_M
QRICH2		missense	2	24	P	56	1	4.59	rs61759535	0.005275	17_74276788_T_Y
SKIV2L2		missense	1	1	D	112	1	5.48	rs142958762	0.004468	5_54645455_C_S
SPAG5		missense	1	2	D	56	0.995	4.24			17_26905701_C_Y
SVEP1		missense	4	30		45	0.911	-2.4	rs41296069	0.055389	9_113244732_G_K
SYNE1	642	missense	1	38	D	101	0.989	3.53	rs34028822	0.004839	6_152757224_G_R
PLK1S1		missense	1	5		76	0.344	4.22			20_21143521_A_M
TNS4		missense	1	5	D	43	1	5.05	rs143122913	0.00022	17_38641181_C_Y
TEK	811	missense	1	7	P	180	1	4.07			9_27158131_C_Y
TRAK2		nonsense	1	7	NA	NA	1	3.25			2_202262876_G_R
TTN	250	missense	3	142		43	1	4.92	rs72648998	0.036691	2_179575511_C_Y
USP41		missense	2	4		21	0.425	99	rs75178771	0.018254	22_20723832_T_Y
C6orf186		missense	1	3	D	22	1	2.84			6_110644001_G_K
ZNF642		missense	1	2	D	121	0.999	0.975	rs144613252	0.001763	1_40961133_A_W

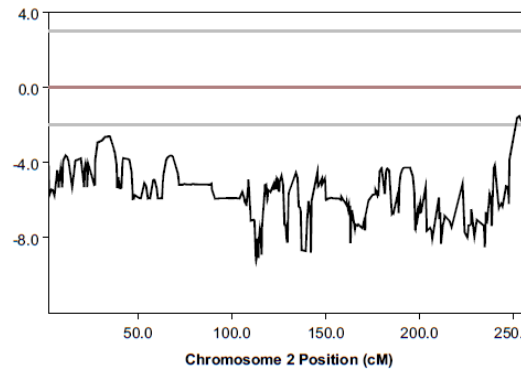
Appendix II: List of 34 possible pathogenic variants found in family D.

Appendix III

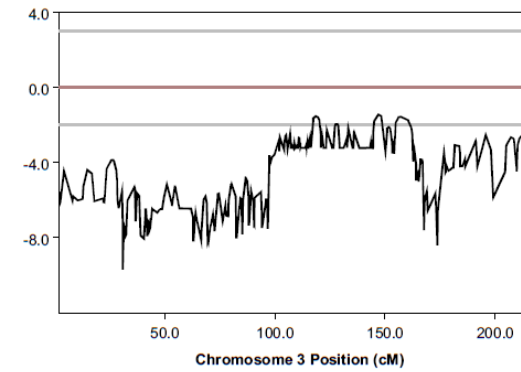
Parametric Analysis for dominant_model



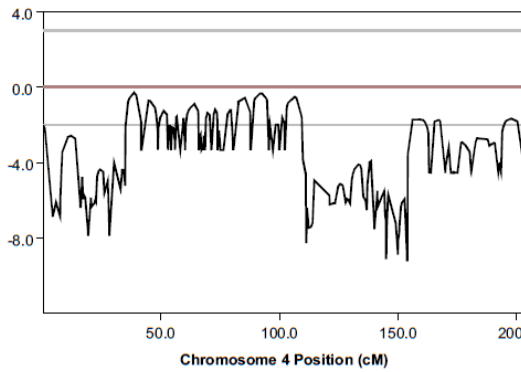
Parametric Analysis for dominant_model



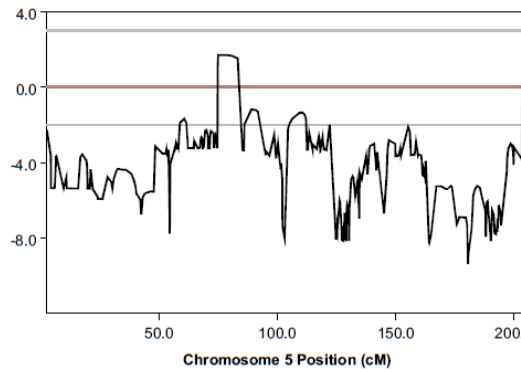
Parametric Analysis for dominant_model



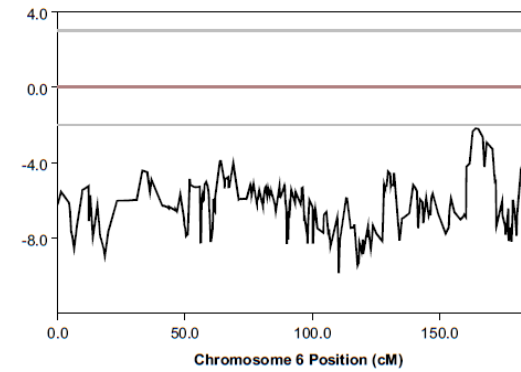
Parametric Analysis for dominant_model



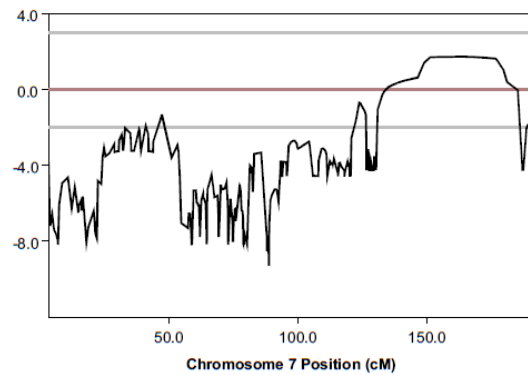
Parametric Analysis for dominant_model



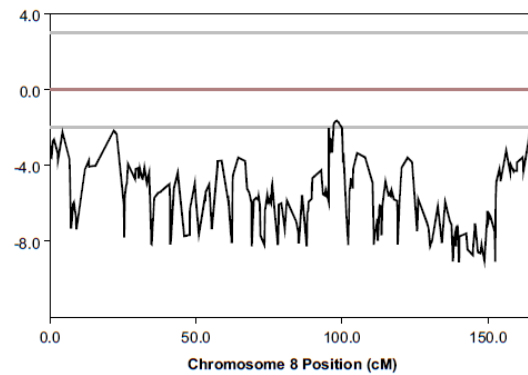
Parametric Analysis for dominant_model



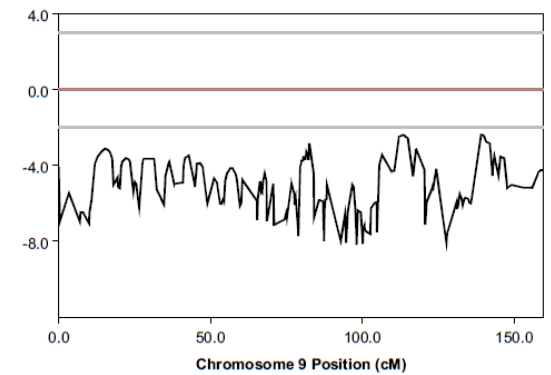
Parametric Analysis for dominant_model



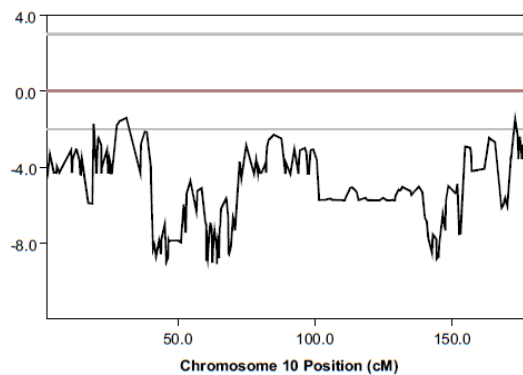
Parametric Analysis for dominant_model



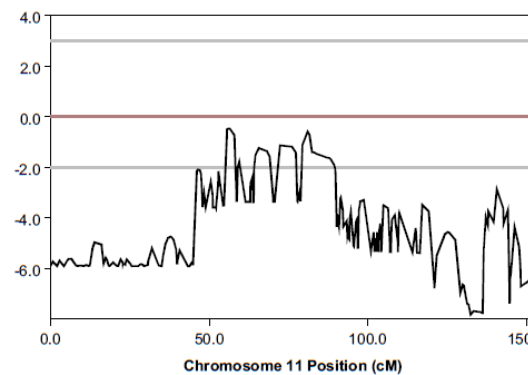
Parametric Analysis for dominant_model



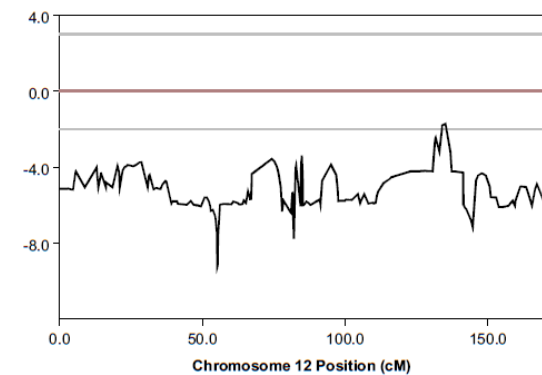
Parametric Analysis for dominant_model



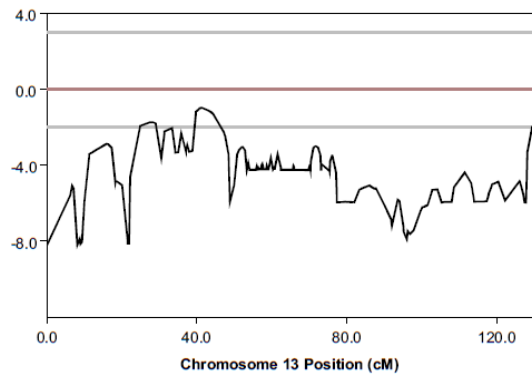
Parametric Analysis for dominant_model



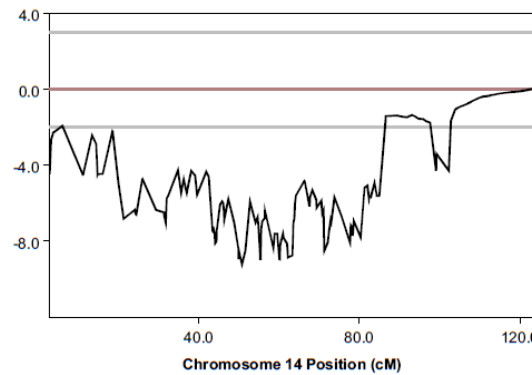
Parametric Analysis for dominant_model



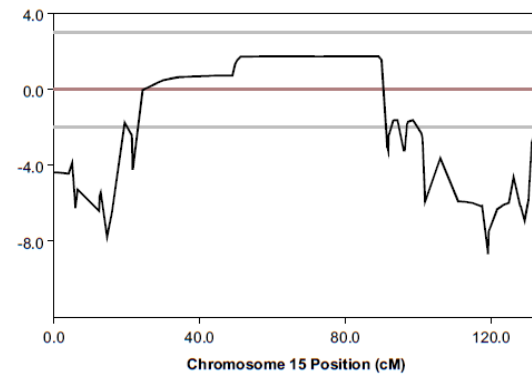
Parametric Analysis for dominant_model



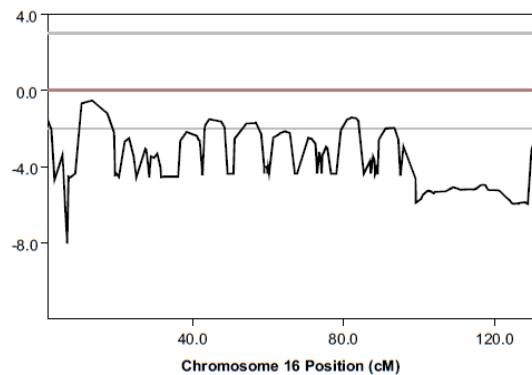
Parametric Analysis for dominant_model



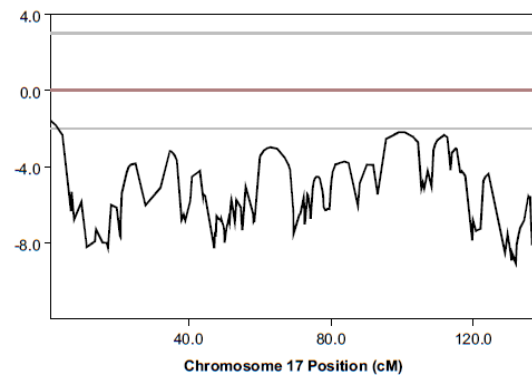
Parametric Analysis for dominant_model



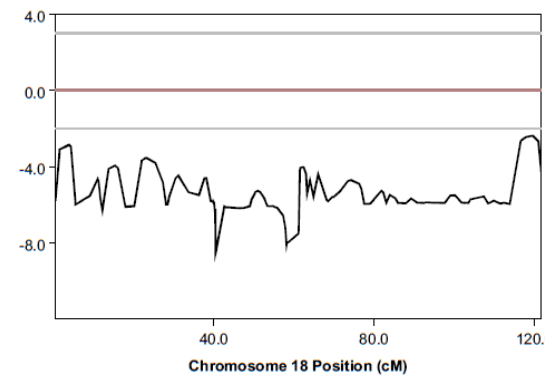
Parametric Analysis for dominant_model



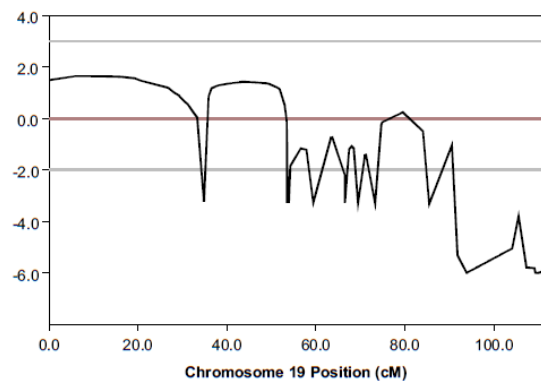
Parametric Analysis for dominant_model



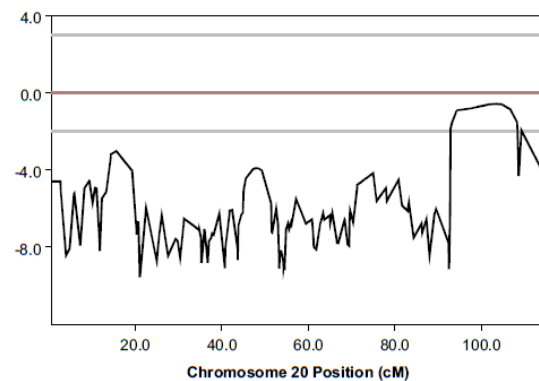
Parametric Analysis for dominant_model



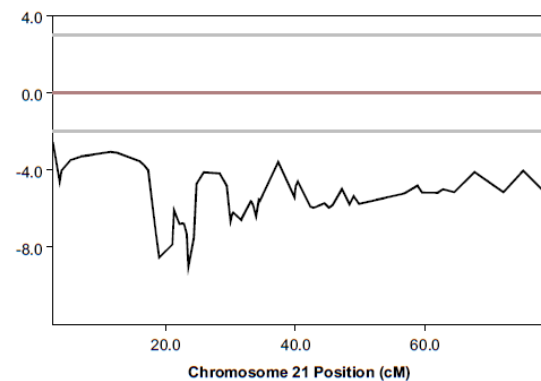
Parametric Analysis for dominant_model



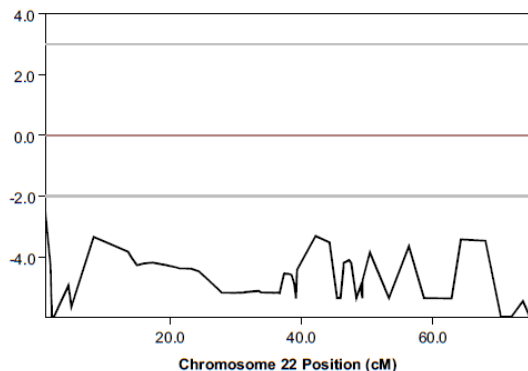
Parametric Analysis for dominant_model



Parametric Analysis for dominant_model

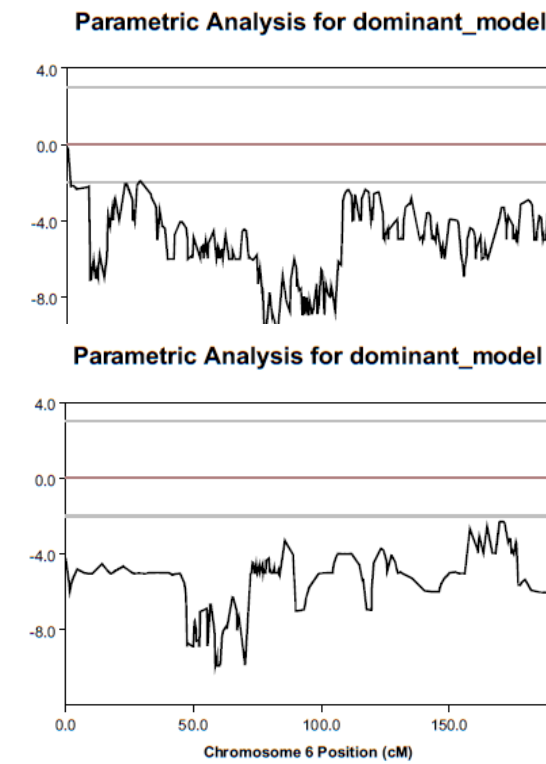
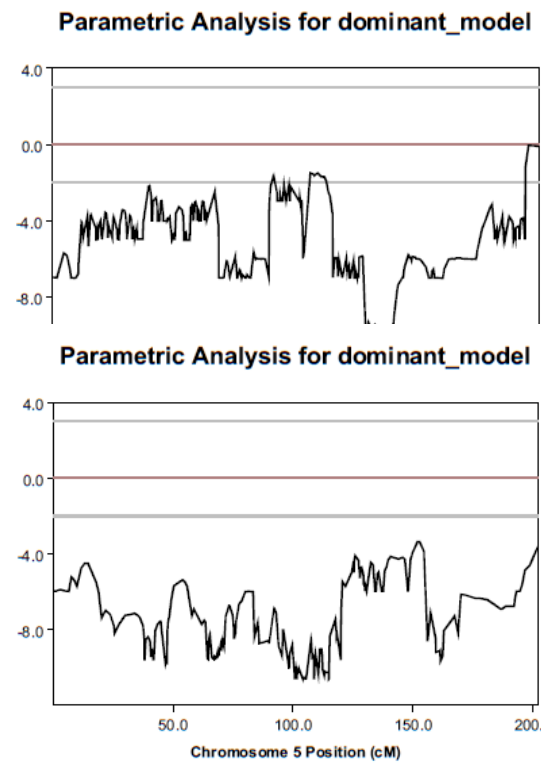
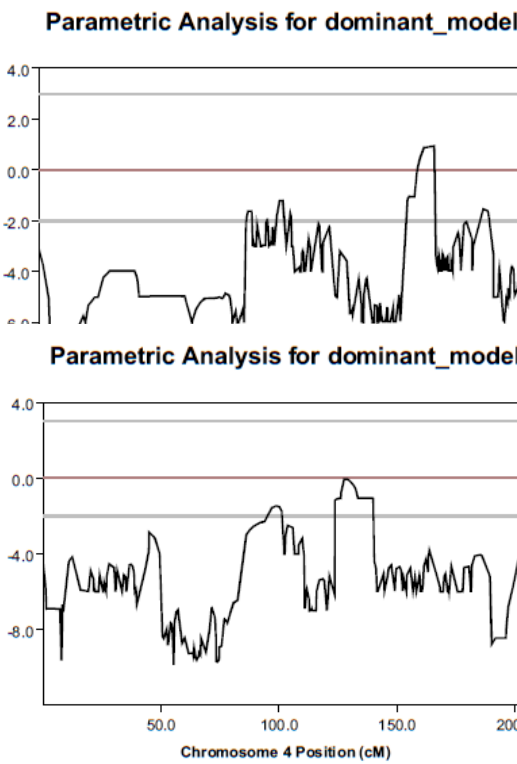


Parametric Analysis for dominant_model

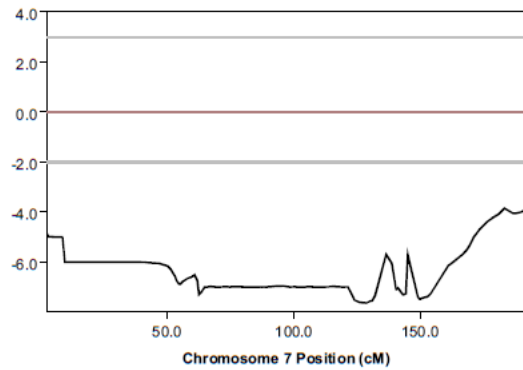


Appendix III: Linkage analysis results for Pedigree F.

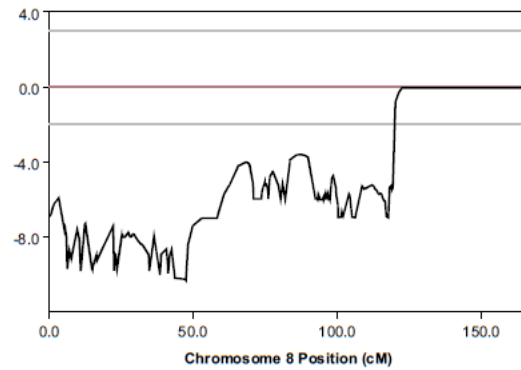
Appendix IV



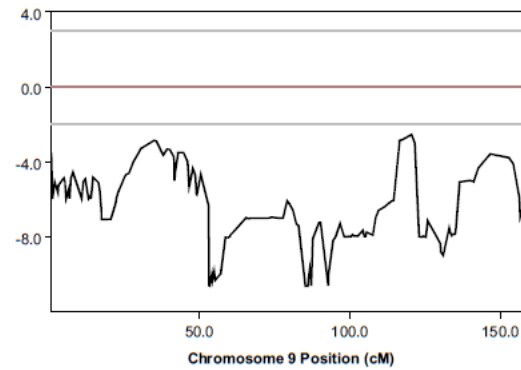
Parametric Analysis for dominant_model



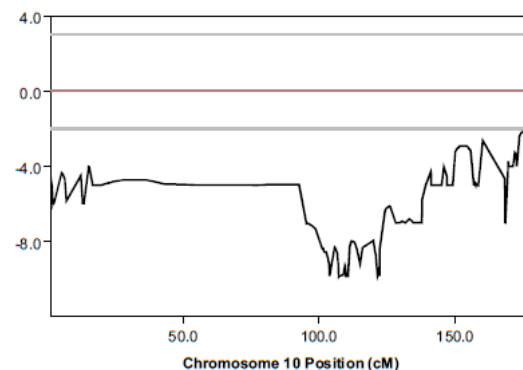
Parametric Analysis for dominant_model



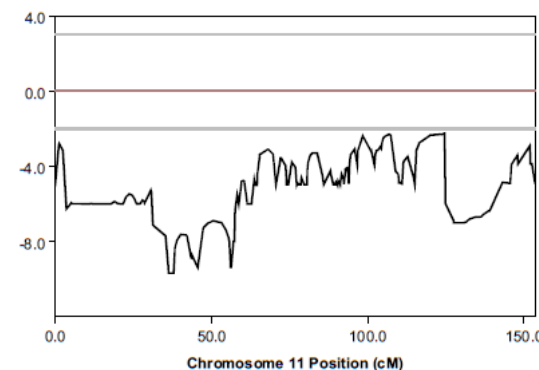
Parametric Analysis for dominant_model



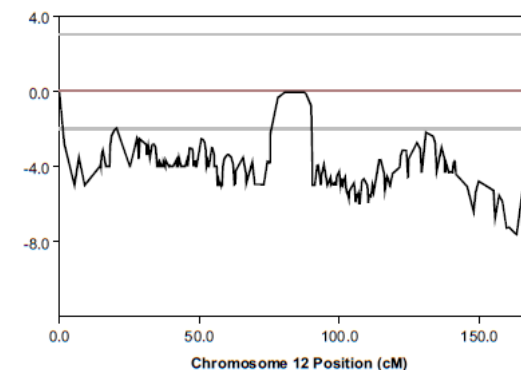
Parametric Analysis for dominant_model



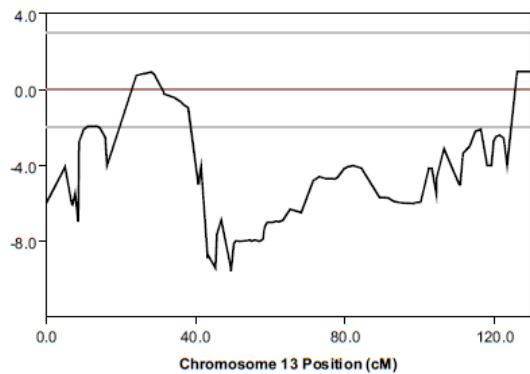
Parametric Analysis for dominant_model



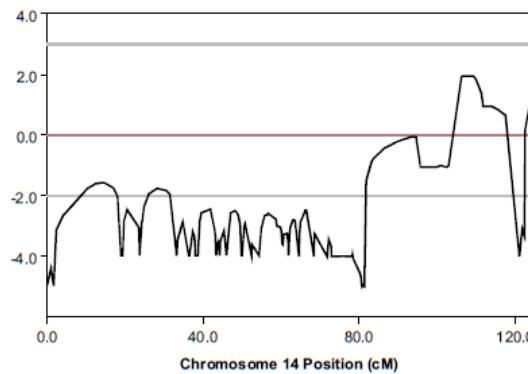
Parametric Analysis for dominant_model



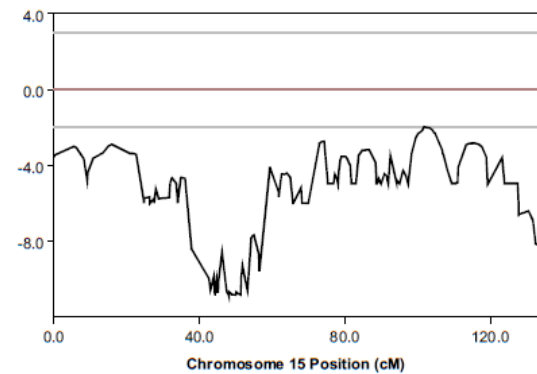
Parametric Analysis for dominant_model



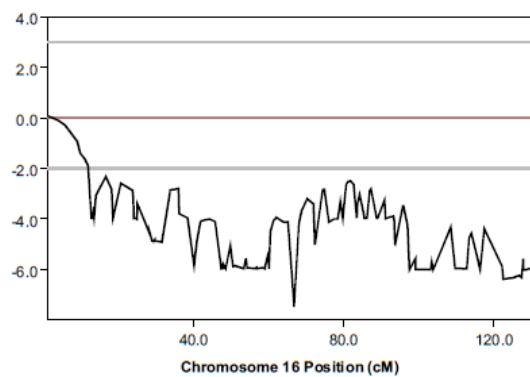
Parametric Analysis for dominant_model



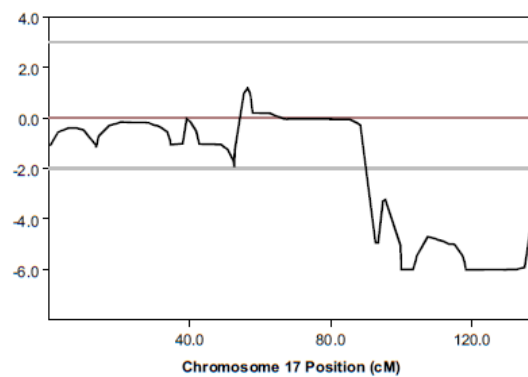
Parametric Analysis for dominant_model



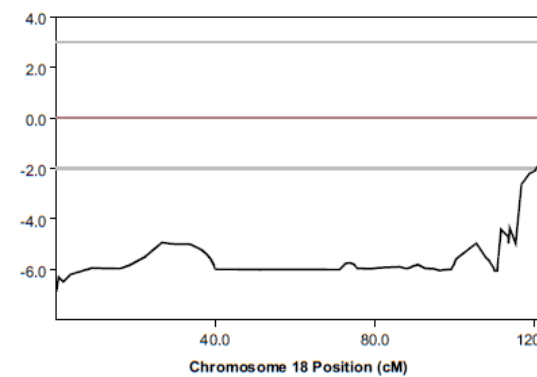
Parametric Analysis for dominant_model

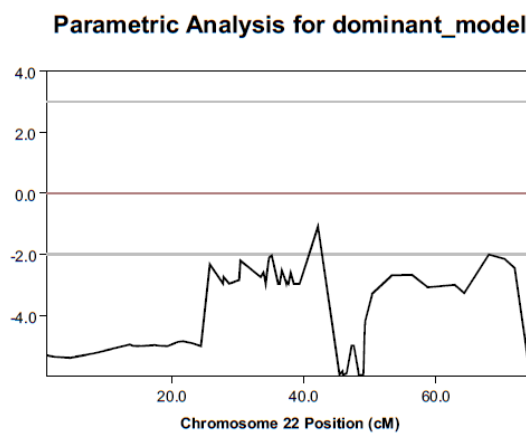
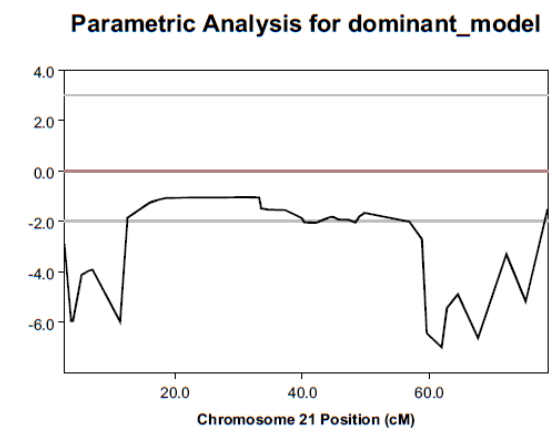
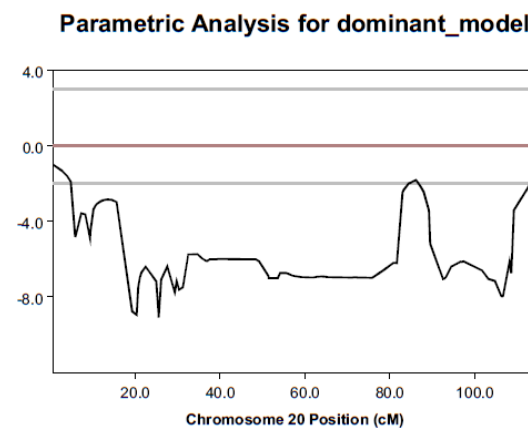
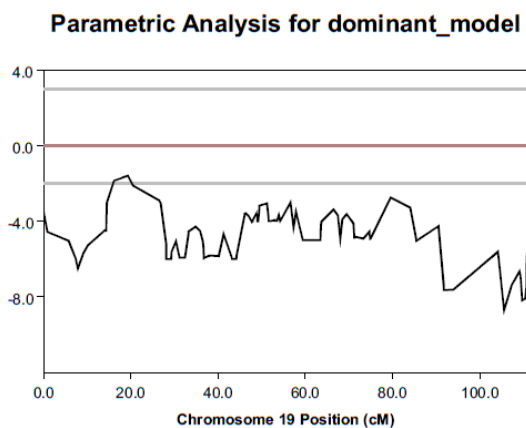


Parametric Analysis for dominant_model



Parametric Analysis for dominant_model





Appendix V

Gene	Exonic	Transcript ID	AD	AR	XLD	XLR	# SNVs	# INDEL	Signature
	Function	(NCBI)	Hom				in gene	in gene	
B3GALT6	missense	NM_080605.3	y	n	n	n	46		1_1168046_G_R
SLC45A1	missense	NM_001080397.1	y	n	n	n	27		1_8403940_C_Y
MYOM3	missense	NM_152372.3	y	n	n	n	89		1_24433663_C_Y
SPTA1	missense	NM_003126.2	y	n	n	n	87		1_158612230_C_Y
SLAMF8	missense	NM_020125.2	y	n	n	n	1		1_159805006_G_R
RCSD1	missense	NM_052862.3	y	n	n	n	13		1_167666340_G_R
CRB1	missense	NM_001193640.1	y	n	n	n	15		1_197326120_G_R
NID1	missense	NM_002508.2	y	n	n	n	67		1_236144975_G_R
C2orf42	missense	NM_017880.1	y	n	n	n	13		2_70408453_A_M
MERTK	missense	NM_006343.2	y	n	n	n	31	1	2_112705097_G_R
NEB	missense	NM_001164507.1	y	n	n	n	224	4	2_152541401_T_K
DOCK10	missense	NM_014689.2	y	n	n	n	60		2_225729789_C_Y
TOP2B	missense	NM_001068.2	y	n	n	n	44		3_25665208_A_R
RNF123	missense	NM_022064.2	y	n	n	n	47		3_49753586_C_Y

CACNA2D3,LRTM1	missense	NM_020678.2	y	n	n	n	7	1	3_54958871_G_R
SLMAP	missense	NM_007159.2	y	n	n	n	11	1	3_57835521_T_W
BBX	missense	NM_001142568.1	y	n	n	n	13	2	3_107435587_G_R
STIM2	missense	NM_001169118.1	y	n	n	n	21		4_27024391_A_R
ANKRD37	missense	NM_181726.2	y	n	n	n	2		4_186318347_A_R
SLC38A9	missense	NM_173514.2	y	n	n	n	14		5_54948489_T_Y
KIF2A	missense	NM_001098511.2	y	n	n	n	11		5_61602334_G_R
RGNEF	missense	NM_001080479.2	y	n	n	n	94		5_73190296_T_K
SLC22A7	missense	NM_006672.3	y	n	n	n	17		6_43267379_G_R
DOPEY1	missense	NM_001199942.1	y	n	n	n	29	2	6_83863904_G_R
NOD1	missense	NM_006092.2	y	n	n	n	30		7_30491667_C_Y
C7orf69,PKD1L1	missense	NM_138295.3	y	n	n	n	30		7_47851554_G_S
RELN	missense	NM_005045.3	y	n	n	n	65	6	7_103234193_T_W
KIAA1549	missense	NM_001164665.1	y	n	n	n	91		7_138537006_C_Y
KIAA1549	missense	NM_001164665.1	y	n	n	n	91		7_138556013_G_R
LRRC61,C7orf29	missense	NM_138434.2	y	n	n	n	13	1	7_150028187_C_M
DNAJC5B	missense	NM_033105.4	y	n	n	n	5		8_66963813_C_Y
SNTB1	missense	NM_021021.3	y	n	n	n	29		8_121561121_C_S
ACO1	missense	NM_002197.2	y	n	n	n	19		9_32449055_A_W
UNC13B	missense	NM_006377.3	y	n	n	n	36		9_35398953_C_Y

BICD2	missense	NM_001003800.1	y	n	n	n	51	1	9_95481425_C_S
C9orf152	missense	NM_001012993.2	y	n	n	n	12	1	9_112969840_G_R
CRAT	missense	NM_000755.3	y	n	n	n	30	1	9_131862217_C_Y
NOTCH1	missense	NM_017617.3	y	n	n	n	303	1	9_139391968_C_Y
CALML3	missense	NM_005185.2	y	n	n	n	8		10_5567319_C_Y
WAC	missense	NM_016628.4	y	n	n	n	8		10_28872390_C_Y
NRG3	missense	NM_001010848.3	y	n	n	n	41	1	10_83635671_C_Y
C11orf46	missense	NM_152316.1	y	n	n	n	3		11_30354488_G_K
C11orf46	missense	NM_152316.1	y	n	n	n	3		11_30354491_A_R
RIN1	missense	NM_004292.2	y	n	n	n	115	1	11_66103561_G_R
P2RY2	missense	NM_002564.2	y	n	n	n	24		11_72946144_G_S
C11orf70	missense-	NM_032930.2	y	n	n	n	2		11_101951947_G_K
	near-splice								
NUAK1	missense	NM_014840.2	y	n	n	n	77		12_106480516_T_Y
FGF9	missense	NM_002010.2	y	n	n	n	4		13_22255252_G_R
MIPEP	stop-gained	NM_005932.3	y	n	n	n	18	1	13_24413808_G_R
GSX1	missense	NM_145657.1	y	n	n	n	42	1	13_28367973_G_R
AP1G2	missense-	NM_003917.2	y	n	n	n	14	1	14_24032794_G_R

	near-splice									
ATG2B	missense	NM_018036.5	y	n	n	n	42	2	14_96792216_G_R	
MGA	missense	NM_001080541.2	y	n	n	n	62		15_41991063_A_W	
NOXO1	missense	NM_144603.2	y	n	n	n	58	1	16_2029312_A_M	
NOXO1	missense	NM_144603.2	y	n	n	n	58	1	16_2029313_G_S	
DNAJA3	missense	NM_001135110.2	y	n	n	n	28		16_4491530_C_S	
PHKG2,C16orf93	stop-gained	NM_001014979.2	y	n	n	n	7	1	16_30770393_G_R	
ATMIN	missense	NM_015251.2	y	n	n	n	38		16_81069612_G_K	
ZBTB4	missense	NM_001128833.1	y	n	n	n	70	3	17_7366934_G_R	
HAP1	missense	NM_001079870.1	y	n	n	n	50	2	17_39888972_T_Y	
SPAG9	missense	NM_001130528.2	y	n	n	n	20		17_49072561_A_M	
BAHCC1	missense	NM_001080519.2	y	n	n	n	338	1	17_79425291_G_K	
GREB1L	missense	NM_001142966.1	y	n	n	n	35	1	18_19075668_G_R	
KLHL14	missense	NM_020805.1	y	n	n	n	21		18_30349890_C_Y	
MYO5B	missense	NM_001080467.2	y	n	n	n	75	2	18_47390707_A_M	
TCF3	splice-5	NM_001136139.2	y	n	n	n	101	1	19_1621835_A_W	
PLIN4	missense	NM_001080400.1	y	n	n	n	485	2	19_4512974_G_R	
PLIN4	missense	NM_001080400.1	y	n	n	n	485	2	19_4513172_G_R	

NCAN	missense	NM_004386.2	y	n	n	n	35		19_19359535_G_R
GGN	missense	NM_152657.3	y	n	n	n	68	2	19_38876865_C_Y
GGN	missense	NM_152657.3	y	n	n	n	68	2	19_38877423_G_K
ATP1A3	missense	NM_152296.3	y	n	n	n	22		19_42492254_C_Y
ZNF160	missense	NM_001102603.1	y	n	n	n	24	1	19_53578346_C_Y
SIRPA	missense	NM_001040022.1	y	n	n	n	61	4	20_1876113_C_Y
PYGB	missense	NM_002862.3	y	n	n	n	32		20_25261702_G_S
SDC4	missense	NM_002999.3	y	n	n	n	7	1	20_43961667_G_R
ZNF335	missense	NM_022095.3	y	n	n	n	47	2	20_44592228_G_R
TRAPP10	missense	NM_003274.4	y	n	n	n	28		21_45502843_T_Y
MRPL40	missense	NM_003776.2	y	n	n	n	12		22_19423268_C_S
SOX10	missense	NM_006941.3	y	n	n	n	31		22_38369872_G_R
SBF1	missense	NM_002972.2	y	n	n	n	137		22_50904250_T_K
PHC2	coding	NM_198040.2	y	n	n	n	46	1	1_33820748_GGCTGCTGCT GTTGTGGCTGT_CGGCTGC TGCTGTTGTGGCTGT/C
MAPKAPK2	coding	NM_004759.4	y	n	n	n	37	1	1_206858675_A-G_A/AGCC
PCDHGB4,PCDHGA8 ,PCDHGB7,PCDHGB 6,PCDHGB5,	coding	NM_018914.2	y	n	n	n	52	3	5_140802723_GTG_CGTG/C

SLC16A10	coding	NM_018593.4	y	n	n	n	18	2	6_111494006_TGG_TTGG/T
CCDC114	coding	NM_144577.3	y	n	n	n	51	1	19_48814908_C-A_C/CACG
LAMA5	coding	NM_005560.3	y	n	n	n	481	1	20_60942086_CCGCGCGCC_GCCGCGCGCC/G
C1orf141	frameshift	NM_001013674.1	y	n	n	n	16	1	1_67558869_TCATT_CTCAT T/C
TDRD5	frameshift	NM_001199085.1	y	n	n	n	26	1	1_179660076_T-G_T/TGAGG
CYBRD1	frameshift	NM_024843.3	y	n	n	n	8	1	2_172411298_TT_CTT/C
CACNA2D3,LRTM1	frameshift	NM_020678.2	y	n	n	n	7	1	3_54952509_CT_GCT/G
SLC16A10	frameshift	NM_018593.4	y	n	n	n	18	2	6_111494010_TTTGTTGGGC TCATGT_ATTTGTTGGGCT CATGT/A
MED23	frameshift	NM_004830.2	y	n	n	n	18	1	6_131939578_A- A_A/AAACG

Appendix V: List of 93 candidate variants found in family K. y = yes; n = no.

References

ABE, A., NUMAKURA, C., SAITO, K., KOIDE, H., OKA, N., HONMA, A., KISHIKAWA, Y. & HAYASAKA, K. 2009. Neurofilament light chain polypeptide gene mutations in Charcot-Marie-Tooth disease: nonsense mutation probably causes a recessive phenotype. *J Hum Genet*, 54, 94-7.

ABECASIS, G. R., CHERNY, S. S., COOKSON, W. O. & CARDON, L. R. 2002. Merlin--rapid analysis of dense genetic maps using sparse gene flow trees. *Nature genetics*, 30, 97-101.

AMABLE, P. R., TEIXEIRA, M. V., CARIAS, R. B., GRANJEIRO, J. M. & BOROJEVIC, R. 2013. Identification of appropriate reference genes for human mesenchymal cells during expansion and differentiation. *PLoS One*, 8, e73792.

ANTONELLIS, A., ELLSWORTH, R. E., SAMBUUGHIN, N., PULS, I., ABEL, A., LEE-LIN, S. Q., JORDANOVA, A., KREMENSKY, I., CHRISTODOULOU, K., MIDDLETON, L. T., SIVAKUMAR, K., IONASESCU, V., FUNALOT, B., VANCE, J. M., GOLDFARB, L. G., FISCHBECK, K. H. & GREEN, E. D. 2003. Glycyl tRNA synthetase mutations in Charcot-Marie-Tooth disease type 2D and distal spinal muscular atrophy type V. *American journal of human genetics*, 72, 1293-9.

ANTONELLIS, A. & GREEN, E. D. 2008. The Role of Aminoacyl-tRNA Synthetases in Genetic Diseases*. *Annual Review of Genomics and Human Genetics*, 9, 87-107.

ANTONELLIS, A., LEE-LIN, S.-Q., WASTERLAIN, A., LEO, P., QUEZADO, M., GOLDFARB, L. G., MYUNG, K., BURGESS, S., FISCHBECK, K. H. & GREEN, E. D. 2006. Functional Analyses of Glycyl-tRNA Synthetase Mutations Suggest a Key Role for tRNA-Charging Enzymes in Peripheral Axons. *The Journal of Neuroscience*, 26, 10397-10406.

AUER-GRUMBACH, M., OLSCHEWSKI, A., PAPIC, L., KREMER, H., MCENTAGART, M. E., UHRIG, S., FISCHER, C., FROHLICH, E., BALINT, Z., TANG, B., STROHMAIER, H., LOCHMULLER, H., SCHLÖTTER-WEIGEL, B., SENDEREK, J., KREBS, A., DICK, K. J.,

PETTY, R., LONGMAN, C., ANDERSON, N. E., PADBERG, G. W., SCHELHAAS, H. J., VAN RAVENSWAAIJ-ARTS, C. M., PIEBER, T. R., CROSBY, A. H. & GUELLY, C. 2010. Alterations in the ankyrin domain of TRPV4 cause congenital distal SMA, scapuloperoneal SMA and HMSN2C. *Nature genetics*, 42, 160-4.

AUER-GRUMBACH, M., SCHLÖTTER-WEIGEL, B., LOCHMULLER, H., STROBL-WILDEMANN, G., AUER-GRUMBACH, P., FISCHER, R., OFFENBACHER, H., ZWICK, E. B., ROBL, T., HARTL, G., HARTUNG, H. P., WAGNER, K. & WINDPASSINGER, C. 2005. Phenotypes of the N88S Berardinelli-Seip congenital lipodystrophy 2 mutation. *Annals of neurology*, 57, 415-24.

AZZEDINE, H., SENDEREK, J., RIVOLTA, C. & CHRAST, R. 2012. Molecular genetics of charcot-marie-tooth disease: from genes to genomes. *Mol Syndromol*, 3, 204-14.

AZZEDINE, H., ZAVADAKOVA, P., PLANTE-BORDENEUVE, V., VAZ PATO, M., PINTO, N., BARTESAGHI, L., ZENKER, J., POIROT, O., BERNARD-MARISSAL, N., ARNAUD GOUTTENOIRE, E., CARTONI, R., TITLE, A., VENTURINI, G., MEDARD, J. J., MAKOWSKI, E., SCHOLS, L., CLAEYS, K. G., STENDEL, C., ROOS, A., WEIS, J., DUBOURG, O., LEAL LOUREIRO, J., STEVANIN, G., SAID, G., AMATO, A., BARABAN, J., LEGUERN, E., SENDEREK, J., RIVOLTA, C. & CHRAST, R. 2013. PLEKHG5 deficiency leads to an intermediate form of autosomal-recessive Charcot-Marie-Tooth disease. *Human molecular genetics*, 22, 4224-32.

BACKELJAUW, P. F. & CHERNAUSEK, S. D. 2012. The Insulin-Like Growth Factors and Growth Disorders of Childhood. *Endocrinology and Metabolism Clinics of North America*, 41, 265-282.

BAINES, A. J. 2010. The spectrin-ankyrin-4.1-adducin membrane skeleton: adapting eukaryotic cells to the demands of animal life. *Protoplasma*, 244, 99-131.

BALASTIK, M., FERRAGUTI, F., PIRES-DA SILVA, A., LEE, T. H., ALVAREZ-BOLADO, G., LU, K. P. & GRUSS, P. 2008. Deficiency in ubiquitin ligase TRIM2 causes accumulation of neurofilament light chain and neurodegeneration. *Proc Natl Acad Sci U S A*, 105, 12016-21.

BALOH, R. H., SCHMIDT, R. E., PESTRONK, A. & MILBRANDT, J. 2007. Altered axonal mitochondrial transport in the pathogenesis of Charcot-Marie-Tooth disease from mitofusin 2 mutations. *The Journal of neuroscience : the official journal of the Society for Neuroscience*, 27, 422-30.

BAMSHAD, M. J., NG, S. B., BIGHAM, A. W., TABOR, H. K., EMOND, M. J., NICKERSON, D. A. & SHENDURE, J. 2011. Exome sequencing as a tool for Mendelian disease gene discovery. *Nature reviews. Genetics*, 12, 745-55.

BANCHS , I., CASASNOVAS, C., MONTERO, J., VOLPINI, V., MARTÍNEZ-MATOS, J.A. 2010 Charcot-Marie-Tooth disease with intermediate conduction velocities caused by a novel mutation in the MPZ gene. *Muscle Nerve* 42(2): 184-188.

BAREL, O., SHORER, Z., FLUSSER, H., OFIR, R., NARKIS, G., FINER, G., SHALEV, H., NASASRA, A., SAADA, A. & BIRK, O. S. 2008. Mitochondrial Complex III Deficiency Associated with a Homozygous Mutation in UQCRC2. *The American Journal of Human Genetics*, 82, 1211-1216.

BARLOW, A. L., MACLEOD, A., NOPPEN, S., SANDERSON, J. & GUÉRIN, C. J. 2010. Colocalization Analysis in Fluorescence Micrographs: Verification of a More Accurate Calculation of Pearson's Correlation Coefficient. *Microscopy and Microanalysis*, 16, 710-724.

BARRELL, B. G., BANKIER, A. T. & DROUIN, J. 1979. A different genetic code in human mitochondria. *Nature*, 282, 189-94.

BARWICK, K. E., WRIGHT, J., AL-TURKI, S., MCENTAGART, M. M., NAIR, A., CHIOZA, B., AL-MEMAR, A., MODARRES, H., REILLY, M. M., DICK, K. J., RUGGIERO, A. M., BLAKELY, R. D., HURLES, M. E. & CROSBY, A. H. 2012. Defective presynaptic choline transport underlies hereditary motor neuropathy. *American journal of human genetics*, 91, 1103-7.

BAX, M., GOLDSTEIN, M., ROSENBAUM, P., LEVITON, A., PANETH, N., DAN, B., JACOBSSON, B. & DAMIANO, D. 2005. Proposed definition and classification of cerebral palsy, April 2005. *Dev Med Child Neurol*, 47, 571-6.

BECK, M., BRICKLEY, K., WILKINSON, H.L., SHARMA, S., SMITH, M., CHAZOT, P.L., POLLARD, S., STEPHENSON, F.A. 2002 Identification,

molecular cloning, and characterization of a novel GABAA receptor-associated protein, GRIF-1. *J Biol Chem.* 277(33):30079-90.

BECK, J., POULTER, M., HENSMAN, D., ROHRER, J. D., MAHONEY, C. J., ADAMSON, G., CAMPBELL, T., UPHILL, J., BORG, A., FRATTA, P., ORRELL, R. W., MALASPINA, A., ROWE, J., BROWN, J., HODGES, J., SIDLE, K., POLKE, J. M., HOULDEN, H., SCHOTT, J. M., FOX, N. C., ROSSOR, M. N., TABRIZI, S. J., ISAACS, A. M., HARDY, J., WARREN, J. D., COLLINGE, J. & MEAD, S. 2013. Large C9orf72 hexanucleotide repeat expansions are seen in multiple neurodegenerative syndromes and are more frequent than expected in the UK population. *American journal of human genetics*, 92, 345-53.

BEETZ, C., PIEBER, T. R., HERTEL, N., SCHABHUTTL, M., FISCHER, C., TRAJANOSKI, S., GRAF, E., KEINER, S., KURTH, I., WIELAND, T., VARGA, R. E., TIMMERMAN, V., REILLY, M. M., STROM, T. M. & AUER-GRUMBACH, M. 2012. Exome sequencing identifies a REEP1 mutation involved in distal hereditary motor neuropathy type V. *American journal of human genetics*, 91, 139-45.

BERCIANO, J., BAETS, J., GALLARDO, E., ZIMON, M., GARCIA, A., LOPEZ-LASO, E., COMBARROS, O., INFANTE, J., TIMMERMAN, V., JORDANOVA, A. & DE JONGHE, P. 2011a. Reduced penetrance in hereditary motor neuropathy caused by TRPV4 Arg269Cys mutation. *J Neurol*, 258, 1413-21.

BERCIANO, J., BAETS, J., GALLARDO, E., ZIMÓN, M., GARCÍA, A., LÓPEZ-LASO, E., COMBARROS, O., INFANTE, J., TIMMERMAN, V., JORDANOVA, A. & DE JONGHE, P. 2011b. Reduced penetrance in hereditary motor neuropathy caused by TRPV4 Arg269Cys mutation. *Journal of Neurology*, 258, 1413-1421.

BERCIANO, J., SEVILLA, T., CASASNOVAS, C., SIVERA, R., VILCHEZ, J. J., INFANTE, J., RAMON, C., PELAYO-NEGRO, A. L. & ILLA, I. 2012. [Guidelines for molecular diagnosis of Charcot-Marie-Tooth disease]. *Neurologia*, 27, 169-78.

BERGER, P., BONNEICK, S., WILLI, S., WYMAN, M. & SUTER, U. 2002. Loss of phosphatase activity in myotubularin-related protein 2 is associated

with Charcot-Marie-Tooth disease type 4B1. *Human molecular genetics*, 11, 1569-79.

BERGER, P., NIEMANN, A. & SUTER, U. 2006. Schwann cells and the pathogenesis of inherited motor and sensory neuropathies (Charcot-Marie-Tooth disease). *Glia*, 54, 243-57.

BERNARD, R., SANDRE-GIOVANNOLI, A., DELAGUE, V. & LÉVY, N. 2006. Molecular genetics of autosomal-recessive axonal Charcot-Marie-Tooth neuropathies. *NeuroMolecular Medicine*, 8, 87-106.

BERRY, E. A., GUERGOVA-KURAS, M., HUANG, L. S. & CROFTS, A. R. 2000. Structure and function of cytochrome bc complexes. *Annu Rev Biochem*, 69, 1005-75.

BERTINI, E., GADISSEUX, J. L., PALMIERI, G., RICCI, E., DI CAPUA, M., FERRIERE, G. & LYON, G. 1989. Distal infantile spinal muscular atrophy associated with paralysis of the diaphragm: a variant of infantile spinal muscular atrophy. *Am J Med Genet*, 33, 328-35.

BERTINI, E. & HOULDEN, H. 2014. Defects of RNA metabolism in the pathogenesis of spinal muscular atrophy. *Neurology*, 82, 1298-9.

BHATTACHARYA, A., CZAPLINSKI, K., TRIFILLIS, P., HE, F., JACOBSON, A. & PELTZ, S. W. 2000. Characterization of the biochemical properties of the human Upf1 gene product that is involved in nonsense-mediated mRNA decay. *RNA*, 6, 1226-35.

BHUVANAGIRI, M., SCHLITTER, A. M., HENTZE, M. W. & KULOZIK, A. E. 2010. NMD: RNA biology meets human genetic medicine. *The Biochemical journal*, 430, 365-77.

BIENIEK, K. F., MURRAY, M. E., RUTHERFORD, N. J., CASTANEDES-CASEY, M., DEJESUS-HERNANDEZ, M., LIESINGER, A. M., BAKER, M. C., BOYLAN, K. B., RADEMAKERS, R. & DICKSON, D. W. 2013. Tau pathology in frontotemporal lobar degeneration with C9ORF72 hexanucleotide repeat expansion. *Acta neuropathologica*, 125, 289-302.

BIESECKER, L. G. 2012. Opportunities and challenges for the integration of massively parallel genomic sequencing into clinical practice: lessons from the ClinSeq project. *Genetics in medicine : official journal of the American College of Medical Genetics*, 14, 393-8.

BITOUN, M., DURIEUX, A. C., PRUDHON, B., BEVILACQUA, J. A., HERLEDAN, A., SAKANYAN, V., URTIZBEREA, A., CARTIER, L., ROMERO, N. B. & GUICHENEY, P. 2009. Dynamin 2 mutations associated with human diseases impair clathrin-mediated receptor endocytosis. *Human mutation*, 30, 1419-27.

BLACK, J.A., CUMMINS, T.R., PLUMPTON, C. 1999 Upregulation of a silent sodium channel after peripheral, but not central, nerve injury in DRG neurons. *J. Neurophysiol.* 82, 2776–2785.

BOUHOUCHE, A., BENOMAR, A., BOUSLAM, N., CHKILI, T. & YAHYAOUI, M. 2006. Mutation in the epsilon subunit of the cytosolic chaperonin-containing t-complex peptide-1 (Cct5) gene causes autosomal recessive mutilating sensory neuropathy with spastic paraplegia. *J Med Genet*, 43, 441-3.

BOUHY, D. & TIMMERMAN, V. 2013. [Animal models of Charcot-Marie-Tooth disease and their relevance for understanding the disease in humans]. *Rev Neurol (Paris)*, 169, 971-7.

BOYER, O., NEVO, F., PLAISIER, E., FUNALOT, B., GRIBOUVAL, O., BENOIT, G., HUYNH CONG, E., ARRONDEL, C., TETE, M. J., MONTJEAN, R., RICHARD, L., KARRAS, A., POUTEIL-NOBLE, C., BALAFREJ, L., BONNARDEAUX, A., CANAUD, G., CHARASSE, C., DANTAL, J., DESCHENES, G., DETEIX, P., DUBOURG, O., PETIOT, P., POUTHIER, D., LEGUERN, E., GUIOCHON-MANTEL, A., BROUTIN, I., GUBLER, M. C., SAUNIER, S., RONCO, P., VALLAT, J. M., ALONSO, M. A., ANTIGNAC, C. & MOLLET, G. 2011. INF2 mutations in Charcot-Marie-Tooth disease with glomerulopathy. *N Engl J Med*, 365, 2377-88.

BRAATHEN, G. J. 2012. Genetic epidemiology of Charcot-Marie-Tooth disease. *Acta Neurol Scand Suppl*, iv-22.

BREWER, M., CHANGI, F., ANTONELLIS, A., FISCHBECK, K., POLLY, P., NICHOLSON, G. & KENNERSON, M. 2008. Evidence of a founder haplotype refines the X-linked Charcot-Marie-Tooth (CMTX3) locus to a 2.5 Mb region. *neurogenetics*, 9, 191-5.

BRICKLEY, K., SMITH, M. J., BECK, M. & STEPHENSON, F. A. 2005. GRIF-1 and OIP106, members of a novel gene family of coiled-coil domain proteins: association in vivo and in vitro with kinesin. *J Biol Chem*, 280, 14723-32.

BRICKLEY, K. & STEPHENSON, F. A. 2011. Trafficking kinesin protein (TRAK)-mediated transport of mitochondria in axons of hippocampal neurons. *J Biol Chem*, 286, 18079-92.

BROSAMLE, C. 2010. The myelin proteolipid DMalpha in fishes. *Neuron Glia Biol*, 6, 109-12.

BROWNLEES, J., ACKERLEY, S., GRIERSON, A. J., JACOBSEN, N. J., SHEA, K., ANDERTON, B. H., LEIGH, P. N., SHAW, C. E. & MILLER, C. C. 2002. Charcot-Marie-Tooth disease neurofilament mutations disrupt neurofilament assembly and axonal transport. *Human molecular genetics*, 11, 2837-44.

BUCCI, C., BAKKE, O. & PROGIDA, C. 2012. Charcot-Marie-Tooth disease and intracellular traffic. *Prog Neurobiol*, 99, 191-225.

BUTTERFIELD, R. J., STEVENSON, T. J., XING, L., NEWCOMB, T. M., NELSON, B., ZENG, W., LI, X., LU, H. M., LU, H., FARWELL GONZALEZ, K. D., WEI, J. P., CHAO, E. C., PRIOR, T. W., SNYDER, P. J., BONKOWSKY, J. L. & SWOBODA, K. J. 2014. Congenital lethal motor neuron disease with a novel defect in ribosome biogenesis. *Neurology*, 82, 1322-30.

CAETANO, J. S., COSTA, C., BAETS, J., ZIMON PHD, M., VENÂNCIO PHD, M., SARAIVA PHD, J., NEGRÃO, L. & FINEZA, I. 2014. Autosomal Recessive Axonal Neuropathy With Neuromyotonia: A Rare Entity. *Pediatric Neurology*, 50, 104-107.

CALHOUN, M.W., THOMAS, J.W., GENNIS, R.B. 1994 The cytochrome oxidase superfamily of redox-driven proton pumps. *Trends Biochem Sci*. 19(8):325-30.

CAMPEAU, P. M., LENK, G. M., LU, J. T., BAE, Y., BURRAGE, L., TURNPENNY, P., ROMAN CORONA-RIVERA, J., MORANDI, L., MORA, M., REUTTER, H., VULTO-VAN SILFHOUT, A. T., FAIVRE, L., HAAN, E., GIBBS, R. A., MEISLER, M. H. & LEE, B. H. 2013. Yunis-Varon syndrome is caused by mutations in FIG4, encoding a phosphoinositide phosphatase. *American journal of human genetics*, 92, 781-91.

CAPALDI, R. A., AGGELER, R., TURINA, P. & WILKENS, S. 1994. Coupling between catalytic sites and the proton channel in F1F0-type ATPases. *Trends Biochem Sci*, 19, 284-9.

CARDAIOLI, E., MALFATTI, E., DA POZZO, P., GALLUS, G. N., CARLUCCIO, M. A., RUFA, A., VOLPI, N., DOTTI, M. T. & FEDERICO, A. 2011. Progressive mitochondrial myopathy, deafness, and sporadic seizures associated with a novel mutation in the mitochondrial tRNASer(AGY) gene. *Journal of the Neurological Sciences*, 303, 142-145.

CARRA, S., BONCORAGLIO, A., KANON, B., BRUNSTING, J. F., MINOIA, M., RANA, A., VOS, M. J., SEIDEL, K., SIBON, O. C. & KAMPINGA, H. H. 2010. Identification of the Drosophila ortholog of HSPB8: implication of HSPB8 loss of function in protein folding diseases. *J Biol Chem*, 285, 37811-22.

CARTONI, R. & MARTINOU, J. C. 2009. Role of mitofusin 2 mutations in the physiopathology of Charcot-Marie-Tooth disease type 2A. *Experimental neurology*, 218, 268-73.

CARVALHO, O. P., THORNTON, G. K., HERTECANT, J., HOULDEN, H., NICHOLAS, A. K., COX, J. J., RIELLY, M., AL-GAZALI, L. & WOODS, C. G. 2011. A novel NGF mutation clarifies the molecular mechanism and extends the phenotypic spectrum of the HSAN5 neuropathy. *Journal of Medical Genetics*, 48, 131-135.

CASSA, C. A., SAVAGE, S. K., TAYLOR, P. L., GREEN, R. C., MCGUIRE, A. L. & MANDL, K. D. 2012. Disclosing pathogenic genetic variants to research participants: quantifying an emerging ethical responsibility. *Genome research*, 22, 421-8.

CASSEREAU, J., CHEVROLLIER, A., GUEGUEN, N., DESQUIRET, V., VERNY, C., NICOLAS, G., DUBAS, F., AMATI-BONNEAU, P., REYNIER, P., BONNEAU, D. & PROCACCIO, V. 2011. Mitochondrial dysfunction and pathophysiology of Charcot-Marie-Tooth disease involving GDAP1 mutations. *Experimental neurology*, 227, 31-41.

CASTAGNA, A. E., ADDIS, J., MCINNES, R. R., CLARKE, J. T., ASHBY, P., BLASER, S. & ROBINSON, B. H. 2007. Late onset Leigh syndrome and ataxia due to a T to C mutation at bp 9,185 of mitochondrial DNA. *Am J Med Genet A*, 143A, 808-16.

CATTERALL, W.A. 2000 Structure and regulation of voltage-gated Ca₂₊ channels. *Annu. Rev. Cell Dev. Biol.* 16, 521–555.

CECCHINI, G. 2003. Function and structure of complex II of the respiratory chain. *Annu Rev Biochem*, 72, 77-109.

CERAMI, C., MARCONE, A., GALIMBERTI, D., ZAMBONI, M., FENOGLIO, C., SERPENTE, M., SCARPINI, E. & CAPPA, S. F. 2013. Novel Evidence of Phenotypical Variability in the Hexanucleotide Repeat Expansion in Chromosome 9. *J Alzheimers Dis.*

CHANCE, P. F. 2004. Genetic evaluation of inherited motor/sensory neuropathy. *Suppl Clin Neurophysiol*, 57, 228-42.

CHEN, H., DETMER, S. A., EWALD, A. J., GRIFFIN, E. E., FRASER, S. E. & CHAN, D. C. 2003. Mitofusins Mfn1 and Mfn2 coordinately regulate mitochondrial fusion and are essential for embryonic development. *J Cell Biol*, 160, 189-200.

CHEN, Y. Z., BENNETT, C. L., HUYNH, H. M., BLAIR, I. P., PULS, I., IROBI, J., DIERICK, I., ABEL, A., KENNERSON, M. L., RABIN, B. A., NICHOLSON, G. A., AUER-GRUMBACH, M., WAGNER, K., DE JONGHE, P., GRIFFIN, J. W., FISCHBECK, K. H., TIMMERMAN, V., CORNBLATH, D. R. & CHANCE, P. F. 2004. DNA/RNA helicase gene mutations in a form of juvenile amyotrophic lateral sclerosis (ALS4). *American journal of human genetics*, 74, 1128-35.

CHEN, Y. Z., HASHEMI, S. H., ANDERSON, S. K., HUANG, Y., MOREIRA, M. C., LYNCH, D. R., GLASS, I. A., CHANCE, P. F. & BENNETT, C. L. 2006. Senataxin, the yeast Sen1p orthologue: characterization of a unique protein in which recessive mutations cause ataxia and dominant mutations cause motor neuron disease. *Neurobiol Dis*, 23, 97-108.

CHIN, L. S., LEE, S. M. & LI, L. 2013. SIMPLE: A new regulator of endosomal trafficking and signaling in health and disease. *Commun Integr Biol*, 6, e24214.

CHING, G. Y. & LIEM, R. K. 1993. Assembly of type IV neuronal intermediate filaments in nonneuronal cells in the absence of preexisting cytoplasmic intermediate filaments. *J Cell Biol*, 122, 1323-35.

CHINNERY P. F. Mitochondrial Disorders Overview. 2000 Jun 8. In: PAGON, R. A., ADAM, M. P., ARDINGER, H.H., et al., editors. GeneReviews®. Seattle

(WA): University of Washington, Seattle; 1993-2014. Available from: <http://www.ncbi.nlm.nih.gov/books/NBK1224/>

CHINNERY, P.F. 2010 Mitochondrial Disorders Overview: Mitochondrial Encephalomyopathies, Mitochondrial Myopathies, Oxidative Phosphorylation Disorders, Respiratory Chain Disorders In GeneReviews [Internet], Pagon RA, Bird TD, Dolan CR, Stephens K. (Seattle: University of Washington)

CHOI, B. O., KOO, S. K., PARK, M. H., RHEE, H., YANG, S. J., CHOI, K. G., JUNG, S. C., KIM, H. S., HYUN, Y. S., NAKHRO, K., LEE, H. J., WOO, H. M. & CHUNG, K. W. 2012. Exome sequencing is an efficient tool for genetic screening of Charcot-Marie-Tooth disease. *Human mutation*, 33, 1610-5.

CHOU, T. F., TIKH, I. B., HORTA, B. A., GHOSH, B., DE ALENCASTRO, R. B. & WAGNER, C. R. 2007. Engineered monomeric human histidine triad nucleotide-binding protein 1 hydrolyzes fluorogenic acyl-adenylate and lysyl-tRNA synthetase-generated lysyl-adenylate. *J Biol Chem*, 282, 15137-47.

CHOW, C.Y., ZHANG, Y., DOWLING, J.J., JIN, N., ADAMSKA, M., SHIGA, K., SZIGETI, K., SHY, M.E., LI, J., ZHANG, X., LUPSKI, J.R., WEISMAN, L.S., MEISLER, M.H. 2007 Mutation of FIG4 causes neurodegeneration in the pale tremor mouse and patients with CMT4J. *Nature*.448(7149):68-72.

CHOW, C. Y., LANDERS, J. E., BERGREN, S. K., SAPP, P. C., GRANT, A. E., JONES, J. M., EVERETT, L., LENK, G. M., MCKENNA-YASEK, D. M., WEISMAN, L. S., FIGLEWICZ, D., BROWN, R. H. & MEISLER, M. H. 2009. Deleterious variants of FIG4, a phosphoinositide phosphatase, in patients with ALS. *American journal of human genetics*, 84, 85-8.

CIAFALONI, E., SANTORELLI, F.M., SHANSKE, S., DEONNA, T., ROULET, E., JANZER, C., PESCIA, G., DIMAURO, S. 1993 Maternally inherited Leigh syndrome. *J Pediatr*. 122, 419–22.

CLEMENT Y. CHOW, Y. Z., JAMES J. DOWLING, NATSUKO JIN, MAJA ADAMSKA,, KENSUKE SHIGA, K. S., MICHAEL E. SHY, JUN LI, XUEBAO ZHANG, JAMES R. & LUPSKI, L. S. W., AND MIRIAM H. MEISLER 2007. Mutation of FIG4 causes neurodegeneration in the pale tremor mouse and patients with CMT4J. *Nature* 448, 68-72.

CLOSE, P., HAWKES, N., CORNEZ, I., CREPPE, C., LAMBERT, C. A., ROGISTER, B., SIEBENLIST, U., MERVILLE, M. P., SLAUGENHAUPT, S. A., BOURS, V., SVEJSTRUP, J. Q. & CHARIOT, A. 2006. Transcription impairment and cell migration defects in elongator-depleted cells: implication for familial dysautonomia. *Mol Cell*, 22, 521-31.

COOK, S. A., JOHNSON, K. R., BRONSON, R. T. & DAVISSON, M. T. 1995. Neuromuscular degeneration (nmd): a mutation on mouse chromosome 19 that causes motor neuron degeneration. *Mamm Genome*, 6, 187-91.

COONROD, E. M., DURTSCHI, J. D., MARGRAF, R. L. & VOELKERDING, K. V. 2012. Developing Genome and Exome Sequencing for Candidate Gene Identification in Inherited Disorders. *Archives of pathology & laboratory medicine*.

CORDIN, O., BANROQUES, J., TANNER, N. K. & LINDER, P. 2006. The DEAD-box protein family of RNA helicases. *Gene*, 367, 17-37.

CORTI, S., LOCATELLI, F., PAPADIMITRIOU, D., DONADONI, C., DEL BO, R., CRIMI, M., BORDONI, A., FORTUNATO, F., STRAZZER, S., MENOZZI, G., SALANI, S., BRESOLIN, N. & COMI, G. P. 2006. Transplanted ALDHhiSSClo neural stem cells generate motor neurons and delay disease progression of nmd mice, an animal model of SMARD1. *Human molecular genetics*, 15, 167-87.

CORTI, S., NIZZARDO, M., NARDINI, M., DONADONI, C., SALANI, S., DEL BO, R., PAPADIMITRIOU, D., LOCATELLI, F., MEZZINA, N., GIANNI, F., BRESOLIN, N. & COMI, G. P. 2009. Motoneuron transplantation rescues the phenotype of SMARD1 (spinal muscular atrophy with respiratory distress type 1). *The Journal of neuroscience : the official journal of the Society for Neuroscience*, 29, 11761-71.

COX, G. A., MAHAFFEY, C. L. & FRANKEL, W. N. 1998. Identification of the mouse neuromuscular degeneration gene and mapping of a second site suppressor allele. *Neuron*, 21, 1327-37.

CREE, L. M., SAMUELS, D. C., DE SOUSA LOPES, S. C., RAJASIMHA, H. K., WONNAPINIJ, P., MANN, J. R., DAHL, H. H. & CHINNERY, P. F. 2008. A reduction of mitochondrial DNA molecules during embryogenesis explains the rapid segregation of genotypes. *Nature genetics*, 40, 249-54.

D'YDEWALLE, C., BENOY, V. & VAN DEN BOSCH, L. 2012. Charcot-Marie-Tooth disease: emerging mechanisms and therapies. *The international journal of biochemistry & cell biology*, 44, 1299-304.

DAHL, H.-H. 1998 Getting to the nucleus of mitochondrial disorders: identification of respiratory chain-enzyme genes causing Leigh syndrome. *Am. J. Hum. Genet.* 63, 1594-1597

DE ANDRADE, D. C., BAUDIC, S., ATTAL, N., RODRIGUES, C. L., CARAMELLI, P., LINO, A. M., MARCHIORI, P. E., OKADA, M., SCAFF, M., BOUHASSIRA, D. & TEIXEIRA, M. J. 2008. Beyond neuropathy in hereditary sensory and autonomic neuropathy type V: cognitive evaluation. *Eur J Neurol.* 15, 712-9.

DE COO, I. F., SMEETS, H. J., GABREELS, F. J., ARTS, N. & VAN OOST, B. A. 1996. Isolated case of mental retardation and ataxia due to a de novo mitochondrial T8993G mutation. *American journal of human genetics*, 58, 636-8.

DE JONGHE P., TIMMERMAN, V., CEUTERICK, C., NELIS , E., DE VRIENDT, E., LÖFGREN, A., VERCROYSEN, A., VERELLEN, C., VAN MALDERGEM, L., MARTIN, J.J., VAN BROECKHOVEN, C. 1999 The Thr124Met mutation in the peripheral myelin protein zero (MPZ) gene is associated with a clinically distinct Charcot-Marie-Tooth phenotype. *Brain : a journal of neurology* 122 (Pt 2): 281-290.

DE LIGT, J., WILLEMSEN, M. H., VAN BON, B. W., KLEEFSTRA, T., YNTEMA, H. G., KROES, T., VULTO-VAN SILFHOUT, A. T., KOOLEN, D. A., DE VRIES, P., GILISSEN, C., DEL ROSARIO, M., HOISCHEN, A., SCHEFFER, H., DE VRIES, B. B., BRUNNER, H. G., VELTMAN, J. A. & VISSERS, L. E. 2012. Diagnostic exome sequencing in persons with severe intellectual disability. *N Engl J Med*, 367, 1921-9.

DE MEIRLEIR, L. 2004. Respiratory chain complex V deficiency due to a mutation in the assembly gene ATP12. *Journal of Medical Genetics*, 41, 120-124.

DE PLANELL-SAGUER, M., SCHROEDER, D. G., RODICIO, M. C., COX, G. A. & MOURELATOS, Z. 2009. Biochemical and genetic evidence for a role of IGHMBP2 in the translational machinery. *Human molecular genetics*, 18, 2115-26.

DEJESUS-HERNANDEZ, M., MACKENZIE, IAN R., BOEVE, BRADLEY F., BOXER, ADAM L., BAKER, M., RUTHERFORD, NICOLA J., NICHOLSON, ALEXANDRA M., FINCH, NICOLE A., FLYNN, H., ADAMSON, J., KOURI, N., WOJTAS, A., SENGDY, P., HSIUNG, G.-YUEK R., KARYDAS, A., SEELEY, WILLIAM W., JOSEPHS, KEITH A., COPPOLA, G., GESCHWIND, DANIEL H., WSZOLEK, ZBIGNIEW K., FELDMAN, H., KNOPMAN, DAVID S., PETERSEN, RONALD C., MILLER, BRUCE L., DICKSON, DENNIS W., BOYLAN, KEVIN B., GRAFF-RADFORD, NEILL R. & RADEMAKERS, R. 2011. Expanded GGGGCC Hexanucleotide Repeat in Noncoding Region of C9ORF72 Causes Chromosome 9p-Linked FTD and ALS. *Neuron*, 72, 245-256.

DELAGUE, V., JACQUIER, A., HAMADOUCH, T., POITELON, Y., BAUDOT, C., BOCCACCIO, I., CHOUERY, E., CHAOUCH, M., KASSOURI, N., JABBOUR, R., GRID, D., MEGARBANE, A., HAASE, G. & LEVY, N. 2007. Mutations in FGD4 encoding the Rho GDP/GTP exchange factor FRABIN cause autosomal recessive Charcot-Marie-Tooth type 4H. *American journal of human genetics*, 81, 1-16.

DETMER, S.A., CHAN, D.C. 2007 Complementation between mouse Mfn1 and Mfn2 protects mitochondrial fusion defects caused by CMT2A disease mutations. *J Cell Biol.* 176(4):405-14.

DIB-HAJJ, S.D., TYRRELL, L., CUMMINS, T.R. 1999 Two tetrodotoxin-resistant sodium channels in human dorsal root ganglion neurons. *FEBS Lett.* 462, 117-120.

DIERS, A., KACZINSKI, M., GROHMANN, K., HUBNER, C. & STOLTENBURG-DIDINGER, G. 2005. The ultrastructure of peripheral nerve, motor end-plate and skeletal muscle in patients suffering from spinal muscular atrophy with respiratory distress type 1 (SMARD1). *Acta neuropathologica*, 110, 289-97.

DIMAUCO, S., DE VIVO, D.C. 1996 Genetic heterogeneity in Leigh syndrome. *Ann. Neurol.* 40, 5-7

DIMAUCO, S. & SCHON, E. A. 2003. Mitochondrial respiratory-chain diseases. *N Engl J Med*, 348, 2656-68.

DIVINCENZO, C., ELZINGA, C. D., MEDEIROS, A. C., KARBASSI, I., JONES, J. R., EVANS, M. C., BRAASTAD, C. D., BISHOP, C. M., JAREMKO, M.,

WANG, Z., LIAQUAT, K., HOFFMAN, C. A., YORK, M. D., BATISH, S. D., LUPSKI, J. R. & HIGGINS, J. J. 2014. The allelic spectrum of Charcot–Marie–Tooth disease in over 17,000 individuals with neuropathy. *Molecular Genetics & Genomic Medicine*, 2, 522-529.

DOMINGUEZ, E., MARAIS, T., CHATAURET, N., BENKHELIFA-ZIYYAT, S., DUQUE, S., RAVASSARD, P., CARCENAC, R., ASTORD, S., PEREIRA DE MOURA, A., VOIT, T. & BARKATS, M. 2011. Intravenous scAAV9 delivery of a codon-optimized SMN1 sequence rescues SMA mice. *Human molecular genetics*, 20, 681-93.

DONG, L., CHAPLINE, C., MOUSSEAU, B., FOWLER, L., RAMSAY, K., STEVENS, J. L. & JAKEN, S. 1995. 35H, a Sequence Isolated as a Protein Kinase C Binding Protein, Is a Novel Member of the Adducin Family. *Journal of Biological Chemistry*, 270, 25534-25540.

DRENTH, J.P., WAXMAN, S.G. 2007 Mutations in sodium-channel gene SCN9A cause a spectrum of human genetic pain disorders. *J Clin Invest.* 117, 3603-9.

DUBOURG, O., AZZEDINE, H., VERNY, C., DUROSIER, G., BIROUK, N., GOUIDER, R., SALIH, M., BOUHOUCHE, A., THIAM, A., GRID, D., MAYER, M., RUBERG, M., TAZIR, M., BRICE, A. & LEGUERN, E. 2006. Autosomal-recessive forms of demyelinating Charcot-Marie-Tooth disease. *Neuromolecular Med*, 8, 75-86.

DUQUE, S., JOUSSEMET, B., RIVIERE, C., MARAIS, T., DUBREIL, L., DOUAR, A. M., FYFE, J., MOULLIER, P., COLLE, M. A. & BARKATS, M. 2009. Intravenous administration of self-complementary AAV9 enables transgene delivery to adult motor neurons. *Mol Ther*, 17, 1187-96.

DURIEUX, A. C., PRUDHON, B., GUICHENEY, P. & BITOUN, M. 2010. Dynamin 2 and human diseases. *Journal of molecular medicine*, 88, 339-50.

DYCK, P.J. 1927. Peripheral Neuropathies. 2nd ed. Philadelphia: Saunders.

ECKART, M., GUENTHER, U.P., IDKOWIAK, J., VARON, R., GROLLE, B., BOFFI, P., VAN MALDERGEM, L., HUBNER, C., SCHUELKE, M., AND VON AU, K. 2012 The natural course of infantile spinal muscular atrophy with respiratory distress type 1 (SMARD1). *Pediatrics* 129, e148–e156.

ECHANIZ-LAGUNA, A., GHEZZI, D., CHASSAGNE, M., MAYENCON, M., PADET, S., MELCHIONDA, L., ROUVET, I., LANNES, B., BOZON, D.,

LATOUR, P., ZEVIANI, M. & MOUSSON DE CAMARET, B. 2013. SURF1 deficiency causes demyelinating Charcot-Marie-Tooth disease. *Neurology*, 81, 1523-30.

EDVARDSON, S., CINNAMON, Y., JALAS, C., SHAAG, A., MAAYAN, C., AXELROD, F. B. & ELPELEG, O. 2012. Hereditary sensory autonomic neuropathy caused by a mutation in dystonin. *Annals of neurology*, 71, 569-72.

EINARSDOTTIR, E., CARLSSON, A., MINDE, J., TOOLANEN, G., SVENSSON, O., SOLDERS, G., HOLMGREN, G., HOLMBERG, D. & HOLMBERG, M. 2004. A mutation in the nerve growth factor beta gene (NGFB) causes loss of pain perception. *Human molecular genetics*, 13, 799-805.

ENGEHOLM, M., SEKLER, J., SCHONDORF, D. C., ARORA, V., SCHITTENHELM, J., BISKUP, S., SCHELL, C. & GASSER, T. 2014. A novel mutation in LRSAM1 causes axonal Charcot-Marie-Tooth disease with dominant inheritance. *BMC Neurol*, 14, 118.

ESCHBACH, J., SINNIGER, J., BOUITBIR, J., FERGANI, A., SCHLAGOWSKI, A.-I., ZOLL, J., GENY, B., RENÉ, F., LARMET, Y., MARION, V., BALOH, R. H., HARMS, M. B., SHY, M. E., MESSADEQ, N., WEYDT, P., LOEFFLER, J.-P., LUDOLPH, A. C. & DUPUIS, L. 2013. Dynein mutations associated with hereditary motor neuropathies impair mitochondrial morphology and function with age. *Neurobiology of Disease*, 58, 220-230.

ESPINÓS, C., CALPENA, E., MARTÍNEZ-RUBIO, D., LUPO, V. 2012 Autosomal recessive Charcot-Marie-Tooth neuropathy. *Adv Exp Med Biol*. 724:61-75

EVGRAFOV, O. V., MERSIYANOVA, I., IROBI, J., VAN DEN BOSCH, L., DIERICK, I., LEUNG, C. L., SCHAGINA, O., VERPOORTEN, N., VAN IMPE, K., FEDOTOV, V., DADALI, E., AUER-GRUMBACH, M., WINDPASSINGER, C., WAGNER, K., MITROVIC, Z., HILTON-JONES, D., TALBOT, K., MARTIN, J.-J., VASSERMAN, N., TVERSKAYA, S., POLYAKOV, A., LIEM, R. K. H., GETTEMANS, J., ROBBERECHT, W., DE JONGHE, P. & TIMMERMAN, V. 2004a. Mutant small heat-shock protein 27 causes axonal Charcot-Marie-Tooth disease and distal hereditary motor neuropathy. *Nature genetics*, 36, 602-606.

EVGRAFOV, O. V., MERSIYANOVA, I., IROBI, J., VAN DEN BOSCH, L., DIERICK, I., LEUNG, C. L., SCHAGINA, O., VERPOORTEN, N., VAN IMPE, K., FEDOTOV, V., DADALI, E., AUER-GRUMBACH, M., WINDPASSINGER, C., WAGNER, K., MITROVIC, Z., HILTON-JONES, D., TALBOT, K., MARTIN, J. J., VASSERMAN, N., TVERSKAYA, S., POLYAKOV, A., LIEM, R. K., GETTEMANS, J., ROBBERECHT, W., DE JONGHE, P. & TIMMERMAN, V. 2004b. Mutant small heat-shock protein 27 causes axonal Charcot-Marie-Tooth disease and distal hereditary motor neuropathy. *Nature genetics*, 36, 602-6.

FABSITZ, R. R., MCGUIRE, A., SHARP, R. R., PUGGAL, M., BESKOW, L. M., BIESECKER, L. G., BOOKMAN, E., BURKE, W., BURCHARD, E. G., CHURCH, G., CLAYTON, E. W., ECKFELDT, J. H., FERNANDEZ, C. V., FISHER, R., FULLERTON, S. M., GABRIEL, S., GACHUPIN, F., JAMES, C., JARVIK, G. P., KITTLES, R., LEIB, J. R., O'DONNELL, C., O'ROURKE, P. P., RODRIGUEZ, L. L., SCHULLY, S. D., SHULDINER, A. R., SZE, R. K., THAKURIA, J. V., WOLF, S. M. & BURKE, G. L. 2010. Ethical and practical guidelines for reporting genetic research results to study participants: updated guidelines from a National Heart, Lung, and Blood Institute working group. *Circ Cardiovasc Genet*, 3, 574-80.

FAIRMAN-WILLIAMS, M. E., GUENTHER, U. P. & JANKOWSKY, E. 2010. SF1 and SF2 helicases: family matters. *Curr Opin Struct Biol*, 20, 313-24.

FASSIER, C., HUTT, J. A., SCHOLPP, S., LUMSDEN, A., GIROS, B., NOTHIAS, F., SCHNEIDER-MAUNOURY, S., HOUART, C. & HAZAN, J. 2010. Zebrafish atlastin controls motility and spinal motor axon architecture via inhibition of the BMP pathway. *Nat Neurosci*, 13, 1380-7.

FATO, R., BERGAMINI, C., LEONI, S., STROCCHI, P. & LENAZ, G. 2008. Generation of reactive oxygen species by mitochondrial complex I: implications in neurodegeneration. *Neurochem Res*, 33, 2487-501.

FAWCETT, K. A., MURPHY, S. M., POLKE, J. M., WRAY, S., BURCHELL, V. S., MANJI, H., QUINLIVAN, R. M., ZDEBIK, A. A., REILLY, M. M. & HOULDEN, H. 2012. Comprehensive analysis of the TRPV4 gene in a large series of inherited neuropathies and controls. *J Neurol Neurosurg Psychiatry*, 83, 1204-9.

FFECTO, F., SHI, Y., HUDA, R., MARTINA, M., SIDDIQUE, T. & DENG, H.-X. 2011a. Mutant TRPV4-mediated Toxicity Is Linked to Increased Constitutive Function in Axonal Neuropathies. *Journal of Biological Chemistry*, 286, 17281-17291.

FFECTO, F., SHI, Y., HUDA, R., MARTINA, M., SIDDIQUE, T. & DENG, H. X. 2011b. Mutant TRPV4-mediated toxicity is linked to increased constitutive function in axonal neuropathies. *Journal of Biological Chemistry*, 286, 17281-17291.

FERGUSON, C.J., LENK, G.M., MEISLER, M.H. 2009 Defective autophagy in neurons and astrocytes from mice deficient in PI(3,5)P(2) *Human molecular genetics* 18(24): 4868-4878.

FERTLEMAN, C. R., BAKER, M. D., PARKER, K. A., MOFFATT, S., ELMSLIE, F. V., ABRAHAMSEN, B., OSTMAN, J., KLUGBAUER, N., WOOD, J. N., GARDINER, R. M., REES, M. 2006 SCN9A mutations in paroxysmal extreme pain disorder: allelic variants underlie distinct channel defects and phenotypes. *Neuron* 52, 767-774.

FINK, J. K. 2013. Hereditary spastic paraplegia: clinico-pathologic features and emerging molecular mechanisms. *Acta neuropathologica*, 126, 307-28.

FISCHER, T.Z., WAXMAN, S.G. 2010 Familial pain syndromes from mutations of the NaV1.7 sodium channel. *Ann N Y Acad Sci.* 1184, 196-207.

FLANIGAN, K., GARDNER, K., ALDERSON, K., GALSTER, B., OTTERUD, B., LEPPERT, M. F., KAPLAN, C. & PTACEK, L. J. 1996. Autosomal dominant spinocerebellar ataxia with sensory axonal neuropathy (SCA4): clinical description and genetic localization to chromosome 16q22.1. *American journal of human genetics*, 59, 392-9.

FLEDRICH, R., SCHLÖTTER-WEIGEL, B., SCHNIZER, T. J., WICHERT, S. P., STASSART, R. M., MEYER ZU HORSTE, G., KLINK, A., WEISS, B. G., HAAG, U., WALTER, M. C., RAUTENSTRAUSS, B., PAULUS, W., ROSSNER, M. J. & SEREDA, M. W. 2012. A rat model of Charcot-Marie-Tooth disease 1A recapitulates disease variability and supplies biomarkers of axonal loss in patients. *Brain : a journal of neurology*, 135, 72-87.

FUJII, T., HATTORI, H., HIGUCHI, Y., TSUJI, M. & MITSUYOSHI, I. 1998. Phenotypic differences between T-->C and T-->G mutations at nt 8993 of mitochondrial DNA in Leigh syndrome. *Pediatr Neurol*, 18, 275-7.

FUKITA, Y., MIZUTA, T.R., SHIROZU, M., OZAWA, K., SHIMIZU, A., AND HONJO, T. 1993 The human S mu bp-2, a DNA-binding protein specific to the single-stranded guanine-rich sequence related to the immunoglobulin mu chain switch region. *J. Biol. Chem.* 268, 17463–17470.

FUKU, N., NISHIGAKI, Y. & TANAKA, M. 2005. [Human mitochondrial genome polymorphism database (mtSNP)]. *Tanpakushitsu Kakusan Koso*, 50, 1753-8.

GAHL, W. A., MARKELLO, T. C., TORO, C., FAJARDO, K. F., SINCAN, M., GILL, F., CARLSON-DONOHUE, H., GROPMAN, A., PIERSON, T. M., GOLAS, G., WOLFE, L., GRODEN, C., GODFREY, R., NEHREBECKY, M., WAHL, C., LANDIS, D. M., YANG, S., MADEO, A., MULLIKIN, J. C., BOERKOEL, C. F., TIFFT, C. J. & ADAMS, D. 2012. The National Institutes of Health Undiagnosed Diseases Program: insights into rare diseases. *Genetics in medicine : official journal of the American College of Medical Genetics*, 14, 51-9.

GAO, W. Q., SHINSKY, N., INGLE, G., BECK, K., ELIAS, K. A. & POWELL-BRAXTON, L. 1999. IGF-I deficient mice show reduced peripheral nerve conduction velocities and decreased axonal diameters and respond to exogenous IGF-I treatment. *J Neurobiol*, 39, 142-52.

GARDNER, K. & BENNETT, V. 1986. A new erythrocyte membrane-associated protein with calmodulin binding activity. Identification and purification. *Journal of Biological Chemistry*, 261, 1339-1348.

GENDRON, T. F., BELZIL, V. V., ZHANG, Y. J. & PETRUCELLI, L. 2014. Mechanisms of toxicity in C9FTLD/ALS. *Acta neuropathologica*, 127, 359-76.

GENTIL, B. J. & COOPER, L. 2012a. Molecular basis of axonal dysfunction and traffic impairments in CMT. *Brain Res Bull*, 88, 444-53.

GENTIL, B. J. & COOPER, L. 2012b. Molecular basis of axonal dysfunction and traffic impairments in CMT. *Brain Research Bulletin*, 88, 444-453.

GESSE, B., AUER-GRUMBACH, M., SCHIRMACHER, A., STROM, T., ZITZELSBERGER, M., RUDNIK-SCHONEBORN, S., ROHR, D., HALFTER, H., YOUNG, P. & SENDEREK, J. 2014. HSJ1-related hereditary neuropathies: Novel mutations and extended clinical spectrum. *Neurology*, 83, 1726-32.

GIJSELINCK I, V. L. T., VAN DER ZEE J, SLEEGERS K, PHILIJENS S, KLEINBERGER G, JANSSENS J, BETTENS K, VAN CAUWENBERGHE C, PERESON S, ENGELBORGH S, SIEBEN A, DE JONGHE P, VANDENBERGHE R, SANTENS P, DE BLEECKER J, MAES G, BÄUMER V, DILLEN L, JORIS G, CUIJT I, CORSMIT E, ELINCK E, VAN DONGEN J, VERMEULEN S, VAN DEN BROECK M, VAERENBERG C, MATTHEIJSENS M, PEETERS K, ROBBERECHT W, CRAS P, MARTIN JJ, DE DEYN PP, CRUTS M, VAN BROECKHOVEN C. 2011. A c9orf72 promotor repeat expansion in a flanders-belgian cohort. *Lancet Neurol*, 54-65.

GILISSEN, C., HOISCHEN, A., BRUNNER, H. G. & VELTMAN, J. A. 2012. Disease gene identification strategies for exome sequencing. *European journal of human genetics : EJHG*, 20, 490-7.

GIUDITTA, A., KAPLAN, B. B., VAN MINNEN, J., ALVAREZ, J. & KOENIG, E. 2002. Axonal and presynaptic protein synthesis: new insights into the biology of the neuron. *Trends Neurosci*, 25, 400-4.

GLATER, E. E., MEGEATH, L. J., STOWERS, R. S. & SCHWARZ, T. L. 2006a. Axonal transport of mitochondria requires milton to recruit kinesin heavy chain and is light chain independent. *The Journal of Cell Biology*, 173, 545-557.

GLATER, E. E., MEGEATH, L. J., STOWERS, R. S. & SCHWARZ, T. L. 2006b. Axonal transport of mitochondria requires milton to recruit kinesin heavy chain and is light chain independent. *J Cell Biol*, 173, 545-57.

GOMEZ-TORTOSA, E., GALLEGOS, J., GUERRERO-LOPEZ, R., MARCOS, A., GIL-NECIGA, E., SAINZ, M. J., DIAZ, A., FRANCO-MACIAS, E., TRUJILLO-TIEBAS, M. J., AYUSO, C. & PEREZ-PEREZ, J. 2013. C9ORF72 hexanucleotide expansions of 20-22 repeats are associated with frontotemporal deterioration. *Neurology*, 80, 366-70.

GONZALEZ, M., MCLAUGHLIN, H., HOULDEN, H., GUO, M., YO-TSEN, L., HADJIVASSILIOU, M., SPEZIANI, F., YANG, X. L., ANTONELLIS, A., REILLY, M. M. & ZUCHNER, S. 2013. Exome sequencing identifies a significant variant in methionyl-tRNA synthetase (MARS) in a family with late-onset CMT2. *J Neurol Neurosurg Psychiatry*, 84, 1247-9.

GRAY, J. S., BIRMINGHAM, J. M. & FENTON, J. I. 2010. Got black swimming dots in your cell culture? Identification of Achromobacter as a novel cell culture contaminant. *Biologicals*, 38, 273-7.

GREENBERG, S. A. & WALSH, R. J. 2005. Molecular diagnosis of inheritable neuromuscular disorders. Part II: Application of genetic testing in neuromuscular disease. *Muscle Nerve*, 31, 431-51.

GRIFFIN, L. B., SAKAGUCHI, R., MCGUIGAN, D., GONZALEZ, M. A., SEARBY, C., ZÜCHNER, S., HOU, Y.-M. & ANTONELLIS, A. 2014. Impaired Function is a Common Feature of Neuropathy-Associated Glycyl-tRNA Synthetase Mutations. *Human mutation*, 35, 1363-1371.

GROHMANN, K., ROSSOLL, W., KOBSAR, I., HOLTmann, B., JABLONKA, S., WESSIG, C., STOLTENBURG-DIDINGER, G., FISCHER, U., HUBNER, C., MARTINI, R. & SENDTNER, M. 2004. Characterization of Igmbp2 in motor neurons and implications for the pathomechanism in a mouse model of human spinal muscular atrophy with respiratory distress type 1 (SMARD1). *Human molecular genetics*, 13, 2031-42.

GROHMANN, K., SCHUELKE, M., DIERS, A., HOFFMANN, K., LUCKE, B., ADAMS, C., BERTINI, E., LEONHARDT-HORTI, H., MUNTONI, F., OUVRIER, R., PFEUFER, A., ROSSI, R., VAN MALDERGEM, L., WILMSHURST, J. M., WIENKER, T. F., SENDTNER, M., RUDNIK-SCHÖNEBORN, S., ZERRES, K. & HUBNER, C. 2001. Mutations in the gene encoding immunoglobulin mu-binding protein 2 cause spinal muscular atrophy with respiratory distress type 1. *Nature genetics*, 29, 75-7.

GROHMANN K, V. R., STOLZ P, SCHUELKE M, JANETZKI C, BERTINI E, BUSHBY K, MUNTONI F, OUVRIER R, VAN MALDERGEM L, GOEMANS NM, LOCHMÜLLER H, EICHHOLZ S, ADAMS C, BOSCH F, GRATTAN-SMITH P, NAVARRO C, NEITZEL H, POLSTER T, TOPALOĞLU H, STEGLICH C, GUENTHER UP, ZERRES K, RUDNIK-SCHÖNEBORN S, HÜBNER C. 2003. Infantile spinal muscular atrophy with respiratory distress Type 1. *Ann Neurol.*, 719-724.

GROHMANN, K., WIENKER, T.F., SAAR, K., RUDNIK-SCHÖNEBORN, S., STOLTENBURG-DIDINGER, G., ROSSI, R., NOVELLI, G., NÜRNBERG, G., PFEUFER, A., WIRTH, B., REIS, A., ZERRES, K., HÜBNER, C. 1999 Diaphragmatic spinal muscular atrophy with respiratory distress is

heterogeneous, and one form is linked to chromosome 11q13-q21. *Am J Hum Genet.* 65(5):1459-62.

GUENTHER, U. P., HANDOKO, L., LAGGERBAUER, B., JABLONKA, S., CHARI, A., ALZHEIMER, M., OHMER, J., PLOTTNER, O., GEHRING, N., SICKMANN, A., VON AU, K., SCHUELKE, M. & FISCHER, U. 2009a. IGHMBP2 is a ribosome-associated helicase inactive in the neuromuscular disorder distal SMA type 1 (DSMA1). *Human molecular genetics*, 18, 1288-300.

GUENTHER, U. P., HANDOKO, L., VARON, R., STEPHANI, U., TSAO, C. Y., MENDELL, J. R., LUTZKENDORF, S., HUBNER, C., VON AU, K., JABLONKA, S., DITTMAR, G., HEINEMANN, U., SCHUETZ, A. & SCHUELKE, M. 2009b. Clinical variability in distal spinal muscular atrophy type 1 (DSMA1): determination of steady-state IGHMBP2 protein levels in five patients with infantile and juvenile disease. *Journal of molecular medicine*, 87, 31-41.

GUENTHER, U. P., VARON, R., SCHLICKE, M., DUTRANNOY, V., VOLK, A., HUBNER, C., VON AU, K. & SCHUELKE, M. 2007. Clinical and mutational profile in spinal muscular atrophy with respiratory distress (SMARD): defining novel phenotypes through hierarchical cluster analysis. *Human mutation*, 28, 808-15.

GUERNSEY, D. L., JIANG, H., BEDARD, K., EVANS, S. C., FERGUSON, M., MATSUOKA, M., MACGILLIVRAY, C., NIGHTINGALE, M., PERRY, S., RIDEOUT, A. L., ORR, A., LUDMAN, M., SKIDMORE, D. L., BENSTEAD, T. & SAMUELS, M. E. 2010. Mutation in the gene encoding ubiquitin ligase LRSAM1 in patients with Charcot-Marie-Tooth disease. *PLoS genetics*, 6.

HAFEZPARAST, M., KLOCKE, R., RUHRBERG, C., MARQUARDT, A., AHMAD-ANNUAR, A., BOWEN, S., LALLI, G., WITHERDEN, A. S., HUMMERICH, H., NICHOLSON, S., MORGAN, P. J., OOZAGEER, R., PRIESTLEY, J. V., AVERILL, S., KING, V. R., BALL, S., PETERS, J., TODA, T., YAMAMOTO, A., HIRAOKA, Y., AUGUSTIN, M., KORTHAUS, D., WATTERL, S., WABNITZ, P., DICKNEITE, C., LAMPEL, S., BOEHME, F., PERAUS, G., POPP, A., RUDELIUS, M., SCHLEGEL, J., FUCHS, H., HRABE DE ANGELIS, M., SCHIAVO, G.,

SHIMA, D. T., RUSS, A. P., STUMM, G., MARTIN, J. E. & FISHER, E. M. 2003. Mutations in dynein link motor neuron degeneration to defects in retrograde transport. *Science*, 300, 808-12.

HARDING, A. E. & THOMAS, P. K. 1980. Hereditary distal spinal muscular atrophy. A report on 34 cases and a review of the literature. *J Neurol Sci*, 45, 337-48.

HARDING, A. E. AND P. K. THOMAS 1980 The clinical features of hereditary motor and sensory neuropathy types I and II *Brain : a journal of neurology* 103(2): 259-280.

HARDING, A. E. AND P. K. THOMAS 1980 Genetic aspects of hereditary motor and sensory neuropathy (types I and II) *J Med Genet* 17(5): 329-336.

HARMS, M. B., ORI-MCKENNEY, K. M., SCOTO, M., TUCK, E. P., BELL, S., MA, D., MASI, S., ALLRED, P., AL-LOZI, M., REILLY, M. M., MILLER, L. J., JANI-ACSADI, A., PESTRONK, A., SHY, M. E., MUNTONI, F., VALLEE, R. B. & BALOH, R. H. 2012. Mutations in the tail domain of DYNC1H1 cause dominant spinal muscular atrophy. *Neurology*, 78, 1714-1720.

HATTORI, N., YAMAMOTO, M., YOSHIHARA, T., KOIKE, H., NAKAGAWA, M., YOSHIKAWA, H., OHNISHI, A., HAYASAKA, K., ONODERA, O., BABA, M., YASUDA, H., SAITO, T., NAKASHIMA, K., KIRA, J., KAJI, R., OKA, N. & SOBUE, G. 2003. Demyelinating and axonal features of Charcot-Marie-Tooth disease with mutations of myelin-related proteins (PMP22, MPZ and Cx32): a clinicopathological study of 205 Japanese patients. *Brain : a journal of neurology*, 126, 134-51.

HERRMANN, D. N. 2008. Experimental therapeutics in hereditary neuropathies: the past, the present, and the future. *Neurotherapeutics*, 5, 507-15.

HIROKAWA, N. & TAKEMURA, R. 2005. Molecular motors and mechanisms of directional transport in neurons. *Nature reviews. Neuroscience*, 6, 201-14.

HIRST, J., SAHLENDER, D. A., LI, S., LUBBEN, N. B., BORNER, G. H. & ROBINSON, M. S. 2008. Auxilin depletion causes self-assembly of clathrin into membraneless cages in vivo. *Traffic*, 9, 1354-71.

HOLLENBECK, P. J. & SAXTON, W. M. 2005. The axonal transport of mitochondria. *J Cell Sci*, 118, 5411-9.

HOLMGREN, A., BOUHY, D., DE WINTER, V., ASSELBERGH, B., TIMMERMANS, J. P., IROBI, J. & TIMMERMAN, V. 2013. Charcot-Marie-Tooth causing HSPB1 mutations increase Cdk5-mediated phosphorylation of neurofilaments. *Acta neuropathologica*, 126, 93-108.

HOLT, I. J., HARDING, A. E., PETTY, R. K. & MORGAN-HUGHES, J. A. 1990. A new mitochondrial disease associated with mitochondrial DNA heteroplasmy. *American journal of human genetics*, 46, 428-33.

HOULDEN, H., KING, R., BLAKE, J., GROVES, M., LOVE, S., WOODWARD, C., HAMMANS, S., NICOLL, J., LENNOX, G., O'DONOVAN, D. G., GABRIEL, C., THOMAS, P. K. & REILLY, M. M. 2006. Clinical, pathological and genetic characterization of hereditary sensory and autonomic neuropathy type 1 (HSAN I). *Brain : a journal of neurology*, 129, 411-25.

HOULDEN, H., LAURA, M., GINSBERG, L., JUNGBLUTH, H., ROBB, S. A., BLAKE, J., ROBINSON, S., KING, R. H. & REILLY, M. M. 2009a. The phenotype of Charcot-Marie-Tooth disease type 4C due to SH3TC2 mutations and possible predisposition to an inflammatory neuropathy. *Neuromuscular disorders : NMD*, 19, 264-9.

HOULDEN, H., LAURA, M., GINSBERG, L., JUNGBLUTH, H., ROBB, S. A., BLAKE, J., ROBINSON, S., KING, R. H. M. & REILLY, M. M. 2009b. The phenotype of Charcot-Marie-Tooth disease type 4C due to SH3TC2 mutations and possible predisposition to an inflammatory neuropathy. *Neuromuscular Disorders*, 19, 264-269.

HOULDEN, H., LAURA, M., WAVRANT-DE VRIEZE, F., BLAKE, J., WOOD, N. & REILLY, M. M. 2008. Mutations in the HSP27 (HSPB1) gene cause dominant, recessive, and sporadic distal HMN/CMT type 2. *Neurology*, 71, 1660-8.

HOULDEN, H. & REILLY, M. M. 2006. Molecular genetics of autosomal-dominant demyelinating Charcot-Marie-Tooth disease. *Neuromolecular Med*, 8, 43-62.

HOUSTEK, J., MRACEK, T., VOJTEJKOVA, A. & ZEMAN, J. 2004. Mitochondrial diseases and ATPase defects of nuclear origin. *Biochimica et biophysica acta*, 1658, 115-21.

HOUSTEK, J., PICKOVA, A., VOJTIŠKOVA, A., MRACEK, T., PECINA, P. & JESINA, P. 2006. Mitochondrial diseases and genetic defects of ATP synthase. *Biochimica et biophysica acta*, 1757, 1400-5.

HUA, Y., SAHASHI, K., RIGO, F., HUNG, G., HOREV, G., BENNETT, C. F. & KRAINER, A. R. 2011. Peripheral SMN restoration is essential for long-term rescue of a severe spinal muscular atrophy mouse model. *Nature*, 478, 123-6.

HUBBARD, J.I. (1974). *The peripheral nervous system*. Plenum Press. p. vii. ISBN 978-0-306-30764-5.

HUBER, N., GUIMARAES, S., SCHRADER, M., SUTER, U. & NIEMANN, A. 2013. Charcot-Marie-Tooth disease-associated mutants of GDAP1 dissociate its roles in peroxisomal and mitochondrial fission. *EMBO Rep*, 14, 545-52.

HUGHES, C. A. & BENNETT, V. 1995. Adducin: a Physical Model with Implications for Function in Assembly of Spectrin-Actin Complexes. *Journal of Biological Chemistry*, 270, 18990-18996.

HUTTNER, I. G., KENNERSON, M. L., REDDEL, S. W., RADOVANOVIC, D. & NICHOLSON, G. A. 2006. Proof of genetic heterogeneity in X-linked Charcot-Marie-Tooth disease. *Neurology*, 67, 2016-21.

INDO, Y. 2002. Genetics of congenital insensitivity to pain with anhidrosis (CIPA) or hereditary sensory and autonomic neuropathy type IV. Clinical, biological and molecular aspects of mutations in TRKA(NTRK1) gene encoding the receptor tyrosine kinase for nerve growth factor. *Clin Auton Res*, 12 Suppl 1, I20-32.

INGMAN, M. & GYLLENSTEN, U. 2006. mtDB: Human Mitochondrial Genome Database, a resource for population genetics and medical sciences. *Nucleic Acids Res*, 34, D749-51.

IONASESCU, V. V., TROFATTER, J., HAINES, J. L., SUMMERS, A. M., IONASESCU, R. & SEARBY, C. 1991. Heterogeneity in X-linked recessive Charcot-Marie-Tooth neuropathy. *American journal of human genetics*, 48, 1075-83.

IROBI, J., DE JONGHE, P. & TIMMERMAN, V. 2004. Molecular genetics of distal hereditary motor neuropathies. *Human molecular genetics*, 13 Spec No 2, R195-202.

IROBI, J., DIERICK, I., JORDANOVA, A., CLAEYS, K. G., DE JONGHE, P. & TIMMERMAN, V. 2006. Unraveling the genetics of distal hereditary motor neuronopathies. *Neuromolecular Med*, 8, 131-46.

IROBI, J., HOLMGREN, A., DE WINTER, V., ASSELBERGH, B., GETTEMANS, J., ADRIAENSEN, D., CEUTERICK-DE GROOTE, C., VAN COSTER, R., DE JONGHE, P. & TIMMERMAN, V. 2012. Mutant HSPB8 causes protein aggregates and a reduced mitochondrial membrane potential in dermal fibroblasts from distal hereditary motor neuropathy patients. *Neuromuscular disorders : NMD*, 22, 699-711.

ISHIURA, H., SAKO, W., YOSHIDA, M., KAWARAI, T., TANABE, O., GOTO, J., TAKAHASHI, Y., DATE, H., MITSUI, J., AHSAN, B., ICHIKAWA, Y., IWATA, A., YOSHINO, H., IZUMI, Y., FUJITA, K., MAEDA, K., GOTO, S., KOIZUMI, H., MORIGAKI, R., IKEMURA, M., YAMAUCHI, N., MURAYAMA, S., NICHOLSON, G. A., ITO, H., SOBUE, G., NAKAGAWA, M., KAJI, R. & TSUJI, S. 2012. The TRK-fused gene is mutated in hereditary motor and sensory neuropathy with proximal dominant involvement. *American journal of human genetics*, 91, 320-9.

ITO, D., FUJISAWA, T., IIDA, H. & SUZUKI, N. 2008. Characterization of seipin/BSCL2, a protein associated with spastic paraplegia 17. *Neurobiology of Disease*, 31, 266-277.

IYER, S., XIAO, E., ALSAYEGH, K., EROSHENKO, N., RIGGS, M. J., BENNETT, J. P., JR. & RAO, R. R. 2012. Mitochondrial gene replacement in human pluripotent stem cell-derived neural progenitors. *Gene therapy*, 19, 469-75.

JABLONKA, S., HOLTMANN, B., SENDTNER, M. & METZGER, F. 2011. Therapeutic effects of PEGylated insulin-like growth factor I in the pmn mouse model of motoneuron disease. *Experimental neurology*, 232, 261-9.

JANKOWSKY, E. 2011. RNA helicases at work: binding and rearranging. *Trends Biochem Sci*, 36, 19-29.

JANSSEN, R. J., VAN DEN HEUVEL, L. P. & SMEITINK, J. A. 2004. Genetic defects in the oxidative phosphorylation (OXPHOS) system. *Expert Rev Mol Diagn*, 4, 143-56.

JEDRZEJOWSKA, M., MADEJ-PILARCZYK, A., FIDZIANSKA, A., MIERZEWSKA, H., PRONICKA, E., OBERSZTYN, E., GOS, M.,

PRONICKI, M., KMIEC, T., MIGDAL, M., MIERZEWSKA-SCHMIDT, M., WALCZAK-WOJKOWSKA, I., KONOPKA, E. & HAUSMANOWA-PETRUSEWICZ, I. 2014. Severe phenotypes of SMARD1 associated with novel mutations of the IGHMBP2 gene and nuclear degeneration of muscle and Schwann cells. *Eur J Paediatr Neurol*, 18, 183-92.

JOHNSTON, J. J., RUBINSTEIN, W. S., FACIO, F. M., NG, D., SINGH, L. N., TEER, J. K., MULLIKIN, J. C. & BIESECKER, L. G. 2012. Secondary variants in individuals undergoing exome sequencing: screening of 572 individuals identifies high-penetrance mutations in cancer-susceptibility genes. *American journal of human genetics*, 91, 97-108.

JONCKHEERE, A. I., SMEITINK, J. A. & RODENBURG, R. J. 2012. Mitochondrial ATP synthase: architecture, function and pathology. *Journal of inherited metabolic disease*, 35, 211-25.

JONES, J. M., ALBIN, R. L., FELDMAN, E. L., SIMIN, K., SCHUSTER, T. G., DUNNICK, W. A., COLLINS, J. T., CHRISP, C. E., TAYLOR, B. A. & MEISLER, M. H. 1993. mnd2: a new mouse model of inherited motor neuron disease. *Genomics*, 16, 669-77.

JORDANOVA, A., DE JONGHE, P., BOERKOEL, C. F., TAKASHIMA, H., DE VRIENDT, E., CEUTERICK, C., MARTIN, J. J., BUTLER, I. J., MANCIAS, P., PAPASOZOMENOS, S., TERESPOLSKY, D., POTOCKI, L., BROWN, C. W., SHY, M., RITA, D. A., TOURNEV, I., KREMENSKY, I., LUPSKI, J. R. & TIMMERMAN, V. 2003. Mutations in the neurofilament light chain gene (NEFL) cause early onset severe Charcot-Marie-Tooth disease. *Brain : a journal of neurology*, 126, 590-7.

JORDANOVA, A., IROBI, J., THOMAS, F. P., VAN DIJCK, P., MEERSCHAERT, K., DEWIL, M., DIERICK, I., JACOBS, A., DE VRIENDT, E., GUERGUELTCHEVA, V., RAO, C. V., TOURNEV, I., GONDIM, F. A., D'HOOGHE, M., VAN GERWEN, V., CALLAERTS, P., VAN DEN BOSCH, L., TIMMERMANS, J. P., ROBBERECHT, W., GETTEMANS, J., THEVELEIN, J. M., DE JONGHE, P., KREMENSKY, I. & TIMMERMAN, V. 2006. Disrupted function and axonal distribution of mutant tyrosyl-tRNA synthetase in dominant intermediate Charcot-Marie-Tooth neuropathy. *Nature genetics*, 38, 197-202.

JOSEPH, S., ROBB, S. A., MOHAMMED, S., LILLIS, S., SIMONDS, A., MANZUR, A. Y., WALTER, S. & WRAIGE, E. 2009. Interfamilial phenotypic heterogeneity in SMARD1. *Neuromuscular disorders : NMD*, 19, 193-5.

KACHHAP, S. K., FAITH, D., QIAN, D. Z., SHABBEER, S., GALLOWAY, N. L., PILI, R., DENMEADE, S. R., DEMARZO, A. M. & CARDUCCI, M. A. 2007. The N-Myc Down Regulated Gene1 (NDRG1) Is a Rab4a Effector Involved in Vesicular Recycling of E-Cadherin. *PLoS One*, 2, e844.

KANEKO, M., SATTA, Y., MATSUURA, E.T., CHIGUSA, S.I. 1993 Evolution of the mitochondrial ATPase 6 gene in Drosophila: Unusually high level of polymorphism in *D. melanogaster*. *Genet Res* 61, 195–204.

KAINDL, A. M., GUENTHER, U. P., RUDNIK-SCHONEBORN, S., VARON, R., ZERRES, K., SCHUELKE, M., HUBNER, C. & VON AU, K. 2008. Spinal muscular atrophy with respiratory distress type 1 (SMARD1). *J Child Neurol*, 23, 199-204.

KARBOWSKI, M. & NEUTZNER, A. 2012. Neurodegeneration as a consequence of failed mitochondrial maintenance. *Acta neuropathologica*, 123, 157-71.

KARDON, J. R. & VALE, R. D. 2009. Regulators of the cytoplasmic dynein motor. *Nat Rev Mol Cell Biol*, 10, 854-65.

KENNERSON, M. L., NICHOLSON, G. A., KALER, S. G., KOWALSKI, B., MERCER, J. F., TANG, J., LLANOS, R. M., CHU, S., TAKATA, R. I., SPECK-MARTINS, C. E., BAETS, J., ALMEIDA-SOUZA, L., FISCHER, D., TIMMERMAN, V., TAYLOR, P. E., SCHERER, S. S., FERGUSON, T. A., BIRD, T. D., DE JONGHE, P., FEELY, S. M., SHY, M. E. & GARBERN, J. Y. 2010. Missense mutations in the copper transporter gene ATP7A cause X-linked distal hereditary motor neuropathy. *American journal of human genetics*, 86, 343-52.

KENNERSON, M. L., YIU, E. M., CHUANG, D. T., KIDAMBI, A., TSO, S. C., LY, C., CHAUDHRY, R., DREW, A. P., RANCE, G., DELATYCKI, M. B., ZUCHNER, S., RYAN, M. M. & NICHOLSON, G. A. 2013. A new locus for X-linked dominant Charcot-Marie-Tooth disease (CMTX6) is caused by mutations in the pyruvate dehydrogenase kinase isoenzyme 3 (PDK3) gene. *Human molecular genetics*, 22, 1404-16.

KHWAJA, O. S., HO, E., BARNES, K. V., O'LEARY, H. M., PEREIRA, L. M., FINKELSTEIN, Y., NELSON, C. A., VOGEL-FARLEY, V., DEGREGORIO, G., HOLM, I. A., KHATWA, U., KAPUR, K., ALEXANDER, M. E., FINNEGAN, D. M., CANTWELL, N. G., WALCO, A. C., RAPPAPORT, L., GREGAS, M., FICHOPOVA, R. N., SHANNON, M. W., SUR, M. & KAUFMANN, W. E. 2014. Safety, pharmacokinetics, and preliminary assessment of efficacy of mecasermin (recombinant human IGF-1) for the treatment of Rett syndrome. *Proceedings of the National Academy of Sciences*, 111, 4596-4601.

KIJIMA, K., NUMAKURA, C., GOTO, T., TAKAHASHI, T., OTAGIRI, T., UMETSU, K. & HAYASAKA, K. 2005. Small heat shock protein 27 mutation in a Japanese patient with distal hereditary motor neuropathy. *J Hum Genet*, 50, 473-6.

KIM, H. J., SOHN, K. M., SHY, M. E., KRAJEWSKI, K. M., HWANG, M., PARK, J. H., JANG, S. Y., WON, H. H., CHOI, B. O., HONG, S. H., KIM, B. J., SUH, Y. L., KI, C. S., LEE, S. Y., KIM, S. H. & KIM, J. W. 2007. Mutations in PRPS1, which encodes the phosphoribosyl pyrophosphate synthetase enzyme critical for nucleotide biosynthesis, cause hereditary peripheral neuropathy with hearing loss and optic neuropathy (cmtx5). *American journal of human genetics*, 81, 552-8.

KIMURA, K., FUKATA, Y., MATSUOKA, Y., BENNETT, V., MATSUURA, Y., OKAWA, K., IWAMATSU, A. & KAIBUCHI, K. 1998. Regulation of the Association of Adducin with Actin Filaments by Rho-associated Kinase (Rho-kinase) and Myosin Phosphatase. *Journal of Biological Chemistry*, 273, 5542-5548.

KITTLER, J. T., THOMAS, P., TRETTER, V., BOGDANOV, Y. D., HAUCKE, V., SMART, T. G. & MOSS, S. J. 2004. Huntington-associated protein 1 regulates inhibitory synaptic transmission by modulating gamma-aminobutyric acid type A receptor membrane trafficking. *Proc Natl Acad Sci U S A*, 101, 12736-41.

KLEIN, C. J., DUAN, X. & SHY, M. E. 2013a. Inherited neuropathies: Clinical overview and update. *Muscle & Nerve*, 48, 604-622.

KLEIN, C. J., WU, Y., KILFOYLE, D. H., SANDRONI, P., DAVIS, M. D., GAVRILOVA, R. H., LOW, P. A. & DYCK, P. J. 2013b. Infrequent SCN9A

mutations in congenital insensitivity to pain and erythromelalgia. *J Neurol Neurosurg Psychiatry*, 84, 386-91.

KLUCKOVA, K., BEZAWORK-GELETA, A., ROHLENA, J., DONG, L. & NEUZIL, J. 2013. Mitochondrial complex II, a novel target for anti-cancer agents. *Biochimica et biophysica acta*, 1827, 552-64.

KOCHANSKI, A. 2004. Mutations in the Myelin Protein Zero result in a spectrum of Charcot-Marie-Tooth phenotypes. *Acta Myol*, 23, 6-9.

KOENE, S., SMEITINK, J. 2011 Mitochondrial medicine. *J Inherit Metab Dis*. 34(2):247-8.

KOK, C., KENNERTON, M. L., SPRING, P. J., ING, A. J., POLLARD, J. D. & NICHOLSON, G. A. 2003. A Locus for Hereditary Sensory Neuropathy with Cough and Gastroesophageal Reflux on Chromosome 3p22-p24. *The American Journal of Human Genetics*, 73, 632-637.

KOLB, S. J., SNYDER, P. J., POI, E. J., RENARD, E. A., BARTLETT, A., GU, S., SUTTON, S., ARNOLD, W. D., FREIMER, M. L., LAWSON, V. H., KISSEL, J. T. & PRIOR, T. W. 2010. Mutant small heat shock protein B3 causes motor neuropathy: utility of a candidate gene approach. *Neurology*, 74, 502-6.

KOROBOVA, F., RAMABHADRAN, V. & HIGGS, H. N. 2013. An actin-dependent step in mitochondrial fission mediated by the ER-associated formin INF2. *Science*, 339, 464-7.

KRIEGER, F., ELFLEIN, N., SAENGER, S., WIRTHGEN, E., RAK, K., FRANTZ, S., HOEFLICH, A., TOYKA, K. V., METZGER, F. & JABLONKA, S. 2014a. Polyethylene glycol-coupled IGF1 delays motor function defects in a mouse model of spinal muscular atrophy with respiratory distress type 1. *Brain : a journal of neurology*.

KRIEGER, F., ELFLEIN, N., SAENGER, S., WIRTHGEN, E., RAK, K., FRANTZ, S., HOEFLICH, A., TOYKA, K. V., METZGER, F. & JABLONKA, S. 2014b. Polyethylene glycol-coupled IGF1 delays motor function defects in a mouse model of spinal muscular atrophy with respiratory distress type 1. *Brain : a journal of neurology*, 137, 1374-93.

KRIEGER, F., METZGER, F. & JABLONKA, S. 2014c. Differentiation defects in primary motoneurons from a SMARD1 mouse model that are insensitive to treatment with low dose PEGylated IGF1. *Rare Dis*, 2, e29415.

KRUER, M. C., JEPPESON, T., DUTTA, S., STEINER, R. D., COTTENIE, E., SANFORD, L., MERKENS, M., RUSSMAN, B. S., BLASCO, P. A., FAN, G., POLLOCK, J., GREEN, S., WOLTJER, R. L., MOONEY, C., KRETZSCHMAR, D., PAISAN-RUIZ, C. & HOULDEN, H. 2013. Mutations in gamma adducin are associated with inherited cerebral palsy. *Annals of neurology*, 74, 805-14.

KU, C. S., COOPER, D. N., POLYCHRONAKOS, C., NAIDOO, N., WU, M. & SOONG, R. 2012. Exome sequencing: dual role as a discovery and diagnostic tool. *Annals of neurology*, 71, 5-14.

KUCHARCZYK, R., RAK, M. & DI RAGO, J. P. 2009a. Biochemical consequences in yeast of the human mitochondrial DNA 8993T>C mutation in the ATPase6 gene found in NARP/MILS patients. *Biochimica et biophysica acta*, 1793, 817-24.

KUCHARCZYK, R., ZICK, M., BIETENHADER, M., RAK, M., COUPLAN, E., BLONDEL, M., CAUBET, S. D. & DI RAGO, J. P. 2009b. Mitochondrial ATP synthase disorders: molecular mechanisms and the quest for curative therapeutic approaches. *Biochimica et biophysica acta*, 1793, 186-99.

LACERDA, A. F., HARTJES, E. & BRUNETTI, C. R. 2014. LITAF mutations associated with Charcot-Marie-Tooth disease 1C show mislocalization from the late endosome/lysosome to the mitochondria. *PLoS One*, 9, e103454.

LAMPERT, A., O'REILLY, A.O., REEH, P., LEFFLER, A. 2010 Sodium channelopathies and pain. *Pflugers Arch.* 460, 249-63.

LARIVIERE, R. C. & JULIEN, J. P. 2004. Functions of intermediate filaments in neuronal development and disease. *J Neurobiol*, 58, 131-48.

LAŠŠUTHOVÁ, P., BROŽKOVÁ, D.Š., KRŮTOVÁ, M., NEUPAUEROVÁ, J., HABERLOVÁ, J., MAZANEC, R., DVORÁČKOVÁ, N., GOLDENBERG, Z., SEEMAN, P. 2015 Mutations in HINT1 are one of the most frequent causes of hereditary neuropathy among Czech patients and neuromyotonia is rather an underdiagnosed symptom. *Neurogenetics* 16(1):43-54.

LATOUR, P., THAUVIN-ROBINET, C., BAUDELET-MERY, C., SOICHOT, P., CUSIN, V., FAIVRE, L., LOCATELLI, M. C., MAYENCON, M., SARCEY, A., BROUSSOLLE, E., CAMU, W., DAVID, A. & ROUSSON, R. 2010. A major determinant for binding and aminoacylation of tRNA(Ala) in cytoplasmic Alanyl-tRNA synthetase is mutated in dominant axonal

Charcot-Marie-Tooth disease. *American journal of human genetics*, 86, 77-82.

LAX, N.Z., TURNBULL, D.M., REEVE, A.K. 2011 Mitochondrial mutations: newly discovered players in neuronal degeneration. *Neuroscientist* 17(6):645-58.

LEAL, A., HUEHNE, K., BAUER, F., STICHT, H., BERGER, P., SUTER, U., MORERA, B., VALLE, G., LUPSKI, J., EKICI, A., PASUTTO, F., ENDELE, S., BARRANTES, R., BERGHOFF, C., BERGHOFF, M., NEUNDÖRFER, B., HEUSS, D., DORN, T., YOUNG, P., SANTOLIN, L., UHLMANN, T., MEISTERERNST, M., SEREDA, M., ZU HORSTE, G., NAVÉ, K.-A., REIS, A. & RAUTENSTRAUSS, B. 2009. Identification of the variant Ala335Val of MED25 as responsible for CMT2B2: molecular data, functional studies of the SH3 recognition motif and correlation between wild-type MED25 and PMP22 RNA levels in CMT1A animal models. *neurogenetics*, 10, 275-287.

LEBLANC, S. E., JANG, S. W., WARD, R. M., WRABETZ, L. & SVAREN, J. 2006. Direct regulation of myelin protein zero expression by the Egr2 transactivator. *J Biol Chem*, 281, 5453-60.

LEE, J. W., BEEBE, K., NANGLE, L. A., JANG, J., LONGO-GUESS, C. M., COOK, S. A., DAVISSON, M. T., SUNDBERG, J. P., SCHIMMEL, P. & ACKERMAN, S. L. 2006. Editing-defective tRNA synthetase causes protein misfolding and neurodegeneration. *Nature*, 443, 50-5.

LEE, M. K., MARSZALEK, J. R. & CLEVELAND, D. W. 1994. A mutant neurofilament subunit causes massive, selective motor neuron death: implications for the pathogenesis of human motor neuron disease. *Neuron*, 13, 975-88.

LEE, S. M., CHIN, L. S. & LI, L. 2012. Charcot-Marie-Tooth disease-linked protein SIMPLE functions with the ESCRT machinery in endosomal trafficking. *J Cell Biol*, 199, 799-816.

LENAZ, G., BARACCA, A., CARELLI, V., D'AURELIO, M., SGARBI, G. & SOLAINI, G. 2004. Bioenergetics of mitochondrial diseases associated with mtDNA mutations. *Biochimica et biophysica acta*, 1658, 89-94.

LENAZ, G., FATO, R., GENOVA, M. L., BERGAMINI, C., BIANCHI, C. & BIONDI, A. 2006. Mitochondrial Complex I: structural and functional aspects. *Biochimica et biophysica acta*, 1757, 1406-20.

LENK, G. M., FERGUSON, C. J., CHOW, C. Y., JIN, N., JONES, J. M., GRANT, A. E., ZOLOV, S. N., WINTERS, J. J., GIGER, R. J., DOWLING, J. J., WEISMAN, L. S. & MEISLER, M. H. 2011. Pathogenic mechanism of the FIG4 mutation responsible for Charcot-Marie-Tooth disease CMT4J. *PLoS genetics*, 7, e1002104.

LERER, I., SAGI, M., MEINER, V., COHEN, T., ZLOTOGORA, J. & ABELIOVICH, D. 2005. Deletion of the ANKRD15 gene at 9p24.3 causes parent-of-origin-dependent inheritance of familial cerebral palsy. *Human molecular genetics*, 14, 3911-20.

LESAGE, S., LE BER, I., CONDROYER, C., BROUSSOLLE, E., GABELLE, A., THOBOIS, S., PASQUIER, F., MONDON, K., DION, P. A., ROCHEFORT, D., ROULEAU, G. A., DURR, A. & BRICE, A. 2013. C9orf72 repeat expansions are a rare genetic cause of parkinsonism. *Brain : a journal of neurology*, 136, 385-91.

LEVY, J. R., SUMNER, C. J., CAVISTON, J. P., TOKITO, M. K., RANGANATHAN, S., LIGON, L. A., WALLACE, K. E., LAMONTE, B. H., HARMISON, G. G., PULS, I., FISCHBECK, K. H. & HOLZBAUR, E. L. F. 2006. A motor neuron disease-associated mutation in p150Glued perturbs dynactin function and induces protein aggregation. *The Journal of Cell Biology*, 172, 733-745.

LI, D. Q., NAIR, S. S. & KUMAR, R. 2013a. The MORC family: new epigenetic regulators of transcription and DNA damage response. *Epigenetics*, 8, 685-93.

LI, J. 2012. Inherited neuropathies. *Seminars in neurology*, 32, 204-14.

LI, J., PARKER, B., MARTYN, C., NATARAJAN, C. & GUO, J. 2013b. The PMP22 gene and its related diseases. *Mol Neurobiol*, 47, 673-98.

LI, L., LORENZO, P. S., BOGI, K., BLUMBERG, P. M. & YUSPA, S. H. 1999. Protein kinase C δ targets mitochondria, alters mitochondrial membrane potential, and induces apoptosis in normal and neoplastic keratinocytes when overexpressed by an adenoviral vector. *Mol Cell Biol*, 19, 8547-58.

LI, S., TIAB, L., JIAO, X., MUNIER, F. L., ZOGRAFOS, L., FRUEH, B. E., SERGEEV, Y., SMITH, J., RUBIN, B., MEALLET, M. A., FORSTER, R. K., HEJTMANCIK, J. F. & SCHORDERET, D. F. 2005. Mutations in PIP5K3 are associated with Francois-Neetens mouchetee fleck corneal dystrophy. *American journal of human genetics*, 77, 54-63.

LI, J., PARKER, B., MARTYN, C., NATARAJAN, C., GUO, J. 2013 The PMP22 gene and its related diseases *Mol Neurobiol* 47(2): 673-698.

LIEPINSH, E., LEONCHIKS, A., SHARIPO, A., GUIGNARD, L. & OTTING, G. 2003. Solution structure of the R3H domain from human Smubp-2. *J Mol Biol*, 326, 217-23.

LIM, S.C., BOWLER, M.W., LAI, T.F., AND SONG, H. 2012. The Ighmbp2 helicase structure reveals the molecular basis for disease-causing mutations in DMSA1. *Nucleic Acids Res.* 40,11009–11022.

LIN, M. T. & BEAL, M. F. 2006. Mitochondrial dysfunction and oxidative stress in neurodegenerative diseases. *Nature*, 443, 787-795.

LINDQUIST, S. G., DUNO, M., BATBAYLI, M., PUSCHMANN, A., BRAENDGAARD, H., MARDOSIENE, S., SVENSTRUP, K., PINBORG, L. H., VESTERGAARD, K., HJERMIND, L. E., STOKHOLM, J., ANDERSEN, B. B., JOHANNSEN, P. & NIELSEN, J. E. 2013. Corticobasal and ataxia syndromes widen the spectrum of C9ORF72 hexanucleotide expansion disease. *Clin Genet*, 83, 279-83.

LIU, C. Y. & KAUFMAN, R. J. 2003. The unfolded protein response. *J Cell Sci*, 116, 1861-2.

LIU, X., DOBBIE, M., TUNNINGLEY, R., WHITTLE, B., ZHANG, Y., ITTNER, L. M. & GOTZ, J. 2011. ENU mutagenesis screen to establish motor phenotypes in wild-type mice and modifiers of a pre-existing motor phenotype in tau mutant mice. *J Biomed Biotechnol*, 2011, 130947.

LIU, Y. T., LAURA, M., HERSHESON, J., HORGAN, A., JAUNMUKTANE, Z., BRANDNER, S., PITTMAN, A., HUGHES, D., POLKE, J. M., SWEENEY, M. G., PROUKAKIS, C., JANSSEN, J. C., AUER-GRUMBACH, M., ZUCHNER, S., SHIELDS, K. G., REILLY, M. M. & HOULDEN, H. 2014. Extended phenotypic spectrum of KIF5A mutations: From spastic paraparesis to axonal neuropathy. *Neurology*, 83, 612-9.

LLORCA, O., MARTIN-BENITO, J., RITCO-VONSOVICI, M., GRANTHAM, J., HYNES, G. M., WILLISON, K. R., CARRASCOSA, J. L. & VALPUESTA, J. M. 2000. Eukaryotic chaperonin CCT stabilizes actin and tubulin folding intermediates in open quasi-native conformations. *EMBO J*, 19, 5971-9.

LOISEAU, D., CHEVROLLIER, A., VERNY, C., GUILLET, V., GUEGUEN, N., DE CRESCENZO, M. A. P., FERRÉ, M., MALINGE, M. C., GUICHET, A., NICOLAS, G., AMATI-BONNEAU, P., MALTHIÈRY, Y., BONNEAU, D. & REYNIER, P. 2007. Mitochondrial coupling defect in Charcot-Marie-Tooth type 2A disease. *Annals of neurology*, 61, 315-323.

LOWE, S. L., WONG, S. H. & HONG, W. 1996. The mammalian ARF-like protein 1 (Arl1) is associated with the Golgi complex. *J Cell Sci*, 109 (Pt 1), 209-20.

LUPSKI, J. R., WISE, C. A., KUWANO, A., PENTAO, L., PARKE, J. T., GLAZE, D. G., LEDBETTER, D. H., GREENBERG, F. & PATEL, P. I. 1992. Gene dosage is a mechanism for Charcot-Marie-Tooth disease type 1A. *Nature genetics*, 1, 29-33.

LYON, G. J. & WANG, K. 2012. Identifying disease mutations in genomic medicine settings: current challenges and how to accelerate progress. *Genome medicine*, 4, 58.

MACASKILL, A. F., BRICKLEY, K., STEPHENSON, F. A. & KITTLER, J. T. 2009. GTPase dependent recruitment of Grif-1 by Miro1 regulates mitochondrial trafficking in hippocampal neurons. *Mol Cell Neurosci*, 40, 301-12.

MAJANDER, A., LAMMINEN, T., JUVONEN, V., AULA, P., NIKOSKELAINEN, E., SAVONTAUS, M.-L. & WIKSTRÖM, M. 1997. Mutations in subunit 6 of the F1F0-ATP synthase cause two entirely different diseases. *FEBS Letters*, 412, 351-354.

MAJID, A., TALAT, K., COLIN, L., CAROLINE, R., HELEN, K. & CHRISTIAN DE, G. 2012. Heterogeneity in spinal muscular atrophy with respiratory distress type 1. *J Pediatr Neurosci*, 7, 197-9.

MAJUMDER, P. K., MISHRA, N. C., SUN, X., BHARTI, A., KHARBANDA, S., SAXENA, S. & KUFE, D. 2001. Targeting of protein kinase C delta to mitochondria in the oxidative stress response. *Cell Growth Differ*, 12, 465-70.

MANDELL, F., FOLKMAN, J., MATSUMOTO, S. 1977 Erythromelalgia. *Pediatrics* 59, 45-48.

MARTIN-JIMENEZ, R., MARTIN-HERNANDEZ, E., CABELLO, A., GARCIA-SILVA, M. T., ARENAS, J. & CAMPOS, Y. 2012. Clinical and cellular consequences of the mutation m.12300G>A in the mitochondrial tRNA(Leu(CUN)) gene. *Mitochondrion*, 12, 288-93.

MARTIN, N., JAUBERT, J., GOUNON, P., SALIDO, E., HAASE, G., SZATANIK, M. & GUENET, J. L. 2002. A missense mutation in Tbce causes progressive motor neuronopathy in mice. *Nature genetics*, 32, 443-7.

MATHIS, S., CORCIA, P., TAZIR, M., CAMU, W., MAGDELAINE, C., LATOUR, P., BIBERON, J., GUENNO, A. M., RICHARD, L., MAGY, L., FUNALOT, B. & VALLAT, J. M. 2014. Peripheral myelin protein 22 gene duplication with atypical presentations: a new example of the wide spectrum of Charcot-Marie-Tooth 1A disease. *Neuromuscular disorders : NMD*, 24, 524-8.

MAYR, J. A., HAVLICKOVA, V., ZIMMERMANN, F., MAGLER, I., KAPLANOVA, V., JESINA, P., PECINOVA, A., NUSKOVA, H., KOCH, J., SPERL, W. & HOUSTEK, J. 2010. Mitochondrial ATP synthase deficiency due to a mutation in the ATP5E gene for the F1 epsilon subunit. *Human molecular genetics*, 19, 3430-9.

MAYSTADT, I., ZARHRATE, M., LANDRIEU, P., BOESPFLUG-TANGUY, O., SUKNO, S., COLLIGNON, P., MELKI, J., VERELLEN-DUMOULIN, C., MUNNICH, A. & VIOLET, L. 2004. Allelic heterogeneity of SMARD1 at the IGHMBP2 locus. *Human mutation*, 23, 525-6.

MCCARTNEY, A. J., ZHANG, Y. & WEISMAN, L. S. 2014. Phosphatidylinositol 3,5-bisphosphate: low abundance, high significance. *Bioessays*, 36, 52-64.

MCLAUGHLIN, H. M., SAKAGUCHI, R., GIBLIN, W., WILSON, T. E., BIESECKER, L., LUPSKI, J. R., TALBOT, K., VANCE, J. M., ZUCHNER, S., LEE, Y. C., KENNISON, M., HOU, Y. M., NICHOLSON, G. & ANTONELLIS, A. 2012. A recurrent loss-of-function alanyl-tRNA synthetase (AARS) mutation in patients with Charcot-Marie-Tooth disease type 2N (CMT2N). *Human mutation*, 33, 244-53.

MCLAUGHLIN, H. M., SAKAGUCHI, R., LIU, C., IGARASHI, T., PEHLIVAN, D., CHU, K., IYER, R., CRUZ, P., CHERUKURI, P. F., HANSEN, N. F.,

MULLIKIN, J. C., BIESECKER, L. G., WILSON, T. E., IONASESCU, V., NICHOLSON, G., SEARBY, C., TALBOT, K., VANCE, J. M., ZUCHNER, S., SZIGETI, K., LUPSKI, J. R., HOU, Y. M., GREEN, E. D. & ANTONELLIS, A. 2010. Compound heterozygosity for loss-of-function lysyl-tRNA synthetase mutations in a patient with peripheral neuropathy. *American journal of human genetics*, 87, 560-6.

MEHLEN, P., PREVILLE, X., CHAREYRON, P., BRIOLAY, J., KLEMENZ, R. & ARRIGO, A. P. 1995. Constitutive expression of human hsp27, Drosophila hsp27, or human alpha B-crystallin confers resistance to TNF- and oxidative stress-induced cytotoxicity in stably transfected murine L929 fibroblasts. *J Immunol*, 154, 363-74.

MELLINS, R.B., HAYS, A.P., GOLD, A.P., BERDON, W.E., BOWDLER, J.D. 1974 Respiratory distress as the initial manifestation of Werdnig-Hoffmann disease. *Pediatrics*. 53(1):33-40.

MENEZES, M. P., WADDELL, L., LENK, G. M., KAUR, S., MACARTHUR, D. G., MEISLER, M. H. & CLARKE, N. F. 2014. Whole exome sequencing identifies three recessive FIG4 mutations in an apparently dominant pedigree with Charcot-Marie-Tooth disease. *Neuromuscular disorders : NMD*.

MERSIYANOVA, I. V., PEREPELOV, A. V., POLYAKOV, A. V., SITNIKOV, V. F., DADALI, E. L., OPARIN, R. B., PETRIN, A. N. & EVGRAFOV, O. V. 2000. A new variant of Charcot-Marie-Tooth disease type 2 is probably the result of a mutation in the neurofilament-light gene. *American journal of human genetics*, 67, 37-46.

MESSINA, M.F., MESSINA, S., GAETA, M., RODOLICO, C., SALPIETRO, DAMIANO, A.M., LOMBARDO, F., FRISAFULLI, G., AND DE LUCA, F. 2012 Infantile spinal muscular atrophy with respiratory distress type I (SMARD 1): an atypical phenotype and review of the literature. *Eur J Paediatr Neurol*. 16, 90–94.

MEYER, S. G., WENDT, A. E., SCHERER, M., LIEBISCH, G., KERKweg, U., SCHMITZ, G. & DE GROOT, H. 2012. Myriocin, an inhibitor of serine palmitoyl transferase, impairs the uptake of transferrin and low-density lipoprotein in mammalian cells. *Archives of biochemistry and biophysics*, 526, 60-8.

MICHELL, A. W., LAURA, M., BLAKE, J., LUNN, M. P., COX, A., GIBBONS, V. S., DAVIS, M. B., WOOD, N. W., MANJI, H., HOULDEN, H., MURRAY, N. M. F. & REILLY, M. M. 2009. GJB1 gene mutations in suspected inflammatory demyelinating neuropathies not responding to treatment. *Journal of Neurology, Neurosurgery & Psychiatry*, 80, 699-700.

MICHELS, J. J., ABELS, J., STEKETEE, J., VAN VLIET, H. H. D. M., VUZEVSKI, V. D. 1985 Erythromelalgia caused by platelet-mediated arteriolar inflammation and thrombosis in thrombocythemia. *Ann. Intern. Med.* 102, 466-471

MILLECAMPUS, S., BOILLÉE, S., LE BER, I., SEILHEAN, D., TEYSSOU, E., GIRAudeau, M., MOIGNEU, C., VANDENBERGHE, N., DANELLBRUNAUD, V., CORCIA, P. et al 2012 Phenotype difference between ALS patients with expanded repeats in C9ORF72 and patients with mutations in other ALS-related genes. *J Med Genet.* 49(4):258-63.

MILONE, M. & BENARROCH, E. E. 2012. Mitochondrial dynamics: general concepts and clinical implications. *Neurology*, 78, 1612-9.

MILTENBERGER-MILTENYI, G., JANECKE, A. R., WANSCHITZ, J. V., TIMMERMAN, V., WINDPASSINGER, C., AUER-GRUMBACH, M. & LOSCHER, W. N. 2007. Clinical and electrophysiological features in Charcot-Marie-Tooth disease with mutations in the NEFL gene. *Arch Neurol*, 64, 966-70.

MISKO, A., JIANG, S., WEGORZEWSKA, I., MILBRANDT, J. & BALOH, R. H. 2010. Mitofusin 2 is necessary for transport of axonal mitochondria and interacts with the Miro/Milton complex. *The Journal of neuroscience : the official journal of the Society for Neuroscience*, 30, 4232-40.

MISKO, A. L., SASAKI, Y., TUCK, E., MILBRANDT, J. & BALOH, R. H. 2012. Mitofusin2 mutations disrupt axonal mitochondrial positioning and promote axon degeneration. *The Journal of neuroscience : the official journal of the Society for Neuroscience*, 32, 4145-55.

MIYATA, Y. 1983. A new mutant mouse with motor neuron disease. *Brain Res*, 312, 139-42.

MOLNAR, G. M., CROZAT, A., KRAEFT, S. K., DOU, Q. P., CHEN, L. B. & PARDEE, A. B. 1997. Association of the mammalian helicase MAH with the pre-mRNA splicing complex. *Proc Natl Acad Sci U S A*, 94, 7831-6.

MORTIMER, S. A., KIDWELL, M. A. & DOUDNA, J. A. 2014. Insights into RNA structure and function from genome-wide studies. *Nature reviews. Genetics*.

MOTIL, J., DUBEY, M., CHAN, W. K. & SHEA, T. B. 2007. Inhibition of dynein but not kinesin induces aberrant focal accumulation of neurofilaments within axonal neurites. *Brain Res*, 1164, 125-31.

MRACEK, T., PECINA, P., VOJTIŠKOVA, A., KALOUS, M., SEBESTA, O. & HOUSTEK, J. 2006. Two components in pathogenic mechanism of mitochondrial ATPase deficiency: energy deprivation and ROS production. *Experimental gerontology*, 41, 683-7.

MURPHY, S.M., LAURA, M., FAWCETT, K., PANDRAUD, A., LIU, Y.T., DAVIDSON, G.L., ROSSOR, A.M., POLKE, J.M., CASTLEMAN, V., MANJI, H. et al. 2012 Charcot-Marie-Tooth disease: frequency of genetic subtypes and guidelines for genetic testing. *J Neurol Neurosurg Psychiatry* 83(7):706-10.

NAKAGAWA, M. & TAKASHIMA, H. 2003. [Molecular mechanisms of hereditary neuropathy: genotype-phenotype correlation]. *Rinsho Byori*, 51, 536-43.

NAKAGAWA, M. & TAKASHIMA, H. 2004. [Update on hereditary neuropathy]. *Rinsho Shinkeigaku*, 44, 991-4.

NARAYANAN, U. G. 2012. Management of children with ambulatory cerebral palsy: an evidence-based review. *J Pediatr Orthop*, 32 Suppl 2, S172-81.

NAVE, K.A., SEREDA, M.W., EHRENREICH, H. 2007 Mechanisms of disease: inherited demyelinating neuropathies--from basic to clinical research. *Nat Clin Pract Neurol*. Aug;3(8):453-64.

NEED, A. C., SHASHI, V., HITOMI, Y., SCHOCH, K., SHIANKA, K. V., MCDONALD, M. T., MEISLER, M. H. & GOLDSTEIN, D. B. 2012. Clinical application of exome sequencing in undiagnosed genetic conditions. *J Med Genet*, 49, 353-61.

NELIS, E., VAN BROECKHOVEN, C., DE JONGHE, P., LOFGREN, A., VANDENBERGHE, A., LATOUR, P., LE GUERN, E., BRICE, A., MOSTACCIUOLO, M. L., SCHIAVON, F., PALAU, F., BORT, S., UPADHYAYA, M., ROCCHI, M., ARCHIDIACONO, N., MANDICH, P., BELLONE, E., SILANDER, K., SAVONTAUS, M. L., NAVON, R., GOLDBERG-STERN, H., ESTIVILL, X., VOLPINI, V., FRIEDL, W.,

GAL, A. & ET AL. 1996. Estimation of the mutation frequencies in Charcot-Marie-Tooth disease type 1 and hereditary neuropathy with liability to pressure palsies: a European collaborative study. *European journal of human genetics : EJHG*, 4, 25-33.

NEVELING, K., MARTINEZ-CARRERA, L. A., HOLKER, I., HEISTER, A., VERRIPS, A., HOSSEINI-BARKOOIE, S. M., GILISSEN, C., VERMEER, S., PENNINGS, M., MEIJER, R., TE RIELE, M., FRIJNS, C. J., SUCHOWERSKY, O., MACLAREN, L., RUDNIK-SCHONEBORN, S., SINKE, R. J., ZERRES, K., LOWRY, R. B., LEMMINK, H. H., GARBES, L., VELTMAN, J. A., SCHELHAAS, H. J., SCHEFFER, H. & WIRTH, B. 2013. Mutations in BICD2, which encodes a golgin and important motor adaptor, cause congenital autosomal-dominant spinal muscular atrophy. *American journal of human genetics*, 92, 946-54.

NICHOLSON, G., LENK, G. M., REDDEL, S. W., GRANT, A. E., TOWNE, C. F., FERGUSON, C. J., SIMPSON, E., SCHEUERLE, A., YASICK, M., HOFFMAN, S., BLOUIN, R., BRANDT, C., COPPOLA, G., BIESECKER, L. G., BATISH, S. D. & MEISLER, M. H. 2011. Distinctive genetic and clinical features of CMT4J: a severe neuropathy caused by mutations in the PI(3,5)P(2) phosphatase FIG4. *Brain : a journal of neurology*, 134, 1959-71.

NICHOLSON, G. A., MAGDELAINE, C., ZHU, D., GREW, S., RYAN, M. M., STURTZ, F., VALLAT, J. M. & OUVRIER, R. A. 2008. Severe early-onset axonal neuropathy with homozygous and compound heterozygous MFN2 mutations. *Neurology*, 70, 1678-81.

NICOLAOU, P., CIANCHETTI, C., MINAIDOU, A., MARROSU, G., ZAMBA-PAPANICOLAOU, E., MIDDLETON, L. & CHRISTODOULOU, K. 2013. A novel LRSAM1 mutation is associated with autosomal dominant axonal Charcot-Marie-Tooth disease. *European journal of human genetics : EJHG*, 21, 190-4.

NIEMANN, A., BERGER, P. & SUTER, U. 2006. Pathomechanisms of mutant proteins in Charcot-Marie-Tooth disease. *NeuroMolecular Medicine*, 8, 217-241.

NIEMANN, A., HUBER, N., WAGNER, K. M., SOMANDIN, C., HORN, M., LEBRUN-JULIEN, F., ANGST, B., PEREIRA, J. A., HALFTER, H., WELZL, H., FELTRI, M. L., WRABETZ, L., YOUNG, P., WESSIG, C.,

TOYKA, K. V. & SUTER, U. 2014. The Gdap1 knockout mouse mechanistically links redox control to Charcot-Marie-Tooth disease. *Brain : a journal of neurology*, 137, 668-82.

NIEMANN, A., RUEGG, M., LA PADULA, V., SCHENONE, A. & SUTER, U. 2005. Ganglioside-induced differentiation associated protein 1 is a regulator of the mitochondrial network: new implications for Charcot-Marie-Tooth disease. *J Cell Biol*, 170, 1067-78.

NIEMANN, A., WAGNER, K. M., RUEGG, M. & SUTER, U. 2009. GDAP1 mutations differ in their effects on mitochondrial dynamics and apoptosis depending on the mode of inheritance. *Neurobiol Dis*, 36, 509-20.

NIJTMANS, L. G., KLEMENT, P., HOUSTEK, J. & VAN DEN BOGERT, C. 1995. Assembly of mitochondrial ATP synthase in cultured human cells: implications for mitochondrial diseases. *Biochimica et biophysica acta*, 1272, 190-8.

NOJI, H. & YOSHIDA, M. 2001. The rotary machine in the cell, ATP synthase. *J Biol Chem*, 276, 1665-8.

NOVARINO, G., FENSTERMAKER, A. G., ZAKI, M. S., HOFREE, M., SILHAVY, J. L., HEIBERG, A. D., ABDELLATEEF, M., ROSTI, B., SCOTT, E., MANSOUR, L., MASRI, A., KAYSERILI, H., AL-AAMA, J. Y., ABDEL-SALAM, G. M., KARMINEJAD, A., KARA, M., KARA, B., BOZORGMEHRI, B., BEN-OMRAN, T., MOJAHEDI, F., MAHMOUD, I. G., BOUSLAM, N., BOUHOUCHE, A., BENOMAR, A., HANEIN, S., RAYMOND, L., FORLANI, S., MASCARO, M., SELIM, L., SHEHATA, N., AL-ALLAWI, N., BINDU, P. S., AZAM, M., GUNEL, M., CAGLAYAN, A., BILGUVAR, K., TOLUN, A., ISSA, M. Y., SCHROTH, J., SPENCER, E. G., ROSTI, R. O., AKIZU, N., VAUX, K. K., JOHANSEN, A., KOH, A. A., MEGAHEDE, H., DURR, A., BRICE, A., STEVANIN, G., GABRIEL, S. B., IDEKER, T. & GLEESON, J. G. 2014. Exome sequencing links corticospinal motor neuron disease to common neurodegenerative disorders. *Science*, 343, 506-11.

OATES, E. C., ROSSOR, A. M., HAFEZPARAST, M., GONZALEZ, M., SPEZIANI, F., MACARTHUR, D. G., LEK, M., COTTERIE, E., SCOTO, M., FOLEY, A. R., HURLES, M., HOULDEN, H., GREENSMITH, L., AUER-GRUMBACH, M., PIEBER, T. R., STROM, T. M., SCHULE, R.,

HERRMANN, D. N., SOWDEN, J. E., ACSADI, G., MENEZES, M. P., CLARKE, N. F., ZUCHNER, S., MUNTONI, F., NORTH, K. N. & REILLY, M. M. 2013. Mutations in BICD2 cause dominant congenital spinal muscular atrophy and hereditary spastic paraplegia. *American journal of human genetics*, 92, 965-73.

ODDING, E., ROEBROECK, M. E. & STAM, H. J. 2006. The epidemiology of cerebral palsy: incidence, impairments and risk factors. *Disabil Rehabil*, 28, 183-91.

OGILVIE, I. & CAPALDI, R. A. 1999. Mutation of the mitochondrial encoded ATPase 6 gene modeled in the ATP synthase of *Escherichia coli*. *FEBS Lett*, 453, 179-82.

ORI-MCKENNEY, K. M., XU, J., GROSS, S. P. & VALLEE, R. B. 2010. A cytoplasmic dynein tail mutation impairs motor processivity. *Nat Cell Biol*, 12, 1228-34.

ORIGONE, P., VERDIANI, S., CIOTTI, P., GULLI, R., BELLONE, E., MARCHESE, R., ABBRUZZESE, G. & MANDICH, P. 2013. Enlarging the clinical spectrum associated with C9orf 72 repeat expansions: findings in an Italian cohort of patients with parkinsonian syndromes and relevance for genetic counselling. *Amyotroph Lateral Scler Frontotemporal Degener*, 14, 479-80.

PALAU, F., ESTELA, A., PLA-MARTIN, D. & SANCHEZ-PIRIS, M. 2009. The role of mitochondrial network dynamics in the pathogenesis of Charcot-Marie-Tooth disease. *Adv Exp Med Biol*, 652, 129-37.

PARK, E., KIM, J. M., PRIMACK, B., WEINSTOCK, D. M., MOREAU, L. A., PARMAR, K. & D'ANDREA, A. D. 2013. Inactivation of Uaf1 causes defective homologous recombination and early embryonic lethality in mice. *Mol Cell Biol*, 33, 4360-70.

PARK, H. J., KIM, H. J., HONG, Y. B., NAM, S. H., CHUNG, K. W. & CHOI, B. O. 2014. A novel INF2 mutation in a Korean family with autosomal dominant intermediate Charcot-Marie-Tooth disease and focal segmental glomerulosclerosis. *J Peripher Nerv Syst*.

PARK, J., LEE, B. S., CHOI, J. K., MEANS, R. E., CHOE, J. & JUNG, J. U. 2002. Herpesviral protein targets a cellular WD repeat endosomal protein to downregulate T lymphocyte receptor expression. *Immunity*, 17, 221-33.

PATEL, K. P., O'BRIEN, T. W., SUBRAMONY, S. H., SHUSTER, J. & STACPOOLE, P. W. 2012. The spectrum of pyruvate dehydrogenase complex deficiency: clinical, biochemical and genetic features in 371 patients. *Mol Genet Metab*, 106, 385-94.

PATZKÓ, Á. & SHY, M. 2011. Update on Charcot-Marie-Tooth Disease. *Current Neurology and Neuroscience Reports*, 11, 78-88.

PEARN, J. & HUDGSON, P. 1979. Distal spinal muscular atrophy. A clinical and genetic study of 8 kindreds. *J Neurol Sci*, 43, 183-91.

PEETERS, K., LITVINENKO, I., ASSELBERGH, B., ALMEIDA-SOUZA, L., CHAMOVA, T., GEUENS, T., YDENS, E., ZIMON, M., IROBI, J., DE VRIENDT, E., DE WINTER, V., OOMS, T., TIMMERMANS, V., TOURNEV, I. & JORDANOVA, A. 2013. Molecular defects in the motor adaptor BICD2 cause proximal spinal muscular atrophy with autosomal-dominant inheritance. *American journal of human genetics*, 92, 955-64.

PEREZ-OLLE, R., JONES, S. T. & LIEM, R. K. 2004. Phenotypic analysis of neurofilament light gene mutations linked to Charcot-Marie-Tooth disease in cell culture models. *Human molecular genetics*, 13, 2207-20.

PERNG, M. D., CAIRNS, L., VAN DEN, I. P., PRESCOTT, A., HUTCHESON, A. M. & QUINLAN, R. A. 1999. Intermediate filament interactions can be altered by HSP27 and alphaB-crystallin. *J Cell Sci*, 112 (Pt 13), 2099-112.

PIERSON, T. M., TART, G., ADAMS, D., TORO, C., GOLAS, G., TIFFT, C. & GAHL, W. 2011. Infantile-onset spinal muscular atrophy with respiratory distress-1 diagnosed in a 20-year-old man. *Neuromuscular disorders : NMD*, 21, 353-5.

PITCEATHLY, R. D., MURPHY, S. M., COTTENIE, E., CHALASANI, A., SWEENEY, M. G., WOODWARD, C., MUDANOHWOO, E. E., HARGREAVES, I., HEALES, S., LAND, J., HOLTON, J. L., HOULDEN, H., BLAKE, J., CHAMPION, M., FLINTER, F., ROBB, S. A., PAGE, R., ROSE, M., PALACE, J., CROWE, C., LONGMAN, C., LUNN, M. P., RAHMAN, S., REILLY, M. M. & HANNA, M. G. 2012. Genetic dysfunction of MT-ATP6 causes axonal Charcot-Marie-Tooth disease. *Neurology*, 79, 1145-54.

PITT, M., HOULDEN, H., JACOBS, J., MOK, Q., HARDING, B., REILLY, M. & SURTEES, R. 2003. Severe infantile neuropathy with diaphragmatic

weakness and its relationship to SMARD1. *Brain : a journal of neurology*, 126, 2682-92.

PLA-MARTÍN, D., RUEDA, C. B., ESTELA, A., SÁNCHEZ-PIRIS, M., GONZÁLEZ-SÁNCHEZ, P., TRABA, J., DE LA FUENTE, S., SCORRANO, L., RENAU-PIQUERAS, J., ALVAREZ, J., SATRÚSTEGUI, J. & PALAU, F. 2013. Silencing of the Charcot-Marie-Tooth disease-associated gene GDAP1 induces abnormal mitochondrial distribution and affects Ca^{2+} homeostasis by reducing store-operated Ca^{2+} entry. *Neurobiology of Disease*, 55, 140-151.

POLKE, J. M., LAURA, M., PAREYSON, D., TARONI, F., MILANI, M., BERGAMIN, G., GIBBONS, V. S., HOULDEN, H., CHAMLEY, S. C., BLAKE, J., DEVILE, C., SANDFORD, R., SWEENEY, M. G., DAVIS, M. B. & REILLY, M. M. 2011. Recessive axonal Charcot-Marie-Tooth disease due to compound heterozygous mitofusin 2 mutations. *Neurology*, 77, 168-73.

PULS, I., JONNAKUTY, C., LAMONTE, B. H., HOLZBAUR, E. L., TOKITO, M., MANN, E., FLOETER, M. K., BIDUS, K., DRAYNA, D., OH, S. J., BROWN, R. H., JR., LUDLOW, C. L. & FISCHBECK, K. H. 2003. Mutant dynactin in motor neuron disease. *Nature genetics*, 33, 455-6.

PULS, I., OH, S. J., SUMNER, C. J., WALLACE, K. E., FLOETER, M. K., MANN, E. A., KENNEDY, W. R., WENDELSCHAFFER-CRABB, G., VORTMEYER, A., POWERS, R., FINNEGAN, K., HOLZBAUR, E. L., FISCHBECK, K. H. & LUDLOW, C. L. 2005. Distal spinal and bulbar muscular atrophy caused by dynactin mutation. *Annals of neurology*, 57, 687-94.

PURCELL, S., NEALE, B., TODD-BROWN, K., THOMAS, L., FERREIRA, M. A., BENDER, D., MALLER, J., SKLAR, P., DE BAKKER, P. I., DALY, M. J. & SHAM, P. C. 2007. PLINK: a tool set for whole-genome association and population-based linkage analyses. *American journal of human genetics*, 81, 559-75.

RAEYMAEKERS, P., TIMMERMAN, V., NELIS, E., DE JONGHE, P., HOOGENDIJK, J. E., BAAS, F., BARKER, D. F., MARTIN, J. J., DE VISSER, M., BOLHUIS, P. A. & ET AL. 1991. Duplication in chromosome

17p11.2 in Charcot-Marie-Tooth neuropathy type 1a (CMT 1a). The HMSN Collaborative Research Group. *Neuromuscular disorders : NMD*, 1, 93-7.

RAFFAN, E. & SEMPLE, R. K. 2011. Next generation sequencing--implications for clinical practice. *British medical bulletin*, 99, 53-71.

RAHMAN, S., BLOK, R. B., DAHL, H. H., DANKS, D. M., KIRBY, D. M., CHOW, C. W., CHRISTODOULOU, J. & THORBURN, D. R. 1996. Leigh syndrome: clinical features and biochemical and DNA abnormalities. *Annals of neurology*, 39, 343-51.

RATTI, A., CORRADO, L., CASTELLOTTI, B., DEL BO, R., FOGH, I., CEREDA, C., TILOCA, C., D'ASCENZO, C., BAGAROTTI, A., PENSATO, V., RANIERI, M., GAGLIARDI, S., CALINI, D., MAZZINI, L., TARONI, F., CORTI, S., CERONI, M., OGGIONI, G. D., LIN, K., POWELL, J. F., SORARU, G., TICOZZI, N., COMI, G. P., D'ALFONSO, S., GELLERA, C. & SILANI, V. 2012. C9ORF72 repeat expansion in a large Italian ALS cohort: evidence of a founder effect. *Neurobiology of aging*, 33, 2528 e7-14.

REILLY, M. M. 2007a. Sorting out the inherited neuropathies 93-105.

REILLY, M. M. 2007b. Sorting out the inherited neuropathies. *Practical Neurology*, 7, 93-105.

REILLY, M. M., MURPHY, S. M. & LAURÁ, M. 2011. Charcot-Marie-Tooth disease. *Journal of the Peripheral Nervous System*, 16, 1-14.

REILLY, M.M., MURPHY, S.M., LAURÁ, M. 2011 Charcot-Marie-Tooth disease *Journal of the Peripheral Nervous System* 16(1): 1-14.

RENGANATHAN, M., CUMMINS, T.R., AND WAXMAN, S.G. 2001 Contribution of Na(v)1.8 sodium channels to action potential electrogenesis in DRG neurons. *J. Neurophysiol.* 86, 629–640.

RENTON, A. E., MAJOUNIE, E., WAITE, A., SIMON-SANCHEZ, J., ROLLINSON, S., GIBBS, J. R., SCHYMICK, J. C., LAAKSOVIRTA, H., VAN SWIETEN, J. C., MYLLYKANGAS, L., KALIMO, H., PAETAU, A., ABRAMZON, Y., REMES, A. M., KAGANOVICH, A., SCHOLZ, S. W., DUCKWORTH, J., DING, J., HARMER, D. W., HERNANDEZ, D. G., JOHNSON, J. O., MOK, K., RYTEN, M., TRABZUNI, D., GUERREIRO, R. J., ORRELL, R. W., NEAL, J., MURRAY, A., PEARSON, J., JANSEN, I. E., SONDERVAN, D., SEELAAR, H., BLAKE, D., YOUNG, K.,

HALLIWELL, N., CALLISTER, J. B., TOULSON, G., RICHARDSON, A., GERHARD, A., SNOWDEN, J., MANN, D., NEARY, D., NALLS, M. A., PEURALINNA, T., JANSSON, L., ISOVIITA, V. M., KAIVORINNE, A. L., HOLTTA-VUORI, M., IKONEN, E., SULKAVA, R., BENATAR, M., WUU, J., CHIO, A., RESTAGNO, G., BORGHERO, G., SABATELLI, M., HECKERMAN, D., ROGAEVA, E., ZINMAN, L., ROTHSTEIN, J. D., SENDTNER, M., DREPPER, C., EICHLER, E. E., ALKAN, C., ABDULLAEV, Z., PACK, S. D., DUTRA, A., PAK, E., HARDY, J., SINGLETON, A., WILLIAMS, N. M., HEUTINK, P., PICKERING-BROWN, S., MORRIS, H. R., TIENARI, P. J. & TRAYNOR, B. J. 2011. A hexanucleotide repeat expansion in C9ORF72 is the cause of chromosome 9p21-linked ALS-FTD. *Neuron*, 72, 257-68.

RINALDI, C., GRUNSEICH, C., SEVRIOUKOVA, I.F., SCHINDLER, A., HORKAYNE-SZAKALY, I., LAMPERTI, C., LANDOURÉ, G., KENNERTON, M.L., BURNETT, B.G., BÖNNEMANN, C et al. 2012 Cowchock syndrome is associated with a mutation in apoptosis-inducing factor. *Am J Hum Genet*. 91(6):1095-102.

RIVIÈRE, J.-B., RAMALINGAM, S., LAVASTRE, V., SHEKARABI, M., HOLBERT, S., LAFONTAINE, J., SROUR, M., MERNER, N., ROCHEFORT, D., HINCE, P., GAUDET, R., MES-MASSON, A.-M., BAETS, J., HOULDEN, H., BRAIS, B., NICHOLSON, GARTH A., VAN ESCH, H., NAFISSI, S., DE JONGHE, P., REILLY, MARY M., TIMMERMAN, V., DION, PATRICK A. & ROULEAU, GUY A. 2011. KIF1A, an Axonal Transporter of Synaptic Vesicles, Is Mutated in Hereditary Sensory and Autonomic Neuropathy Type 2. *The American Journal of Human Genetics*, 89, 219-230.

RIZZA, T., VAZQUEZ-MEMIJE, M. E., MESCHINI, M. C., BIANCHI, M., TOZZI, G., NESTI, C., PIEMONTE, F., BERTINI, E., SANTORELLI, F. M. & CARROZZO, R. 2009. Assaying ATP synthesis in cultured cells: a valuable tool for the diagnosis of patients with mitochondrial disorders. *Biochemical and biophysical research communications*, 383, 58-62.

ROBERTS, R. C., PEDEN, A. A., BUSS, F., BRIGHT, N. A., LATOUCHE, M., REILLY, M. M., KENDRICK-JONES, J. & LUZIO, J. P. 2010. Mistargeting

of SH3TC2 away from the recycling endosome causes Charcot–Marie–Tooth disease type 4C. *Human molecular genetics*, 19, 1009-1018.

ROBUSTO, M., FANG, M., ASSELTA, R., CASTORINA, P., PREVITALI, S. C., CACCIA, S., BENZONI, E., DE CRISTOFARO, R., YU, C., CESARANI, A., LIU, X., LI, W., PRIMIGNANI, P., AMBROSETTI, U., XU, X., DUGA, S. & SOLDÀ, G. 2014. The expanding spectrum of PRPS1-associated phenotypes: three novel mutations segregating with X-linked hearing loss and mild peripheral neuropathy. *European journal of human genetics : EJHG*.

RODRIGUEZ, P. Q., LOHKAMP, B., CELSI, G., MACHE, C. J., AUER-GRUMBACH, M., WERNERSON, A., HAMAJIMA, N., TRYGGVASON, K. & PATRAKKA, J. 2013. Novel INF2 mutation p. L77P in a family with glomerulopathy and Charcot-Marie-Tooth neuropathy. *Pediatr Nephrol*, 28, 339-43.

ROSSOR, A. M., KALMAR, B., GREENSMITH, L. & REILLY, M. M. 2012. The distal hereditary motor neuropathies. *J Neurol Neurosurg Psychiatry*, 83, 6-14.

ROTTIER, A., AUER-GRUMBACH, M., JANSSENS, K., BAETS, J., PENNO, A., ALMEIDA-SOUZA, L., VAN HOOF, K., JACOBS, A., DE VRIENDT, E., SCHLÖTTER-WEIGEL, B., LÖSCHER, W., VONDRAČEK, P., SEEMAN, P., DE JONGHE, P., VAN DIJCK, P., JORDANOVA, A., HORNEMANN, T. & TIMMERMAN, V. 2010. Mutations in the SPTLC2 Subunit of Serine Palmitoyltransferase Cause Hereditary Sensory and Autonomic Neuropathy Type I. *The American Journal of Human Genetics*, 87, 513-522.

RUBINO, F., PIREDDA, R., CALABRESE, F. M., SIMONE, D., LANG, M., CALABRESE, C., PETRUZZELLA, V., TOMMASEO-PONZETTA, M., GASPARRE, G. & ATTIMONELLI, M. 2012. HmtDB, a genomic resource for mitochondrion-based human variability studies. *Nucleic Acids Res*, 40, D1150-9.

RUDNIK-SCHONEBORN, S., STOLZ, P., VARON, R., GROHMANN, K., SCHACHTELE, M., KETELSEN, U. P., STAVROU, D., KURZ, H., HUBNER, C. & ZERRES, K. 2004. Long-term observations of patients with

infantile spinal muscular atrophy with respiratory distress type 1 (SMARD1). *Neuropediatrics*, 35, 174-82.

RUSTIN, P., BOURGERON, T., PARFAIT, B., CHRETIEN, D., MUNNICH, A. & RÖTIG, A. 1997. Inborn errors of the Krebs cycle: a group of unusual mitochondrial diseases in human. *Biochimica et Biophysica Acta (BBA) - Molecular Basis of Disease*, 1361, 185-197.

SAMAD, T. A., REBBAPRAGADA, A., BELL, E., ZHANG, Y., SIDIS, Y., JEONG, S.-J., CAMPAGNA, J. A., PERUSINI, S., FABRIZIO, D. A., SCHNEYER, A. L., LIN, H. Y., BRIVANLOU, A. H., ATTISANO, L. & WOOLF, C. J. 2005. DRAGON, a Bone Morphogenetic Protein Co-receptor. *Journal of Biological Chemistry*, 280, 14122-14129.

SAMAD, T. A., SRINIVASAN, A., KARCHEWSKI, L. A., JEONG, S. J., CAMPAGNA, J. A., JI, R. R., FABRIZIO, D. A., ZHANG, Y., LIN, H. Y., BELL, E. & WOOLF, C. J. 2004. DRAGON: a member of the repulsive guidance molecule-related family of neuronal- and muscle-expressed membrane proteins is regulated by DRG11 and has neuronal adhesive properties. *The Journal of neuroscience : the official journal of the Society for Neuroscience*, 24, 2027-36.

SAMUELS, D. C., WONNAPINIJ, P., CREE, L. M. & CHINNERY, P. F. 2010. Reassessing evidence for a postnatal mitochondrial genetic bottleneck. *Nature genetics*, 42, 471-2; author reply 472-3.

SANTORELLI, F.M., TANJI, K., SANO, M., SHANSKE, S., EL-SHAHAWI, M., KRANZ-EBLE, P., DIMAURO, S., DE VIVO, D.C. 1997 Maternally inherited encephalopathy associated with a single-base insertion in the mitochondrial tRNATrp gene. *Ann Neurol*. 42, 256-60.

SAPORTA, A. S., SOTTILE, S. L., MILLER, L. J., FEELY, S. M., SISKIND, C. E. & SHY, M. E. 2011. Charcot-Marie-Tooth disease subtypes and genetic testing strategies. *Annals of neurology*, 69, 22-33.

SAUVANET, C., DUVEZIN-CAUBET, S., DI RAGO, J. P. & ROJO, M. 2010. Energetic requirements and bioenergetic modulation of mitochondrial morphology and dynamics. *Seminars in cell & developmental biology*, 21, 558-65.

SCHABHUTTL, M., WIELAND, T., SENDEREK, J., BAETS, J., TIMMERMANN, V., DE JONGHE, P., REILLY, M. M., STIEGLBAUER, K., LAICH, E.,

WINDHAGER, R., ERWA, W., TRAJANOSKI, S., STROM, T. M. & AUER-GRUMBACH, M. 2014a. Whole-exome sequencing in patients with inherited neuropathies: outcome and challenges. *J Neurol.*

SCHABHUTTL, M., WIELAND, T., SENDEREK, J., BAETS, J., TIMMERMAN, V., DE JONGHE, P., REILLY, M. M., STIEGLBAUER, K., LAICH, E., WINDHAGER, R., ERWA, W., TRAJANOSKI, S., STROM, T. M. & AUER-GRUMBACH, M. 2014b. Whole-exome sequencing in patients with inherited neuropathies: outcome and challenges. *J Neurol*, 261, 970-82.

SCHENONE, A., NOBBIO, L., MONTI BRAGADIN, M., URSINO, G. & GRANDIS, M. 2011. Inherited neuropathies. *Curr Treat Options Neurol*, 13, 160-79.

SCHERER, S. S. & KLEOPA, K. A. 2012. X-linked Charcot-Marie-Tooth disease. *J Peripher Nerv Syst*, 17 Suppl 3, 9-13.

SCHERER, S. S. & WRABETZ, L. 2008. Molecular Mechanisms of Inherited Demyelinating Neuropathies. *Glia*, 56, 1578-1589.

SCHMALBRUCH, H., JENSEN, H. J., BJAERG, M., KAMIENIECKA, Z. & KURLAND, L. 1991. A new mouse mutant with progressive motor neuronopathy. *J Neuropathol Exp Neurol*, 50, 192-204.

SCHMITTGEN, T. D. & LIVAK, K. J. 2008. Analyzing real-time PCR data by the comparative C(T) method. *Nat Protoc*, 3, 1101-8.

SCHON, ERIC A. & PRZEDBORSKI, S. 2011. Mitochondria: The Next (Neurode)Generation. *Neuron*, 70, 1033-1053.

SCHON, E. A., SANTRA, S., PALLOTTI, F. & GIRVIN, M. E. 2001. Pathogenesis of primary defects in mitochondrial ATP synthesis. *Seminars in cell & developmental biology*, 12, 441-8.

SEVILLA, T. & VILCHEZ, J. J. 2004. [Different phenotypes of Charcot-Marie-Tooth disease caused by mutations in the same gene. Are classical criteria for classification still valid?]. *Neurologia*, 19, 264-71.

SENDEREK, J., BERGMANN, C., RAMAEKERS, V.T., NELIS, E., BERNERT, G., MAKOWSKI, A., ZÜCHNER, S., DE JONGHE, P., RUDNIK-SCHÖNEBORN, S., ZERRES, K., SCHRÖDER, J.M. 2003 Mutations in the ganglioside-induced differentiation-associated protein-1 (GDAP1) gene in intermediate type autosomal recessive Charcot-Marie-Tooth neuropathy. *Brain : a journal of neurology* 126(Pt 3): 642-649.

SGARBI, G., BARACCA, A., LENAZ, G., VALENTINO, L. M., CARELLI, V. & SOLAINI, G. 2006. Inefficient coupling between proton transport and ATP synthesis may be the pathogenic mechanism for NARP and Leigh syndrome resulting from the T8993G mutation in mtDNA. *The Biochemical journal*, 395, 493-500.

SHEKARABI, M., MOLDRICH, R. X., RASHEED, S., SALIN-CANTEGREL, A., LAGANIÈRE, J., ROCHEFORT, D., HINCE, P., HUOT, K., GAUDET, R., KURNIAWAN, N., SOTOCINAL, S. G., RITCHIE, J., DION, P. A., MOGIL, J. S., RICHARDS, L. J. & ROULEAU, G. A. 2012. Loss of neuronal potassium/chloride cotransporter 3 (KCC3) is responsible for the degenerative phenotype in a conditional mouse model of hereditary motor and sensory neuropathy associated with agenesis of the corpus callosum. *The Journal of neuroscience : the official journal of the Society for Neuroscience*, 32, 3865-76.

SHISHEVA, A. 2012. PIKfyve and its Lipid products in health and in sickness. *Curr Top Microbiol Immunol*, 362, 127-62.

SHY, M. E. 2006. Peripheral neuropathies caused by mutations in the myelin protein zero. *J Neurol Sci*, 242, 55-66.

SHY, M. E., JANI, A., KRAJEWSKI, K., GRANDIS, M., LEWIS, R. A., LI, J., SHY, R. R., BALSAMO, J., LILIEN, J., GARBERN, J. Y. & KAMHOLZ, J. 2004. Phenotypic clustering in MPZ mutations. *Brain : a journal of neurology*, 127, 371-84.

SHY, M. E. & PATZKO, A. 2011. Axonal Charcot-Marie-Tooth disease. *Current opinion in neurology*, 24, 475-83.

SIGURGARDOTTIR, S., HELGASON, A., GULCHER, J. R., STEFANSSON, K. & DONNELLY, P. 2000. The mutation rate in the human mtDNA control region. *American journal of human genetics*, 66, 1599-609.

SIMON-SANCHEZ, J., DOPPER, E. G., COHN-HOKKE, P. E., HUKEMA, R. K., NICOLAOU, N., SEELAAR, H., DE GRAAF, J. R., DE KONING, I., VAN SCHOOOR, N. M., DEEG, D. J., SMITS, M., RAAPHORST, J., VAN DEN BERG, L. H., SCHELHAAS, H. J., DE DIE-SMULDERS, C. E., MAJOOR-KRAKAUER, D., ROZEMULLER, A. J., WILLEMSSEN, R., PIJNENBURG, Y. A., HEUTINK, P. & VAN SWIETEN, J. C. 2012. The

clinical and pathological phenotype of C9ORF72 hexanucleotide repeat expansions. *Brain : a journal of neurology*, 135, 723-35.

SIMONE, C., NIZZARDO, M., RIZZO, F., RUGGIERI, M., RIBOLDI, G., SALANI, S., BUCCHIA, M., BRESOLIN, N., COMI, G.P., CORTI, S. 2014 iPSC-Derived neural stem cells act via kinase inhibition to exert neuroprotective effects in spinal muscular atrophy with respiratory distress type 1. *Stem Cell Reports*. 3(2):297-311.

SISKIND, C. E., PANCHAL, S., SMITH, C. O., FEELY, S. M., DALTON, J. C., SCHINDLER, A. B. & KRAJEWSKI, K. M. 2013. A review of genetic counseling for Charcot Marie Tooth disease (CMT). *J Genet Couns*, 22, 422-36.

SITARZ, K. S., YU-WAI-MAN, P., PYLE, A., STEWART, J. D., RAUTENSTRAUSS, B., SEEMAN, P., REILLY, M. M., HORVATH, R. & CHINNERY, P. F. 2012. MFN2 mutations cause compensatory mitochondrial DNA proliferation. *Brain : a journal of neurology*, 135, e219, 1-3; author reply e220, 1-3.

SKRE, H. 1974 Genetic and clinical aspects of Charcot-Marie-Tooth's disease. *Clin Genet* 6(2): 98-118.

SMITH, M. J., POZO, K., BRICKLEY, K. & STEPHENSON, F. A. 2006. Mapping the GRIF-1 binding domain of the kinesin, KIF5C, substantiates a role for GRIF-1 as an adaptor protein in the anterograde trafficking of cargoes. *J Biol Chem*, 281, 27216-28.

SONG, B.W., HUANG, Y.H., TSAI, P.C., HUANG, C.C., PAN, H.C., LU, Y.C., CHIEN, H.J., LIU, T.T., CHANG, M.H., LIN, K.P et al. 2013 Exome sequencing identifies GNB4 mutations as a cause of dominant intermediate Charcot-Marie-Tooth disease. *American journal of human genetics* 92(3): 422-430.

SPIEGEL, R., KHAYAT, M., SHALEV, S. A., HOROVITZ, Y., MANDEL, H., HERSHKOVITZ, E., BARGHUTI, F., SHAAG, A., SAADA, A., KORMAN, S. H., ELPELEG, O. & YATSIV, I. 2011. TMEM70 mutations are a common cause of nuclear encoded ATP synthase assembly defect: further delineation of a new syndrome. *Journal of Medical Genetics*, 48, 177-82.

SPINOSA, M. R., PROGIDA, C., DE LUCA, A., COLUCCI, A. M., ALIFANO, P. & BUCCI, C. 2008. Functional characterization of Rab7 mutant proteins associated with Charcot-Marie-Tooth type 2B disease. *The Journal of neuroscience : the official journal of the Society for Neuroscience*, 28, 1640-8.

SPRINZL, M., HORN, C., BROWN, M., IOUDOVITCH, A. & STEINBERG, S. 1998. Compilation of tRNA sequences and sequences of tRNA genes. *Nucleic Acids Research*, 26, 148-153.

STALPERS, X. L., VERRIPS, A., POLL-THE, B. T., COBBEN, J.-M., SNOECK, I. N., DE COO, I. F. M., BROOKS, A., BULK, S., GOOSKENS, R., FOCK, A., VERSCHUUREN-BEMELMANS, C., SINKE, R. J., DE VISSER, M. & LEMMINK, H. H. 2013. Clinical and mutational characteristics of spinal muscular atrophy with respiratory distress type 1 in the Netherlands. *Neuromuscular Disorders*, 23, 461-468.

STEWART, J. B., FREYER, C., ELSON, J. L., WREDENBERG, A., CANSU, Z., TRIFUNOVIC, A. & LARSSON, N.-G. 2008. Strong Purifying Selection in Transmission of Mammalian Mitochondrial DNA. *PLoS Biol*, 6, e10.

STUM, M., MCLAUGHLIN, H. M., KLEINBRINK, E. L., MIERS, K. E., ACKERMAN, S. L., SEBURN, K. L., ANTONELLIS, A. & BURGESS, R. W. 2011. An assessment of mechanisms underlying peripheral axonal degeneration caused by aminoacyl-tRNA synthetase mutations. *Mol Cell Neurosci*, 46, 432-43.

SUMNER, C. J., D'YDEWALLE, C., WOOLEY, J., FAWCETT, K. A., HERNANDEZ, D., GARDINER, A. R., KALMAR, B., BALOH, R. H., GONZALEZ, M., ZUCHNER, S., STANESCU, H. C., KLETA, R., MANKODI, A., CORNBLATH, D. R., BOYLAN, K. B., REILLY, M. M., GREENSMITH, L., SINGLETON, A. B., HARMS, M. B., ROSSOR, A. M. & HOULDEN, H. 2013. A dominant mutation in FBXO38 causes distal spinal muscular atrophy with calf predominance. *American journal of human genetics*, 93, 976-83.

SUN, X., FONTAINE, J. M., REST, J. S., SHELDEN, E. A., WELSH, M. J. & BENNDORF, R. 2004. Interaction of Human HSP22 (HSPB8) with Other Small Heat Shock Proteins. *Journal of Biological Chemistry*, 279, 2394-2402.

SURAWEERA, A., LIM, Y., WOODS, R., BIRRELL, G. W., NASIM, T., BECHEREL, O. J. & LAVIN, M. F. 2009. Functional role for senataxin, defective in ataxia oculomotor apraxia type 2, in transcriptional regulation. *Human molecular genetics*, 18, 3384-96.

SUTER, U. & SCHERER, S. S. 2003. Disease mechanisms in inherited neuropathies. *Nature reviews. Neuroscience*, 4, 714-26.

SUTOVSKY, P., MORENO, R. D., RAMALHO-SANTOS, J., DOMINKO, T., SIMERLY, C. & SCHATTEN, G. 1999. Development: Ubiquitin tag for sperm mitochondria. *Nature*, 402, 371-372.

TACHI, N., KIKUCHI, S., KOZUKA, N. & NOGAMI, A. 2005. A new mutation of IGHMBP2 gene in spinal muscular atrophy with respiratory distress type 1. *Pediatr Neurol*, 32, 288-90.

TAKASHIMA, H. 2006. [Molecular genetics of inherited neuropathies]. *Rinsho Shinkeigaku*, 46, 1-18.

TAKASHIMA, H. 2012. [Genetic diagnosis and molecular pathology of inherited neuropathy]. *Rinsho Shinkeigaku*, 52, 399-404.

TANABE, K. & TAKEI, K. 2012. Dynamin 2 in Charcot-Marie-Tooth disease. *Acta Med Okayama*, 66, 183-90.

TAYLOR, R. W. & TURNBULL, D. M. 2005. Mitochondrial DNA mutations in human disease. *Nature reviews. Genetics*, 6, 389-402.

TAZIR, M., BELLATACHE, M., NOUIOUA, S. & VALLAT, J.-M. 2013. Autosomal recessive Charcot-Marie-Tooth disease: from genes to phenotypes. *Journal of the Peripheral Nervous System*, 18, 113-129.

THORBURN, D.R., RAHMAN, S. Mitochondrial DNA-Associated Leigh Syndrome and NARP. 2003 Oct 30. In: PAGON, R. A., ADAM, M. P., ARDINGER, H.H., et al., editors. GeneReviews®. Seattle (WA): University of Washington, Seattle; 1993-2014. Available from: <http://www.ncbi.nlm.nih.gov/books/NBK1173/>

TOLEDO-ARAL, J.J., MOSS, B.L., HE, Z.J., KOSZOWSKI, A.G., WHISENAND, T., LEVINSON, S.R., WOLF, J.J., SILOS-SANTIAGO, I., HALEGOUA, S., MANDEL, G. 1997 Identification of PN1, a predominant voltage-dependent sodium channel expressed principally in peripheral neurons. *Proc. Natl. Acad. Sci.* 94, 1527-1532.

TORIELLI, L., TIVODAR, S., MONTELLA, R. C., IACONE, R., PADOANI, G., TARSINI, P., RUSSO, O., SARNATARO, D., STRAZZULLO, P., FERRARI, P., BIANCHI, G. & ZURZOLO, C. 2008. alpha-Adducin mutations increase Na/K pump activity in renal cells by affecting constitutive endocytosis: implications for tubular Na reabsorption. *Am J Physiol Renal Physiol*, 295, F478-87.

TSURUSAKI, Y., SAITO, S., TOMIZAWA, K., SUDO, A., ASAHINA, N., SHIRAISHI, H., ITO, J., TANAKA, H., DOI, H., SAITSU, H., MIYAKE, N. & MATSUMOTO, N. 2012. A DYNC1H1 mutation causes a dominant spinal muscular atrophy with lower extremity predominance. *neurogenetics*, 13, 327-32.

TURNBULL, H. E., LAX, N. Z., DIODATO, D., ANSORGE, O. & TURNBULL, D. M. 2010. The mitochondrial brain: From mitochondrial genome to neurodegeneration. *Biochimica et biophysica acta*, 1802, 111-21.

TUUPANEN, S., HANNINEN, U. A., KONDELIN, J., VON NANDELSTADH, P., CAJUSO, T., GYLFE, A. E., KATAINEN, R., TANSKANEN, T., RISTOLAINEN, H., BOHM, J., MECKLIN, J. P., JARVINEN, H., RENKONEN-SINISALO, L., ANDERSEN, C. L., TAIPALE, M., TAIPALE, J., VAHTERISTO, P., LEHTI, K., PITKANEN, E. & AALTONEN, L. A. 2014. Identification of 33 candidate oncogenes by screening for base-specific mutations. *Br J Cancer*, 111, 1657-62.

TWELVETREES, A. E., YUEN, E. Y., ARANCIBIA-CARCAMO, I. L., MACASKILL, A. F., ROSTAING, P., LUMB, M. J., HUMBERT, S., TRILLER, A., SAUDOU, F., YAN, Z. & KITTLER, J. T. 2010. Delivery of GABAARs to synapses is mediated by HAP1-KIF5 and disrupted by mutant huntingtin. *Neuron*, 65, 53-65.

UGUR, S. A. & TOLUN, A. 2008. A deletion in DRCTNNB1A associated with hypomyelination and juvenile onset cataract. *European journal of human genetics : EJHG*, 16, 261-4.

VACCARI, I., DINA, G., TRONCHÈRE, H., KAUFMAN, E., CHICANNE, G., CERRI, F., WRABETZ, L., PAYRASTRE, B., QUATTRINI, A., WEISMAN, L. S., MEISLER, M. H. & BOLINO, A. 2011. Genetic Interaction between MTMR2 and FIG4 Phospholipid Phosphatases Involved in Charcot-Marie-Tooth Neuropathies. *PLoS genetics*, 7, e1002319.

VALLAT, J. M., TAZIR, M., CALVO, J. & FUNALOT, B. 2009. [Hereditary peripheral neuropathies]. *Presse Med*, 38, 1325-34.

VAN DER POL, W. L., TALIM, B., PITT, M. & VON AU, K. 2013. 190th ENMC international workshop: Spinal muscular atrophy with respiratory distress/distal spinal muscular atrophy type 1: 11–13 May 2012, Naarden, The Netherlands. *Neuromuscular Disorders*, 23, 602-609.

VAN MEERBEKE, J. P. & SUMNER, C. J. 2011. Progress and promise: the current status of spinal muscular atrophy therapeutics. *Discov Med*, 12, 291-305.

VAN SPRONSEN, M., MIKHAYLOVA, M., LIPKA, J., SCHLAGER, M. A., VAN DEN HEUVEL, D. J., KUIJPERS, M., WULF, P. S., KEIJZER, N., DEMMERS, J., KAPITEIN, L. C., JAARSMA, D., GERRITSEN, H. C., AKHMANOVA, A. & HOOGENRAAD, C. C. 2013. TRAK/Milton motor-adaptor proteins steer mitochondrial trafficking to axons and dendrites. *Neuron*, 77, 485-502.

VANDESOMPELE, J., DE PRETER, K., PATTYN, F., POPPE, B., VAN ROY, N., DE PAEPE, A. & SPELEMAN, F. 2002. Accurate normalization of real-time quantitative RT-PCR data by geometric averaging of multiple internal control genes. *Genome Biol*, 3, RESEARCH0034.

VERHOEVEN, K., DE JONGHE, P., VAN DE PUTTE, T., NELIS, E., ZWIJSEN, A., VERPOORTEN, N., DE VRIENDT, E., JACOBS, A., VAN GERWEN, V., FRANCIS, A., CEUTERICK, C., HUYLEBROECK, D. & TIMMERMAN, V. 2003. Slowed conduction and thin myelination of peripheral nerves associated with mutant rho Guanine-nucleotide exchange factor 10. *American journal of human genetics*, 73, 926-32.

VERMA, A. 2014. Tale of two diseases: amyotrophic lateral sclerosis and frontotemporal dementia. *Neurol India*, 62, 347-51.

VESTER, A., VELEZ-RUIZ, G., MCLAUGHLIN, H. M., LUPSKI, J. R., TALBOT, K., VANCE, J. M., ZUCHNER, S., RODA, R. H., FISCHBECK, K. H., BIESECKER, L. G., NICHOLSON, G., BEG, A. A. & ANTONELLIS, A. 2013a. A loss-of-function variant in the human histidyl-tRNA synthetase (HARS) gene is neurotoxic in vivo. *Human mutation*, 34, 191-9.

VESTER, A., VELEZ-RUIZ, G., MCLAUGHLIN, H. M., PROGRAM, N. C. S., LUPSKI, J. R., TALBOT, K., VANCE, J. M., ZÜCHNER, S., RODA, R. H., FISCHBECK, K. H., BIESECKER, L. G., NICHOLSON, G., BEG, A. A. &

ANTONELLIS, A. 2013b. A Loss-of-Function Variant in the Human Histidyl-tRNA Synthetase (HARS) Gene is Neurotoxic In Vivo. *Human mutation*, 34, 191-199.

VIOLLET, L., ZARH RATE, M., MAYSTADT, I., ESTOURNET-MATHIAUT, B., BAROIS, A., DESGUERRE, I., MAYER, M., CHABROL, B., LEHEUP, B., CUSIN, V., BILLETTE DE VILLEMEUR, T., BONNEAU, D., SAUGIER-VEBER, P., TOUZERY-DE VILLEPIN, A., DELAUBIER, A., KAPLAN, J., JEANPIERRE, M., FEINGOLD, J. & MUNNICH, A. 2004. Refined genetic mapping of autosomal recessive chronic distal spinal muscular atrophy to chromosome 11q13.3 and evidence of linkage disequilibrium in European families. *European journal of human genetics : EJHG*, 12, 483-8.

VOO, I., ALLF, B. E., UDAR, N., SILVA-GARCIA, R., VANCE, J. & SMALL, K. W. 2003. Hereditary motor and sensory neuropathy type VI with optic atrophy. *American Journal of Ophthalmology*, 136, 670-677.

WADA, M., TOH, S., TANIGUCHI, K., NAKAMURA, T., UCHIUMI, T., KOHNO, K., YOSHIDA, I., KIMURA, A., SAKISAKA, S., ADACHI, Y. & KUWANO, M. 1998. Mutations in the canilicular multispecific organic anion transporter (cMOAT) gene, a novel ABC transporter, in patients with hyperbilirubinemia II/Dubin-Johnson syndrome. *Human molecular genetics*, 7, 203-7.

WAI, T., TEOLI, D. & SHOUBRIDGE, E. A. 2008. The mitochondrial DNA genetic bottleneck results from replication of a subpopulation of genomes. *Nature genetics*, 40, 1484-8.

WAGNER, O.I., ASCAÑO, J., TOKITO, M., LETERRIER, J.F., JANMEY, P.A., HOLZBAUR, E.L. 2004 The interaction of neurofilaments with the microtubule motor cytoplasmic dynein. *Mol Biol Cell*. 15(11):5092-100.

WANG, G. L., WANG, C. Y., CAI, X. Z., CHEN, W., WANG, X. H. & LI, F. 2010. Identification and expression analysis of a novel CW-type zinc finger protein MORC2 in cancer cells. *Anat Rec (Hoboken)*, 293, 1002-9.

WANG, J., FANG, P., SCHIMMEL, P. & GUO, M. 2012. Side chain independent recognition of aminoacyl adenylates by the Hint1 transcription suppressor. *The journal of physical chemistry. B*, 116, 6798-805.

WANG, X., WINTER, D., ASHRAFI, G., SCHLEHE, J., WONG, Y. L., SELKOE, D., RICE, S., STEEN, J., LAVOIE, M. J. & SCHWARZ, T. L. 2011. PINK1

and Parkin target Miro for phosphorylation and degradation to arrest mitochondrial motility. *Cell*, 147, 893-906.

WARDE-FARLEY, D., DONALDSON, S. L., COMES, O., ZUBERI, K., BADRAWI, R., CHAO, P., FRANZ, M., GROUIOS, C., KAZI, F., LOPES, C. T., MAITLAND, A., MOSTAFAVI, S., MONTOJO, J., SHAO, Q., WRIGHT, G., BADER, G. D. & MORRIS, Q. 2010. The GeneMANIA prediction server: biological network integration for gene prioritization and predicting gene function. *Nucleic Acids Res*, 38, W214-20.

WARNER, J. P., BARRON, L. H., GOUDIE, D., KELLY, K., DOW, D., FITZPATRICK, D. R., BROCK, D. J. 1996 A general method for the detection of large CAG repeat expansions by fluorescent PCR *J Med Genet*, 33, 1022-6.

WAXMAN, S.G. 2007 Nav1.7, its mutations, and the syndromes that they cause. *Neurology*. 69(6):505-7.

WEEDON, M. N., HASTINGS, R., CASWELL, R., XIE, W., PASZKIEWICZ, K., ANTONIADI, T., WILLIAMS, M., KING, C., GREENHALGH, L., NEWBURY-ECOB, R. & ELLARD, S. 2011. Exome sequencing identifies a DYNC1H1 mutation in a large pedigree with dominant axonal Charcot-Marie-Tooth disease. *American journal of human genetics*, 89, 308-12.

WEI, Y. H. 1998. Oxidative stress and mitochondrial DNA mutations in human aging. *Proc Soc Exp Biol Med*, 217, 53-63.

WEISKE, J. & HUBER, O. 2006. The histidine triad protein Hint1 triggers apoptosis independent of its enzymatic activity. *J Biol Chem*, 281, 27356-66.

WETERMAN, M. A., SORRENTINO, V., KASHER, P. R., JAKOBS, M. E., VAN ENGELEN, B. G., FLUITER, K., DE WISSEL, M. B., SIZAROV, A., NURNBERG, G., NURNBERG, P., ZELCER, N., SCHELHAAS, H. J. & BAAS, F. 2012. A frameshift mutation in LRSAM1 is responsible for a dominant hereditary polyneuropathy. *Human molecular genetics*, 21, 358-70.

XIA, C. H., ROBERTS, E. A., HER, L. S., LIU, X., WILLIAMS, D. S., CLEVELAND, D. W. & GOLDSTEIN, L. S. 2003. Abnormal neurofilament transport caused by targeted disruption of neuronal kinesin heavy chain KIF5A. *J Cell Biol*, 161, 55-66.

XIA, Y., BABITT, J. L., BOULEY, R., ZHANG, Y., DA SILVA, N., CHEN, S., ZHUANG, Z., SAMAD, T. A., BRENNER, G. J., ANDERSON, J. L.,

HONG, C. C., SCHNEYER, A. L., BROWN, D. & LIN, H. Y. 2010. Dragon Enhances BMP Signaling and Increases Transepithelial Resistance in Kidney Epithelial Cells. *Journal of the American Society of Nephrology*, 21, 666-677.

XIA, Y., CORTEZ-RETAMOZO, V., NIEDERKOFLER, V., SALIE, R., CHEN, S., SAMAD, T. A., HONG, C. C., ARBER, S., VYAS, J. M., WEISSLEDER, R., PITTEL, M. J. & LIN, H. Y. 2011. Dragon (repulsive guidance molecule b) inhibits IL-6 expression in macrophages. *J Immunol*, 186, 1369-76.

XU, W. Y., GU, M. M., SUN, L. H., GUO, W. T., ZHU, H. B., MA, J. F., YUAN, W. T., KUANG, Y., JI, B. J., WU, X. L., CHEN, Y., ZHANG, H. X., SUN, F. T., HUANG, W., HUANG, L., CHEN, S. D. & WANG, Z. G. 2012. A nonsense mutation in DHTKD1 causes Charcot-Marie-Tooth disease type 2 in a large Chinese pedigree. *American journal of human genetics*, 91, 1088-94.

Y. MATSUOKAA, X. LIB AND V. BENNETTA 1999. Adducin structure function and regulation. *Cell. Mol. Life Sci.* , 884-895.

YLIKALLIO, E., POYHONEN, R., ZIMON, M., DE VRIENDT, E., HILANDER, T., PAETAU, A., JORDANOVA, A., LÖNNQVIST, T. & TYYNISMAA, H. 2013a. Deficiency of the E3 ubiquitin ligase TRIM2 in early-onset axonal neuropathy. *Human molecular genetics*, 22, 2975-83.

YLIKALLIO, E., PÖYHÖNEN, R., ZIMON, M., DE VRIENDT, E., HILANDER, T., PAETAU, A., JORDANOVA, A., LÖNNQVIST, T. & TYYNISMAA, H. 2013b. Deficiency of the E3 ubiquitin ligase TRIM2 in early-onset axonal neuropathy. *Human molecular genetics*, 22, 2975-2983.

ZARA, F., BIANCHERI, R., BRUNO, C., BORDO, L., ASSERETO, S., GAZZERRO, E., SOTGIA, F., WANG, X. B., GIANOTTI, S., STRINGARA, S., PEDEMONTI, M., UZIEL, G., ROSSI, A., SCHENONE, A., TORTORI-DONATI, P., VAN DER KNAAP, M. S., LISANTI, M. P. & MINETTI, C. 2006. Deficiency of hyccin, a newly identified membrane protein, causes hypomyelination and congenital cataract. *Nature genetics*, 38, 1111-3.

ZHANG, X., CHOW, C.Y., SAHENK, Z., SHY, M.E., MEISLER, M.H., LI J 2008 Mutation of FIG4 causes a rapidly progressive, asymmetric neuronal degeneration. *Brain*. 131(Pt 8):1990-2001.

ZHANG, M., CHEN, L., WANG, S. & WANG, T. 2009. Rab7: roles in membrane trafficking and disease. *Biosci Rep*, 29, 193-209.

ZHAO, C., TAKITA, J., TANAKA, Y., SETOU, M., NAKAGAWA, T., TAKEDA, S., YANG, H. W., TERADA, S., NAKATA, T., TAKEI, Y., SAITO, M., TSUJI, S., HAYASHI, Y. & HIROKAWA, N. 2001. Charcot-Marie-Tooth Disease Type 2A Caused by Mutation in a Microtubule Motor KIF1B β . *Cell*, 105, 587-597.

ZHAO, H., RACE, V., MATTHIJS, G., DE JONGHE, P., ROBBERECHT, W., LAMBRECHTS, D. & VAN DAMME, P. 2014. Exome sequencing reveals HINT1 mutations as a cause of distal hereditary motor neuropathy. *European journal of human genetics : EJHG*, 22, 847-850.

ZHU, Q., COUILLARD-DESPRES, S. & JULIEN, J. P. 1997. Delayed maturation of regenerating myelinated axons in mice lacking neurofilaments. *Experimental neurology*, 148, 299-316.

ZIMON, M., BAETS, J., ALMEIDA-SOUZA, L., DE VRIENDT, E., NIKODINOVIC, J., PARMAN, Y., BATTALOGLU, E., MATUR, Z., GUERGUELTCHEVA, V., TOURNEV, I., AUER-GRUMBACH, M., DE RIJK, P., PETERSEN, B. S., MULLER, T., FRANSEN, E., VAN DAMME, P., LOSCHER, W. N., BARISIC, N., MITROVIC, Z., PREVITALI, S. C., TOPALOGLU, H., BERNERT, G., BELEZA-MEIRELES, A., TODOROVIC, S., SAVIC-PAVICEVIC, D., ISHPEKOVA, B., LECHNER, S., PEETERS, K., OOMS, T., HAHN, A. F., ZUCHNER, S., TIMMERMAN, V., VAN DIJCK, P., RASIC, V. M., JANECKE, A. R., DE JONGHE, P. & JORDANOVA, A. 2012. Loss-of-function mutations in HINT1 cause axonal neuropathy with neuromyotonia. *Nature genetics*, 44, 1080-3.

ZIMON, M., BAETS, J., AUER-GRUMBACH, M., BERCIANO, J., GARCIA, A., LOPEZ-LASO, E., MERLINI, L., HILTON-JONES, D., MCENTAGART, M., CROSBY, A. H., BARISIC, N., BOLTSHAUSER, E., SHAW, C. E., LANDOURE, G., LUDLOW, C. L., GAUDET, R., HOULDEN, H., REILLY, M. M., FISCHBECK, K. H., SUMNER, C. J., TIMMERMAN, V., JORDANOVA, A. & JONGHE, P. D. 2010. Dominant mutations in the cation channel gene transient receptor potential vanilloid 4 cause an unusual spectrum of neuropathies. *Brain : a journal of neurology*, 133, 1798-809.

ZSURKA, G. & KUNZ, W. S. 2013. Mitochondrial involvement in neurodegenerative diseases. *IUBMB Life*, 65, 263-272.

ZU, T., LIU, Y., BANEZ-CORONEL, M., REID, T., PLETNIKOVA, O., LEWIS, J., MILLER, T. M., HARMS, M. B., FALCHOOK, A. E., SUBRAMONY, S. H., OSTROW, L. W., ROTHSTEIN, J. D., TRONCOSO, J. C. & RANUM, L. P. 2013. RAN proteins and RNA foci from antisense transcripts in C9ORF72 ALS and frontotemporal dementia. *Proc Natl Acad Sci U S A*, 110, E4968-77.

ZUCHNER, S., DE JONGHE, P., JORDANOVA, A., CLAEYS, K. G., GUERGUELTCHEVA, V., CHERNINKOVA, S., HAMILTON, S. R., VAN STAVERN, G., KRAJEWSKI, K. M., STAJICH, J., TOURNEV, I., VERHOEVEN, K., LANGERHORST, C. T., DE VISSER, M., BAAS, F., BIRD, T., TIMMERMAN, V., SHY, M. & VANCE, J. M. 2006. Axonal neuropathy with optic atrophy is caused by mutations in mitofusin 2. *Annals of neurology*, 59, 276-81.

ZUCHNER, S., MERSIYANOVA, I. V., MUGLIA, M., BISSAR-TADMOURI, N., ROCHELLE, J., DADALI, E. L., ZAPPIA, M., NELIS, E., PATITUCCI, A., SENDEREK, J., PARMAN, Y., EVGRAFOV, O., JONGHE, P. D., TAKAHASHI, Y., TSUJI, S., PERICAK-VANCE, M. A., QUATTRONE, A., BATTALOGLU, E., POLYAKOV, A. V., TIMMERMAN, V., SCHRODER, J. M. & VANCE, J. M. 2004. Mutations in the mitochondrial GTPase mitofusin 2 cause Charcot-Marie-Tooth neuropathy type 2A. *Nature genetics*, 36, 449-51.

ZUCHNER, S., NOUREDDINE, M., KENNERTON, M., VERHOEVEN, K., CLAEYS, K., DE JONGHE, P., MERORY, J., OLIVEIRA, S. A., SPEER, M. C., STENGER, J. E., WALIZADA, G., ZHU, D., PERICAK-VANCE, M. A., NICHOLSON, G., TIMMERMAN, V. & VANCE, J. M. 2005. Mutations in the pleckstrin homology domain of dynamin 2 cause dominant intermediate Charcot-Marie-Tooth disease. *Nature genetics*, 37, 289-94.